Development of Miniature Enzymatic Biofuel Cells as Potential Power Sources for Implantable Medical Devices

Du Toit, Hendrik

Award date:
2015

Awarding institution:
University of Bath

DEVELOPMENT OF MINIATURE ENZYMATIC BIOFUEL CELLS AS POTENTIAL POWER SOURCES FOR IMPLANTABLE MEDICAL DEVICES

Hendrik du Toit
A thesis submitted for the degree of Doctor of Philosophy
University of Bath
Department of Chemical Engineering
November 2014

ABSTRACT

Since the first implantation of a cardiac pacemaker numerous efforts have been made to develop miniature implantable power devices, which would be able to run continuously for long periods of time without the need for replacement. In this context enzymatic biofuel cells (EBFCs) represent an attractive alternative, as they work at body temperature, are light and easy to miniaturise. Additionally, enzymatic biofuel cells can generate energy from the metabolites already present in physiological fluids, and produce waste products that naturally occur in the human body.

With a view to improving the biocompatibility of such devices, the use of highly porous gold (hPG) as a non-toxic high surface area alternative to the carbon nanotube based materials currently used was here investigated. The process for directly depositing hPG onto conductive surfaces was further developed to improve the stability of the deposited hPG films. The possibility of depositing these films on a range of different materials was also investigated. In particular it was shown that hPG films could also be deposited on very low cost materials, such as graphite composites. It was also demonstrated that these hPG electrodes exhibited potential for the direct electro-oxidation of aldehyde group containing sugars. The potential use of hPG electrodes as abiotic glucose sensors was consequently investigated and found to give stable amperometric responses between 0 and 50 mM, with a strong glucose dependant response even at the lowest concentration investigated of 0.5 µM.

However, since hPG electrodes were found to be susceptible to a large degree of interference and fouling in biological solutions, the use of glucose oxidase (GOx) on hPG electrodes was investigated in order to increase the specificity and stability of such electrodes in biological systems. A rapid and simple technique for the direct and functional deposition of GOx onto hPG was developed without using foreign electron mediators. These hPG-GOx electrodes were found to act as glucose sensors with extremely high sensitivity (22.7 µA mM^{-1} cm^{-2}), and a linear response to glucose in a range of between 50 µM and10 mM.

Finally EBFCs that exhibit continuous flow through were developed using fast prototyping techniques that employ 3D printed moulds. These EBFCs employed hPG-GOx electrodes coupled with hPG and laccase electrodes in order to generate power from glucose. The continuous and stable power production from a flow through EBFC for up to 30 days was subsequently demonstrated for the first time, with a peak power output of approximately 2 µW.

TABLE OF CONTENTS

ACKNOWLEDGMENTS

This thesis would not have been possible without the support of friends and family, and in particular the support of my parents, Johann and Karin du Toit.

I would first like to thank my supervisor, Dr. Mirella Di Lorenzo, not only for her support and guidance throughout the course of this research, but also for being so understanding over the years and allowing me the freedom to pursue the ambitions of a mad scientist. I would also like to thank my second supervisor, Prof. Frank Marken for all of his support and guidance throughout my PhD, and in particular for the use of his laboratory and research equipment at the start of my PhD.

I would like to thank John Mitchels and Ursula Potter from the Microscopy and Analysis Suite at the University of Bath for all of their help with electron microscopy and in particular for allowing me the opportunity to use much of their equipment to manufacture gold based materials. A large portion of the work I have conducted throughout the course of this project would not have been possible without their understanding and their enthusiasm to try something new.

Finally, I would like to thank the administrative and technical staff in the Department of Chemical Engineering, and University of Bath for funding my research and my studentship.

DECLARATION OF WORK DONE IN CONJUNCTION WITH OTHERS

Some preparations of graphite-hPG and carbon fibre-hPG electrodes (according to my protocols) were performed by Jia Huei Chong (in the capacity as a 3rd year undergraduate student for her research project) and Matthew Monti (in the capacity as a paid research assistant).

Iontophoresis extracts from pig skin were prepared and supplied by Sarah Cordery from Prof Richard Guy's group in the Department of Pharmacy and Pharmacology, University of Bath.

TABLE OF FIGURES

NOMENCLATURE

Symbol	Definition	Units
A	Area	cm^2
C	Capacitance	F
c	Concentration	M
E	Potential	V, mV
E^θ	Standard potential of reaction	V
F	Faraday's constant	$C\ mol^{-1}$
I	Current	A, µA
j	Current density	$\mu A\ cm^{-2}$
k	Arbitrary constant	-
K_M	Michaelis-Menten constant	M
l	Width of depletion/diffusion layer	m
l_c	Plate separation	m
Q	Charge	C
R	Resistance	kΩ
R	Ideal gas constant	$J\ K^{-1}\ mol^{-1}$
R^2	Coefficient of determination	-
T	Temperature	K
t	Time	s, h, days
u	Flow velocity	$m\ s^{-1}$, $cm\ min^{-1}$
V	Rate of reaction	$M\ s^{-1}$
ε	Dielectric constant	-
ε_0	Permittivity of free space	-
ν	Scan rate	$mV\ s^{-1}$

ABBREVIATIONS

Abbreviation	Definition
ABFC	Abiotic biofuel cell
AFM	Atomic force microscopy
CE	Counter electrode
CNT	Carbon nanotubes
CV	Cyclic voltammetry
DC	Direct current
DET	Direct electron transfer
DMSO	Dimethyl Sulfoxide
EBFC	Enzymatic biofuel cell
EDC	N-ethyl-N′-(3-dimethylaminopropyl)carbodiimide
E_{ox}/E_{red}	Oxidised or reduced forms of an enzyme
ESA	(Electrochemically-) Effective surface area
FAD	Flavin adenine dinucleotide
FESEM	Field emission scanning electron microscopy
GDH	Glucose dehydrogenase
GOx	Glucose oxidase from *Aspergillus niger*
hPG	Highly porous gold
IPA	Isopropyl alcohol/2-proponol
LAC	Laccase(s)
MBFC	Microbial biofuel cell
MET	Mediated electron transfer
NHS	N-hydroxysuccinimide
nPG	Nanoporous gold
P	Product
PAA	Porous anodic alumina
PBS	Phosphate buffered saline
PDMS	Polydimethylsiloxane
PQQ	Pyrroloquinoline quinone
RE	Reference electrode
RvLAC	Laccase from *Rhus vernicifera*
S	Substrate
SCE	Saturated calomel electrode
SEM	Scanning electron microscopy
TvLAC	Laccase from *Trametes versicolor*
WE	Working electrode

1. INTRODUCTION

1.1. A BRIEF OVERVIEW OF BIOFUEL CELLS

The term biofuel cell is used to describe any fuel cell in which the fuel stock's energy is derived from biological carbon fixation [1]. Fuel cells that use ethanol, carbohydrates, proteins, amino acids or lipids can all be described as biofuel cells if the route for fuel production involved the use of biological matter whether it is plant, animal or microbial based. Depending on the complexity of the biofuel used, the method for efficiently extracting chemical energy from the fuel stock varies as well. For fuels such as methanol or ethanol simple platinum and ruthenium based catalysts can be used to chemically extract energy, whereas for more complex molecules, such as proteins, microbial based fuel cells are required [2, 3]. Biofuel cells can be broken down into 3 sub classes: abiotic biofuel cells (ABFC) (fuel cells which generate power from biofuels without the use of any biological mechanisms); microbial biofuel cells (MBFC) (fuel cells that generate power from biofuels using living micro-organisms); and enzymatic biofuel cells (EBFC) (fuel cells that generate power from biofuels with the aid of enzymes) [4-6].

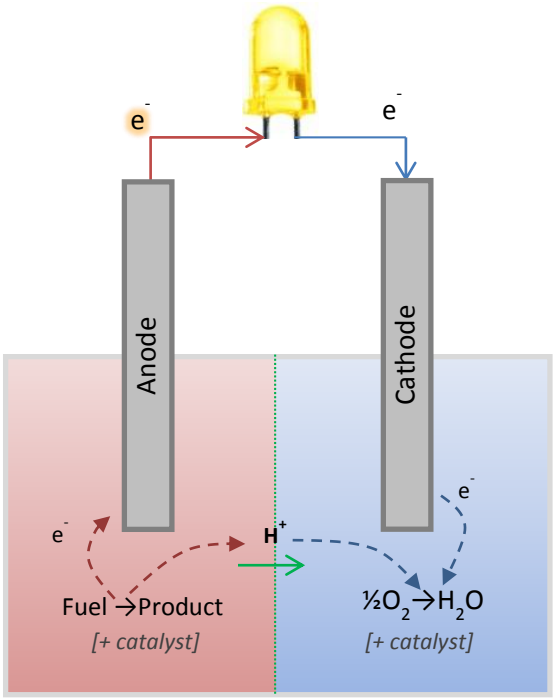

Figure 1: General fuel cell schematic

The first use of ABFCs can be traced back to the birth of implantable biofuel cells in the 1970s (see Section 2.1.1.). These devices were typically very inefficient, since they could only achieve very low conversion of glucose. In recent years however, with the building pressure to find alternative energy sources to fossil fuels, there has been a marked resurgence in research into

ABFCs, this time not limited to implantable fuel cells, but rather to larger devices, such as direct ethanol fuel cells.

The overall reaction scheme for all fuel cells is shown in Figure 1. At the anodic half-cell the fuel is reacted (usually with the help of a catalyst, either on the electrode surface, or in solution), resulting in the release of an electron and a proton. The electron is conducted through the anode to the cathodic half-cell whilst the proton remains in solution. Since most catalysts lack specificity the fuel and the oxidant have to be separated and thus the proton diffuses to the cathodic half-cell via a proton exchange membrane [7]. The drop in pH at the cathodic half-cell then facilitates the electrochemical reaction between an oxidant (typically oxygen) and an electron from the cathode. This is the simplest case, usually adopted in ABFCs with metal catalysts on the anode facilitating the oxidation of biofuels.

The first work on developing a fully characterised MBFC (arguably the oldest fuel cell technology in existence) was reported in 1911. Here the principle aim was not to generate power but to develop a live sensor for microbial activity by determining their electrical potential [8]. Since then there has always been significant interest in MBFCs, but like most fuel cell research, it had a massive boost in interest with the birth of the space age in the 1960s and 1970s. During this time there were numerous projects conducted worldwide investigating the possibility of using biofilms of bacteria such as *E. coli* and *C. butyricum* at the anode [9]. A significant military backing with extensive research was conducted by the United States Department of Defence [10].

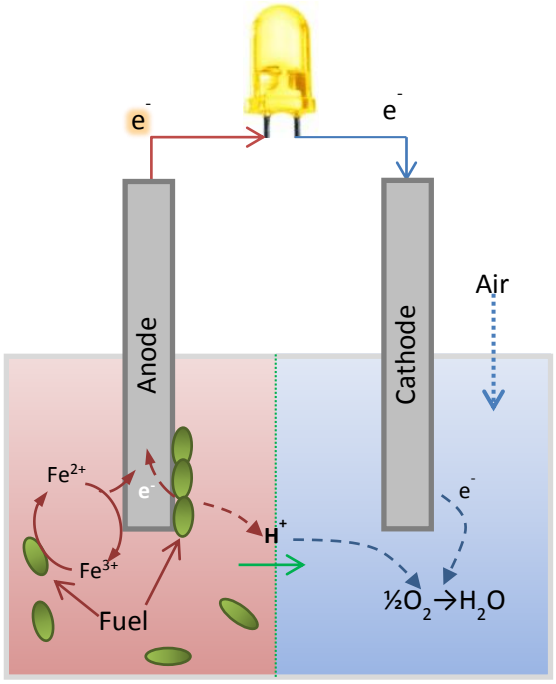

Figure 2: General schematic for microbial biofuel cells

Similarly to abiotic systems, MBFCs function by using microbes as a catalyst for production of protons from fuels [11]. The transfer of electrons from the microbes subsequently occurs, either directly through conducting biofilms, or aided with the use of electron carriers or mediators (Figure 2). Typically a dual chamber system is used with a proton exchange membrane in the middle, though it is also very common in to use a single chamber MBFC with the cathode "open to air" [12-14].

The exact origin of EBFCs is hard to determine since many techniques involving the use of microbes in biofuel cells could potentially have relied on the lyses of microbes used. For example, in 1966 Kenneth Lewis described a method which takes advantage of metabolic pathways both inside and outside of microbial cell membranes in order to fully oxidise glucose, which in actuality could only be achieved by lyses of the cells [5]. Hence this technique could be considered as an enzyme based method for generating energy since no living microbes are required, but instead freshly lysed ones.

The first intentional use of enzymes in a biofuel cell occurred in 1962, when the use of glucose oxidase in solution in glucose dependant biofuel cells was tested [11]. Since then many researchers have moved their focus to enzymatic biofuel cells since they are more specific and can achieve higher levels of conversion than metal catalysts. They can also function at low temperatures utilising traditional fuels such as ethanol, and carbohydrates such as glucose which was previously not considered a commercial fuel source [4].

In comparison EBFCs can be much simpler in their design depending on the method adopted. In the case where enzymes are in solution the exact same general design that is used for ABFCs has to be adopted in order to separate the oxidising enzymes from the reducing enzymes [4]. Contrarily if the enzymes are immobilised onto the surfaces of the anode and cathode then there is no need for a proton exchange membrane [15]. Consequently a much simpler design can be implemented since the specificity of enzymes on each bioelectrode ensures that there is no interference from the oxidant at the anode and *vice versa.* Thus EBFCs can be much smaller in size than both ABFCs and MBFCs and they can be used with mixed fuels and oxidants (Figure 3).

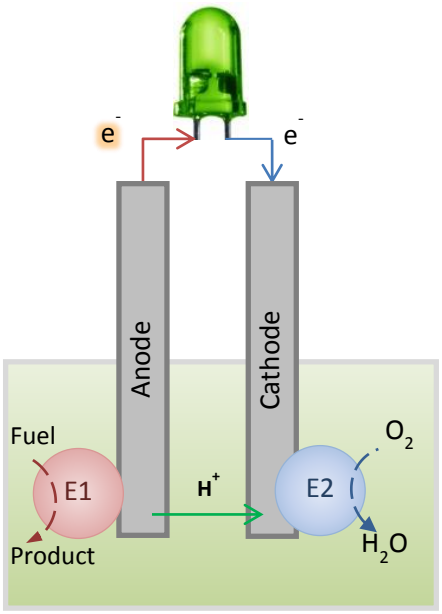

Figure 3: Schematics of an EBFC utilising immobilised enzymes (E1 and E2)

Unfortunately, however, the power density from such biofuel cells is typically much lower than obtained in non-biological fuel cells. This is due to the physical size of the chemical mechanisms employed here. In a hydrogen fuel cell for example, the metal catalyst is conductive and is itself the electrode. Consequently the entire electrode surface can be active for oxidation. The oxidation of hydrogen occurs in high densities on the electrode surface and the electrons produced are immediately conducted away as illustrated in Figure 4.

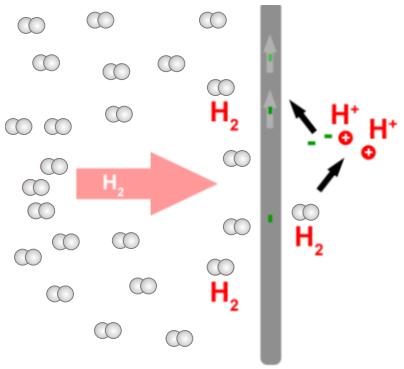

Figure 4: Schematic of hydrogen oxidation on a catalytic electrode in a hydrogen fuel cell

Conversely, in EBFCs, the catalyst is much larger and thus each oxidation site (the enzyme's active site) requires relatively large surface areas of electrode. The enzymes are also typically not conductive or only weakly conductive, and thus there is more time and energy expended in transferring the electrons from the enzymes to the conductive surface of the electrodes. This is demonstrated in Figure 5, which shows a simplified mechanism of reaction for a glucose oxidase (GOx) electrode. Once a molecule of glucose (which is relatively large in size) has successfully reached an immobilised GOx (which is sparsely distributed), diffused to the active site (which is

buried deep inside the enzyme) and been oxidised, the released electrons then have to be transferred from the enzyme to the electrode surface which typically occurs through secondary reactions.

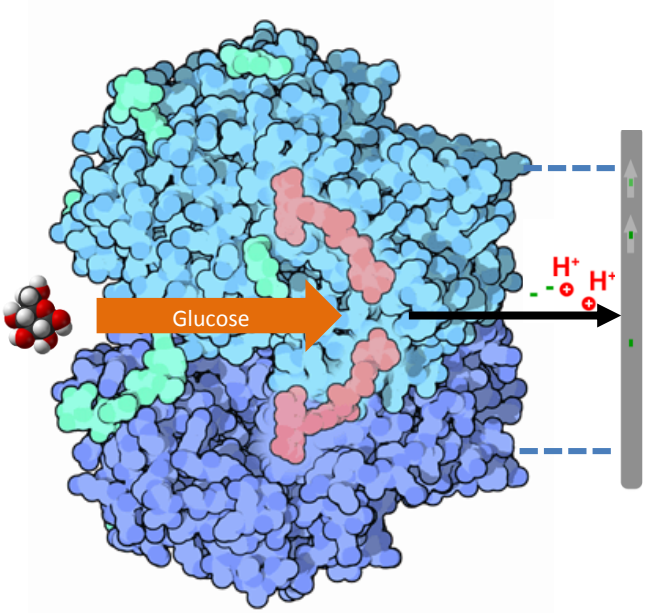

Figure 5: Simplified schematic of reaction scheme involved with a GOx bioelectrode

Consequently, though EBFCs do not require proton exchange membranes, they do require extremely large surface area electrodes to generate useful levels of power.

1.2. PROJECT AIMS AND OBJECTIVES

The aim of this project is to produce a biocompatible fuel cell that can generate power from metabolites found naturally in blood or interstitial fluids in the human body with a view to potential implantation.

The obvious choice for a fuel stock for this purpose is glucose, since it is found in relatively high concentrations in blood (approximately 1.0 g l^{-1} under normal conditions) and also in the interstitial fluid of the human body (at concentration of approximately 0.5 g l^{-1}) [16]. Glucose is also very dense in energy providing up to 16 kJ g^{-1} by generating 12 electrons per molecule during complete oxidation [17]. The waste metabolites produced from the incomplete oxidation of glucose (such as gluconic acid) are also naturally present in the human body and as such can easily be disposed of without the risk of waste toxicity. Other possible fuel stocks include lipids and amino acids, however these are much harder to metabolise electrochemically and as such are not well established for use in fuel cells.

As far as the choice for oxidants is concerned, there is only one clear choice and that is dissolved dioxygen. This is because most other oxidants present in the human body vary greatly in

concentration and are alkaline. Thus a fuel cell that uses oxidants other than oxygen would have a variable power output and would risk changing the pH of the blood with serious health consequences.

Hence, the focus of this project is to create a glucose-oxygen fuel cell following the reaction scheme shown below.

$$\underbrace{C_6H_{12}O_6}_{glucose} \rightarrow \underbrace{C_6H_{10}O_6}_{D-glucono-1,5-lactone} + 2e^- + 2H^+ \qquad \text{Equation 1}$$

$$C_6H_{10}O_6 + H_2O \rightarrow \underbrace{C_6H_{12}O_7}_{Gluconic\ Acid} \qquad \text{Equation 2}$$

$$\tfrac{1}{2}O_2 + 2e^- + 2H^+ \rightarrow H_2O \qquad \text{Equation 3}$$

First glucose is reacted to D-glucono-1,5-lactone in the anodic half-cell, which is subsequently hydrolysed to form gluconic acid (Equations 1 and 2). Whilst the electrons pass through the circuit to generate electric current, the hydrogen ions migrate to the cathodic half-cell where they react with oxygen and electrons from the cathode to form water (Equation 3).

Each type of biofuel cell discussed is capable of facilitating this reaction scheme. However, since the use of microbes inside the human body would not be commonly supported, and since catalysts in solution would wash away or potentially stimulate an immune response, only two potential approaches are obvious.

The first is to develop an ABFC where the catalyst is on the electrode surface. This presents a challenge since most known noble metal catalysts which are active towards glucose oxidation at low temperatures are also active for the reduction of oxygen. Thus the simultaneous presence of glucose and oxygen at both electrodes would lead to an electrochemical short-circuit [18], and therefore special measures would need to be taken to separate oxygen from the blood plasma or interstitial fluid in the anodic half-cell. The second approach is to develop an EBFC utilising immobilised enzymes, since enzymes illustrate a very high level of specificity, are generally active at low temperatures and could easily be used with fuel and oxidant mixtures (as illustrated by Figure 3).

In either case, attention should be given to the types of materials used to ensure biocompatibility, biostability and to prevent long term toxicity of the device. Hence the following objectives should be achieved by this project:

- Produce stable and biocompatible electrodes which will act as a substrate for the attachment of electrocatalysts.

- Functionalise two different electrodes with catalysts (either metal or enzyme based) so as to give them specificity for the oxidation of glucose and the reduction of oxygen respectively.
- Develop a prototype fuel cell utilising these electrodes which can produce a stable power output from a glucose and oxygen mixture.

2. LITERATURE REVIEW

Figure 6: "A sweet idea". Reprinted with permission from copyright holder (see reference) [19].

Since the first implantation of a cardiac pacemaker in 1960 [20], numerous efforts have been made to develop miniature implantable power devices, which would be able to run continuously for long periods of time without the need for replacement. Many different technologies have been considered such as mechanical [21] and thermoelectric [22] power generators which take advantage of the excess energy created by the human body. Technologies such as inductive power transfer *via* radiofrequencies have also been investigated for the continuous supply of power or for recharging electronic devices such as cochlear implants [23]. Each technology comes with its own limitations. Mechanical power generators only produce power when a person is moving and thus would not produce power when someone is sleeping. Thermoelectric power generation relies on the presence on a significant temperature gradient between the body and the surrounding air, and so would fail to produce power on a hot day. Inductive power transfer techniques on the other hand require the use of an external power source which may not always be available. By definition inductive power transfer techniques also use strong magnetic and electrical fields which could cause interference with the standard operation of medical implants such as pacemakers [24].

The use of nuclear powered devices was also very common initially as these devices were able to produce the required power output and could last for decades without the need for any maintenance [25]. Ultimately this type of device was abandoned in the 1980s in favour of lithium based power cells. The main reason for this was that the associated cost of refining the

radioactive material required to power the devices was extremely high, with a single nuclear powered pacemaker costing approximately £1,000 in 1974 (equivalent to £9,250 in 2014) [26].

In this context, biofuel cells which use naturally occurring metabolites as fuel (typically glucose) are a promising alternative for power production. This is due to the fact that such biofuel cells are not prone to the same fluctuations in energy production, since the concentrations of metabolites remain constant due to homeostasis. Many different types of so-called implantable biofuel cells made from biocompatible materials have been developed since the 1970s. In theory such fuel cells would be able to mimic many of the metabolic pathways found within living organisms, and thus produce power from energy sources naturally found within living organisms. Such devices also have the added benefit of producing the same waste products as the living organism. They could thus use established waste metabolism routes to dispose of the by-products produced during the production of power.

2.1. IMPLANTABLE OR POTENTIALLY IMPLANTABLE BIOFUEL CELLS

2.1.1. ABIOTIC BIOFUEL CELLS

Research in the field of implantable ABFCs date back to the early 1970s. These early efforts were motivated by the short life-time of the zinc/mercury oxide batteries at that time. The first truly implantable ABFC prototypes were developed at the American Hospital Supply Corporation in 1970 [27]. Here an ABFC was implanted in the flank of a dog and delivered stable power output of 2.2 µW cm^{-2} with an open circuit potential (OCP) of 0.5 V. In another study ABFCs were implanted in the veins of sheep. This time the initial power output was drastically improved with the ABFC delivering 40 µW cm^{-2}, but stability was lacking with the power rapidly decreasing within an hour of operation [28].

To overcome problems associated with low catalyst specificity researchers largely adopted one of two different separation concepts.

In the first separation concept a phase separation of oxygen is achieved at the cathode. A hydrophobic membrane allows for the diffusion of gaseous oxygen but prevents aqueous glucose from reaching the cathode (Figure 7). At the anode oxygen is removed from the interstitial fluid by the use of a sacrificial layer. Here oxygen can directly react with glucose on the surface of a noble metal catalyst. This reduces the oxygen concentration in the interior of the anode, where glucose then is electrooxidized at a potential more negative than the cathode potential. Since some glucose is consumed by the direct reaction with oxygen a surplus of glucose over oxygen is a prerequisite for this embodiment. The advantage of the concept is that

platinum and other highly active noble metals can be used as catalysts for both the anode and the cathode reaction [27].

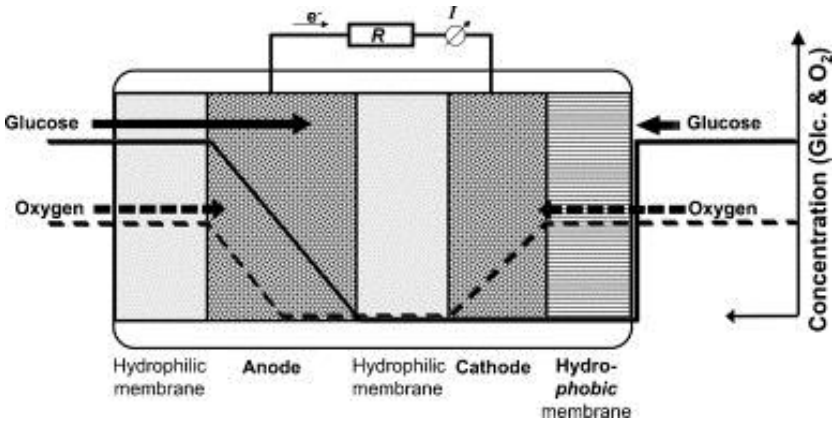

Figure 7: ABFC with hydrophobic membrane at the cathode and sacrificial layer at the anode. Reprinted with permission from copyright holder (see reference) [29].

In the second reactant separation concept an oxygen-selective cathode catalyst is used. By arranging the anode sandwiched between the cathode and an impermeable surface (or alternatively between two cathodes [30, 31]) the interior of the fuel cell is depleted from oxygen, and the anodic glucose oxidation takes place under predominantly anoxic conditions (Figure 8).

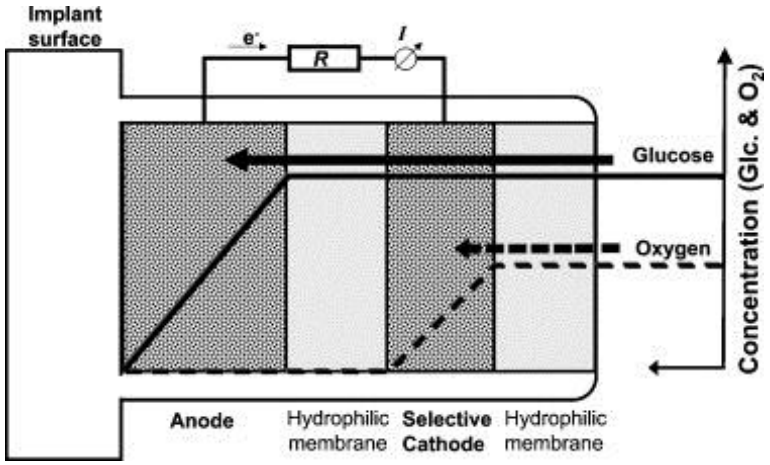

Figure 8: ABFC with oxygen-selective cathode catalyst. Reprinted with permission from copyright holder (see reference) [29].

Here again it is important that the concentration of glucose is in excess compared to the concentration of oxygen since it is crucial that all of the oxygen is depleted before reaching the anode.

In spite of some promising early results, the introduction of lithium based power cells brought about a momentary conclusion to research into implantable biofuel cells, with the last reported study on implantable glucose fuel cells being conducted in 1981 [6, 29]. This was due to low catalyst specificity, unsatisfying power output densities, and inflammatory issues of these devices [18].

In recent years, with the developments in miniaturised fuel cells made in the technology sectors, the development of newer low powered medical devices (modern pacemakers typically require less than 10 µW of power to run [32]) and with the increased concern for using renewable energy sources, the use of biofuel cells as an alternative power source for implantable medical devices is quickly becoming a more realisable goal.

After more than 20 years the concept of using ABFCs to power implantable medical devices was picked up again in 2006 with the development of a direct glucose fuel cell to power implantable micro-electro-mechanical systems [33]. Here the ABFC utilised platinum on an activated carbon framework to catalyse the oxidation of glucose to gluconic acid. They chose to sandwich their electrodes in a PVA hydrogel membrane matrix following a cathode-anode-cathode design (Figure 9). Using this design they were able to achieve an average power density of 2 µW cm^{-2} over a period of 7 days in a "physiological solution" [33].

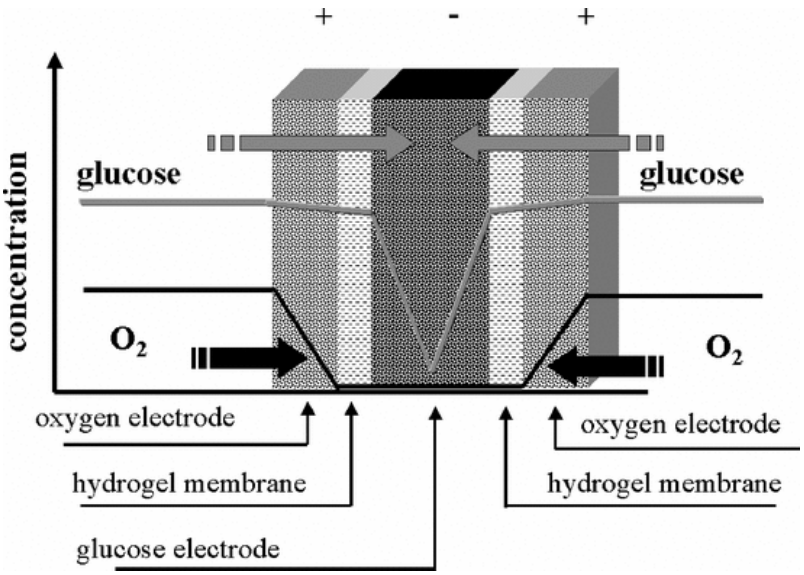

Figure 9: Double layer ABFC with oxygen-selective cathodes. Reprinted with permission from copyright holder (see reference) [33].

In the years that followed these prototypes were improved due to the development of highly selective hydrophilic membranes which allow oxygen diffusion and hamper glucose diffusion at a rate much faster than is possible with a phase separation membrane [29]. The use of porous platinum films instead of porous carbon was also adopted to improve biocompatibility.

By 2010 a Raney-platinum film (a porous platinum and zinc alloy) fuel cell with specially engineered mesoporous silica membranes was developed. This device was not only smaller than previous prototypes (the entire cell was only 490 µm thick, see Figure 10), but it also exhibited a higher power density reported at 4.4 µW cm^{-2} [2].

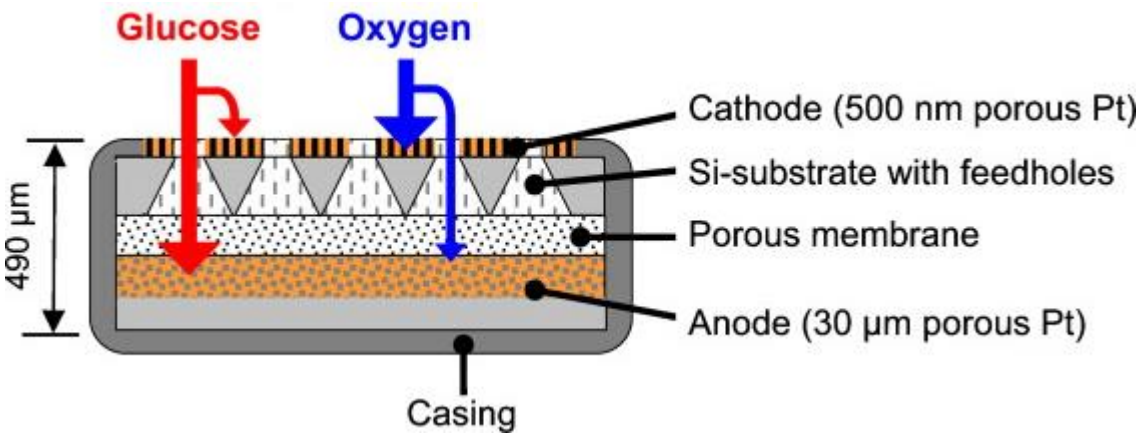

Figure 10: ABFC with highly selective membranes facilitating oxygen transfer to cathode, and glucose transfer to anode. Reprinted with permission from copyright holder (see reference) [2].

This design was subsequently improved upon by other researchers who managed to synthesise functionalised silica membranes that were just 270 nm thick. This design was postulated to be superior to polymer membranes (that are typically tens of micrometres thick), and would thus be suitable for use inside blood vessels. This device was able to achieve power densities of up to 10 µW cm^{-2} when conducting *in vivo* experiments using a live pig [34].

Researchers also discovered that Raney-platinum films exhibit exceptional tolerance to oxygen whilst maintaining their reactivity towards glucose [2]. This meant that they were capable of a higher degree of selectivity towards glucose and could thus be used in physiological solutions without separating glucose and oxygen. This led to the development of a single layer glucose fuel cell, which can be used to coat medical implants such as pacemakers. By using designs of this form the fuel cell can be implanted along with the medical implant without the need for any added invasive medical procedures (Figure 11). This single layer design does however have the drawback of having twice the superficial area than more established layered fuel cells and was reported to produce a maximum of 2.2 µW cm^{-2} during short term trials [35]. Thus such a design may not be suited for small scale *in vivo* glucose sensors where it is preferred to have as small a device as possible.

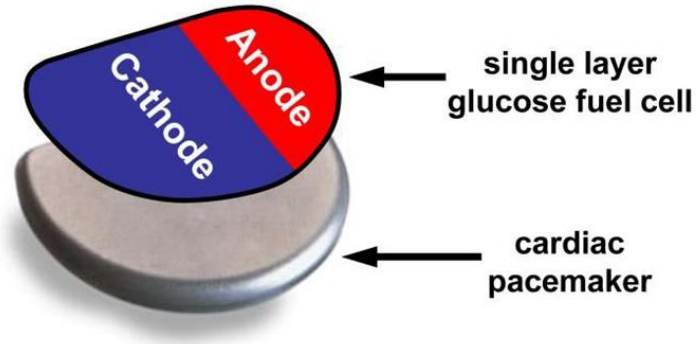

Figure 11: Schematic of single layer ABFC and its placement on a cardiac pacemaker. Reprinted with permission from copyright holder (see reference) [36]

2.1.2. ENZYMATIC BIOFUEL CELLS

Significant advances in the wiring of enzymes (methods for enhancing the electro-connectivity from enzymes to electrode surfaces) have recently provided a promising alternative to abiotic systems for *in vivo* applications. This has led to the development of a range of prototype devices which have been proven capable of generating power when implanted in living organisms (Figure 12).

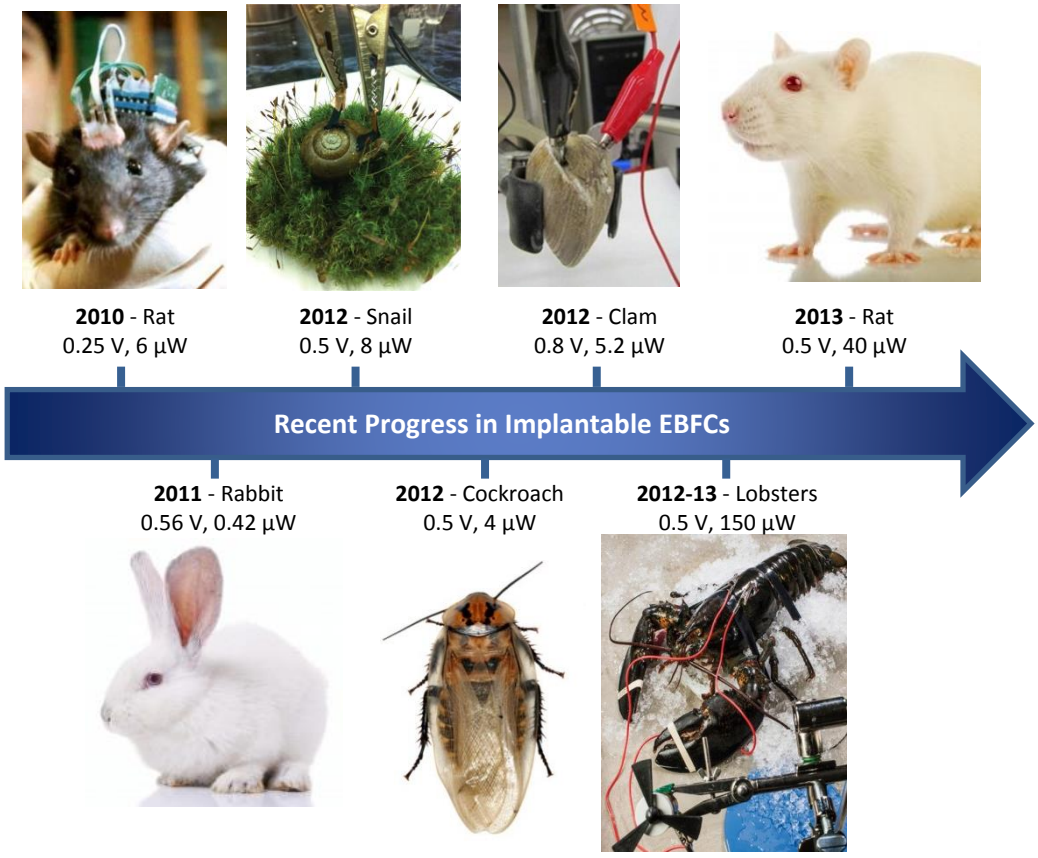

Figure 12: EBFCs implanted into live animals [37-44]

In particular improvements in nanostructured materials have enhanced enzyme wiring by lowering the overpotentials of glucose oxidation and oxygen reduction. At the anode (typically comprised of GOx or pyrroloquinoline quinone (PQQ) dependent glucose dehydrogenase (GDH)) the catalytic oxidation of glucose can be induced at potentials between -0.4 V and -0.1 V against a saturated calomel electrode (SCE). Cathodes (comprised of laccases (LAC) or bilirubin oxidase (BOD)) can achieve oxygen reduction at potentials between 0.5 V and 0.6 V vs SCE. This means that OCP of such EBFCs can reach values of up to 1 V, which is higher than is possible in existing ABFCs employing platinum based catalysts at both the anode and cathode. These higher potential differences have facilitated the use of boost converters (DC to DC potential step-up converters) for power management and thus the powering of real electronics devices. In addition to improving enzyme wiring, the development of nanostructured electrodes also

greatly improves the surface area and thus the number of wired enzymes per surface or volume [45].

The first example of an EBFC implanted in an animal came in 2010 when a research group from the Université Joseph Fourier in France surgically implanted a EBFC in a rat [43]. Here it was postulated that covalently bound enzymes have greatly reduced functionality, and as thus they opted to encapsulate the enzymes they used. This strategy also allowed them to use a combination of different enzymes and electron mediators in the same electrodes. Their design consisted of an enzyme and graphite mixture compressed into pellets, which they encapsulated in dialysis tubing. This protected the enzymes from metabolites in the bodies of rats and, in theory, would protect the rats from any potential carcinogenic effects of implanted graphite [46]. During an *in vivo* experiment with a rat they measured an initial open circuit potential of 0.275V with a power density of 24.4 μW ml^{-1}, which then reduced to a steady value of 0.22 V with a power density of 7.5 μW ml^{-1} for several hours more [43]. Long term power production was not demonstrated here and ultimately the long stability of such a device is questionable due to the use of mediated electron transfer (MET) techniques that utilise free moving redox active particles (see Section 2.2.1.). However, no signs of inflammation or rejection were observed over a 3 month period when the fuel cell was not in constant use.

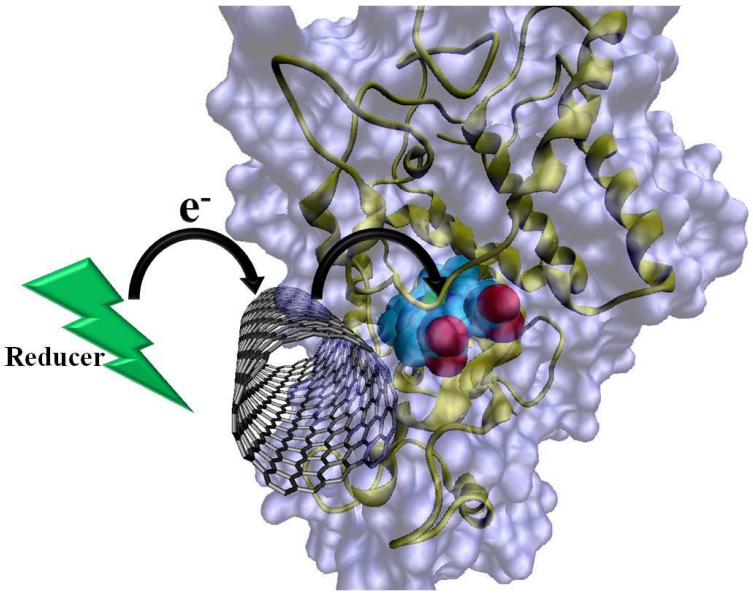

Figure 13: Illustration of protein and CNT intertwinement. Reprinted with permission from copyright holder (see reference) [47].

With a view to improving the stability of implanted EBFCs many researchers turned their focus to the use of carbon nanotubes (CNTs) and their composites. Due to their size and shape CNTs are able to intertwine with the enzymes, thus allowing for direct wiring from the enzyme's active

site to the electrode surface without affecting the activity of the enzyme [47]. As a result direct electron transfer (DET) between the enzyme and electrode surface can be achieved (Figure 13).

By utilising Bucky paper (a CNT aggregate), a research group from Clarkson University in the United States of America has managed to create several different prototype EBFCs which they implanted in invertebrates [38, 41, 44]. Though these examples of implantable EBFCs disregarded any complications that could arise in mammals (such as biocompatibility, toxicity, sterilization and immune responses), they made great advances in proving the levels of power production possible. In one case they even showed that two fuel cells implanted in lobsters could power a digital watch for approximately 1 hour (Figure 14), and five EBFCs running in simulated physiological conditions could generate enough power for the normal operation of a pacemaker for 5 hours [44].

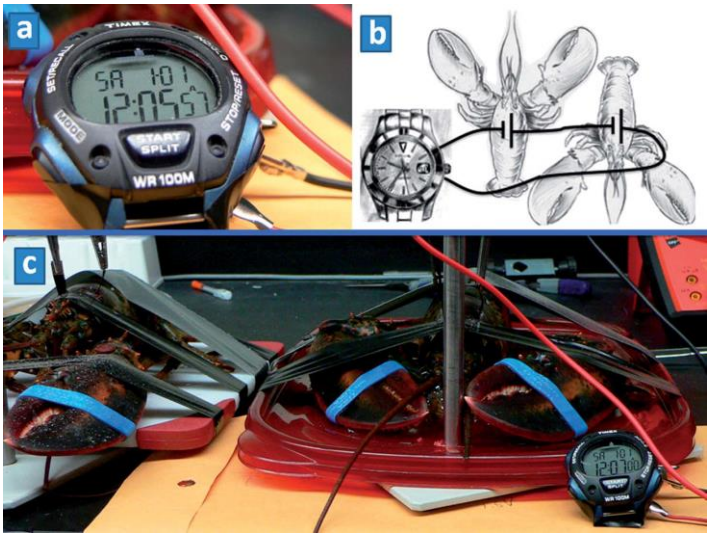

Figure 14: Two lobsters implanted with EBFCs connected in series to power a digital watch. Reprinted with permission from copyright holder (see reference) [44].

To better simulate the conditions within the human body many researchers have instead turned to implanting EBFCs in lab animals such as rats and rabbits.

With a view to powering subcutaneous implants a research group from Tohoku University in Japan developed a 'semi-implantable' EBFC. The device consisted of a needle tip enzymatic anode with an external air breathing cathode utilising carbon nanoparticle composites [42]. In this way the problems associated with the low oxygen levels in living organisms could easily be overcome, and thus power production was only limited to the concentration of glucose. This means that their device could potentially be a viable candidate for live glucose sensing with minimal invasive procedures. When this device was tested in the vein of a rabbit (see Figure 15) a power output as high as 0.42 µW was generated. This is a substantial achievement since the anode fits inside a needle with a cross section of just 0.057 cm^2.

Figure 15: Needle tip anode and external cathode EBFC implanted in a rabbit's ear. Reprinted with permission from copyright holder (see reference) [42].

Though this type of technology may be well suited for small subcutaneous or sensing purposes, in order to develop a fully implantable EBFCs for use with medical devices such as pacemakers one of two approaches must be followed. Devices can either be designed for the potential implantation in the soft tissue, or for the potential implantation in blood vessels. Each of these strategies come with their own advantages and disadvantages [29, 43, 48]. In the case of devices to be implanted in the soft tissue, the system is limited by lower concentrations of glucose and oxygen, and is reliant solely on diffusion for the supply and removal of reactants and waste products respectively. Devices designed for use in blood vessels would exhibit continuous flow through operation. These devices benefit by having higher concentrations of glucose and oxygen which are continuously supplied by the flow of blood. The continuous flow does however induce extra strains on the system, since the flow could result in the removal of enzymes from the electrodes and interfere with the electron transfer between enzymes and the electrode surface [29].

Many research groups have focused on the implantation of EBFC in the soft tissue of animals. In an extension to their pioneering work utilising compressed enzyme and graphite disks implanted in a rat the research group from the Université Joseph Fourier (in collaboration with a group from the Université de Grenoble) developed new EBFCs using compressed enzyme and CNT pellets [49] (see Figure 16).

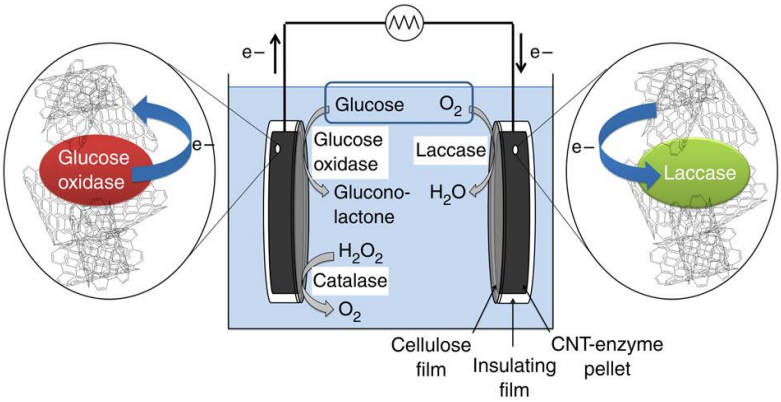

Figure 16: EBFC with compressed enzyme and CNT pellets as electrodes. Reprinted with permission from copyright holder (see reference) [49].

Interestingly here they only partially relied on the DET between GOx and the CNT electrodes. Instead of adopting a simple DET or MET mechanism they relied on the production of H_2O_2 from GOx which they then oxidised using a secondary enzyme (catalase). Therefore this device relied on a two stage DET mechanism with H_2O_2 as an intermediate electron mediator. When implanted in a rat special measures had to be taken to ensure biocompatibility. The pellet fuel cell was first wrapped and sealed in a dialysis bag and then sealed in a biocompatible Dacron bag (conventionally used for implants) [37]. When EBFC was implanted in the retroperitoneal space of a rat it delivered a maximum power output of 40 µW and had an OCP of 0.57 V. This was sufficient to charge a capacitor and (with the aid of a boost converter) intermittently power an LED and an electric thermometer (Figure 17).

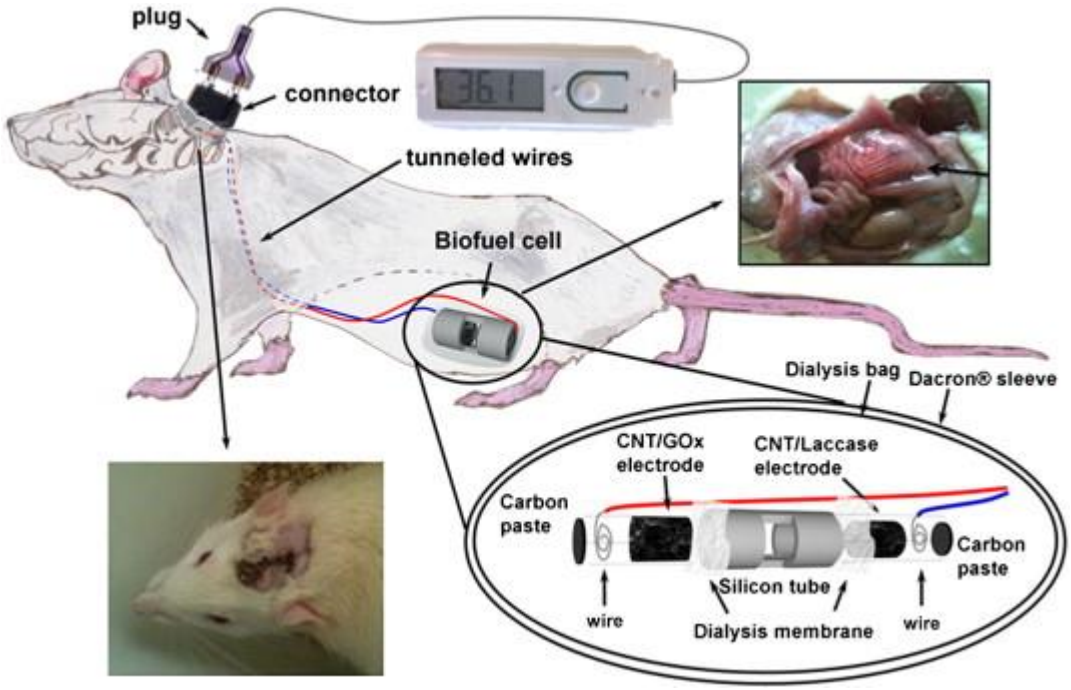

Figure 17: EBFC implanted in the abdomen of a rat powering an electric thermometer. Reprinted with permission from copyright holder (see reference) [18, 37].

Following on from their work with invertebrates, the research group from Clarkson University also ventured to EBFCs implanted in rats. Here they used the same Bucky paper based enzymatic electrodes developed previously but this time placed the electrodes directly in contact with partially excised cremaster muscle whilst the rat was under anaesthesia [50](Figure 18).

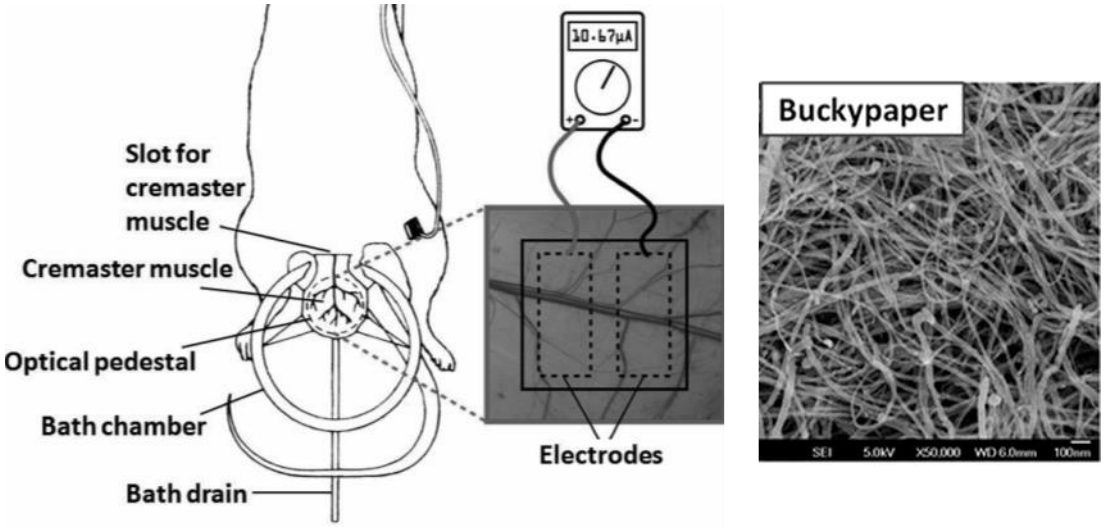

Figure 18: Enzymatic Bucky paper bioelectrodes on the surgically exposed cremaster tissue of a rat. Reprinted with permission from copyright holder (see references) [50, 51].

Though this meant that strictly speaking the EBFC was not implanted into the rat, this setup gave a very good approximation of the operating conditions an implanted EBFC would experience. In contrast to their results with invertebrates, the OCP in this case was only 0.14 V and a maximum power output of only 0.35 µW was achieved.

One more research group has also advanced their EBFC research to the point of implantation. This group (based in Brazil) developed a hybrid enzymatic/abiotic fuel cell which utilised a GOx and modified carbon fibre anode, and a platinum and carbon fibre cathode [52]. When this fuel cell was tested *in vitro* they yielded 24 nW of power and when implanted into the jugular vein of a rat the fuel cell produced a mere 9.5 nW of power over a 24 hour period of operation. This is predominantly due to the small size of the fuel cell with a reported electrode area of just $1x10^{-4}$ cm^2. This small electrode size was necessary since the use of a catheter bag around the fuel cell greatly increased its overall size and thus the potential for scaling of such a fuel cell was limited.

The EBFCs reported so far relied on the use of carbon based electrode materials such as CNTs, carbon nanoparticle composites or carbon fibres. These electrodes have problems related with their long term biocompatibility, toxicity and stability (owing to the fact that many are in fact biodegradable) [53, 54]. In these cases special measures have to be taken to isolate the EBFC from the interstitial fluid or blood of the host, greatly increasing the overall size of the devices. Thus focus has recently turned to developing EBFCs that rely on the use of more stable and biocompatible electrode materials such as gold. In order to create devices that can match the performance of carbon based EBFCs, it is therefore important to create gold surfaces that mimic the properties that make carbon based electrodes so well suited for enzyme wiring and

immobilisation. In this context the use of nanostructured gold is considered a promising alternative.

A research collaborative with members from Russia, Sweden and Austria recently made major advances in this new emerging field. They developed an EBFC consisting of gold microwire electrodes modified with gold nanoparticles [55]. The resulting nanostructures are similar in morphology to nanoporous gold (nPG) films (Figure 19). Their EBFC was implanted in the brain of a rat where it generated 2 µW cm^{-2} of power from the glucose found in cerebrospinal fluid.

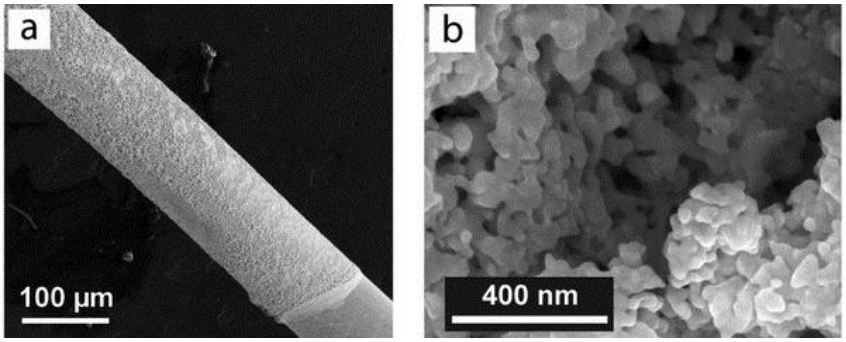

Figure 19: Gold nanowires modified with gold nanoparticle aggregates. Reprinted with permission from copyright holder (see reference) [55] .

The same research collaborative went on to develop a concept design for an EBFC in a contact lens. This device could be used to provide live data on a patient's glucose levels by generating electrical energy from human lachrymal liquid (Figure 20) [56].

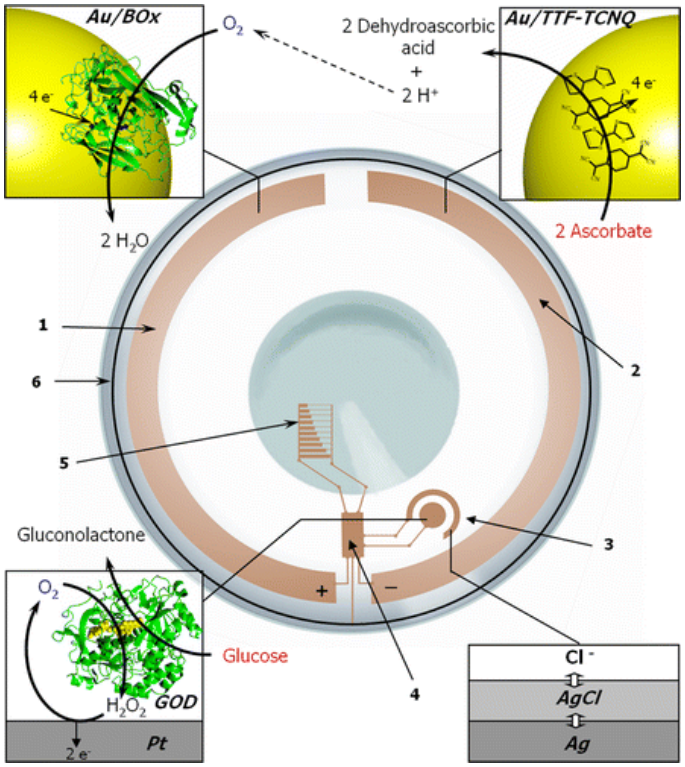

Figure 20: A concept design for a EBFC coupled with a glucose sensor on a contact lens. Reprinted with permission from copyright holder (see reference) [56].

Here the idea was to use gold electrodes modified with gold nanoparticles and enzymes to produce power (this time utilising ascorbate as fuel) which would be coupled with a third GOx electrode to facilitate glucose sensing. Using a rudimentary prototype fuel cell, they were able to generate an average of 9.4 nW of power from human tears using electrodes with surface areas of approximately 10^{-3} cm^2.

Six months after the above concept designs were published, Google reported that they too were developing contact lenses which could sense glucose levels in diabetics (Figure 21) [57]. Although they state that the production of these lenses in collaboration with the pharmaceutical company Novartis will soon start [58], there is no information that is publically available on the type of fuel cell or sensing technology employed here, nor is there any information on the device's performance.

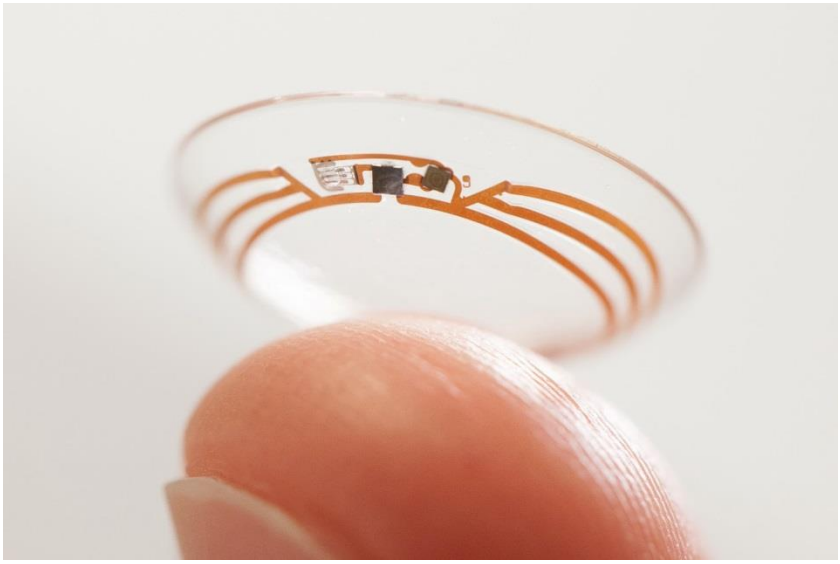

Figure 21: Prototype 'smart' contact lenses for glucose sensing developed by Google[x] (Google's secret projects division) [57].

Though many other research groups have also embarked on the journey towards the production of implantable fuel cells, the majority of these projects still rely on the use of separate oxygen and glucose feeds [59-64] or on the use of mediators in solution [65-67]. However, there is some promising early research into developing EBFCs which do not rely on separating fuel from oxidant, utilise mediators or use unstable materials.

A notable contribution to this research came from a research group from Kyoto University in Japan. Here they developed enzymatic electrodes by immobilising enzymes on functionalised nPG films [68]. When using a GOx anode and a LAC cathode in an EBFC at slightly acidic conditions (Figure 22) they were able to generate a maximum power output of 4.7 µW, though no indication is given on how long they were able to maintain this level of power.

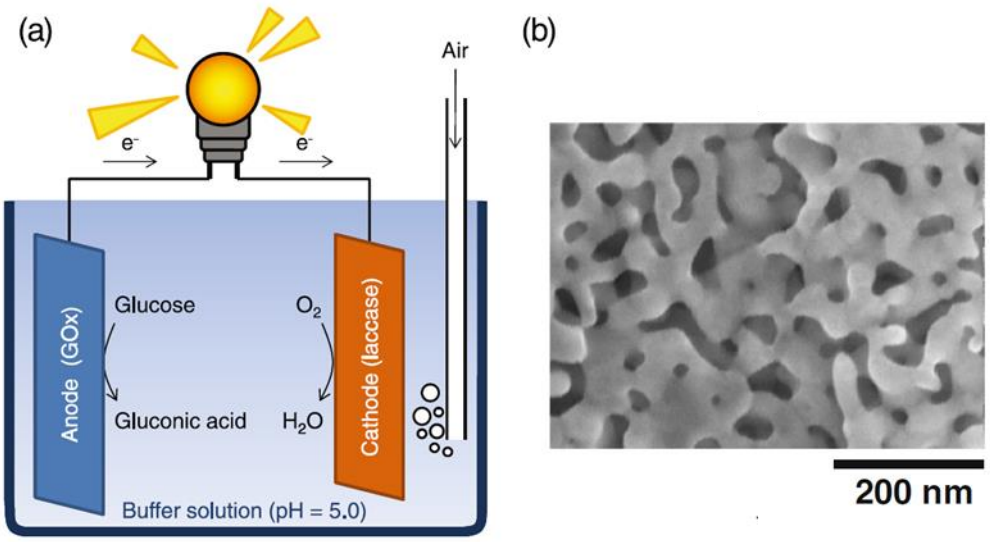

Figure 22: A rudimentary nPG EBFC. A- schematic of experimental setup, B- SEM image of nPG film. Reprinted with permission from copyright holder (see reference) [68].

Another group has also made advances using nPG surfaces in EBFC development. This group (a collaborative between Irish and Austrian researchers) used osmium based polymers co-immobilised with enzymes on a nPG support (Figure 23). The use of an osmium polymer allowed them to drastically increase the efficiency of electron transfer since osmium based compounds are very popular in MET mechanisms. This method could therefore be described as employing MET, but since the osmium polymer is immobilised with the enzyme and not free moving, the pitfalls usually encountered with MET techniques are negated [69].

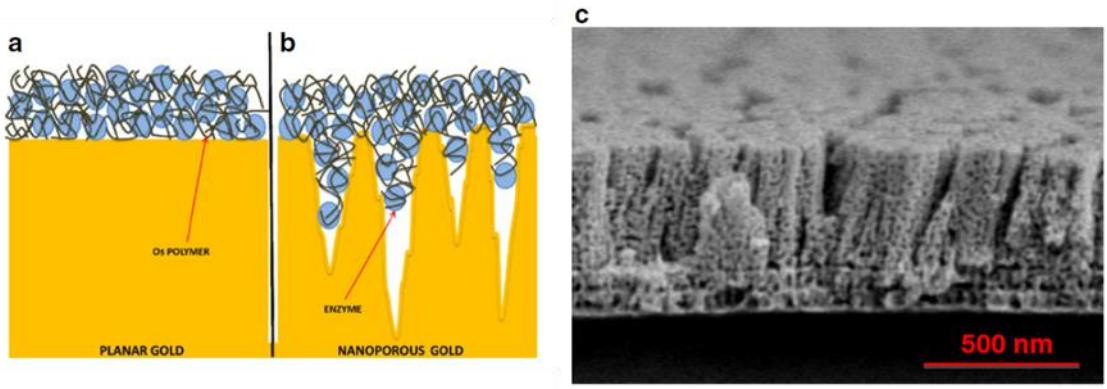

Figure 23: nPG-based electrodes used in osmium mediated EBFC. A,B- Schematic of osmium polymer and enzyme immobilisation on polished gold and nPG respectively, C- SEM of nPG structure used here. Reprinted with permission from copyright holder (see reference) [69].

Using these electrodes with GOx at the anode and LAC at the cathode a maximum power output of 7.3 µW was achieved from a rudimentary prototype EBFC under physiological conditions. This power output had a rapid decay of 50% within the first 100 minutes of operation, and no further data is given on the long term stability of this EBFC.

2.2. THE CHOICE AND IMMOBILISATION OF ENZYMES

Though a wide range of enzymes have been used to oxidise glucose the most prevalent choice is GOx [70]. GOx has long been of interest in many industries, and is widely used in conjunction with peroxidase in kinetic assays for the determination of free glucose concentration. GOx assays are used to measure glucose levels in blood samples, bioreactors and alcoholic fermentation processes.

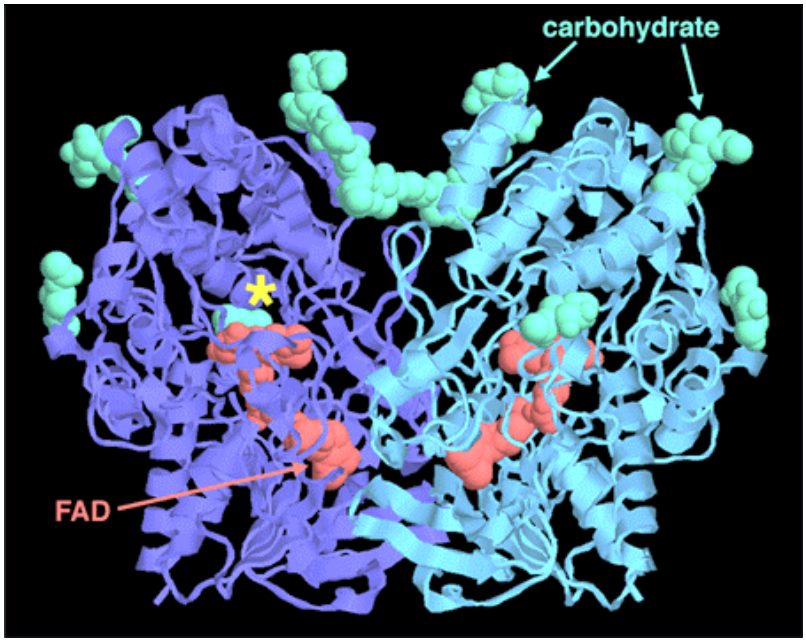

Figure 24: Structure of GOx. Star indicates active site of enzyme [71].

These work by taking advantage of the hydrogen peroxide by-product produced during the oxidation of glucose, which is formed due to the pairing of GOx and the cofactor flavin adenine dinucleotide (FAD) (see Figure 24). During the oxidation of glucose the FAD is used as an electron acceptor reducing it to $FADH_2$ (Equation 4). It is the $FADH_2$ which is then oxidised by dioxygen to produce hydrogen peroxide, which reacts with peroxidase to illicit a visible colour change (due to the presence of a haem cofactor) (Equations 5 and 6) [72].

$$\underbrace{C_6H_{12}O_6}_{glucose} + FAD \xrightarrow{GOx} \underbrace{C_6H_{10}O_6}_{D-glucono-1,5-lactone} + FADH_2 \qquad \text{Equation 4}$$

$$FADH_2 + O_2 \rightarrow FAD + H_2O_2 \qquad \text{Equation 5}$$

$$Peroxidase[Fe(III)] + H_2O_2 \rightarrow Peroxidase[Fe(IV)]O + H_2O \qquad \text{Equation 6}$$

Glucose oxidase is also of particular interest in electrochemistry due to its potential applications in glucose sensors for sufferers of diabetes. Unlike when GOx is used in kinetic assays the intention here is for the $FADH_2$ cofactor to pass electrons to the electron surface, either directly

(Equation 7), or through the oxidation of hydrogen peroxide at the electrode surface (an oxygen-mediated system) (Equation 8).

$$FADH_2 \xrightarrow{electrode} FAD + 2H^+ + 2e^- \qquad \text{Equation 7}$$

$$H_2O_2 \xrightarrow{electrode} O_2 + 2H^+ + 2e^- \qquad \text{Equation 8}$$

As far as the enzymes in the cathodic half-cell are concerned, LAC seams the obvious enzyme on which to focus. LAC is capable of the direct reduction of oxygen to form water and thus follows the ideal reaction scheme for the cathodic half-cell (see Equation 3 in Section 1.2.).

In stark contrast to GOx, LAC is not dependant on a cofactor, has an easily accessed active site and is relatively conductive. In fact LAC has a channel that passes through it, so reactants can access the active site from two different sides or continuously flow through it (see Figure 25). The enzyme's amine and carboxylic acid terminal groups are also exposed allowing for easy immobilisation by covalent linking [73]. Furthermore, since LAC is a copper metalloenzyme, it contains several conductive copper complexes. A trinuclear copper centre is situated at the enzyme's active site and another mononuclear copper centre is located close to the enzymes surface. When LAC is immobilised on an electrode these copper centres act as electron relays which allow for the rapid transfer of electrons between the active site and the surface of the electrode.

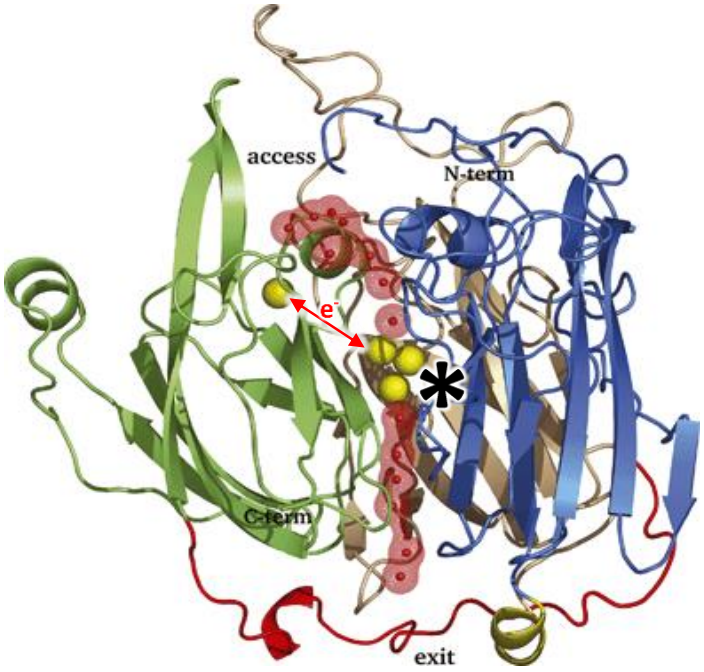

Figure 25: Structural diagram of LAC. The red region indicates channel through enzyme. N-term and C-term refer to amine carboxylic acid terminal groups respectively. Yellow spheres indicate copper complexes. Asterisk indicates active site of enzyme [73].

Thus it is relatively simple to use LAC in the construction of enzymatic electrodes which exhibit DET. The applications of a LAC electrode are much less grand than those of a GOx electrode, and has been of little use until recently. This is because its potential for use in waste water treatment or for the use in an oxygen sensitive half-cell in biofuel cells has become a focal point in recent history [74].

2.2.1. DIRECT AND MEDIATED ELECTRON TRANSFER

The vast majority of enzymes that have been used in biofuel cells to date have not been shown to be able to support the efficient transfer of electrons between the substrate and the electrode surface during oxidation and reduction. Thus small redox active particles and polymers have been utilised as electron carriers in MET mechanisms (Figure 26). Typical mediators include organic dyes, ferrocene and its derivatives, modified vitamin complexes, and conducting salts [75].

These mediators are often preferential for use with NAD^+ and FAD dependant enzymes, such as GOx, as they can react directly with either the enzymes themselves or their cofactors to become charged. If the mediator is in solution their diffusion to the electrode surface then allows for a more rapid electron transfer compared to the direct transfer from the enzyme itself [76]. Alternatively the mediators can also be polymerised directly onto the electrode surface or co-immobilised onto the electrode surface with the reacting enzymes to further enhance the rate of electron transfer [77, 78].

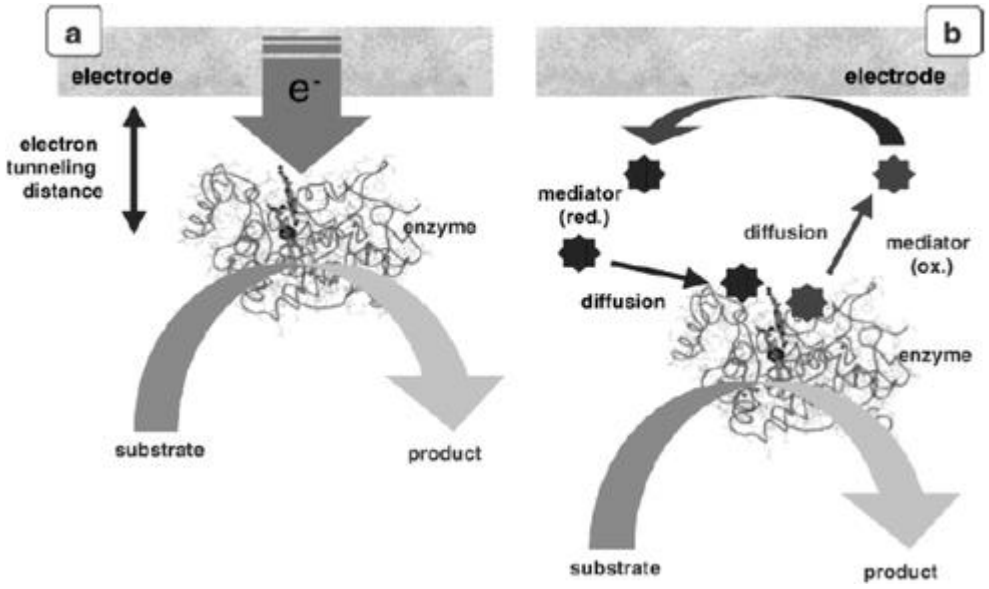

Figure 26: Electron transfer mechanisms utilized in biofuel cell technology. A- DET, B- MET. Reprinted with permission from copyright holder (see reference) [79].

The use of redox active electron carriers as mediators does have its own drawbacks since the mediators often have short lifespans, can leach away from the electrode surface or are not biocompatible. Consequently, the use of enzymes capable of DET became the main focus of many researchers in the 1980s. Major advancements came when examining transition metal rich enzymes such as LAC, which is capable of catalysing the reduction of oxygen to water through the direct catalytic transfer of electrons between the substrates and electrode surface [79].

In most EBFCs developed so far DET has been achieved at the anode by using electrodes modified by CNTs. These nanowires present properties such as hydrophobic outer walls which allow for strong adsorption of enzymes for enzyme wiring, which facilitate electron transfer between enzyme active site and electrode [45]. DET has also been demonstrated possible when using PQQ dependant enzymes. PQQ dependent enzymes contain a haem group which is able to exist in several different redox states, which function as electron acceptors in a similar matter to the redox active metal centres in enzymes such as LAC. In particular PQQ-GDH has been used to great success at the anode of EBFCs [44, 50, 80].

The power outputs obtained from EBFCs using DET mechanisms is typically much lower than those achieved when using MET mechanisms [81]. This is due to the direct correlation between the electron transfer rate and the proximity and orientation of the enzymes active site to the electrode surface [82]. Thus by using fast diffusing mediators the rate of electron transfer and overall power output can be increased. Alternatively DET can be improved by the specific immobilisation of enzymes in a favourable orientation which controls the proximity of the enzyme's active site to the electrode surface [79]. Another method for improving electron transfer is *via* the immobilisation of mediator molecules onto the surface of the electrode or onto the enzymes themselves which then act as electron relays. The latter is technically still considered MET since the electron relays lower the maximum potential difference obtainable [78].

2.2.2. PHYSICAL ADSORPTION

Physical adsorption is the simplest method for enzyme immobilisation. The method relies on a physical interaction between the enzyme and the surface of the electrode (by hydrogen bonds, salt linkages, and Van der Waal's forces), that usually requires no reagents and only a minimum number of activation steps [83]. Thus adsorption is cheap, easily carried out, and tends to be less disruptive to the enzyme protein than chemical means of attachment [84].

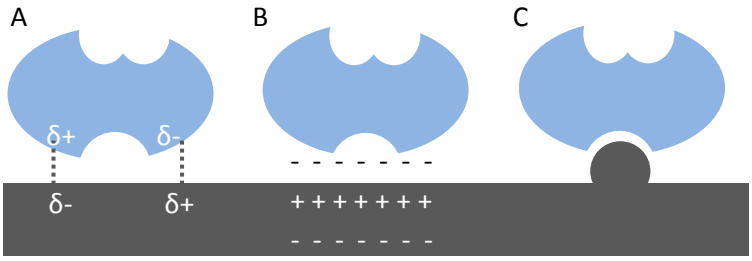

Figure 27: Popular physical adsorption mechanisms; A – Van der Waals forces, B – ionic bonding, C – affinity binding

Another approach is the use of hydrophobic interactions [85]. Hydrophobic adsorption has long been used as a chromatographic principle and relies on well-known experimental variables such as pH, salt concentration, and temperature [86]. Due to the size and hydrophobic nature of CNTs they have been shown to be able to intertwine with and spontaneously adsorb enzymes. Thus much success has been reported utilising hydrophobic physical adsorption with CNTs and GOx, even achieving DET since the CNTs are able to come in very close proximity to the FAD centre in flavoenzymes such as GOx [87, 88].

Porous gold has also been investigated for possible use as a substrate for adsorbed enzymes with a particular focus to creating LAC electrodes. One study reported that with regards to amount of enzymes immobilised, specific activity, and enzyme leakage, a physical adsorption method (which involved simply incubating enzymes in freshly prepared nPG), and the covalent coupling method gave highly comparable results. They also conducted further studies on the morphology and the nPG 'particle size' and found that with smaller nPG structures (close to those of gold nanoparticles) the adsorption affinity could be greatly improved and thus the enzyme loading increased whilst decreasing leakage, without using any reagents to facilitate binding [89]. This suggests that the adsorption here is driven by affinity binding (improved Van der Waal's or hydrogen bonding abetted by the complimentary morphologies of enzyme and substrate (Figure 27)).

Due to the weak bonds involved, however, adsorption methods are typically reversible. Desorption of enzymes can result from changes in temperature, pH, ionic strength or even the presence of substrate [90]. Adsorption is therefore not the most prevalent method for developing reusable enzymatic electrodes or electrodes intended for constant use. It is however often used as a first step prior to the covalent coupling or entrapment methods described later.

2.2.3. ELECTROSTATIC ATTRACTION

Electrostatic attraction is also an adsorption method but, unlike the physical adsorption methods discussed so far, is an active process and not a passive one. Here the idea is to take

advantage of the ionic nature of proteins. Much like amino acids, enzymes can exist as cations, zwitterions or anions depending on the ambient pH (see Figure 28). Moreover the strength of an enzymes ionic charge can be controlled by controlling the pH of the solution.

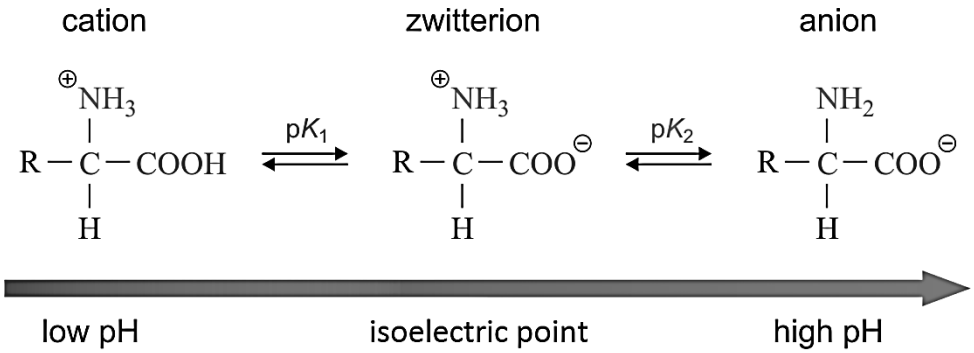

Figure 28: Ionic nature of amino acids [91]

Immobilisation by electrostatic attraction takes advantage of this charge on enzymes by applying a potential to an electrode of opposite charge to the enzyme [89]. Thus enzymes can attach to the electrode by ionic bonding. Furthermore applying a charge to the electrode induces a local electrical field which can actually draw enzymes from the solution to the electrode surface, greatly increasing the enzyme loading [92].

This method is however still reversible. Changing the charge on the electrode after immobilisation can result in enzyme detachment and even repel enzymes from the electrode surface. For the purpose of using electrostatic attraction immobilisation in fuel cells it is thus important to use enzymes with charges which are complimentary to the electrodes. Specifically a negatively charged enzyme should be used at the anode and a positively charged enzyme should be used at the cathode.

Since the pH of a fuel cell system is often fixed, and the choice of enzymes is often limited, finding an enzyme with the right complimentary charge at the given pH is often not possible and thus this method cannot always be implemented.

2.2.4. COVALENT COUPLING

The immobilisation of enzymes by the formation of covalent bonds is among the most widely used methods. The greatest advantage of such methods is the fact that the immobilisation procedure is considered irreversible, and thus the enzyme will not detach upon use [85]. In the ideal situation this is achieved by forming a peptide bond with either the amine or carboxylic acid terminal groups of the enzyme. This is not always possible since the terminal groups of a protein are often folded in to inaccessible positions. Thus the side chains of the following amino acids are frequently used to form peptide or sulphide bonds: lysine (amino group), aspartic and

glutamic acids (carboxylic group), and cysteine (thiol group). However, in order to ensure that the activity of the enzymes is not affected, it is important to ensure that amino acids essential for catalytic activity are not involved in the covalent coupling process [93].

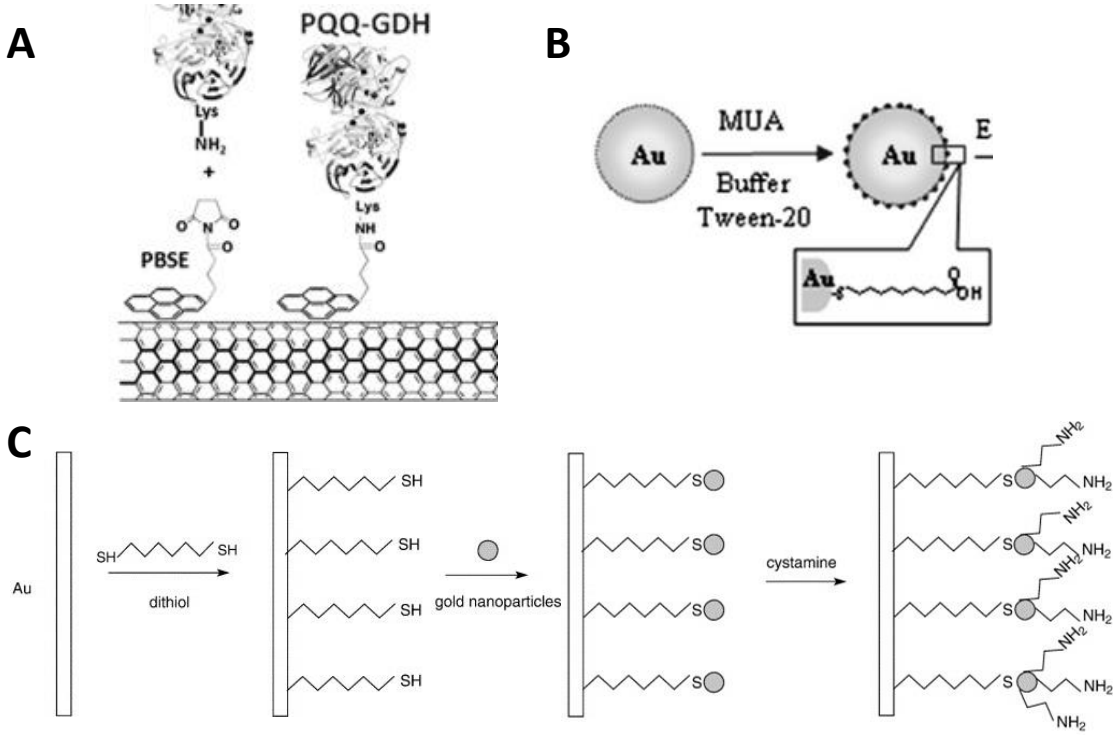

Figure 29: Examples of surface functionalisation techniques employed; A - a) immobilisation of PQQ-GDH on CNTs functionalised with 1-pyrenebutanoic acid succinimidyl ester (an NHS ester) [51], B – functionalisation of gold with carboxyl-terminated alkanethiols [94], C - functionalisation of gold by stepwise assembly of dithiol, gold nanoparticles and cystamine [95]. Reprinted with permission from copyright holders (see references).

In order to facilitate the formation of bonds between the electrode surface and the enzyme, complimentary reactive groups have to be present on the electrode surface. Functionalising the electrode surface with unstable ester, amine, carboxylic acid or thiol groups is therefore necessary [77, 94] (see Figure 29 for examples).

Subsequently these groups have to be activated by destabilising them to ensure reaction between the enzyme and the functionalised electrode surface. This is typically achieved using an EDC/NHS coupling method (Figure 30). This method destabilises carboxylic acid groups by the two step formation of a reactive ester to which amine groups will readily bind. Depending on the stability structure of the enzyme this method can either be employed to first functionalise the electrode surface, or in situ with the enzyme to functionalise carboxylic acids on the enzyme. A variation of this method is also employed to facilitate the formation of disulphide bonds between thiols [96].

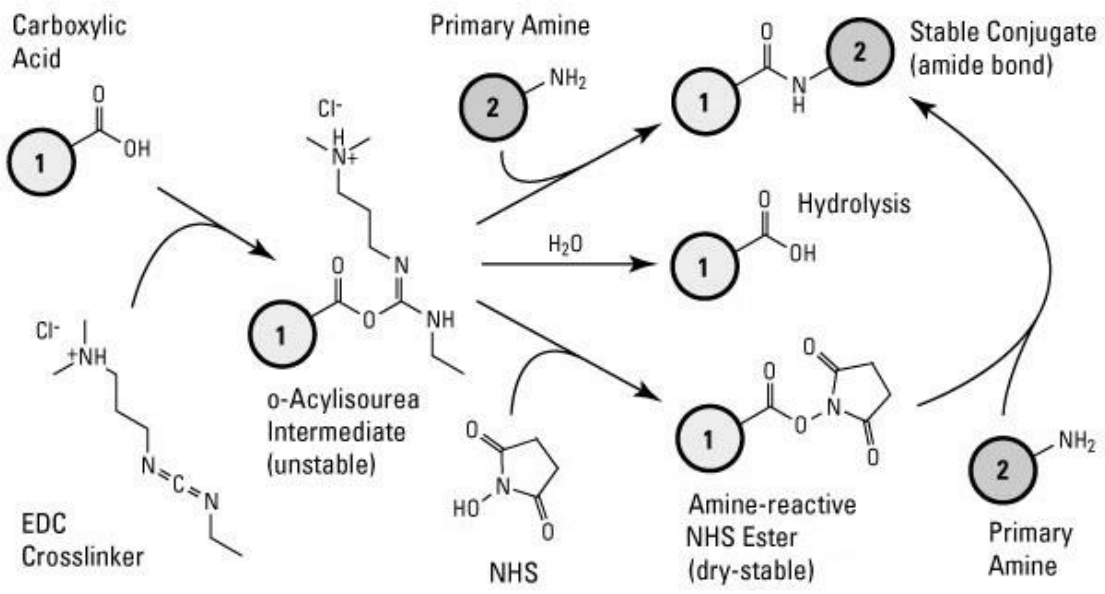

Figure 30: EDC/NHS coupling [97]

2.2.5. ENTRAPMENT

The entrapment method is based on the occlusion of an enzyme within a polymer which allows the substrate and products to freely pass through but retains the enzyme [98]. There are different approaches to entrapping enzymes such as gel encapsulation, sandwich entrapment and micro-encapsulation (Figure 31). The practical use of these methods is typically limited by mass transfer limitations through membranes or gels.

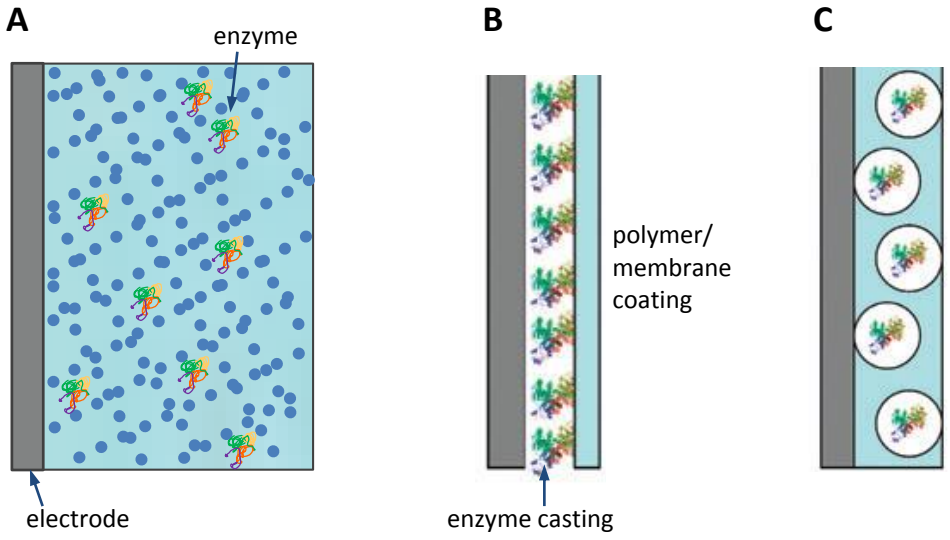

Figure 31: Enzyme entrapment methods; A – gel encapsulation, B – sandwich entrapment, C – microencapsulation [79, 99].

Gel encapsulation technology is based on the formation of metal or semi-metal oxide matrices around enzymes. The materials concerned are mostly oxides, in particular silica, alumina, aluminosilicates, titanium dioxide and zirconium dioxide. The most common material for the

encapsulation of enzymes is SiO_2 [100]. Silica is prevalent due to the fact that the resultant gels can be tailored to a large range of porous textures, surface functionalities and processing conditions, and can thus be adapted to a particular enzyme [101].

In the process of constructing a gel matrix, the enzyme acts as a template around which a porous wall is built by the chemical condensation of a silica gel network, so that its nanocapsule size is usually much larger than most of the pores which prevail in the gel walls (Figure 31A). Consequently the enzyme is immobilised within the gel, whilst substrates and electron mediators can freely move around, allowing for immobilisation without inhibiting enzyme activity. This technique is not ideal for the construction of reusable bioelectrodes since the use of MET techniques is necessary to obtain an electrochemical response [79], and thus electrodes that employ gel encapsulation are generally intended for single use [102].

Sandwich entrapment techniques involve the layering of enzyme followed by coating in another material (typically a polymer or a sol–gel matrix) (see Figure 31B). This coating has the effect of limiting mass transport of substrates to the active site of the enzyme. Furthermore, many systems have employed a three layer system consisting of an initial coating of material, followed by an enzyme layer, followed by the entrapment coating, to enhance the stability of the enzyme by eliminating the diffusion of enzyme in all directions [103]. Nafion polymers have also been used to coat modified electrodes, but have been demonstrated to reduce enzyme activity due to the acidic side chains of Nafion resulting in a hostile environment for the enzymes [104]. Some success has been reported however, when following the same basic principles of this technique, but instead utilising a fragmented electrode. In particular the use of graphite particles mixed with GOx and ferrocene subsequently compressed into a pellet before encapsulation in a dialysis membrane has been shown to produce electrodes which could function continuously in a biofuel cell [46]. This method thus allows for high level of proximity of the enzymes to conductive surfaces of the composite electrode and thus no doubt also employs a degree of localised adsorption of enzymes to graphite fragments.

Microencapsulation is merely the physical entrapment of an enzyme in matrices or the pores of a membrane **at the electrode surface** (see Figure 31C). It therefore typically follows the same principles behind either gel encapsulation or sandwich entrapment, but with a much greater degree of control (through electrochemical assembly for example) in order to produce very thin functional matrices around enzymes, or embedding of enzymes within a thin membrane coating.

Success has been reported with the controlled assembly of simple CNT and chitosan matrices [105], as well as with more complicated CNT, poly-cation polyethylenimine and Nafion matrices

[106], and dithiol-gold nanoparticle-cystamine matrices constructed by sequential self-assembly [107], with all achieving a DET response from GOx.

Microencapsulation of enzymes at the electrode surface has also been achieved using modified Nafion membranes that eliminate their acidity, while altering the size of the micellar pores for the encapsulation of an individual enzyme [108]. This method of encapsulation was also shown to protect the encapsulated enzymes from temperature increases and external changes in pH [109].

2.2.5. COMPARATIVE ANALYSIS OF IMMOBILISATION METHODS

Table 1 shows a comparison of the different immobilisation techniques considered here in terms of their relative stability, complexity, time taken to perform and the types of electron transfer techniques achievable in each case. With a view to constructing devices with long term stability irreversible processes are preferred. Of these covalent coupling of the enzyme to the electrode surface appears to be the best since it is versatile and allows for immobilisation of enzymes with minimal loss of activity without eliminating the possibility for DET.

Table 1: Qualitative comparison of different enzyme immobilisation techniques [51, 87-89, 92, 94, 95, 101, 103, 105]

Immobilisation Method	Stability and Permanence	Complexity	Time	Electron Transfer
Van der Waals Adsorption	Very Low	Low	~24 hrs	DET/MET
Ionic Bonding	Low	Low	~24 hrs	DET/MET
Affinity Binding	Variable (sensitive to pH)	Variable (controlling surface morphology can be complex)	~24 hrs	DET/MET
Electrostatic Attraction	Variable (sensitive to pH and charge)	Low	<1 hr	DET/MET
Covalent Coupling	Irreversible	High	hours to days	DET/MET
Gel Encapsulation	Irreversible (but subject to mediator leeching)	High	72 hrs – 1 week	MET
Sandwich Entrapment	Irreversible	Variable	<1 hr	DET/MET (reduced activity)
Micro Encapsulation	Irreversible (improved pH resistance)	High	~24 hrs	DET/MET

With a view to creating functional devices using fast and simple processes, electrostatic attraction methods are best. Electrostatic attraction is however highly dependent on numerous

factors (such as the isoelectric point of the enzyme and the eventual charge on the electrode), so cannot often be effectively employed. This is especially the case if the isoelectric point of the enzyme is close to the operating pH of the system, since a simple change in pH can then reverse the polarity of the enzyme resulting in detachment. When this method is applicable however, the enhanced electrostatic attraction by the application of a potential difference results in improved enzyme loadings greatly increasing performance and minimising waste.

2.3. DEVELOPMENT OF POROUS GOLD SURFACES

The development of biocompatible and non-toxic glucose sensors could allow for *in vivo* sensing of glucose levels and live control of insulin levels via an implantable insulin pump. The same biocompatible electrodes could also be used to generate power for implantable devices, such as insulin pumps or even cardiac pacemakers. This presents certain challenges and restrictions as few materials are considered to be truly biocompatible with even carbon based electrodes considered by many to be toxic with recent research suggesting that they cause T lymphocyte apoptosis [53].

Thus novel techniques are considered here to create biocompatible electrodes which exhibit the same properties which make carbon electrodes so well suited for enzyme immobilisation. The use of both nPG and other porous gold structures seems the obvious choice as gold is biocompatible, there are numerous tried and tested techniques for its manufacture, and it is a good surface for the immobilisation of enzymes [89].

2.3.1. CHEMICAL DE-ALLOYING

By far the most prevalent technique for the manufacture of nPG is by the simultaneous sputtering of both gold and silver, followed by the selective chemical etching of silver. Typically a small adhesion layer (5-10 nm) of chromium is used followed by a thicker gold layer of around 100-200 nm. This is followed by a thick (200-500 nm) layer of gold and silver (the ratio of gold and silver used here will determine the eventual pore size of the nPG produced (Figure 32)). Finally the silver is chemically etched from the sample using concentrated nitric acid. This method, though easily reproduced and highly effective, can be costly since a large amount of gold is used to sputter such large thicknesses, and thus this method is not a viable choice for the commercial manufacture of nPG electrodes [110].

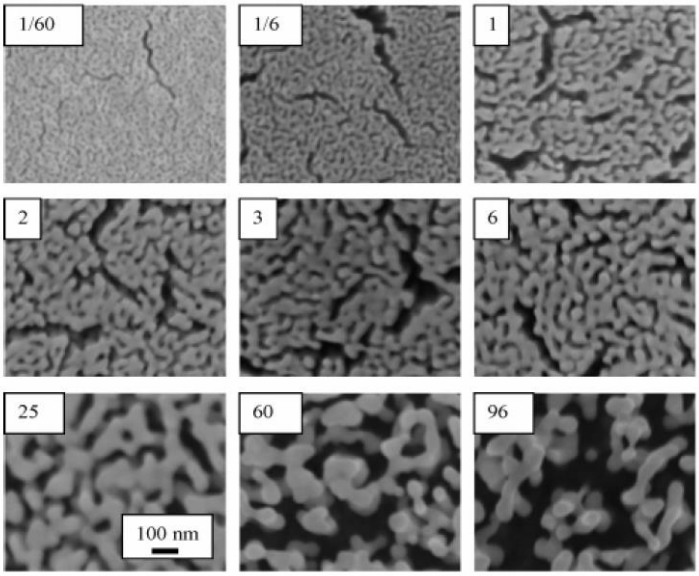

Figure 32: nPG films produced by de-alloying of sputtered gold and silver films [110]. Reprinted with permission from copyright holder (see reference).

An alternative, and more cost effective method, is in instead use commercially available gold and silver alloys [111, 112]. These can be etched to create unsupported nPG surfaces, though less control over pore size is possible since composition of the alloy is less controlled than the aforementioned dual sputtering method.

Other researchers have also reported great success when simply utilising low purity gold as a starting point. For example the use of de-alloyed 12-carat gold has been reported for the construction of platinum decorated nPG [113]. In this case concentrated nitric acid is used to dissolve out all of the gold impurities except for the trace amounts of platinum typically present resulting in a nPG gold structure of similar morphology as those obtained from purer gold and silver alloys (Figure 33). The remaining platinum impurity reportedly improves the catalytic activity of the nPG produced.

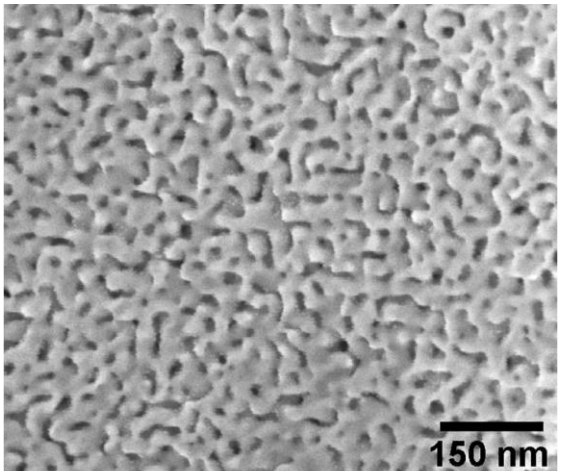

Figure 33: nPG produced by the chemical de-alloying of 12-carat gold [113].

2.3.2. ELECTROCHEMICAL ALLOYING AND DE-ALLOYING

In a similar manner as the chemical de-alloying methods already described many reaserchers have developed techniques for the controlled electrochemical alloying and/or de-alloying of nPG surfaces. The most analogous of these methods is through the electro deposition of a gold and silver alloy followed by the selective chemical etching of silver using nitric acid [114]. Here solutions containing varied amounts of $KAg(CN)_2$ and $KAu(CN)_2$ are used, with varied electrodeposition potentials to control the ratio of gold and silver deposited on a gold support. The chemical etching of silver then occurs in the same style as previously discussed.

Another method developed as a more versatile alternative to de-alloying of gold and silver films is the electrochemical alloying and de-alloying of gold and zinc. Here any gold surface greater than 200 nm in thickness can be converted into nPG (thus gold wires and sheets could easily be turned into unsupported nPG surfaces), which has a lot of potential for the commercial production of nPG. This method simply requires the cyclic electrodeposition and dissolution of zinc onto a gold surface which then systematically results in the formation of small pores in the gold surface (see Figure 34A). Extensively repeating this process yields a gold morphology which is similar to that created by the de-alloying of gold and silver films (Figure 34B and C)[115, 116].

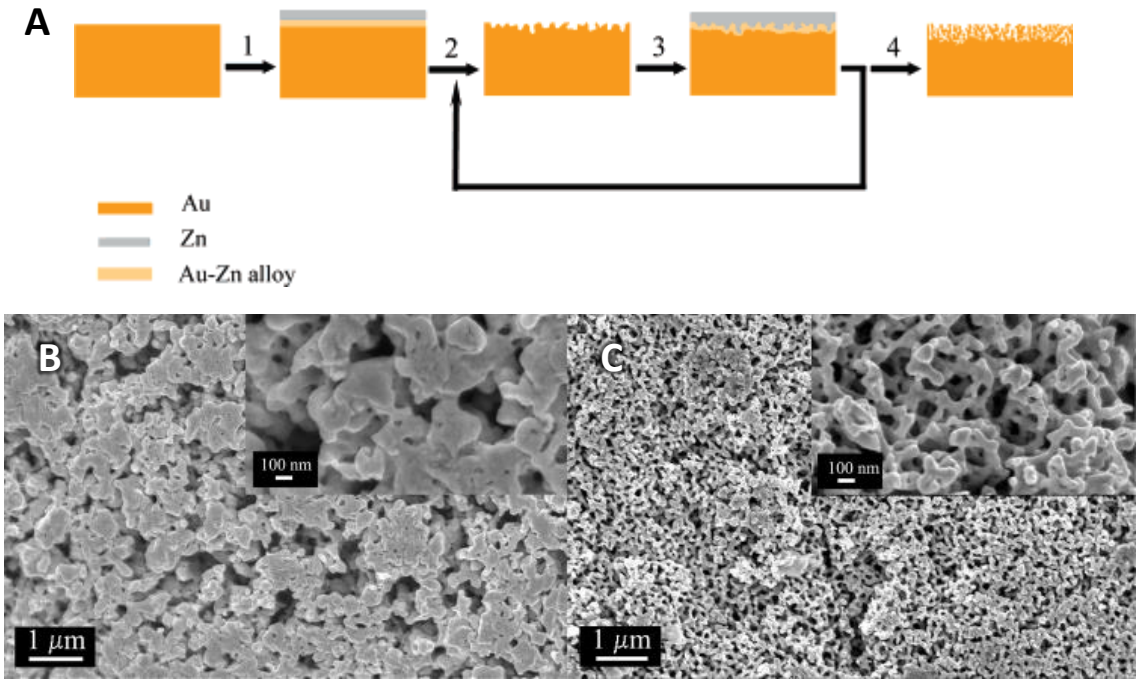

Figure 34: Alloying and dealloying process and FESEM of resultant gold surfaces; A – electrochemical cycle employed, B and C - electrodes after different cycle times of alloying/dealloying in $ZnCl_2$ electrolyte at 120 °C. (10 cycles and 30 cycles respectively). Reprinted with permission from copyright holder (see reference) [116].

2.3.3. DIRECT ELECTROCHEMICAL DEPOSITION OR DISSOLUTION

Another widely used method to create porous gold films is through direct electrodeposition. Here gold nanoparticles are reduced from an aqueous electrolyte containing $HAuCl_4$, and subsequently form gold nanoparticle aggregates resulting in a porous gold film without the need for any de-alloying processes [117-119]. These methods typically create a much less developed porous structure (see Figure 35) since the continued deposition of gold nanoparticles can fill the porous structure already created, and are thus this technique is usually combined with templating procedures which maintain the underlying porous structure already developed (discussed later).

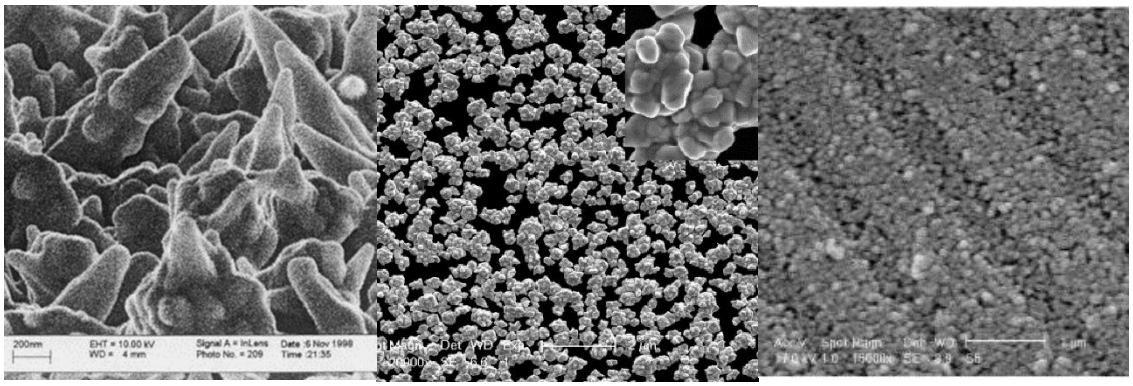

Figure 35: Porous gold films created by the deposition and aggregation of gold nanoparticles. Reprinted with permission from copyright holders (see references) [117-119].

Another electrochemically driven process utilises the electrodissolution, disproportionation and deposition of gold and its chlorides [120, 121]. In this method gold (from a pure gold substrate) undergoes active electrodissolution in either HCl or KCl solution to form $AuCl_2^-$ ions, which spontaneously disproportionate to $AuCl_4^-$ and atomised gold. The gold atoms then aggregate and deposit back on the gold substrate forming a nPG film (see Figure 36).

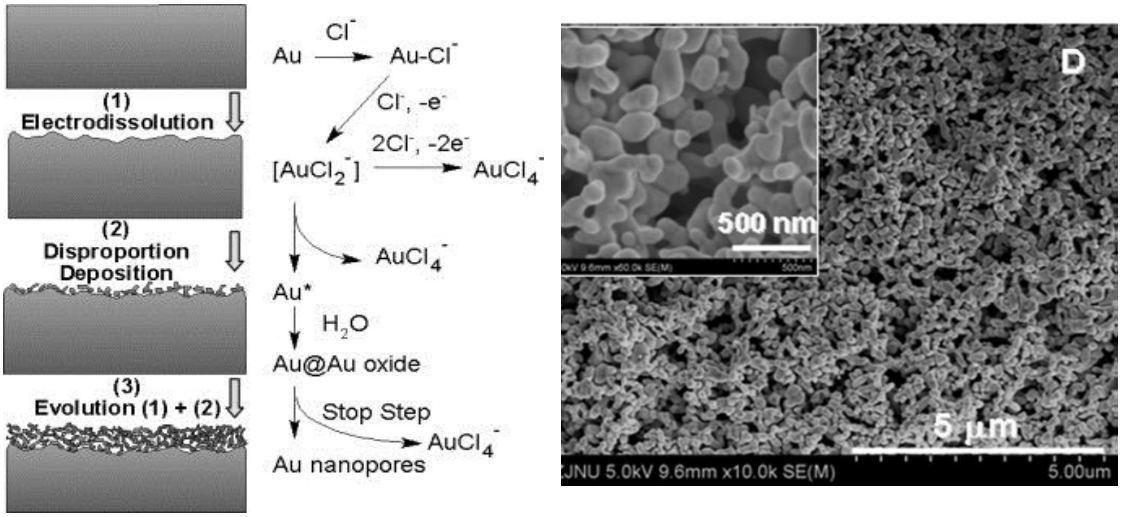

Figure 36: Electrodissolution of gold, disproportionation of its chlorides and deposition of gold, and the resulting nPG structure. Reprinted with permission from copyright holders (see references) [120, 121].

2.3.4. TEMPLATED ELECTROCHEMICAL DEPOSITION

Templated electrochemical deposition is a simple method that combines electrochemical deposition techniques with a template to better control where deposition takes place, and thus affect control on the morphology of the porous structure created [122]. The templates typically take the form of a conductive membrane [123, 124], or a layer of assembled particles [125, 126] which can either be preassembled prior to gold deposition (for a higher degree of control), or they can be assembled simultaneously as the deposition of gold to give a much more randomised structure.

Porous anodic alumina (PAA) membranes have been used as template for the creation of porous gold surfaces either in the form of gold nanotubes [123], or in the form of gold nanorod clusters [124]. In order to produce gold nanotubes, a $HAuCl_4$ electrolyte is used to effectively create structured gold nanoparticle agglomerates inside the pores of the PAA membrane. Subsequently, when the PAA membrane is removed by dissolution, the gold structure that remains is in the form of porous gold nanotubes (Figure 37A). In order to create gold nanorod clusters a highly conductive substrate is used under the membrane and a $KAu(CN)_2$ electrolyte is instead used. This allow for the more even growth of gold nanorods into the membrane from one side only. Once the membrane is removed (by dissolution) the resulting gold nanorods form agglomerates as shown in Figure 37B.

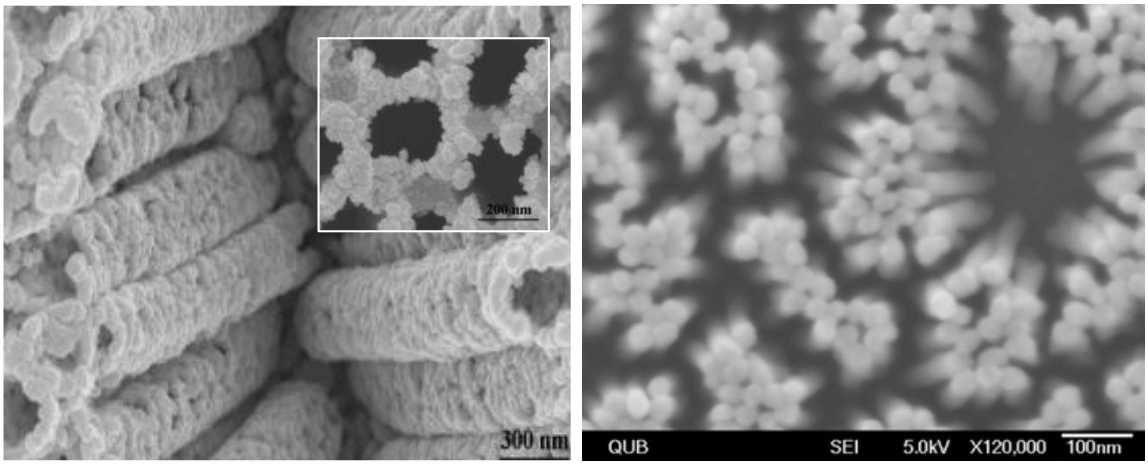

Figure 37: Gold structures grown in PAA membrane; A - FESEM images of gold nanotubes array after the removal of PAA membrane and with PAA membrane (insert) [123], B – FESEM of gold nanorod agglomerates [124]. Reprinted with permission from copyright holders (see references)

Both polystyrene spheres and silica microspheres have also been used to great success for the creation of porous gold via the use of a preassembled template [126-129]. In both cases the procedure is the same; template formation on a conducting substrate, electrochemical deposition of gold from solution, and the dissolution of the template with an appropriate solvent

or acid. The resulting structure when using either polystyrene or silica is a remarkably similar micro honeycomb-like structure as shown in Figure 38.

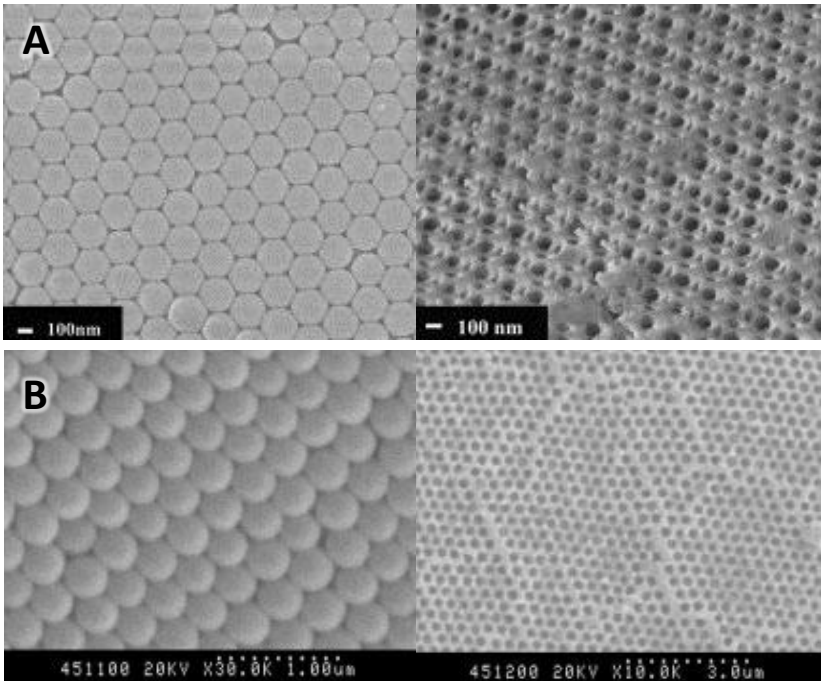

Figure 38: Porous gold structures created by preassembled particle template: A - SEM image of a polystyrene template and the resulting 3D film [126], SEM image of silica microsphere template and the resulting 3D structure [127]. Reprinted with permission from copyright holders (see references).

The simultaneous assembly of porous gold and a template has been demonstrated with the use of colloidal gold and silver nanoparticles [125], and with hydrogen gas templating [130]. When using gold and silver colloids, nanoparticles are deposited onto a conductive substrate in alternative layers creating a complex array of gold and silver particles. The silver particles are subsequently removed by selective dissolution to create a 3D porous gold structure (Figure 39). Here control over the pore sizes obtained can be closely controlled by the sizes of silver particles employed.

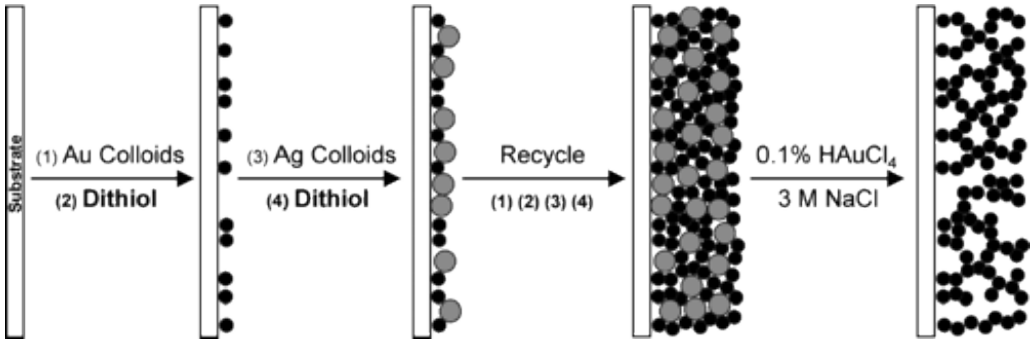

Figure 39: Porous gold deposition by simultaneous assembly of gold and silver nanoparticles, and subsequent dissolution of silver [125]. Reprinted with permission from copyright holder (see reference).

By far the most rapid method for the production of porous gold structures considered here is the direct electrodeposition of highly porous gold (hPG) films (porous gold with a wide pore size

distribution ranging from the nano to micro scales), with the aid of a hydrogen gas template bubble [130]. Here a relatively high deposition potential is applied to the target electrode in order to simultaneously deposit gold (from a $HAuCl_4$ electrolyte) and hydrolyse water to form hydrogen gas bubbles at the surface of the electrode. The hydrogen gas bubbles act as a dynamic template which constantly moves and changes in 'particle' size. The resulting structure is a hPG film with pores ranging from 10 – 50 µm down to less than 10 nm (see Figure 40). Thus an extremely high surface area is achieved since the larger pores (which would not be limited by mass transfer inefficiencies) are themselves lined with nanopores akin to those observed with nPG films [130, 131].

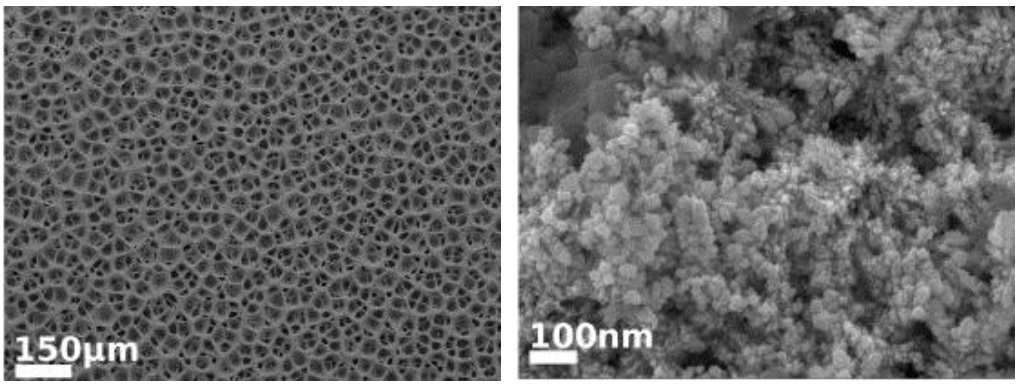

Figure 40: SEM of hPG films created by direct electrodeposition with a hydrogen bubble template [130]. Reprinted with permission from copyright holder (see reference).

2.3.5. GALVANIC EXCHANGE OF OTHER POROUS METALS

An alternate solution for the production of porous gold surfaces is to instead create a porous structure from another more reactive metal, and then to substitute this metal for gold by galvanic exchange. Galvanic exchange occurs when the metal ions in solution react with solid metals and ionise them. The original metal ion from solution loses its charge and deposits on the substrate surface while the original solid metal is dissolved into solution (Equation 9).

$$Metal\ A^{+}{}_{(aq)} + Metal\ B\ {}_{(s)} \rightarrow Metal\ A\ {}_{(s)} + Metal\ B^{+}{}_{(aq)} \qquad \text{Equation 9}$$

Galvanic exchange for the production of porous gold surfaces has been demonstrated using both copper and nickel as sacrificial templates. In order to maintain the same structure as the original solid metal it is important that the total atomic size of the new metal deposited is similar to that of the original metal structure. This can be achieved through the use of metals of similar atomic size so that the metal lattice structure remains unchanged. In the case of copper researchers chose to use a highly porous copper structure (created by hydrogen bubble template) in order to synthesise a hPG film [132]. Since both copper and gold have empirical atomic radii of 135 pm the direct galvanic exchange of copper for gold is possible here [133]. Thus researchers chose

to use a gold (I) electrolyte ($KAu(CN)_2$) here. Figure 41 shows the process utilised here, the initial copper structure, and the resulting hPG structures produced.

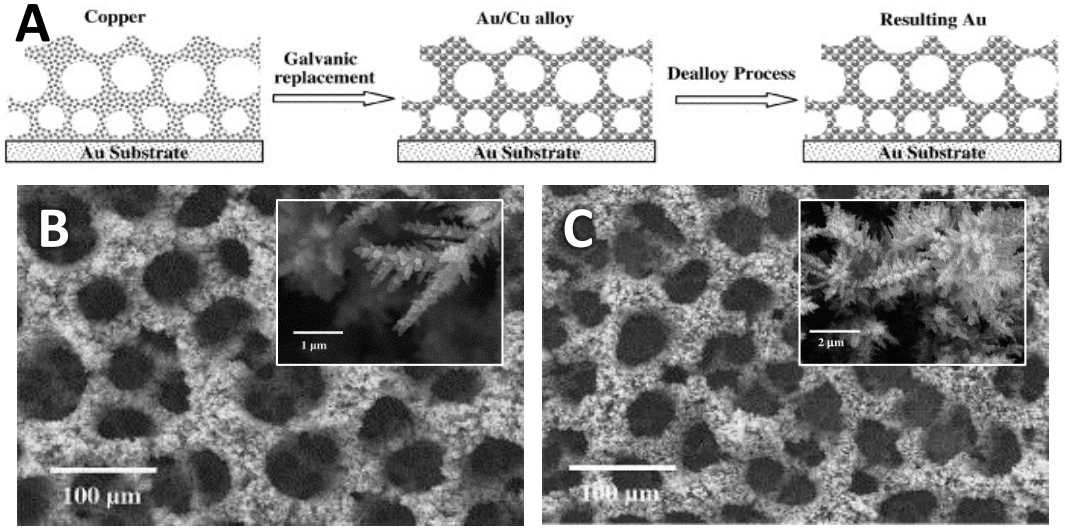

Figure 41: Galvanic exchange of copper for gold; A – summary of process used, B – initial highly porous copper structure, C – resultant hPG structures [132]. Reprinted with permission from copyright holder (see reference).

Alternatively the use of uneven charges between the metal ions deposited and the metal ions produced can be used to change the porosity of the existing metal structure. For example using a gold (III) electrolyte (such as $HAuCl_4$) will result in the production of three nickel ions from solid nickel for every one gold atom deposited (Equation 10). Thus the resultant metal structure produced from galvanic exchange can be more porous than the original [134].

$$Au^{3+}{}_{(aq)} + 3Ni\ {}_{(s)} \rightarrow Au_{(s)} + 3Ni^{+}{}_{(aq)} \qquad \text{Equation 10}$$

This technique has been employed by researchers to create porous gold nanorods. Initially nickel nanorods were produced (using a PAA membrane), and then the nickel was subsequently replaced with gold from a $HAuCl_4$ electrolyte. Figure 42 shows the initial nickel nanorods and the resulting porous gold nanorods produced.

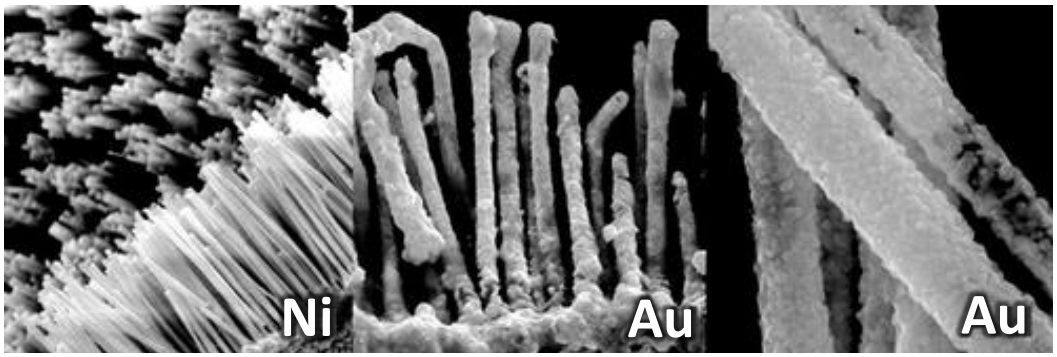

Figure 42: SEM images of initial nickel nanorods and resultant porous gold nanorods produced by galvanic exchange reaction [134]. Reprinted with permission from copyright holder (see reference).

2.3.6. COMPARISON OF DIFFERENT METHODS FOR CREATING POROUS GOLD SURFACES

Table 2 show a qualitative comparison of the different methods reviewed for creating porous gold structures. As it can be seen here, there is a very large difference between the different methods with regards to their complexity, ability to increase surface area and, perhaps most crucially for gold based materials, their respective costs.

Methods which achieve nanoporous structures on the gold surface typically enhance the surface area of the chosen materials by the greatest factor. This is especially true of gas templating methods such as the hydrogen templating method reviewed, since here extremely large pore size distributions are achieved resulting in pores within pores, within pores.

All of the methods reviewed here are relatively fast to conduct with the longest method taking only several hours, so no method can be excluded purely on the time required to perform it. Some methods, however, require a lot of time to prepare the materials. For example, preparing specific compositions of gold and silver alloys for chemical de-alloying can take a very long time.

Table 2: Comparison of different techniques for creating porous gold surfaces [113, 116, 118, 120, 130, 132]

Technique	Surface Area Enhancement	Complexity	Time Taken	Cost
Chemical De-alloying	High	Low (if alloys are purchased) to High	20 mins – 1 hr	Medium to Very High
Electrochemical Alloying and De-alloying	High	Medium	10 – 15 mins	Medium
Direct Electrochemical Deposition	Medium	Medium	5 – 10 mins	Low
Dissolution and Disproportionation	High	Low	5 mins	Medium
Solid Template	Medium	High	~ 2 hrs	Low
Gas Template	Very High	Low	20 s	Low
Galvanic Exchange	Low (typically requires porous starting material)	Low	2 hrs	Low to Medium

With regards to cost the best methods are those that do not require a gold base to create the porous gold structure. Methods which employ targeted deposition of gold (such as direct deposition, solid or gas templates and galvanic exchange) are thus prevalent here, since they do not require large amounts of gold and can, in theory, be used to create porous gold surfaces on any conductive surface.

Thus, with respect to cost, complexity and surface area enhancement, the best method to focus on is the use of a gas templating method such as hydrogen bubble templated electrodeposition of hPG.

2.4. ANALYSIS OF CURRENT PROGRESS AND PROJECT STRATEGIES

Though the possibility of developing implantable biofuel cells capable of producing power in the human body was of much interest in the past, since the development of reliable lithium ion based cells, interest in this subject has wavered. However, due to improvements made in reducing the power requirement of medical implants such as pacemakers, and due to the vast expansion of research into powered medical devices (including ocular implants, nerve relays and implantable insulin pumps), the possibility of using miniaturised biofuel cells has again become a topic of much interest.

Most devices focus on the use of intercellular fluid to supply glucose and oxygen (a fuel and an oxidant) and are thus dependant on the diffusion on these metabolites which are typically at concentrations much lower than in blood. Operation of an implantable fuel cell in a blood vessel would thus allow for much greater power outputs due to the higher concentrations of glucose and oxygen, and would not be limited by the diffusion of metabolites.

ABFCs typically exhibit low specific power outputs (relative to their size) and poor selectivity of their catalytic reactions. This means that larger devices are necessary in order to generate the desired levels of power. Unfortunately, due to the fact that they employ similar catalysts at the anode and the cathode, the OCP of these devices is also typically very low. This makes it very difficult to achieve working potentials that can easily be scaled up using boost converters to power real world devices. In this context EBFCs, are a promising alternative since the theoretical OCPs of around 1 V can be achieved here, and very high specific power outputs are possible. Thus EBFCs can be much smaller than ABFCs while still achieving useful power outputs.

A lack of stability is probably the greatest obstacle to overcome in the development of an implantable biofuel cell. This is especially true when examining the current progress of implantable EBFCs. Here, even though many researchers have boasted impressive maximum power outputs, the continual production of power has yet to be realised, with most devices exhibiting rapid decays in power output within minutes or hours of operation. Only ABFCs have thus far been shown to continuously produce power for extended periods of time in the order of months. In theory EBFCs should be limited by enzyme stability. However since the enzymes

employed typically exhibit native stabilities of several days, weeks or even months in some cases, the source of instability is most likely due to other factors such as interference or enzyme leeching.

The approach to improving the overall stability of EBFCs taken by most researchers is to move away from MET mechanisms and develop better materials that can facilitate DET mechanisms. CNTs and other carbon based materials have often been used to some success in this area. However the long term stability and toxicity of such materials is still disputed. Thus a promising approach taken recently is to use nanostructured metals (in particular porous gold surfaces) to improve the stability of the base electrode material. However work using porous gold surfaces as a substrate for enzyme immobilisation is still in its infancy with most researchers still focusing on the catalytic potential of porous gold itself. This means that there is a lot of potential for novel developments focusing on combining these relatively new technologies with enzymatic fuel cell technologies.

Focus has to be given to the choice and functional immobilisation of enzymes, as well as techniques for developing porous gold electrode materials which are stable and non-toxic.

3. MATERIALS AND METHODS

3.1. MATERIALS

Table 3 outlines the different materials used in this project as well as their respective suppliers.

Table 3: List of Materials and Corresponding Suppliers

Material	Synonym	Supplier	Catalogue #
1,6-Hexanedithiol, 97%		Alfa Aesar	L06686
4-Morpholineethanesulfonic acid Hydrate	MES	Sigma-Aldrich	M2933
4-Nitrobenzenediazonium tetrafluoroborate 97%		Sigma-Aldrich	294438
6-Mercapto-1-hexanol		Sigma-Aldrich	451088
AZ 326 MIF Developer		MicroChemicals	
AZ nLOF 2070 Photoresist		MicroChemicals	
Carbon Cloth		Easy Composites	
Carbon Fibres		Easy Composites	
Dimethyl Sulfoxide	DMSO	Sigma-Aldrich	D5879
Glucose		Sigma-Aldrich	158968
Gold (III) Chloride trihydrate		Sigma-Aldrich	520918
Gold foil ≥99.99% trace metals basis		Sigma-Aldrich	265810
Gold wire		Cookson Precious Metals	
GOx		Sigma-Aldrich	G6125
Hydrochloric acid (37% wt)		Fisher Scientific	10000180
LAC from *Rhus vernicifera*	RvLAC	Sigma-Aldrich	L2157
LAC from *Trametes versicolor*	TvLAC	Sigma-Aldrich	51639
Mars Micro Mechanical Pencil Leads		Staedtler	
N-(3-Dimethylaminopropyl)-N′-ethylcarbodiimide hydrochloride	EDC	Sigma-Aldrich	E7750
N-Hydroxysuccinimide	NHS	Sigma-Aldrich	130672
Nitric acid (68% wt)		Fisher Scientific	
Platinum wire		Cookson Precious Metals	
Polydimethylsiloxane (PDMS-3625)		Dow Corning	
Potassium Chloride		Sigma-Aldrich	P5405
Potassium Phosphate monobasic		Sigma-Aldrich	P5655
Sodium Chloride		Sigma-Aldrich	71380
Sodium Hydroxide		Sigma-Aldrich	06203
Sodium Phosphate dibasic		Sigma-Aldrich	S9763
Tetra-n-butylammonium tetrafluoroborate, 99%		Alfa Aesar	A16688
Tungsten foil ≥99.9% trace metals basis		Sigma-Aldrich	267546
Urea, ACS, 99.0-100.5%		Alfa Aesar	36428

In addition to the reagents listed, a stock solution of phosphate buffered saline (PBS) was made with the following constituents; 137 mM NaCl, 2.7 mM KCl, 10 mM Na_2HPO_4, 2mM KH_2PO_4. The

pH of this solution was then adjusted to 7.1 with the drop wise addition of 1M solutions of HCl and NaOH. This stock solution was subsequently used in all electrode characterisations.

Additional gold (III) chloride ($HAuCl_4$) was also synthesised from high purity gold. This was achieved in several stages. First a known quantity of gold was dissolved in aqua regia (a 1:3 volumetric ratio of concentrated HNO_3 and HCl) under a low heat. Excess nitric acid was then removed from this solution by continually heating and reducing with a 2 M hydrochloric acid solution. This stage was repeated until the colour of the solution changed from bright orange to yellow, and no further gas bubbles were formed. This solution was then reduced down to a slurry in order to remove any excess hydrochloric acid before finally being diluted to the required concentration with distilled water.

3.2. ELECTROCHEMICAL PRINCIPLES AND ANALYTICAL METHODS

3.2.1. OPERATION PRINCIPLES OF A POTENTIOSTAT

Potentiostats are extremely versatile pieces of hardware which can be used to conduct an array of different electrochemical including cell testing, corrosion analysis, biosensor testing, electroplating and determination of capacitance [135]. Essentially a potentiostat is used to control the potential difference between two electrodes whilst measuring the resultant flow of current. Though the potential difference and current observed can be measured between the same two electrodes (a working electrode (WE) and counter electrode (CE)), if analysis of a single electrode is required it is prevalent to introduce a third electrode (a reference electrode (RE)) into the system which is isolated from the bulk solution by a salt bridge. This is due to the fact that the potential measured between two electrodes will include contributions from the CE-electrolyte interface and the electrolyte itself [7]. This three-electrode cell setup is the most common electrochemical cell setup used in electrochemistry (see Figure 43) [136].

In this case, the current flows between the CE and the WE. The potential difference is controlled between the WE and the CE and measured between the RE and WE. The potential between the WE and CE usually is not measured. This is the potential applied by the system and it is adjusted so that the potential difference between the WE and RE will be equal to the potential difference specified.

Throughout this project potentiostats were used for electrode modification and analysis. Two different models of potentiostat were used, namely the μAUTOLABIII and the Autolab PGSTAT128N, both supplied by Metrohm UK. In each case the experimental setup was the same (see Figure 43). Gold disk electrodes (2 mm diameter) and saturated calomel electrodes (SCE)

were purchased from IJ Cambria Scientific Ltd. A platinum rod counter electrode was supplied by Metrohm UK.

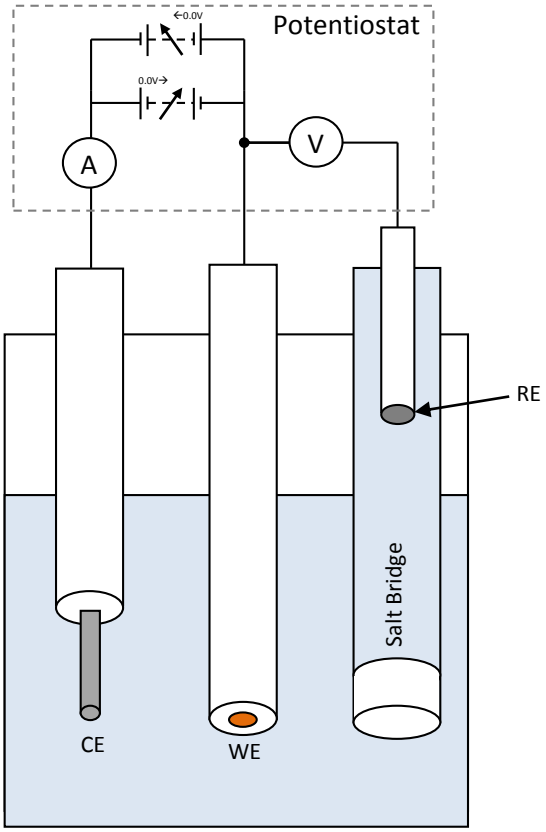

Figure 43: Experimental setup with simplified circuit diagram of a potentiostat

3.2.2. CYCLIC VOLTAMMETRY

Cyclic voltammetry (CV) is a very useful electrochemical technique since it can determine the capacitance of the electrode in the given electrolyte, as well as determining the potentials at which reactions (both relating to the electrode surface and the bulk solution) occur. CV scans are performed using a potentiostat in the three electrode configuration described earlier. Here the potential applied between the electrode of interest (the WE) and the CE is varied such that the potential difference between the WE and the RE varies at a constant rate (the scan rate, *v*) as specified in the control system (see Figure 44a). The resulting current signals (measured between the WE and CE) corresponding to this change in potential difference are then recorded to create a CV curve, also known as a voltammogram (see Figure 44b) [137].

There are two components to the current observed:

- a capacitive component resulting from re-distribution of charged and polar species at the electrode surface (see Section 3.2.2.1.), and

- a faradaic component resulting from exchange of electrons between the electrode and redox species. This is dependent on the standard potential of the reaction, the mass transport of the redox species to the electrode surface and the rates of reaction [138] (see Section 3.2.2.2.).

Depending on the shape of the curves produced and the number of peaks observed CV scans can determine whether a reaction is reversible or irreversible, whether the reaction results in a change of the electrode surface or the electrolyte, how many reaction stages there are and even how many electrons are involved.

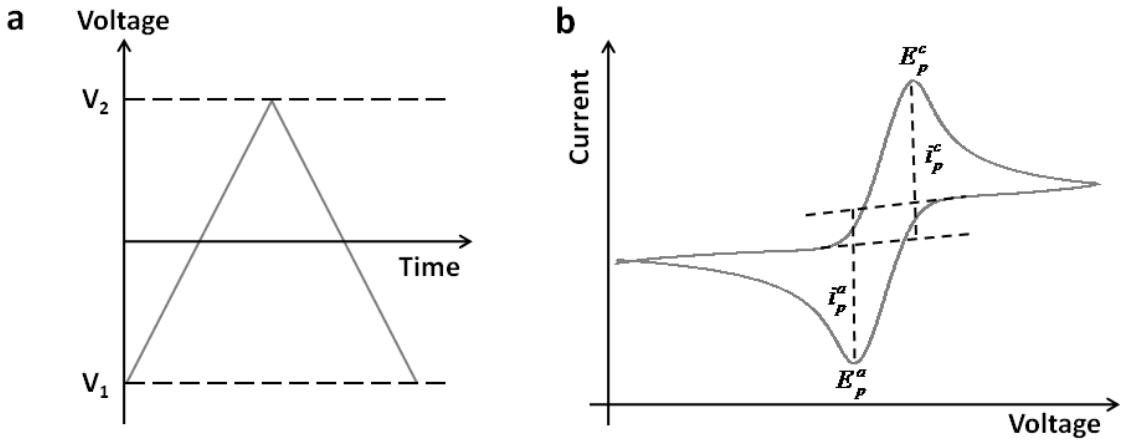

Figure 44: CV waveform (a) and typical CV curve (b) [139].

3.2.2.1. CAPACITIVE CURRENT AND EFFECTIVE SURFACE AREA

During a CV scan the electrode-solution interface will behave as a parallel-plate capacitor [140]. When a potential is applied across a capacitor, charge will accumulate on one plate of a capacitor.

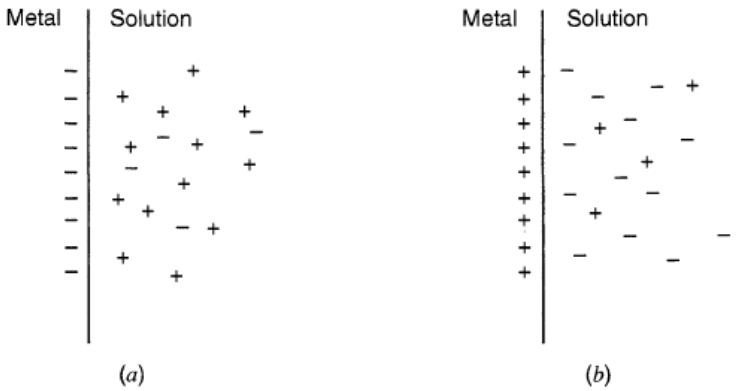

Figure 45: Electrode-electrolyte interface acting as a capacitor with a charge on the metal, Q, (a) positive and (b) negative [135].

During this charging process, a current (called the charging current) will flow. The charge on a capacitor consists of an excess of electrons on one plate and a deficiency of electrons on the other. Similarly the capacitance, C, of an electrode in solution is due to the build-up of charge due to an excess or deficiency of electrons on the metal electrode (see Figure 45).

For a simple parallel plate capacitor, charge on the capacitor, *Q*, is proportional to the voltage drop across the capacitor, *E:*

$$Q = CE \qquad \text{Equation 11}$$

To calculate the magnitude of the charging current, we differentiate Equation 11 with respect to time, *t,* and assume that capacitance is constant:

$$\frac{dQ}{dt} = C\frac{dE}{dt} \qquad \text{Equation 12}$$

Recognizing that *dQ/dt* is an expression for current, I, and *dE/dt* is the potential scan rate, ν, we obtain:

$$I = C\nu \qquad \text{Equation 13}$$

The charging current in this case corresponds to the difference in anodic and cathodic current observed, *ΔI*, during a CV scan (see Figure 46).

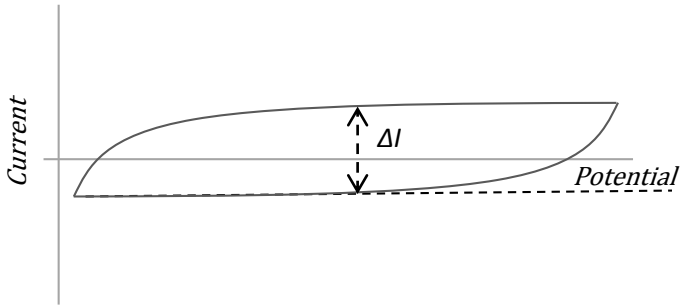

Figure 46: Illustration of CV scan showing charging current

The surface area of flat (nonporous) electrodes can be determined easily by conducting CV scans in an electrolyte such as PBS. This can be done if we again assume that the capacitance of the electrode is constant, and take into account Helmholtz model of electrochemical capacitance where: ε is the dielectric constant of the material separating the parallel plates; ε_0 is the permittivity of free space; l_c is the separation between the plates; and *A* is the area of the electrode (Equation 14) [135].

$$\frac{C}{A} = \frac{\varepsilon\varepsilon_0}{l_c} \qquad \text{Equation 14}$$

Assuming that the area of the electrode remains constant as well this can simply be incorporated into Equation 13 to show that the charging current is proportional to the area of the electrode and the scan rate (Equation 15).

$$I = kAv \qquad \text{Equation 15}$$

This does not strictly hold true with porous electrodes since there is a large surface area of the electrode which is electrochemically ineffective due to limitations related to diffusion of particles capable of carrying charge into the pores (see Figure 47).

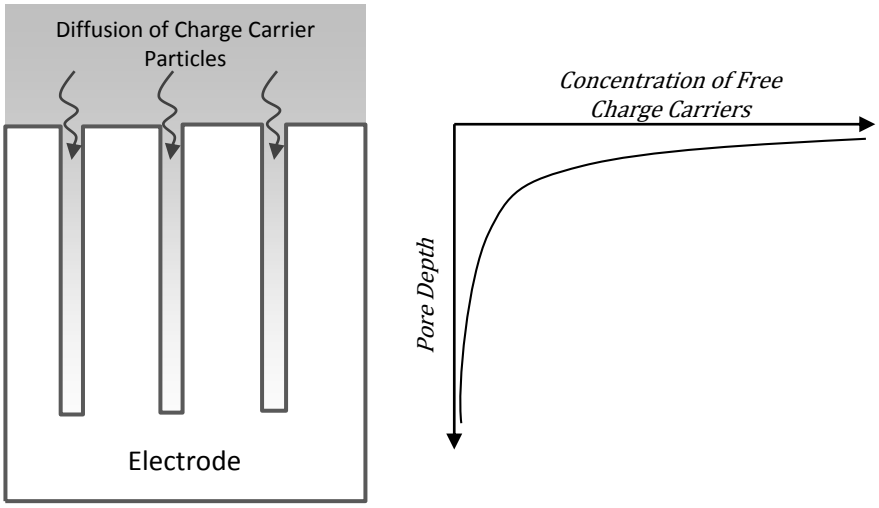

Figure 47: Loss of electrochemical activity within pores

Once the supply of charge carriers within the pores have been exhausted the system relies on diffusion of new charge carriers into the pores. Since the pores are electro-active the charge carriers are reacted electrochemically as they diffuse into the pores resulting in a concentration gradient into the pores. Hence, though the actual surface area of the electrode may be very high, only a small amount of this surface is readily exposed to charge carriers from the bulk of the solution and is electrochemically effective.

Thus the proportionality of current observed to surface area of the electrode is only strictly valid for flat electrodes (where the entire surface area of the electrode is readily exposed to charge carriers from the bulk of the solution). However it can still be used to determine an approximation for the electrochemically effective surface area (ESA) of the electrode [141].

Using a polished gold electrode with a known surface area a set of cyclic scans are conducted in a region where no reaction between gold and any component in PBS is evident and thus only the charging current owing to the capacitance of the system is measured. The surface area of the polished electrode ($SA_{polished}$) is then divided by this charging current ($\Delta I_{polished}$) to determine

a scalar which can be used to determine the effective surface area of a porous electrode under the same conditions (see Equation 16).

$$ESA = \Delta I_{porous} \times \frac{SA_{polished}}{\Delta I_{polished}} \qquad \text{Equation 16}$$

Once the ESA of a hPG electrode has been determined, data collected using the potentiostat can be normalised to negate for the differences in current observed by simply using the current per square centimetres of ESA in figures instead of the absolute value for current itself.

3.2.2.2. FARADAIC CURRENT FLOWS

The faradaic component of current flow in a CV scan depends on the standard potential of the reaction, the mass transport of the redox species to the electrode surface and the rates of reaction at the electrode surface. For a reversible oxidation and reduction a strong peak is observed in both the forward and reverse scans with the current observed returning to its capacitance level after the peak is observed (see Figure 48A).

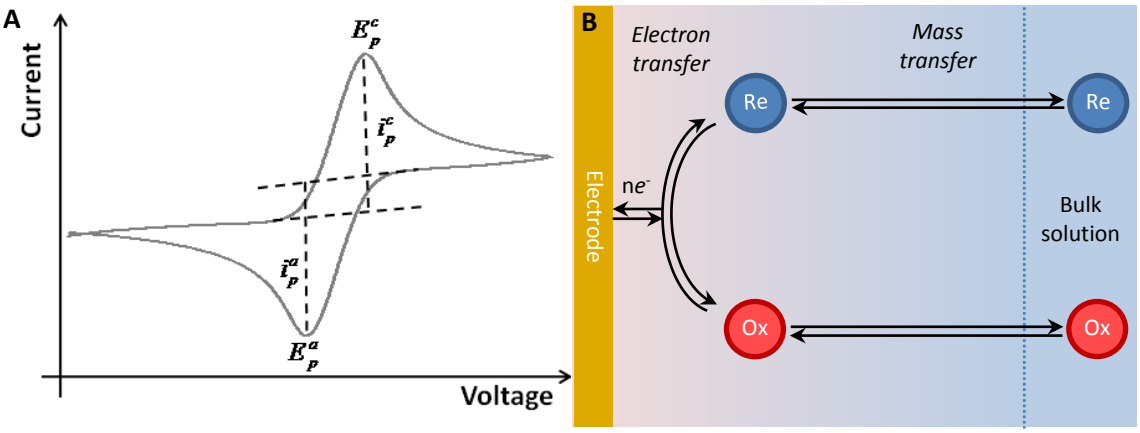

Figure 48: Typical CV scan for reversible oxidation and reduction; A- CV scan, B- diagram illustrating mechanisms involved in this case [139, 142]

In this case the oxidation and reduction current peaks correspond to the reversible oxidation and reduction of a redox species such as shown by Equation 17 (where *Red* and *Ox* refer to the oxidised and reduced forms of the redox species respectively, k_{ox} and k_{red} are the respective rate constants and *n* refers to the number of electrons required for the reaction to occur).

$$Red \underset{k_{red}}{\overset{k_{ox}}{\rightleftharpoons}} Ox + ne^- \qquad \text{Equation 17}$$

As the scan begins (from the left hand side of the current/potential difference (or voltage) plot) only a very low level of current is observed (owing to the capacitance of the system). Then, as the potential difference is increased towards the oxidation potential, the current increases as

more of the *Red* is converted to *Ox*. This behaviour is described by the Nernst equation (Equation 18), which predicts the relationship between the concentration of the different redox species, *[Red]* and *[Ox]*, and the applied potential difference, *E*, where E^{Θ} is the standard potential of reaction, F is Faraday's constant, R is the gas constant and T is the temperature in Kelvins [7].

$$E = E^{\theta} - \frac{RT}{nF}\ln\frac{[Red]}{[Ox]} \qquad \text{Equation 18}$$

When the potential difference is increased past the reduction potential, the current decreases, having formed a peak. This peak occurs, since at some point the diffusion layer has grown sufficiently above the electrode so that the flux of reactant to the electrode is not fast enough to satisfy that required by the Nernst equation and thus the current begins to drop [137]. The faradaic current is then controlled by the rate of diffusion to the electrode and thus becomes mass transfer limited (see Figure 48B). Hence, the faradaic current, i_f, will depend on the concentration gradient of *Red* at the electrode surface as described by Equation 19 where, A is the area of the electrode and D is the diffusion coefficient of *Red*.

$$i_f = nFAD\left(\frac{d[Red]}{dx}\right)_{x=0} \qquad \text{Equation 19}$$

These equations can be used to describe and predict the behaviour of reversible redox reactions that occur by direct interaction with the electrode surface. However, in situations where the driving force behind the production of current is not the result of the direct oxidation or reduction of reactants on the surface of the electrode, or where the processes involved are largely irreversible, the system becomes more complicated. This is generally the case when enzymes or other catalysts are involved, along with any other system where electron mediators are employed.

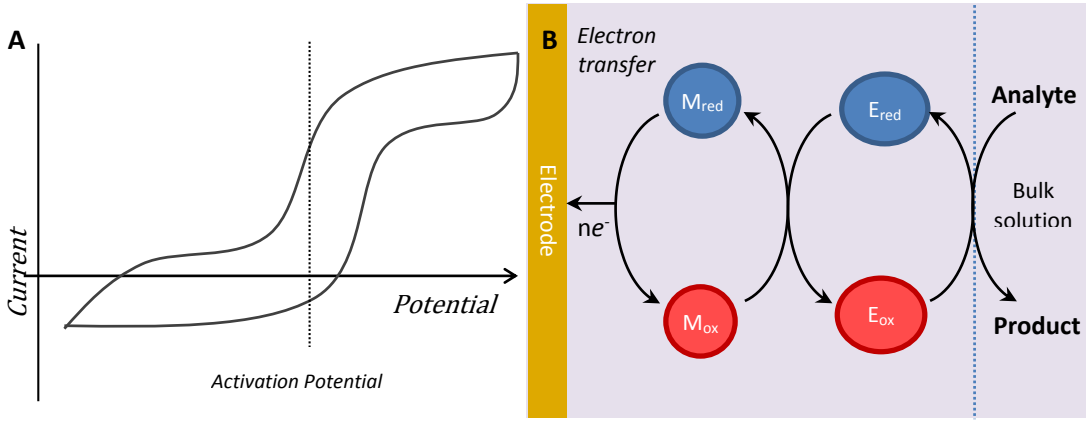

Figure 49: Typical CV scan of a MET enzyme system and mechanisms involved (A and B respectively).

Figure 49 shows a typical CV scan and the electron transfer mechanisms involved for a MET enzyme system. In this case the faradaic current is no longer dependant on the diffusion of a reduced or oxidised species from the bulk of the solution. Instead the concentration of the reduced species (the reduced form of the mediator, M_{red}) at the electrode surface is maintained by a reaction with the enzyme. Thus once the potential of the CV scan exceeds the oxidation potential of the mediator (or the activation potential of the system) the current flow is constant and only dependant on the rate of production of M_{red} from the reduced form of the enzyme (E_{red}). Accordingly the magnitude of this current flow will depend on the concentration of the analyte which will affect the rate at which E_{red} is formed (assuming the concentration of the enzyme itself is not a limiting factor).

3.2.3. CHRONO-AMPEROMETRY

Chrono-amperometry scans rely on the use of a single potential rather than a scan range. Here the current observed at a given potential is carefully monitored over a period of several minutes (typically 5-10 minutes), in order to see if current remained stable at given concentrations of an analyte, or whether it decayed. As with CV scans there are several different components which make up the current observed here.

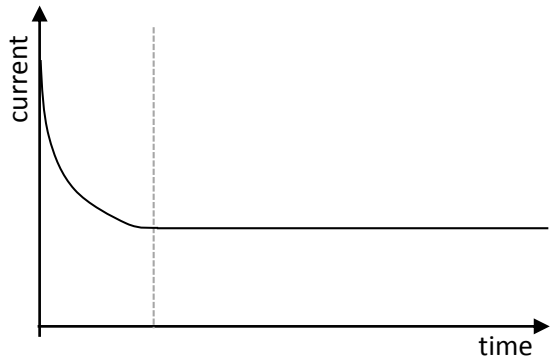

Figure 50: Typical chrono-amperometric scan

Figure 50 show a typical chrono-amperometric scan. At the beginning of such a scan a relatively large current is observed followed by a rapid decay in current. This decay behaviour can usually be attributed to either the system's capacitance (ie the flow of current from a sudden shift in potential difference), or due to the formation of a diffusive layer as the supply of reactants at the surface is rapidly exhausted. If the current decays to nothing then it can be assumed that no further reactions are taking place and thus the current was either solely due to capacitance or due to the electrode surface itself acting as a reactant (eg due to metal oxidation). If current is still observed following this rapid decay phase then this suggests that an equilibrium has been

reached. In the case of a catalysed system (such as with enzymes) the magnitude of this current will depend exclusively on the bulk concentration of the analyte.

Chrono-amperometry it therefore a very important tool for the production of electrochemical sensors since it can be used to directly relate the concentration of an analyte to the level of current flow, thus truning a chemical signal into an electrical one [143, 144].

3.2.4 POLARISATION

In an ideal scenario the potential difference of a fuel cell would only depend on the difference between the potential at which the fuel can be oxidised and the potential at which the oxidant can be reduced (ie the OCP). In reality however the operating potential difference of a fuel cell is always less than the OCP due to polarisation (the reduction of potential difference when current is flowing) of the fuel cell [145]. Polarisation curves (a plot of cell potential against current or current density) are thus used to assess fuel cell performance and to better quantify and characterise the different sources of polarisation.

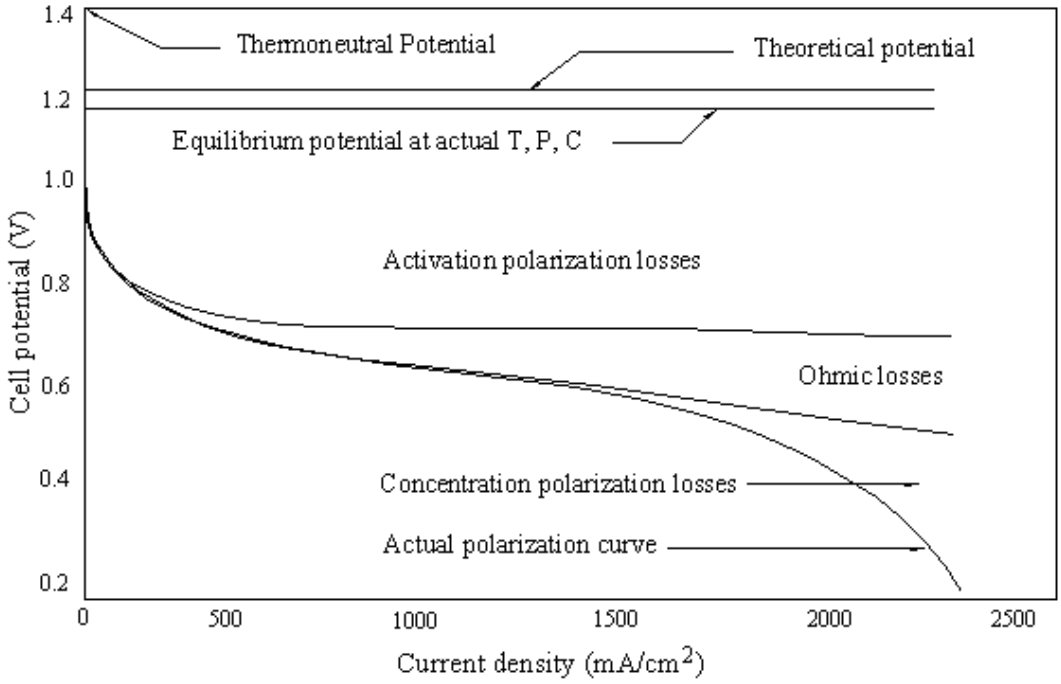

Figure 51: Polarisation curve illustrating different sources of overpotentials [145]

There are three sources of overpotentials which result in fuel cell polarisation as illustrated by Figure 51, namely the activation overpotential, the ohmic overpotential, and the concentration overpotential. The activation overpotential is caused by the flow of current which occurs due to a shift away from the equilibrium position of the anodic and cathodic half reactions. The ohmic overpotential is the result of the sum of the ionic, electronic and contact resistances and is thus governed by Ohm's law. The concentration overpotential is the result of mass transport

limitations in the system. These arise when higher current flows result in the depletion of reactants at either the anode or cathode.

Though polarisation curves are useful for determining the overall cell performance, it does not give any information about the individual components in the cell. Instead it gives the indications on the sum total inefficiencies of the system. Unlike techniques such as CV and chrono-amperometry however, polarisation curves do not require an application of current through the system, but instead passively monitors current flow. It therefore has less of a chance of damaging the cell during analysis.

Polarisation curves also give very useful information on the parameters required in order to maximise a fuel cell's performance. Since the same data can be used to determine power density, polarisation curves are often coupled with power density curves which show at which potential and cell resistance the power is maximised (see Figure 52).

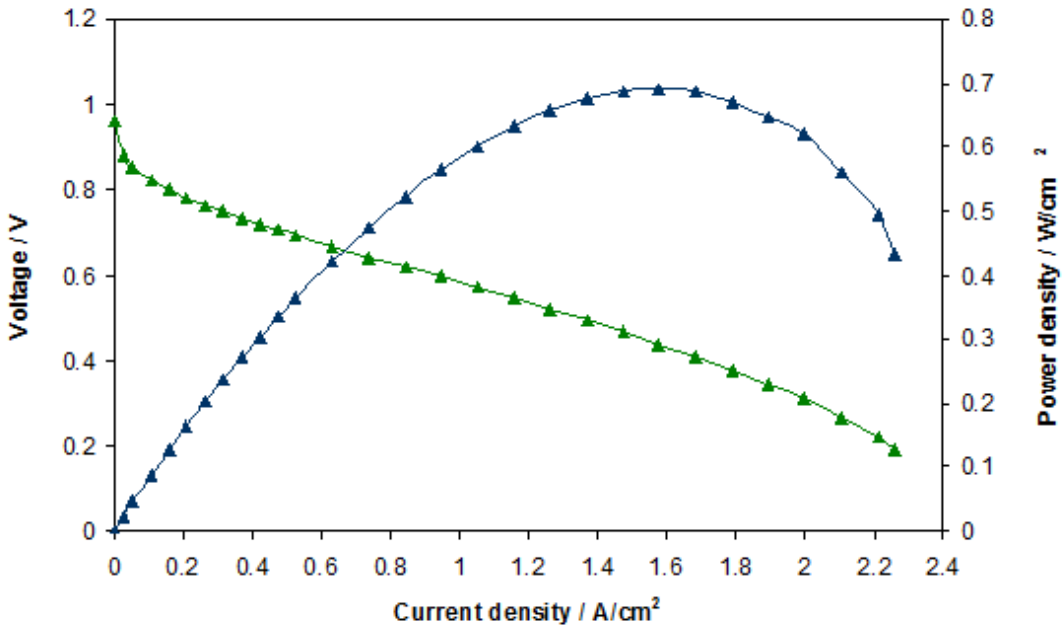

Figure 52: Typical polarisation and power density curve [146].

3.3. EXPERIMENTAL METHODS

3.3.1. DEPOSITION OF hPG FILMS

Though many techniques for the production of nPG or hPG electrodes were considered, it was decided to use a simple hydrogen templated electroplating method in order to directly deposit hPG onto the surface of gold electrodes (see Figure 53). This method was chosen due to two key reasons; the associated cost of using this method was considered to be by far the lowest, and

the method was considered to be the most versatile since, in theory, it could be used for many different shapes and sizes of electrodes such as electrodes patterned on glass or gold wire electrodes. Several variations of this method were used based on a method adapted from literature [130].

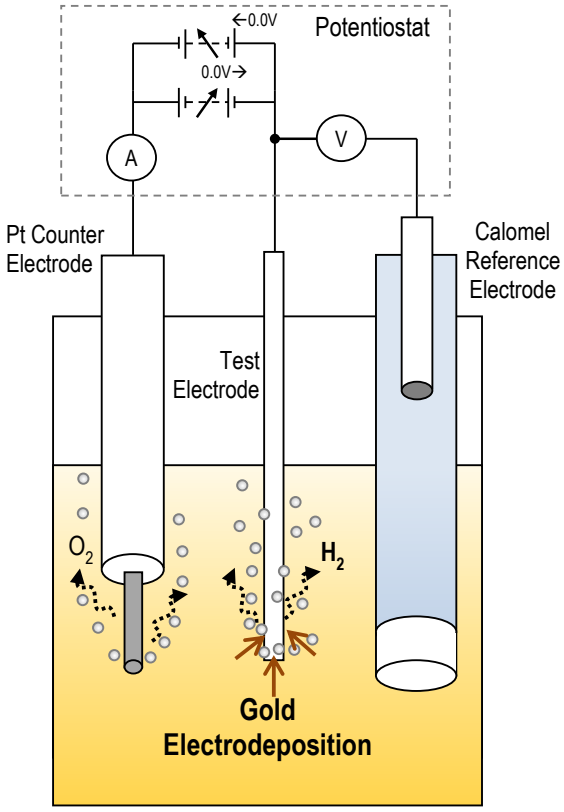

Figure 53: Schematic of experimental setup used to directly deposit hPG by potentiostatic control

The hPG was fabricated by direct electrodeposition from an aqueous electrolyte consisting of 0.1 M $HAuCl_4$ and 1 M NH_4Cl. Though many different deposition potentials and procedures were investigated (see Chapter 4) the most common protocol used when employing potentiostatic control is as follows:

- deposition potential set to -0.7 V (vs. SCE) for 5 s,
- deposition potential set to -1.5 V (vs. SCE) for 5 s,
- deposition potential set to -2.5 V (vs. SCE) for 5 s,
- deposition potential set to -4.0 V (vs. SCE) for 10 s.

When using a simple two electrode setup with a DC power supply (Basetech BT-305 variable bench-top power supply unit) the potential applied across the two electrodes was stepped down to -10 V (at a rate of approximately 1 V s^{-1} by manual control) and then maintained at this potential for 10 s. This was done in accordance to the actual potential applied across the working electrode and counter electrode when using a potentiostat with a three electrode setup.

3.3.2. DEVELOPMENT OF MICRO-ELECTRODES

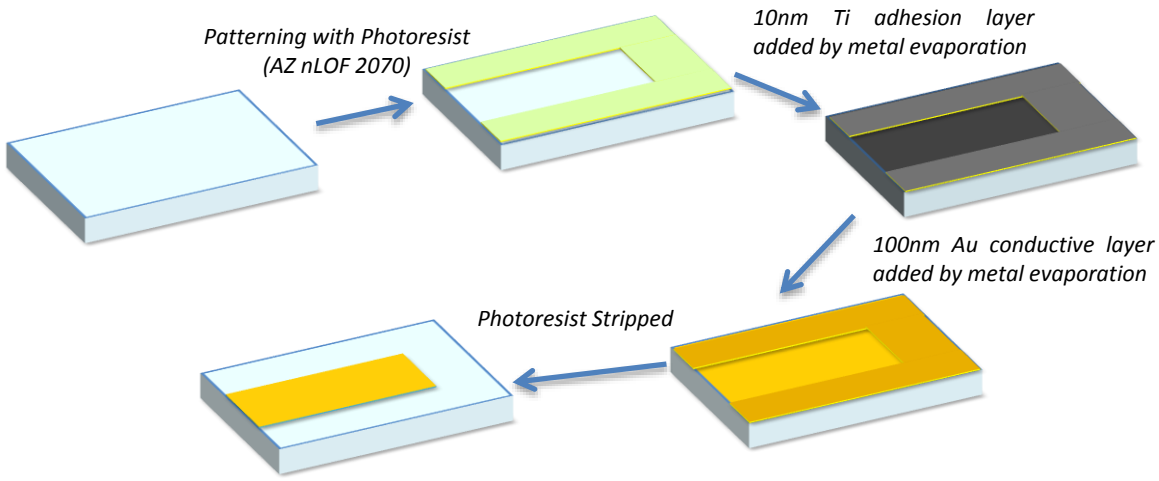

Figure 54: Sequence of events used to pattern electrodes onto glass slides using negative lift-off photolithography

'Micro-Electrodes' were created by first patterning thin film gold electrodes onto specially prepared glass slides by using a process known as negative lift-off photolithography (see Figure 54). This technique allows the user to pattern complex patterns onto a substrate (typically glass or a silicon wafer) using a photomask, a high intensity ultra-violet light source and a heat stable photoresist. Metal can subsequently be deposited (either by metal evaporation or by sputtering) over the photoresist patterns in order to create simple circuit boards, or in this case, an electrode on a glass slide. Following the deposition of a large bar shaped electrode onto the glass slide the exposed surface area of the electrode and electrical contact was controlled with the application of a second layer of photoresist as shown in Figure 55.

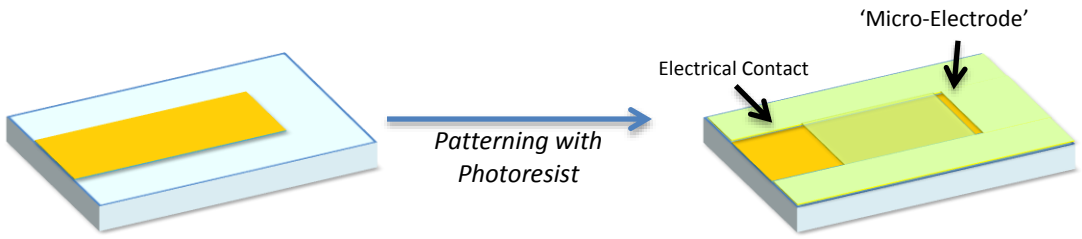

Figure 55: Application of an insulating photoresist layer to control exposed surface area of electrode

3.3.2.1. SAMPLE PREPARATION FOR LIFT-OFF PHOTOLITHOGRAPHY

Since the process of photolithography relies on the use of an ultraviolet (UV) light sensitive photoresist, exposure of the microelectrodes to UV light had to be controlled during sample preparation. Work therefore had to be carried out in a controlled environment. Initially this was achieved using the David Bullett Nanofabrication Facility at the University of Bath but, in order

to reduce cost, a photolithography glove box of our own design and making was later utilised (Figure 56).

Figure 56: A UV light-free environment; A – the David Bullett Nanofabrication Facility, B – a photolithography glove box of our own design and making.

Glass slides were cleaned using several cleaning protocols relying on the sequential use of acetone, 2-proponol (IPA) and distilled water in a sonicated water bath. This was followed by an abrasive dry and polish using polymer based clean room grade tissues. Once the slides were cleaned they were spin coated with the AZ nLOF 2070 photoresist at 3000 rpm for 30 seconds (using a *Headway Research PWM32 Spinner System* or an *INSTRAS SCK-100 Spin Coater*) using a protocol outlined by the distributer [147] (see Figure 57).

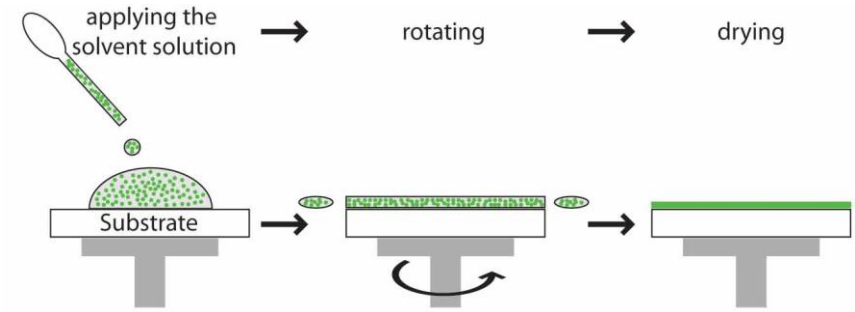

Figure 57: Schematic of spin coating process [148].

Since the standard thickness of this photoresist is 7µm, and the desired thickness of the metal layer is no greater than 0.2µm, several dilutions of the photoresist were also tested with the intension of conserving the amount of photoresist used. The most successful dilution used was an 80:20 %/v mixture of the photoresist and acetone as it resulted in fast development and lift-off, and showed no noticeable difference in the quality of the electrodes produced when using the same coating protocol. It also has a much lower viscosity and as such could be applied very conservatively.

This was followed by a soft bake stage involving heating for the samples for 2 minutes at 110°C using a contact hot plate. This ensured that any excess solvents were removed from the photoresist prior to exposure.

To ensure adequate cross-linking, the photoresist has to be exposed to 180mJ cm^{-2} of UV light (365 nm). After this a post exposure bake was performed for 2 minutes at 110°C using a contact hot plate. Samples were taken straight from the post exposure bake stage and then submerged in an ammonium hydroxide based developer (AZ 826 MIF). Development occurred under light agitation for a minimum of 2 minutes, and at least 30 seconds after developing appeared completed by visual analysis.

3.3.2.2. METAL DEPOSITION

The sequential deposition of a titanium adhesion layer and the gold micro electrodes was achieved by either thermal evaporation of both metals or by DC sputter coating of titanium and thermal evaporation of gold.

For thin film electrodes (up to 50 nm thick) the sole use of thermal evaporation was employed with the *BOC Edwards 306 Manual Vacuum Coater* and the experimental setup shown in Figure 58. Initially a 5 nm adhesion layer of titanium was evaporated onto patterned glass slides, which was subsequently followed a 20 - 50 nm gold layer by thermal evaporation.

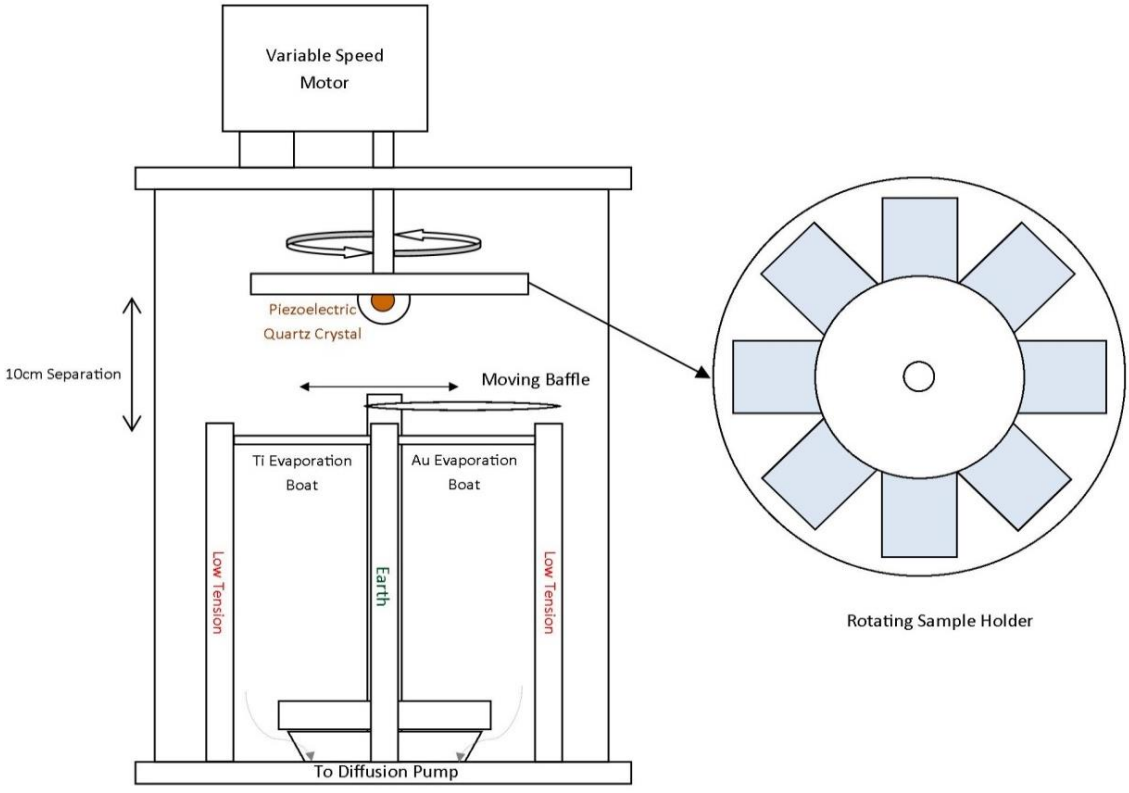

Figure 58: Schematic of current thermal evaporation setup

Though this method was successfully employed for the production of thin film gold electrodes up to 50 nm thick, unfortunately this method proved ineffective for depositing thicker gold electrodes of up to 200 nm thick. This was due to the loss of samples due to the extreme heat required to evaporate thicker titanium adhesion films (approximately 20 – 30 nm thick).

Thus it was decided to investigate sputtering the titanium adhesion layers onto the glass prior to evaporating the gold, as this could be performed at much lower temperatures. A simple DC sputter method was implemented in which a very high current was applied to the target metal while the vacuum chamber is flooded with argon. This presented several obstacles, especially with metals such as titanium which has an enthalpy of atomisation of 471 kJ mol^{-1} (compared to 368 kJ mol^{-1} for gold, and 338 kJ mol^{-1} for copper), as any other connecting metal would likely sputter before a high enough current is achieved to allow for titanium sputtering [149]. Thus all surfaces and connectors in line with the titanium sputter head have to be thoroughly insulated from the ionised argon. A prototype DC sputter head developed here (Figure 59) relied on the use of PDMS to insulate all connectors and the copper heat sink plate.

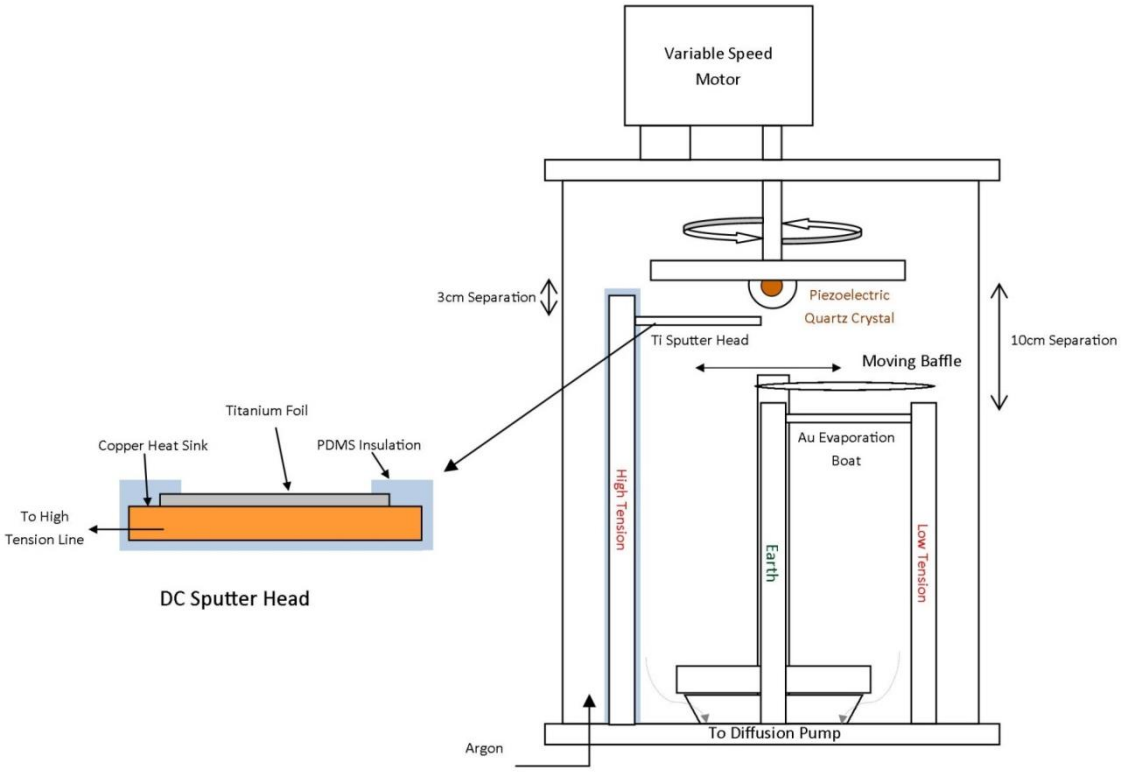

Figure 59: Schematic sputter and evaporation chamber

3.3.3. IONTOPHORESIS AND ELECTROOSMOSIS

Transdermal fluids from pig skin obtained by iontophoresis (Figure 60A) were prepared and supplied by the Department of Pharmacy and Pharmacology at the University of Bath. These were obtained by using a sample of pig skin with a 5 mM NaCl solution as both the electrode-

side saline and as the subcutaneous fluid. Though the composition of these extracts would be different from sweat or extracts obtained by electroosmosis (Figure 60B), the same constituent compounds would be observed in each case. As such these extracts served as an approximation for the kind of transdermal fluids that would be obtained from a living subject.

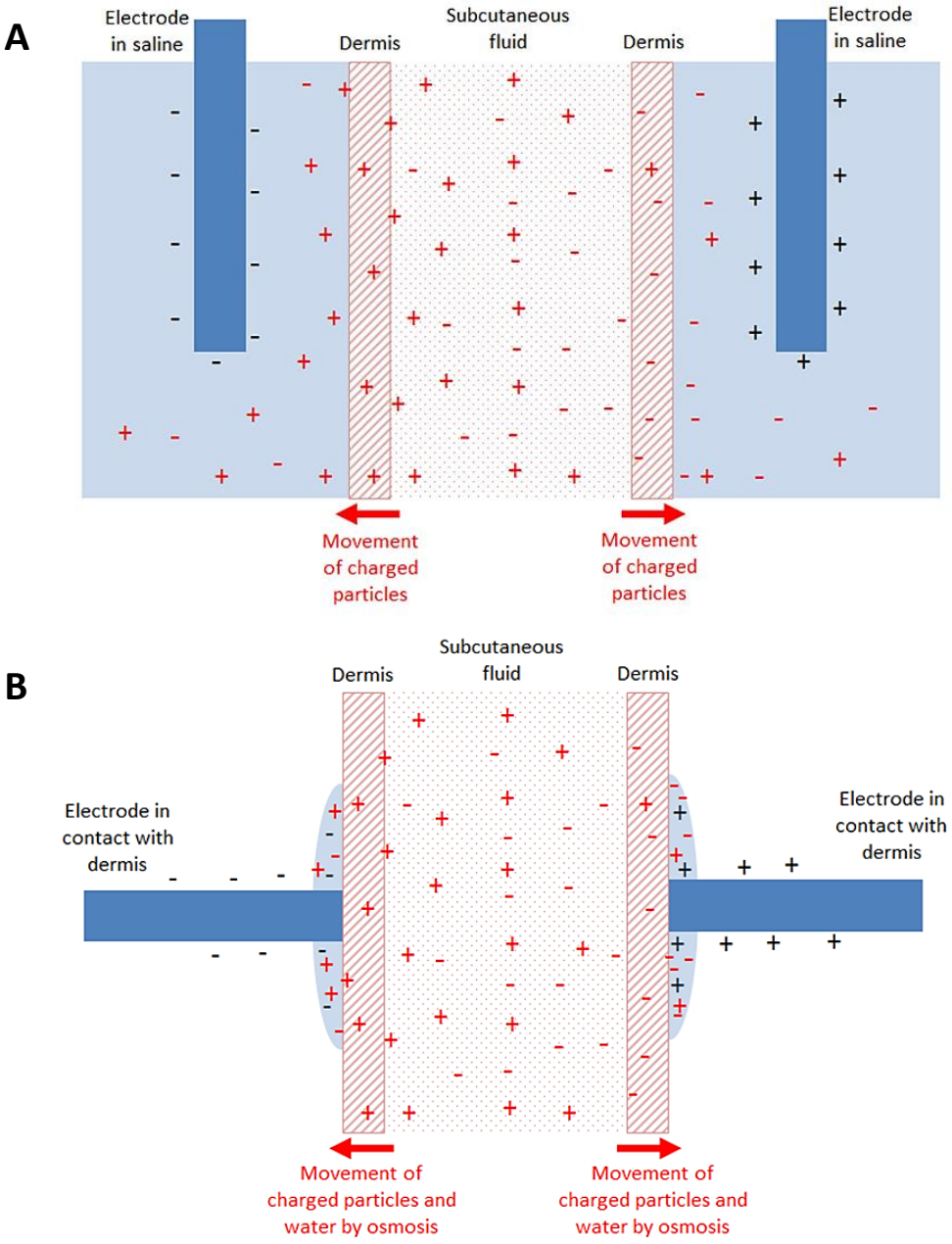

Figure 60: Principles of Iontophoresis and Electroosmosis (A and B respectively).

3.3.4. IMMOBILISATION OF GOx

GOx was immobilised using a simple potential cycling method developed during this project which employs electrostatic attraction. This method takes advantage of the fact that GOx from *Aspergillus niger* has an isoelectric point at pH 4.2 and thus is negatively charged in our stock PBS solution [150].

In order to electrochemically attract and adsorb GOx, six CV scans were conducted between 0.42 V and 0.60 V (vs. SCE) at a scan rate of 1 mV s^{-1}, in a PBS solution containing 15 mg ml^{-1} GOx (approximately 270 U ml^{-1} as per activity rating of manufacturer). This relatively positive scan range allowed the enzyme to be drawn to the hPG electrodes and attach by a combination of physical adsorption and electrostatic attraction. Detachment of GOx would thus not be observed in use as a glucose sensor (since a positive potential is again applied) and in its use as the anode in a fuel cell since again a positive potential is maintained on the electrode.

The amount of GOx immobilised onto the hPG electrodes, was estimated by performing a kinetic assay (provided by Megazyme Ltd.) of the enzyme solution before and after the immobilisation procedure and assuming no enzyme losses during the process [92].

3.3.5. IMMOBILISATION OF LAC

Initially this project was focussed on the use of a fungal LAC from *Trametes versicolor* (TvLAC) for the production of an oxygen reducing anode, since it is cheaper and more readily available than laccases from other sources. However, since TvLAC has an isoelectric point at pH 3.2 [151], it would also carry a negative charge in PBS and thus would detach from a negatively charged anode if simple immobilisation methods such as adsorption or electrostatic attraction were employed. It was thus pertinent to use permanent immobilisation techniques such as covalent linking or entrapment.

Some initial experiments utilising complex techniques from literature [89, 152, 153] gave inconclusive results so it was decided to use a much simpler amine functionalised aniline/polyaniline technique which has been proven to be successful on gold [154-157]. In this technique amine functionalised polyaniline acts as an enzyme binding site and a potential electron relay. In order to limit the formation of long chain polyanilines, and instead encourage the formation of an aniline monolayer on the surface, it is important to use a non-polar electrolyte such as acetonitrile or acetone [154]. An aniline monolayer is preferential since it would decrease the distance between the enzyme and the gold surface and thus electron transfer could either occur directly, or through short relays [157]. This method had the added benefit of reportedly being highly successful with numerous enzymes including LAC and GOx [77, 154].

The functionalisation of hPG electrodes occurred as follows. An anhydrous acetone electrolyte containing 2 mM p-nitrophenyldiazonium tetrafluoroborate and 100 mM tetrabutylammonium tetrafluoroborate was prepared. The hPG electrodes were submerged in this electrolyte and two

cyclic scans were performed between 0.6 V and -0.6 V at a scan rate of 100 mV s^{-1}. This stage facilitated the attachment of nitro-phenyl groups on the electrode surface.

The electrodes were then taken to a 10% ethanol and water solution containing 0.1 M potassium chloride and two cyclic scans were performed from 0.0 V to -1.4 V at a scan rate of 100 mV s^{-1}. This stage facilitated the exchange of nitro groups for amino groups required for enzyme attachment (see Figure 61).

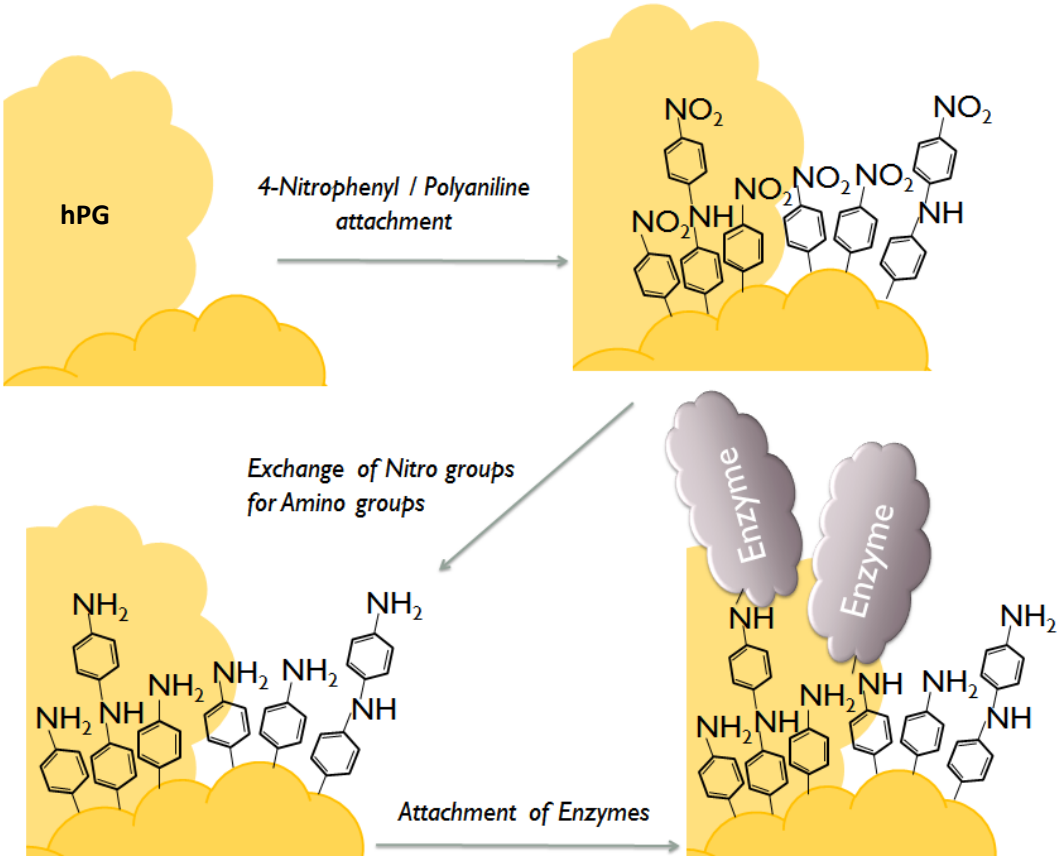

Figure 61: Schematic showing sequence of events during enzyme attachment

Following functionalisation the hPG electrodes were used either directly with LAC or underwent further modification by thiol blotting. Thiol blotting was achieved by overnight incubation (at room temperature) of the already functionalised hPG electrodes in an aqueous solution containing 10 mM 6-mercapto-1-hexanol. 'Blotting' of the thiols then occurred by self-assembly on the non-functionalised facets of the hPG surface. The hPG electrodes were taken from their previous solution and rinsed several times using PBS prior to enzyme attachment.

Enzyme attachment was either achieved by incubation with the raw enzyme in a PBS solution, or by incubation with an activated enzyme solution. In the first case functionalised hPG electrodes were then placed in 1 ml of a PBS solution containing 270 active units of LAC (as per activity rating of manufacturer) and left at room temperature for 2 hours, or incubated overnight

at 4°C. In the latter, 270 units of LAC was first activated by incubation for 30 minutes in 0.38 ml of a 50 mM aqueous sodium periodate solution (a weak oxidiser). This LAC solution was made up to 1.0 ml by the addition of 0.62 ml of a 100 mM Na_2HPO_4 solution and the functionalised hPG electrodes were subsequently submerged in this LAC solution for 90 minutes to allow adsorption and absorption of LAC onto and into the hPG surface.

Finally the electrodes were taken from the LAC solution and, after repeated rinsing in a 10 mM 2-morpholinoethanesulfonate (MES) buffer, were submerged in a solution containing 10 mM MES, 20 mM N-hydroxysuccinimide and 40 mM 1-(3-dimethylaminopropyl)-3-ethylcarbodiimide for 2 hours before being rinsed with and stored in PBS until required. This stage ensured crosslinking between enzymes immobilised on the surface by adsorption.

The use of TvLAC was subsequently followed with experiments utilising LAC from *Rhus vernicifera* (RvLAC) since it has an optimum pH between 6.8 and 7.4 and as such was determined more suitable since the pH of a physiological buffer is usually between 7.1 and 7.4 [158]. In both cases the immobilisation procedure was the same.

3.3.6. FUEL CELL MANUFACTURE AND OPERATION

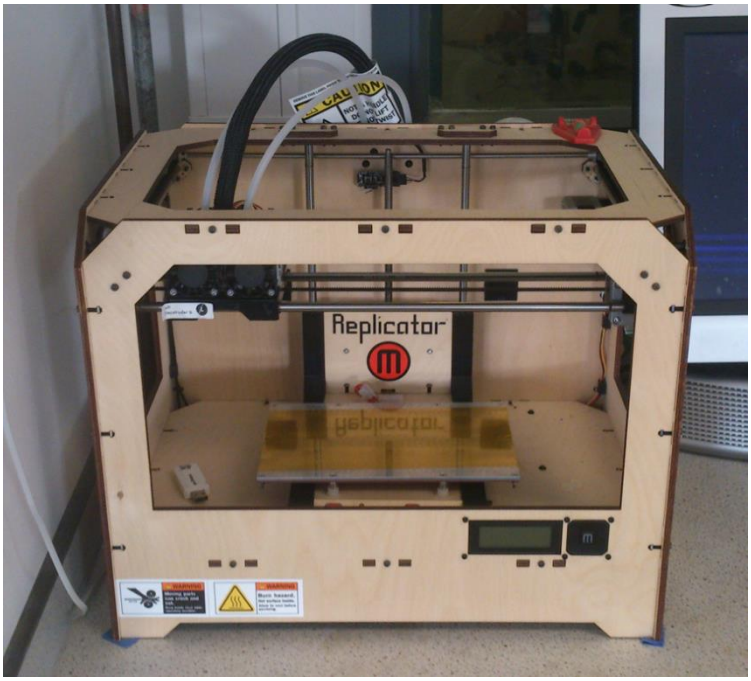

Figure 62: Makerbot Replicator Desktop 3D printer.

The fuel cells were prepared from 3D designed PDMS channels secured between acrylic plastic. Two different fuel cell designs were considered. In the first design two 1 cm long enzymatic electrodes were placed in parallel channels (each with a 3 mm x 3 mm cross-sectional area) separated by a PBMS wall (Figure 63A). In the second fuel cell pleated electrodes were used to

increase the electrode surface area within a similar fuel cell volume. These were made by repeatedly folding 3 cm long electrodes to occupy a 1 cm by 0.5 cm area. These electrodes were not physically separated from each other, but rather positioned in the channel (10 mm x 3 mm cross-sectional area) such that the electrolyte flowed over the LAC electrode and the GOx electrode sequentially (Figure 63B).

The channels through which the feed solution would flow and all other voids in the final fuel cell design were 3D printed in polylactic acid, using the Makerbot Replicator Desktop 3D printer (Figure 62). This was then used as a mould over which PDMS was cast to create the final fuel cell design (Figure 63C). Once the enzymatic electrodes were inserted, the voids around the bare wires was sealed using silicon sealant and the PDMS fuel cell was clamped between two pieces of acrylic plastic (Figure 63D).

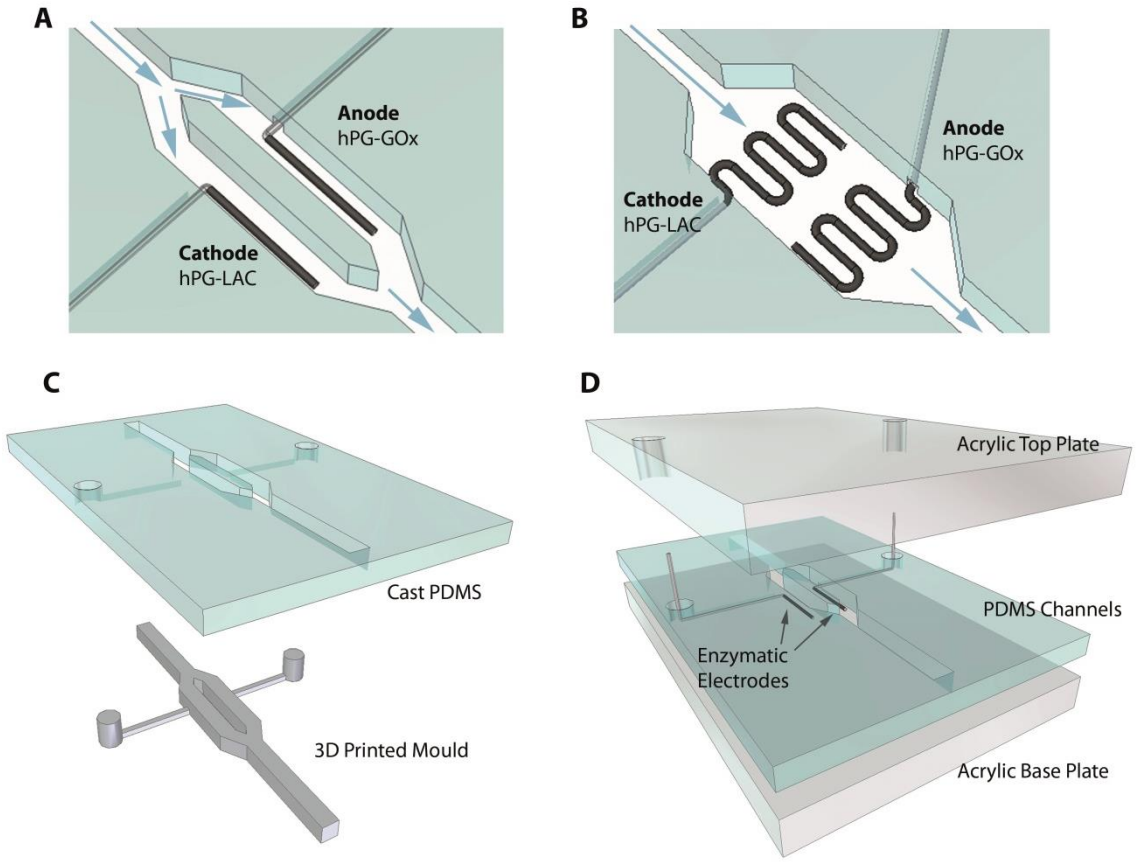

Figure 63: Schematic of fuel cell construction and different configurations considered; A – the 3D printed channels and cast PDMS negative, B – electrode arrangement within constructed fuel cell (exploded), C – parallel channel fuel cell design, D – single channel fuel cell with pleated electrodes (from our unpublished work [159]).

The constructed fuel cells were consequently placed inside an incubator at 37°C and continuously fed with a PBS solution containing 27 mM glucose at a rate of 0.35 ml min^{-1} (Figure 64). The feed solution was aerated prior to entering the incubator and passed through a tubing

coil inside the incubator which acted as a heat exchanger ensuring the feed solution reached 37°C. Finally the feed solution passed through a drip to remove any gas bubbles that evolved in the process of heating the solution prior to entering the fuel cell as the presence of air bubbles in the fuel cell can cause fluctuations in power output.

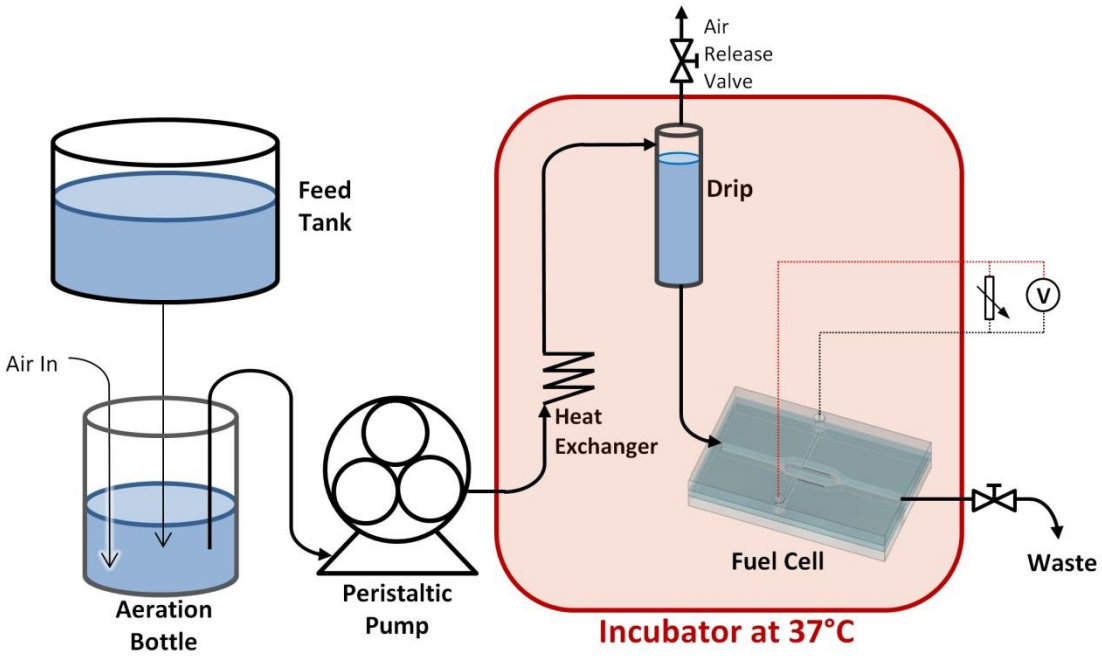

Figure 64: Experimental setup used during fuel cell operation

3.3.7. OTHER ANALYTICAL METHODS

The surface morphology of the NPG electrodes as well as the quality of the microelectrodes produced were analysed using a *Hitachi S-4300* field emission scanning electron microscope (FESEM) and a *JEOL JSM6480LV* scanning electron microscope (SEM). In addition to this visual analysis was used as a quick check to ensure adequate porosity of samples (since highly porous samples appeared black, whereas less porous samples appeared dark gold or brown after electroplating [160]). In addition to this, the thickness of the gold and titanium films produced was verified using a *Veeco/Digital Instruments Nanoscope III SPM* atomic force microscope (AFM).

4. FABRICATION OF HIGHLY POROUS GOLD ELECTRODES

Though many techniques for the production of nPG or hPG electrodes were considered, it was decided to use a simple hydrogen templated electroplating method in order to directly deposit hPG onto the surface of gold electrodes. This method was chosen due to two key reasons; the associated cost of using this method was considered to be by far the lowest, and the method was considered to be the most versatile since, in theory, it could be used for many different shapes and sizes of electrodes such as electrodes patterned on glass or gold wire electrodes. Several variations of this method were used based on a method adapted from literature [130].

4.1. hPG GOLD DEPOSITION

Initially hPG films were deposited onto gold disk test electrodes using a method taken from literature [130]: An aqueous electrolyte was prepared consisting of 0.1 M $HAuCl_4$ and 1 M NH_4Cl. Gold was then potentiostatically deposited using a working potential (*E*) equal to -4 V (vs. SCE) and a platinum counter electrode. This potential was maintained for 20 s to allow sufficient gold deposition and rapid hydrogen gas evolution.

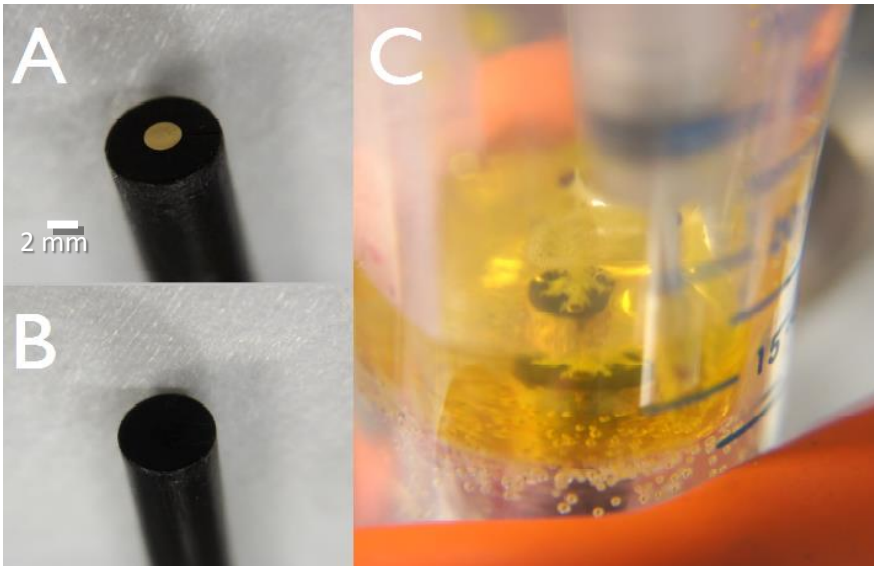

Figure 65: hPG deposition; gold disk electrode before and after electrodeposition of hPG (A and B respectively), C- image showing rapid evolution and removal of gas from upward facing gold disk electrode during electroplating process

The resulting hPG gold structure appeared black (see Figure 65) indicating a very high level of porosity in the nanometre scale [130]. However, due to the rapid evolution and removal of hydrogen gas, the gold structure produced was unstable, so much so, that pieces of black hPG would flake off of the surface of the gold disk if it was disturbed revealing the original polished surface. SEM images of the gold surface revealed that the hPG was not evenly distributed across

the gold surface, but instead occurred in sparsely distributed clusters (Figure 66). Thus it was decided to try and develop a new electroplating protocol which could stabilise the NPG structure by improving the adhesion of the NPG to the gold surface.

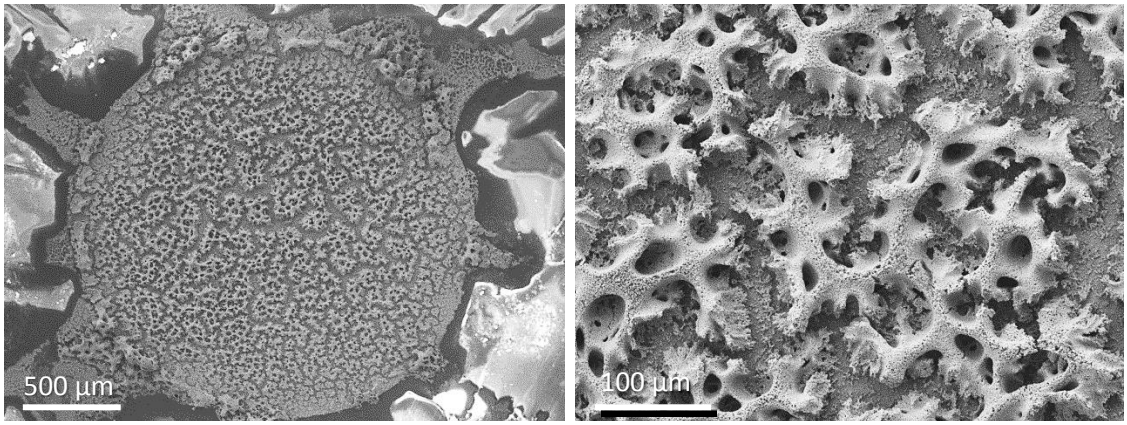

Figure 66: SEM images of hPG deposited on a gold disk electrode using a technique from literature.

Following some experimentation, it was discovered that the visible evolution of hydrogen gas first occurs at a working potential of -0.7 V (vs. SCE). At this potential the evolution of hydrogen gas is slow and thus it can be assumed that the gold structure is less porous. Visual comparison of two electrodes prepared at -0.7V and -4.0V showed that the one prepared at -0.7 was much lighter in colour (a rusty brown) compared to the one prepared at -4.0V which was black. This suggests that, as expected, the average pore size of gold electroplated at this potential is much higher, since less light is adsorbed (assuming that light is absorbed when the pore size nears the wavelength of light). The electrode prepared using the much less negative potential of -0.7 V also exhibited no signs of flaking suggesting that adhesion of the electroplated gold was stronger.

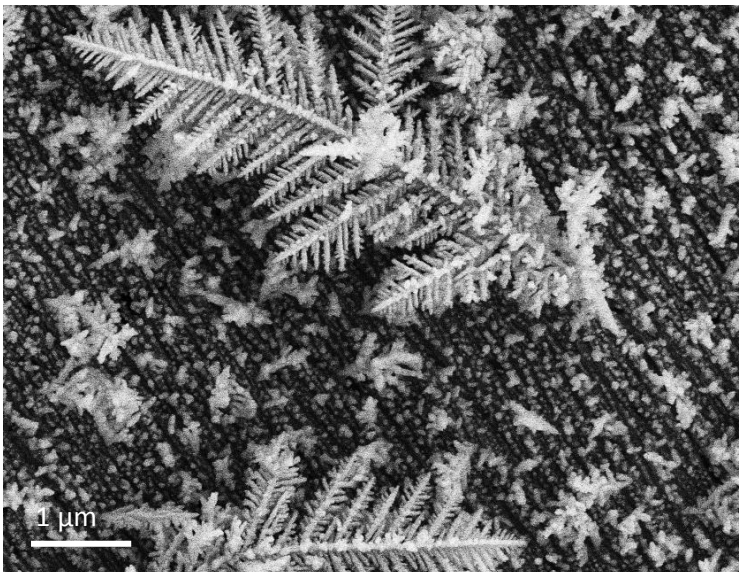

Figure 67: Feather-like gold microcrystals produced by direct electrodeposition at -0.7 V (vs. SCE).

FESEM analysis of the gold structures produced by electrodeposition at -0.7 V revealed an array of feather-like gold microcrystals (Figure 67). It was postulated that these microcrystals grown on the surface of the electrode could act as an anchoring system to prevent hPG from flaking off of the surface. It was thus decided to use a multi stage deposition process in order to improve the adhesion of the NPG. Initially the working potential was set to -0.7 V for a period of 5 seconds, after which the working potential of the electrode was gradually stepped down to -4.0 V and maintained at this potential for a further 10 seconds. The resulting hPG structures produced were stable and exhibited no signs of flaking. SEM analysis of electrodes produced in this fashion showed a very developed hPG film with extremely high degree of porosity. The pore size were in the 10-50 µm range and were themselves lined with pores, some as small as 5 nm (Figure 68).

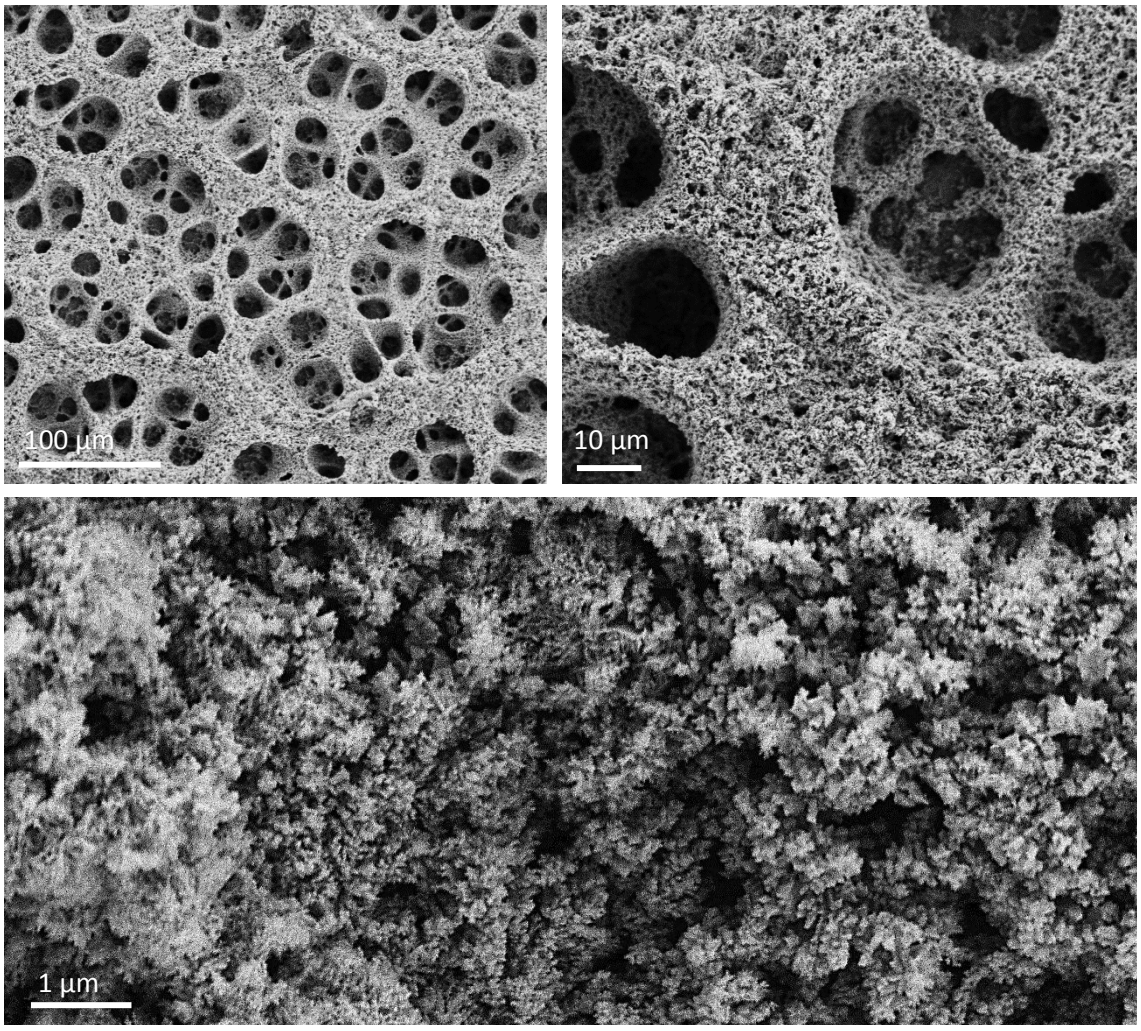

Figure 68: SEM images of hPG films produced by multi-step down potentials.

4.2. CHARACTERISATION

Figure 69 compares the general CV scans obtained from a polished gold disk electrode and a hPG disk electrode produced between -0.8 and 0.8 V (vs. SCE). As it can be seen there is a stark difference between the two cases which is not merely limited by the differences in current observed. In general the hPG appears to be much more reactive than the polished gold electrode. The polished gold electrode does not appear to exhibit any reactions in the scan range considered, except for the reduction of oxygen at potentials below -0.2 V (vs. SCE) [161].

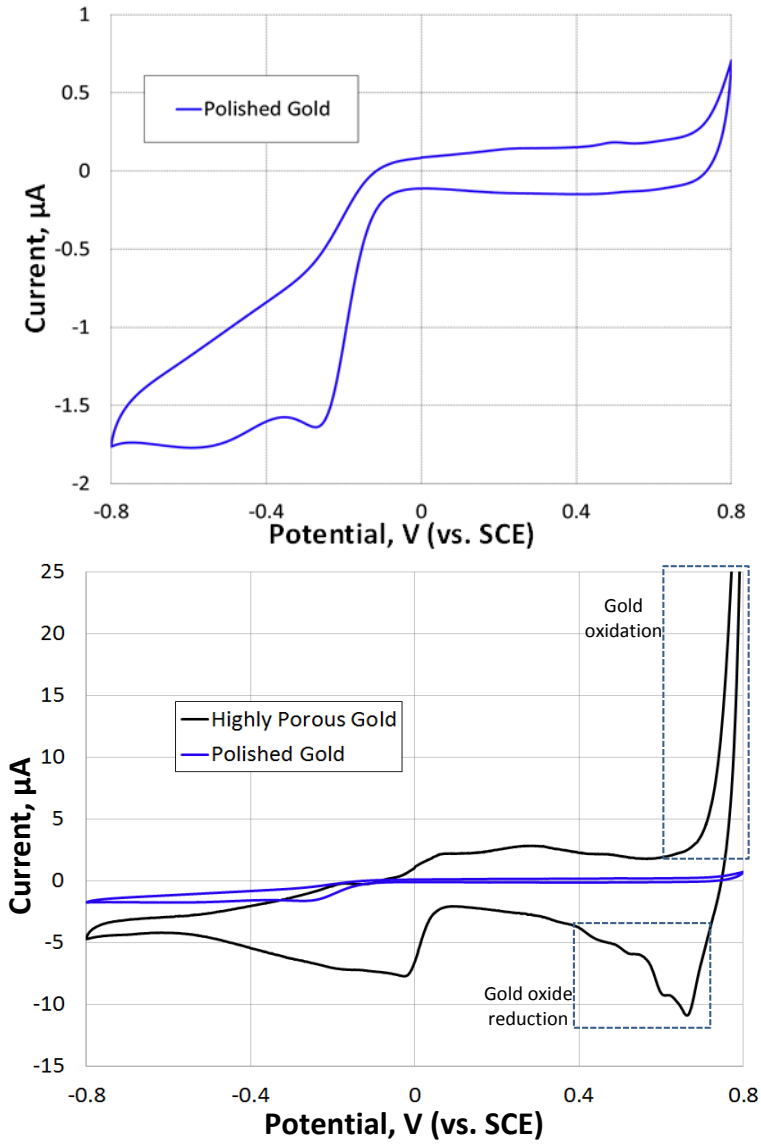

Figure 69: CV scans of polished gold disk electrode (2 mm diameter) and same electrode deposited with hPG film. Scans were performed in PBS at a rate of 10 mV s^{-1} and in both cases the second scan is shown here.

In contrast a several reactions appear to be occurring on the hPG surface. Most notably the oxidation of gold begins to occur at 0.7 V (vs. SCE), which is a much less positive potential than

expected (gold oxidation in an aqueous electrolyte typically occurs at approximately 1.2 V (vs. SCE) [162]). The oxidation of gold is accompanied by a sequence of reduction peaks observed from 0.7 – 0.5 V (vs. SCE) on the reverse scan (these do not occur in the absence of the oxidation on the forward scan as demonstrated later in Figure 73).

The reduction of oxygen also appears to occur at a much less negative potential than is typical with polished gold (approximately +0.05 V (vs. SCE)). This reaction is verified in Figure 70 where CV scans were conducted in the same range as before, but this time in the absence of oxygen.

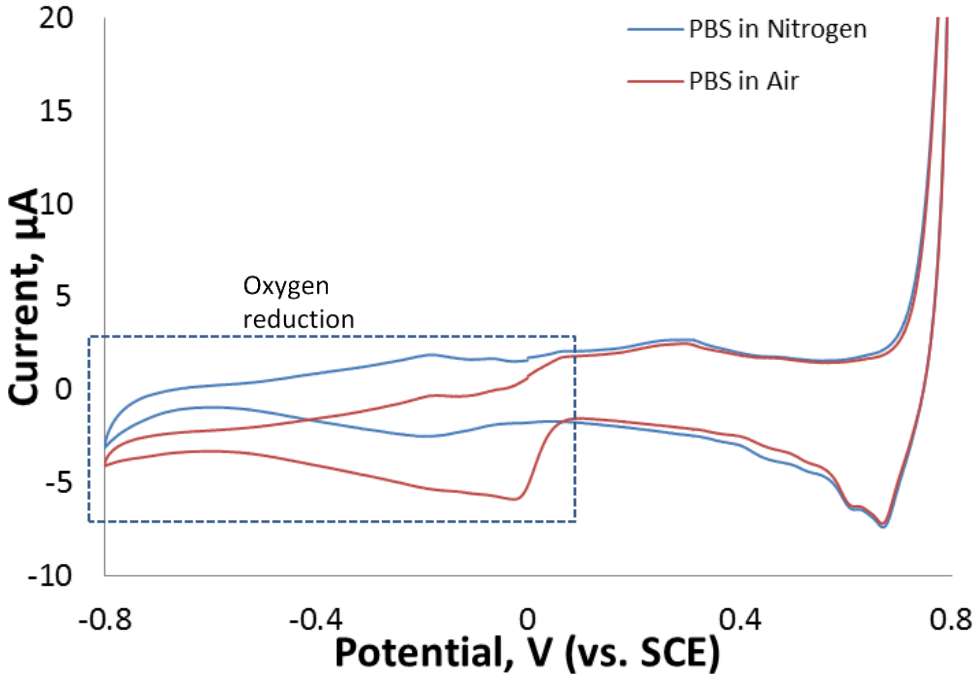

Figure 70: CV scans of hPG disk electrode (2 mm diameter) in the presence and absence of oxygen. Scans were performed in aerated PBS and deoxygenated PBS solutions at a rate of 10 mV s^{-1} and in both cases the second scan is shown here.

In addition to an apparent higher reactivity for standard gold reactions (oxygen reduction and gold oxidation and reduction), there also appears to be weak oxidation peak at approximately 0.3 V (vs. SCE). Interestingly the magnitude of this peak, and its corresponding reduction peak, increases with continued cycling (Figure 71).

This suggests that the continued cycling of the applied potential on the hPG electrode works to activate this redox reaction at the gold surface. A redox peak in this region has commonly been reported in literature when using gold nanoparticle composite electrodes [163]. In these cases this redox peak is attributed to the reduction and oxidation of phosphate contained in the PBS buffer which does not occur on smooth gold surfaces.

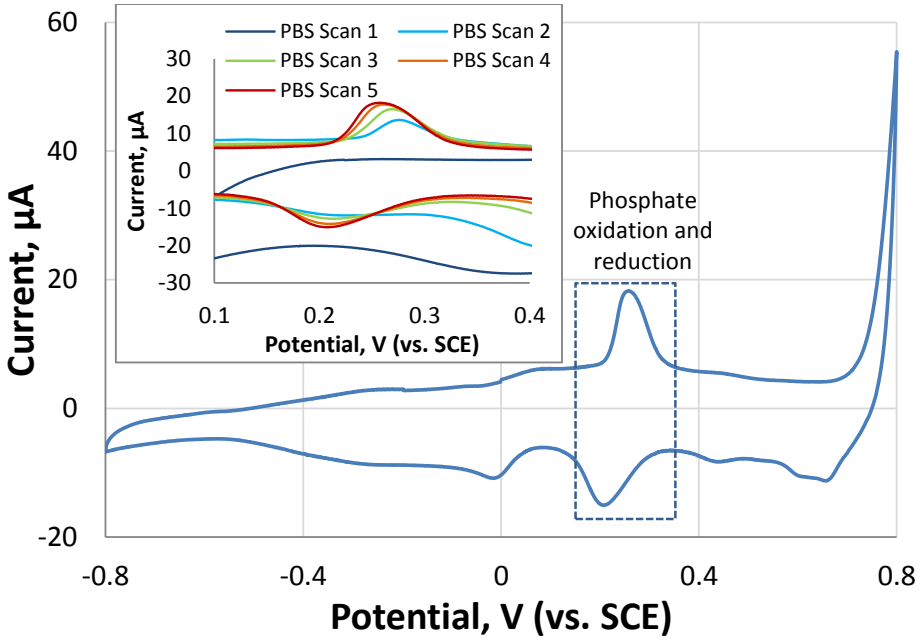

Figure 71: Sixth CV scan of a hPG electrode and the evolution of the redox peak observed at 0.3 V (insert). Scans were performed in PBS at a rate of 5mV s^{-1}.

Since it is clear that the hPG surface created here is highly reactive, and as such reacts to compounds which polished gold does not react to, extra care has to be taken to isolate the exact origins of each peak witnessed here. This is especially true when using redox mediators in solution such as ferrocence, which typically exhibits a redox peak at approximately 0.3 V (vs. SCE), and so could be confused with the phosphate peak demonstrated to occur here.

To complicate things further, in the presence of glucose, a pronounced glucose oxidation peak is also observed in this same region (Figure 72).

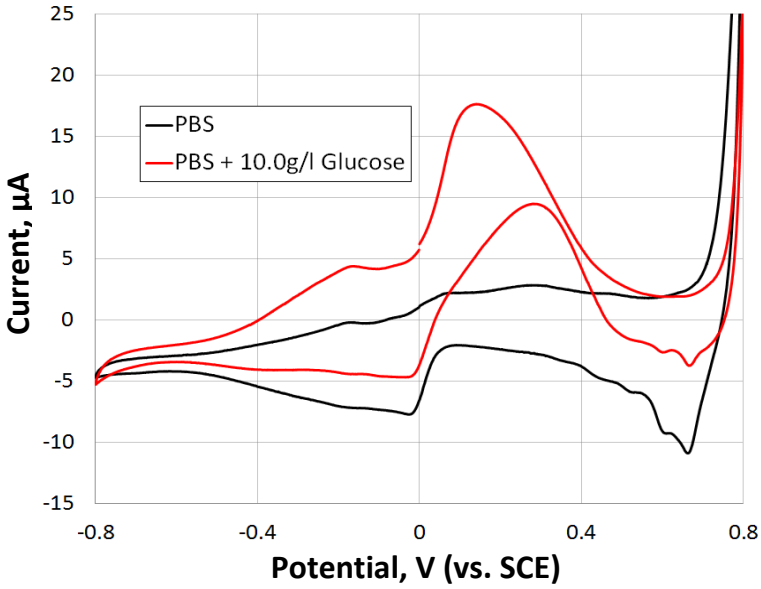

Figure 72: CV scans illustrating the oxidation of glucose on hPG. Scans conducted in PBS and a PBS solution containing 10 g l^{-1} glucose. Scans were performed at a scan rate of 5 mV s^{-1} and the second scan is shown in both cases.

The oxidation of glucose to gluconic acid at neutral pH is typically not possible on smooth gold surfaces, though much research has been conducted into the development of non-enzymatic glucose sensors which utilise gold nanoparticle composites or nPG films [113, 120, 164, 165].

This has been a topic of keen interest since non-enzymatic glucose sensors would not be affected by temperature and pH, or be denatured by toxins and harsh storage conditions such as the enzymatic sensors widely in use currently [166].

4.3. SURFACE AREA - ESA

The surface area of the hPG films was determined electrochemically by their ESA. Though this does not give the absolute surface area of the hPG, it gives the surface area freely accessible to the electrolyte so serves as a more accurate determination of the surface area available for electrochemical analysis. The ESA was determined as described in Section 3.2.2.2. by comparison of the capacitance of a polished gold disk electrode and that of a hPG electrode. In order to measure the capacitance of an electrode it is key to analyse the electrodes in a potential range where no oxidation or reduction peaks are observed. It was thus decided to measure the capacitance by in the potential range between 0.425 V and 0.6 V, since no oxidation or reduction peaks are observed in this scan range providing that the gold surface has not been oxidised. Figure 73 shows the typical CV scans obtained from both polished gold and hPG films.

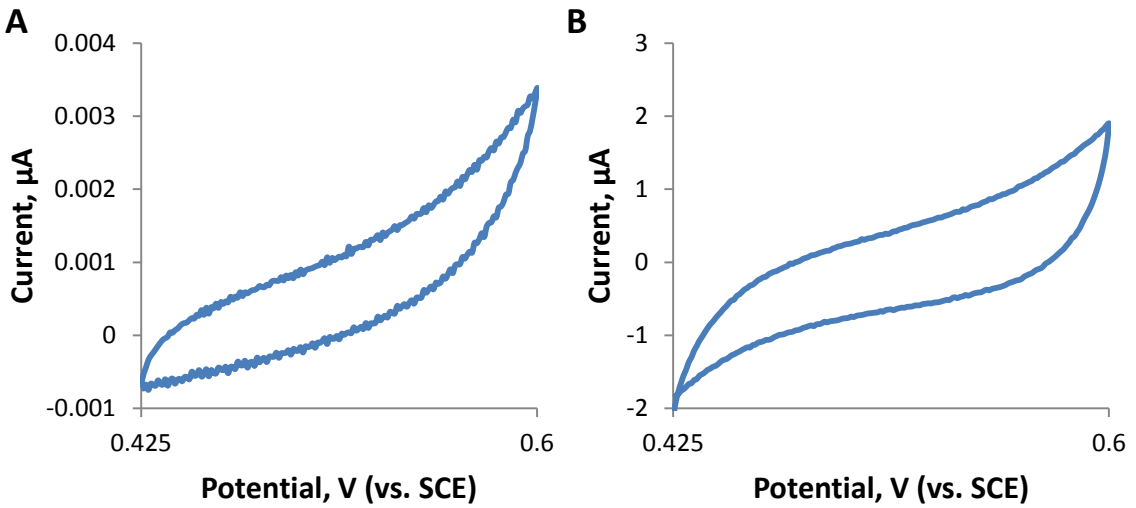

Figure 73: Determining the capacitance of polished gold and hPG films; A – CV scan of polished gold disk electrode (2 mm diameter), B – CV scan of hPG film on same electrode. In both cases scans were performed in PBS between 0.425 and 0.6 V at a scan rate of 1 mV s^{-1}. The third CV scan is shown in each case.

There is a stark difference in the current observed in each case with the polished gold showing current levels in the nA range and the hPG showing current in the µA range. The ESA of the hPG was determined to be approximately 28.99 cm^2 with a standard deviation of 18% (from 9 replicates). In comparition the surface area of the polished gold electrode was calculated to be

only 0.03 cm^2. This means that the direct electrodeposition of hPG films increases the ESA of an electrode by a factor of approximately 1000.

4.4. hPG ON ALTERNATE BASE MATERIALS

4.4.1. LAB-ON-A-CHIP SCALE ELECTRODES

The applicability of the methodology adopted to produce hPG electrodes on thin-film gold electrodes was subsequently investigated. The intent here was to demonstrate the possibility of implementing this method for the direct electro-deposition of hPG films on a lab-on-a-chip scale electrode, and thus to develop cost-effective miniature devices or disposable test strips with varied geometries.

Thin film gold electrodes of a range of different thicknesses were prepared on glass slides as described in Section 3.3.2. and hPG was subsequently deposited as per the existing protocol. Unfortunately however initial tests showed that during the rapid evolution of hydrogen gas at -4.0 V the patterned electrodes were often damaged resulting in a very low success rate (Figure 74). Even when thicker gold film electrodes were employed (up to 150 nm thick) there was a large degree of detachment of the underlying gold film (Figure 74C).

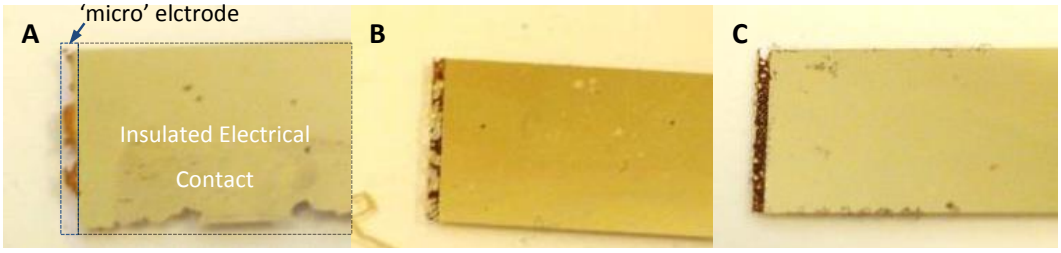

Figure 74: Detachment observed during electroplating for gold film thicknesses of 20 nm (A), 100 nm (B) and 150 nm (C).

An investigation into the levels of detachment observed at different deposition potentials revealed that the majority of gold film detachment only occurred when the applied potential was more negative than -2.5 V (vs. SCE). Thus it was decided to use the weaker potential of -2.5 V during the electrodeposition of hPG onto electrodes patterned on glass slides. The resulting electrodes showed a much lower degree of detachment of the underlying gold films (Figure 75).

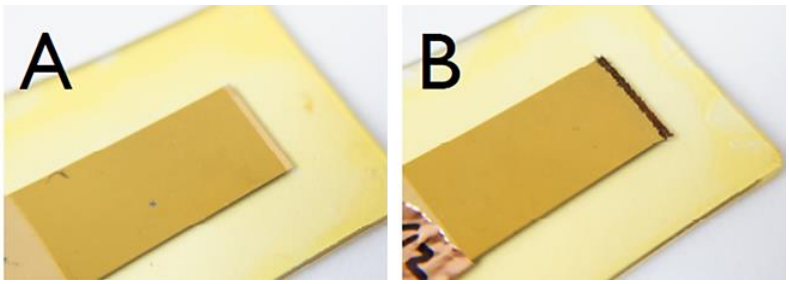

Figure 75: 'Lab-on-a-chip' scale electrodes before (A), and after (B) electrodeposition of hPG at -2.5 V (vs. SCE)

FESEM analysis of the hPG electrodes produced at this potential showed that there was a greater variance in the morphology of the deposited gold (Figure 76). This is most probably due to the fact that the gold foam was much less developed at weaker deposition potentials. A mixture of different structures is observed which are comparable with those observed at the different stages of hPG deposition onto gold disk electrode. Again large pores were formed, but this time the inside of the pores contained some of the feather-like gold structures observed previously after deposition at -0.7 V (Figure 76C, D). Along the ridges of these pores however the structure of the gold was comparable with that observed on gold disk electrodes at the end of the electrodeposition process (Figure 76B).

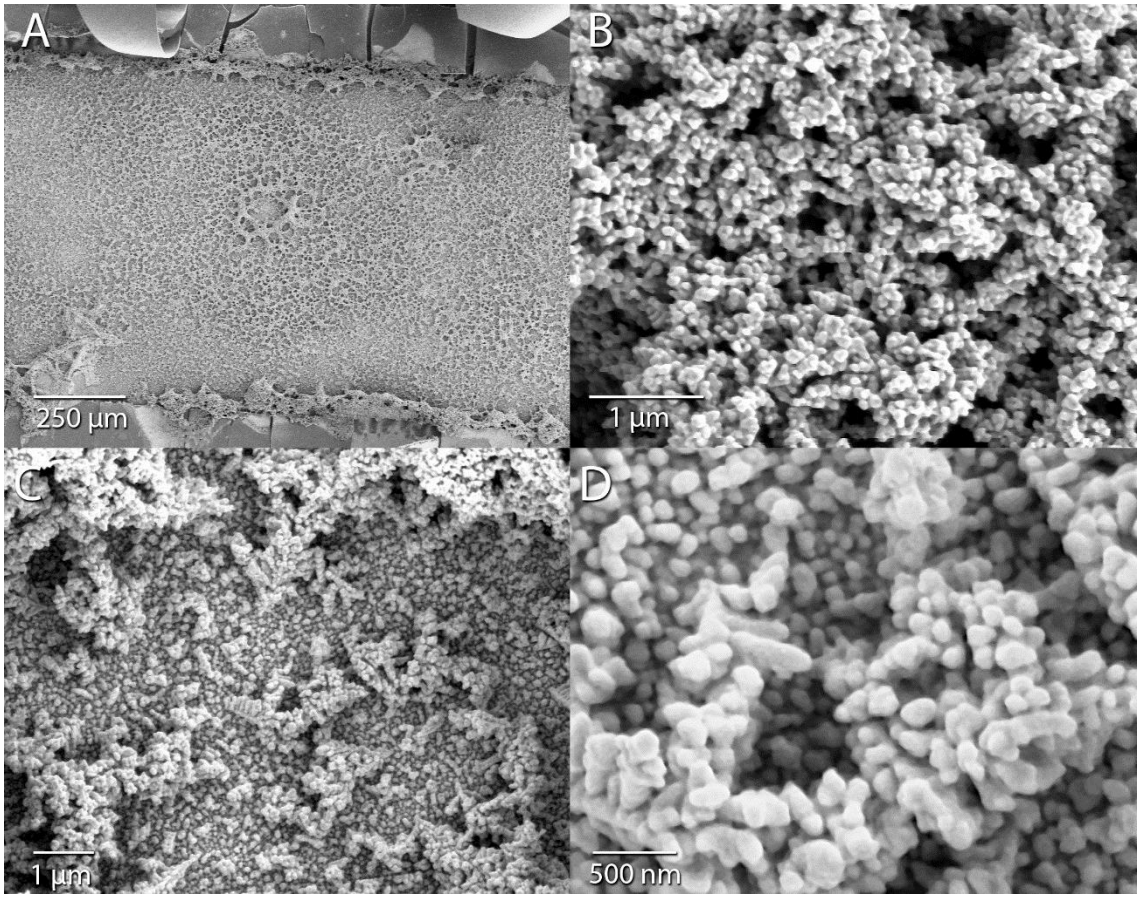

Figure 76: FESEM images of different regions on the hPG patterned microelectrode: A - whole electrode view (flaking on edges due to chemical treatment of photoresist); B - view of gold structures on large pore ridges, C and D - different gold structures within large pores.

Thus, for the first time it was demonstrated that the direct electrodeposition of nPG is viable for use on thin film (100 nm thick) gold electrodes [131]. Since this method uses much less gold than the established Au/Ag dealloying methods previously used for producing porous gold structures on thin gold film electrodes, it can be considered to be a much cheaper method for producing porous gold structures on the lab-on-a-chip scale.

4.4.2. METAL AND CARBON ALTERNATIVES

Up to this point the direct electrodeposition of hPG had only been demonstrated on gold surfaces. To increase the scope of these type of electrodes, and to potentially reduce the cost associated with such high surface area gold electrodes, it was decided to investigate the possibility of the direct electrodeposition of hPG films onto alternate materials.

The first alternate material considered was the use of 0.5 mm thick platinum wires. Initially, the same protocol established for the deposition of hPG films onto gold disk electrodes was used. FESEM analysis of the hPG surfaces deposited onto platinum wires in this fashion revealed a very highly developed hPG film with a wide pore size distribution analogous to the porous gold films obtained on gold disk electrodes (Figure 77). The weight increase corresponding to the deposition of hPG revealed that approximately 1 mg of gold was deposited for every 1 cm of platinum wire (based on the total weight increase of 30 samples). Thus approximately 6 mg of gold is required per 1 cm^2 of electrodeposited hPG. Additionally, due to the rigidity of platinum wire in comparison to high purity gold wires, these hPG on platinum electrodes were much more stable than pure gold electrodes, since they were less susceptible to accidental damage. Consequently electrodes such as these were later used in continuous flow EBFCs developed during this project (Chapter 7).

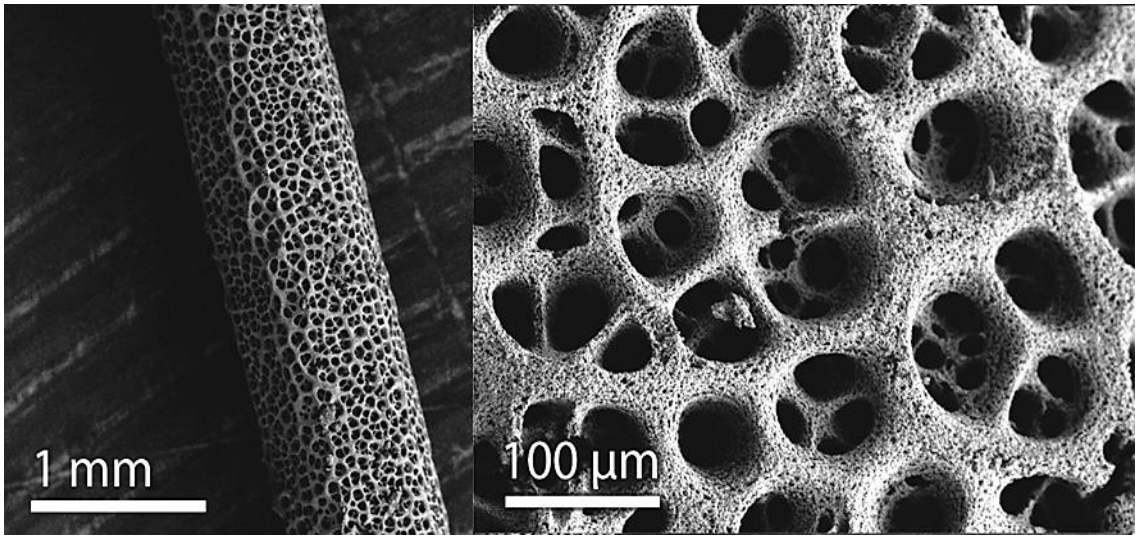

Figure 77: FESEM of hPG film deposited on a platinum wire under potentiostatic control [159]. Approximately 1 mg of gold was deposited here.

Unfortunately, due to the relatively high potentials involved, the resulting current required for the sustained electrodeposition of hPG films was accordingly high. Therefore in order to maintain potentiostatic control this method could only be applied to electrodes with relatively small surface areas so that the corresponding current levels required fell within the capabilities

of the potentiostat (< 1 A). This limited the surface area on which hPG could be deposited to approximately 0.31 cm^2 (or a 2 cm long piece of 0.5 mm thick platinum wire).

It was thus decided to develop a protocol for the deposition of hPG onto conductive surfaces without the need for potentiostatic control. This was achieved by simply measuring the actual applied potential between the WE and CE during electrodeposition using a voltmeter. It was determined that at -4 V (vs. SCE) the potential applied between the WE and CE was approximately 10 V. Using a bench top DC power supply this potential was then applied between two pieces of platinum wire to see if the same types of hPG structures could be realised. Figure 78 shows the FESEM of a 3 cm long piece of platinum wire which has been pleated to minimise superficial size. As shown, the structures produced in this fashion are the same as those produced under potentiostatic control with a comparable pore size distribution.

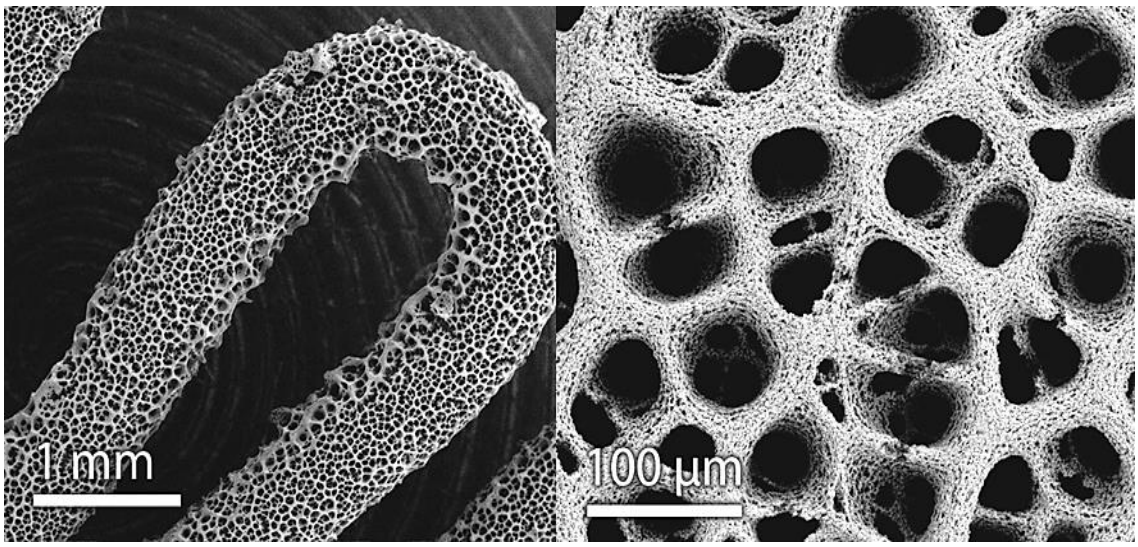

Figure 78: FESEM of hPG film deposited on a platinum wire under manual control with a DC power supply [159].

Regrettably the use of noble metals as the base for hPG deposition has very high associated costs. Much cheaper conductive surfaces were therefore also considered. Initially hPG was deposited onto copper electrodes. Though deposition appeared successful, with a black porous layer being formed analogous to the hPG films already produced, the underlying copper surfaces quickly underwent oxidation leading to a blue-green colourisation. Since similar galvanic responses were probable with many other transition metals, it was decided to instead focus on the use of cheap carbon-based materials which would not readily oxidise. The possibility of such 'gold plated carbon' electrodes would greatly reduce the cost of producing such extremely high surface area electrodes which exhibit high levels of reactivity to many chemicals including glucose.

The use of graphite was first considered since it is highly conductive and would have minimal resistance to the flow of current. Initially very high purity graphite was used. By experimenting with different deposition potentials gold deposition onto graphite first became evident at approximately -0.5 V (vs. SCE). It was thus decided to deposit gold at this potential for FESEM analysis, as well at -0.7 V (vs. SCE). Figure 79 shows the different crystal structures produced at these potentials.

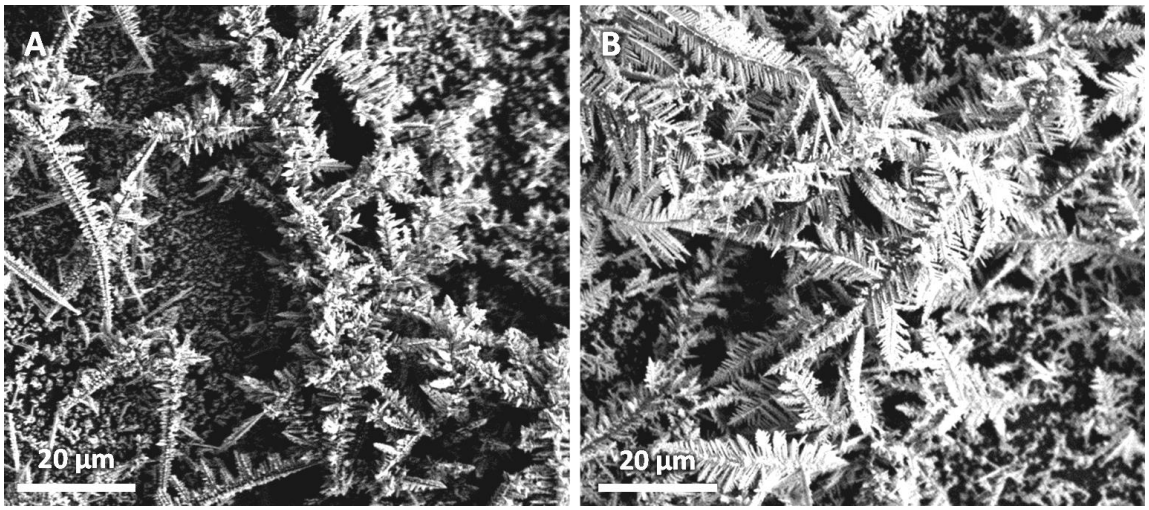

Figure 79: FESEM of crystalline gold structures electrodeposited onto high quality graphite; A – structures produced after 20 s at -0.5 V (vs. SCE), B – structures produced after 20 s at -0.7 V (vs. SCE).

As shown, marked differences between the crystalline structures produced in each case are observed here. When the less negative potential of -0.5 V (vs. SCE) is used a central spine is formed out of which gold structures grow in two planes forming cross shaped stacks. The growth of gold also appears to be perpendicular to the central spine. In contrast the typical featherlike crystal structures are formed at -0.7 V (vs. SCE). These appear to grow only in a single plane (thus forming 'flat' feathers), and growth occurs at a 45° angle from the central spine. Though these results are quite interesting, and further investigation is warranted to determine the effects of these different crystal morphologies, this only served to confirm that the same structures of gold are evident when using the same deposition potentials on gold and on graphite.

Following these experiments, it was decided to use much lower quality graphite which is cheaper and more readily available than the high quality graphite. Graphite composites which normally serve as mechanical pencil leads were consequently employed. To verify that the same deposition potentials resulted in the same hPG structures a preliminary deposition was carried out at -0.7 V (vs. SCE).

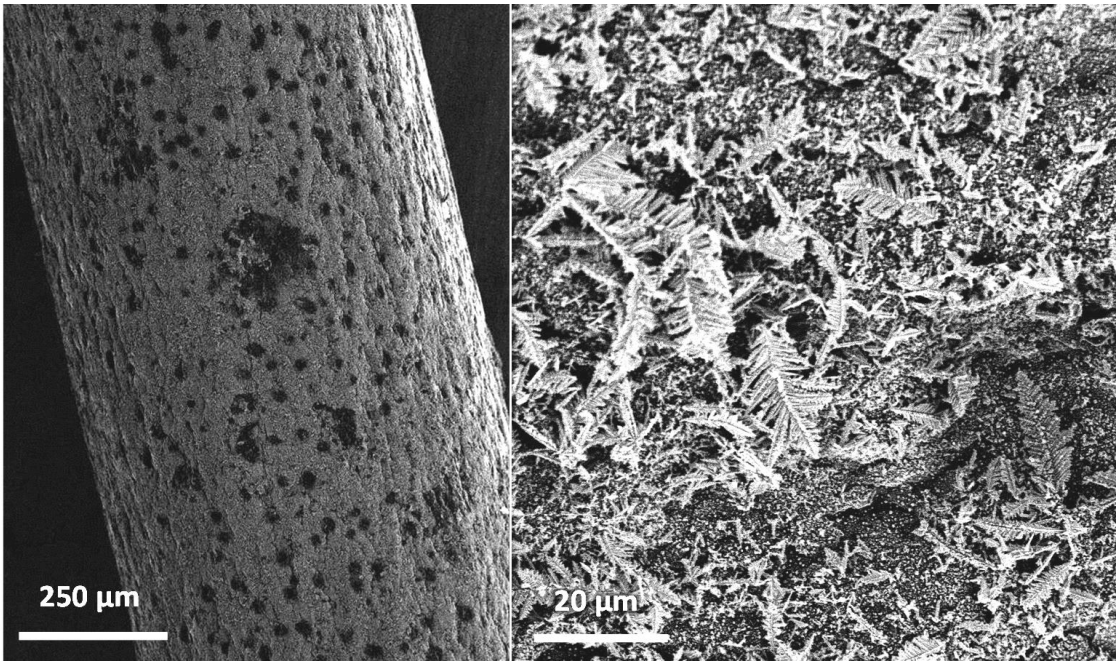

Figure 80: FESEM of mechanical pencil graphite after deposition for 5 s at -0.7 V (vs. SCE).

Figure 80 shows FESEM images of the mechanical pencil graphite after this stage. The typical featherlike gold crystal structures that occur at this potential were observed. Additionally these images revealed that this low quality graphite was itself already littered with pores. This means that the underlying graphite electrode already has an elevated surface area. This textured surface should serve to improve the attachment of the hPG and hence reduce flaking.

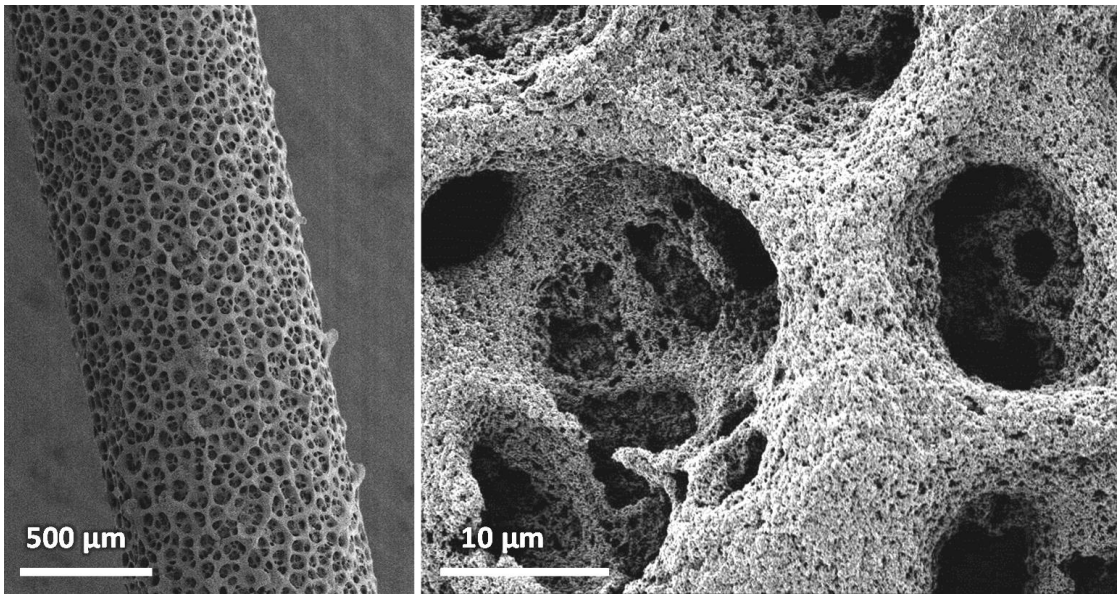

Figure 81: FESEM of mechanical pencil graphite after full hPG deposition.

Figure 81 shows the morphology of the hPG-graphite electrode produced after the subsequent full deposition of hPG according to the established protocols. The same porous structure is observed, which demonstrates the possibility of also using cheap carbon based materials as a base for hPG deposition. These extremely high surface area electrodes exhibit the same

properties as hPG electrodes on gold or platinum, but at a fraction of the cost. This achievement greatly increases the commercial viability of such electrodes.

The use of graphite based electrodes also has their own drawbacks. The principle problem associated with such electrodes is the possibility of accidental breakage since graphite of this type is extremely brittle. With a view to creating low-cost, flexible hPG composite electrodes it was thus decided to investigate the possibility of using carbon fibres as a base for hPG deposition.

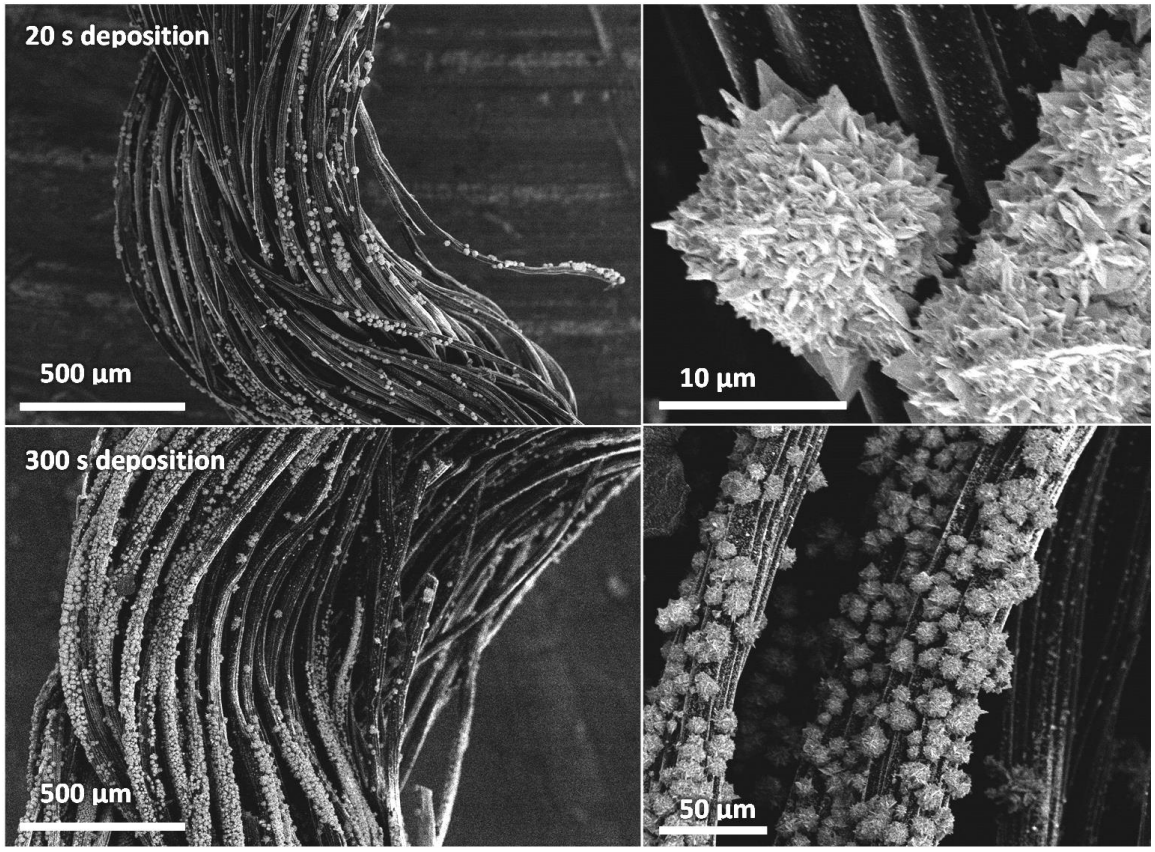

Figure 82: FESEM of jagged gold clusters formed by direct electrodeposition onto carbon fibres

Initially carbon fibres were used on their own as the WE in a standard three electrode potentiostatic setup. The same existing protocols were used as already established. Unfortunately however the carbon fibres were unable to achieve current levels high enough to result in the evolution of hydrogen gas. Instead a very slow rate of gold deposition was evident on the carbon fibres. Analysis by FESEM of the morphology of the gold structures produced revealed a series of gold clusters on the surface of the carbon fibres (Figure 82). These were clusters where broadly spherical in nature with sharp jagged crystal edges. Interesting there was little distribution in the size of these clusters with all observed clusters measuring between 10 and 20 µm. Even when the deposition step at -4 V (vs. SCE) was extended to 300 s these clusters remained exactly the same size though the overall coverage of these clusters was much higher.

In an attempt to try and increase the level of gold deposition and to produce more developed gold structures it was decided to instead use carbon cloth threaded with a gold wire during the direct electrodeposition of gold. The gold wire would serve to increase the overall conductivity of the system during deposition and allow the simultaneous evolution of hydrogen gas and deposition of gold. Any gold structures produced on the gold surface would also in theory develop around the surrounding carbon fibres, and would thus remain after the subsequent removal of the gold wire.

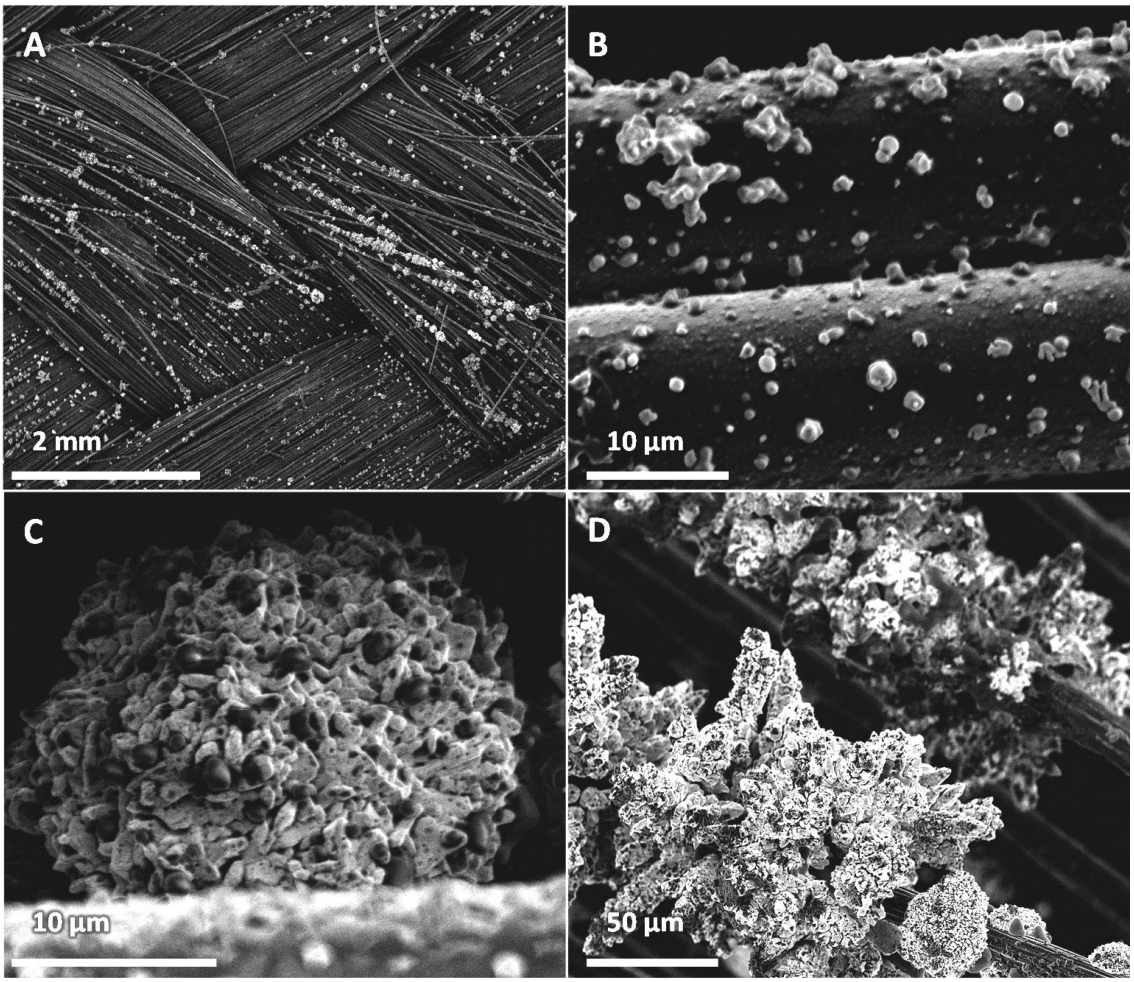

Figure 83: FESEM of different gold structures formed on carbon cloth following electrodeposition with an interwoven gold wire; A – overall view of the carbon cloth, B – small formations of gold on carbon fibres, C – spherical gold clusters formed in between carbon fibres, D – more developed amorphous gold crystal growths on carbon fibres.

Figure 83 shows FESEM images of the different gold morphologies observed in this case. A range of different structures were obtained. In general the carbon fibres showed a high level of surface roughening with small growths of gold (Figure 83B). These most probably served as seeding sites for the subsequent growth of different gold crystal structures. In between some of the fibres several spherical gold clusters were also observed (Figure 83C). In contrast to the clusters produced previously these did not have sharp jagged edges. Instead these clusters were much

more analogous to the types of structures created when producing porous gold nanoparticle agglomerates by direct electrodeposition [117] (see also Section 2.3.3.). Finally some of the carbon fibres also had much more developed amorphous gold crystalline structures (Figure 83D). These structures seemed to contain elements which were similar to the crystal structures produced previously. Ultimately however, these structures were not stable, since they detached from the carbon cloth during electrochemical analysis. It was thus concluded that a rigid base was required for the deposition of hPG, since the rigid crystal structures show poor adhesion to such a flexible base.

4.4. RECOVERY, REUSE AND RECYCLING OF GOLD

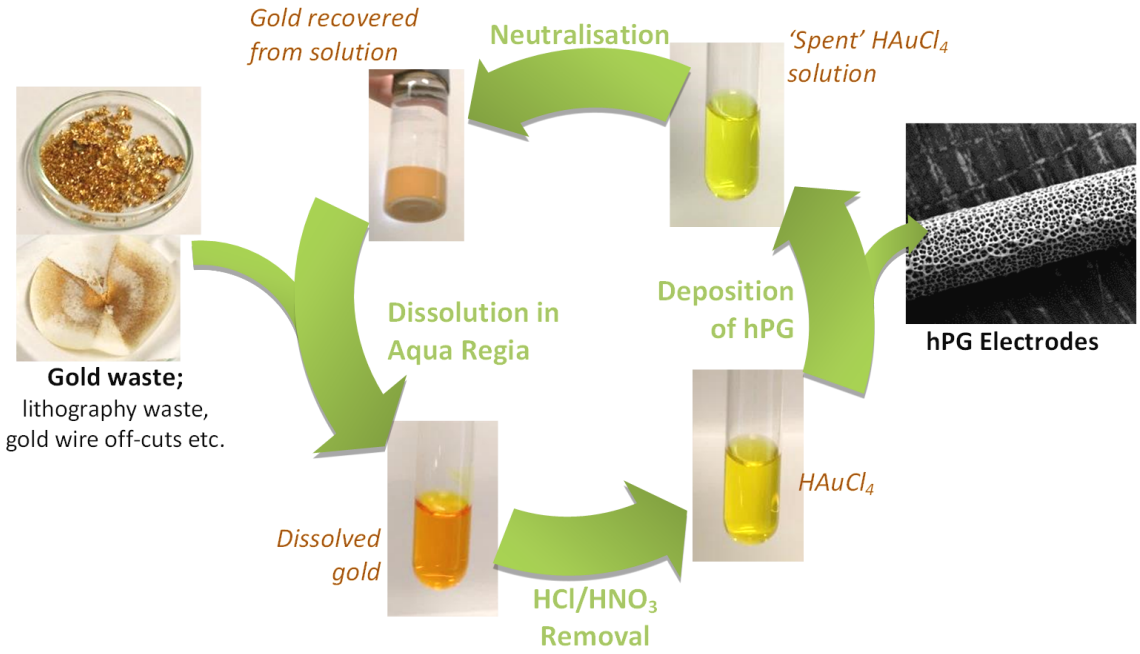

Figure 84: Gold recovery and $HAuCl_4$ synthesis cycle.

Though only very small amounts of gold are required to produce these hPG surfaces (approximately 15 pence of gold per cm^2 of hPG film deposited or 2.4 pence of gold per 1 cm long hPG wire), the associated cost of the gold involved in these processes can be quite high. This is due to the large amounts of unreacted gold still left in solution after the electrodeposition process. Additionally lots of gold waste is produced in the manufacture of microelectrodes or from the production of hPG electrodes on gold wires. In order to reduce the associated cost of producing such hPG surfaces, it is thus imperative to try and recover or repurpose as much of the gold containing waste as possible. In this project the solution was to use the gold waste to synthesise $HAuCl_4$ which could then be used in later depositions of hPG.

This resulted in the gold recycle loop shown in Figure 84. Gold recovered from spent electrodeposition solution, along with any other pieces of waste gold where weighed and then

dissolved in aqua regia (a 1:3 volumetric ratio of concentrated HNO_3 and HCl, or approximately a 1:2 molar ratio of said acids). The dissolution of gold in aqua regia results in the production of $HAuCl_4$ as per Equations 20 and 21.

$$Au + HNO_3 + 4HCl \rightleftarrows HAuCl_4 + NO + 2H_2O \qquad \text{Equation 20}$$

$$Au + 3HNO_3 + 4HCl \rightleftarrows HAuCl_4 + 3NO_2 + 3H_2O \qquad \text{Equation 21}$$

The dissolution of gold in this fashion had the added benefit of separating out trace amounts of titanium impurities from the adhesion layer used in the production of lab-on-a-chip scale electrodes, since titanium is one of a few metals which is impervious to aqua regia. Following the dissolution of gold in aqua regia, excess HNO_3 and HCl has to be removed. Fortunately the decomposition of HNO_3 in the presence of HCl spontaneously occurs at a very slow rate as per Equation 22.

$$HNO_{3_{(aq)}} + 3HCl_{(aq)} \rightarrow NO_{(g)} + 1½Cl_{2_{(g)}} + 2H_2O_{(l)} \qquad \text{Equation 22}$$

Since the molar ratio of aqua regia is less than the stoichiometric ratio of this decomposition, the removal of HNO_3 is achieved by the addition of a large volume of HCl under low heat. Once HNO_3 has decomposed a visible colour change from dark orange to yellow is evident (Figure 84) and the evolution of gas bubbles ceases. At this point excess HCl is removed by reducing to a slurry under a low heat. The synthesised $HAuCl_4$ is then diluted to the required concentration and used to create the hPG deposition electrolyte.

Once the hPG deposition electrolyte has been used, any unreacted gold chloride is precipitated out of the solution by neutralising the solution with the addition of NaOH. The precipitated gold is then washed several times with distilled water before being dried, ready for dissolution in aqua regia restarting the cycle.

5. HIGHLY POROUS GOLD ELECTRODES AS ABIOTIC GLUCOSE SENSORS

5.1. ELECTROCHEMICAL RESPONSE OF hPG TO ALDEHYDE GROUP CONTAINING SUGARS

As discussed previously, long range CV scans conducted on freshly prepared hPG disk electrodes in the presence of glucose revealed a clear glucose-dependent response. In particular, a strong oxidising peak on the forward scan was observed at approximately 0.15 V, as previously found to be the case on nPG films [113]. Accordingly the magnitude of the current peak changed with the concentration of glucose in the electrolyte (Figure 85).

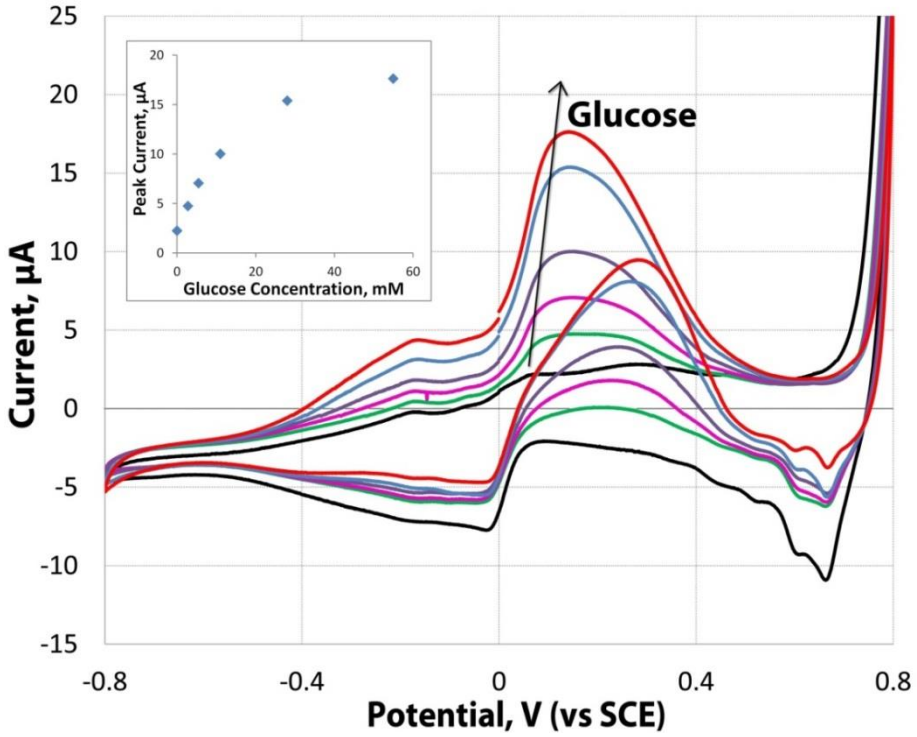

Figure 85: CV scans at 5 mV s^{-1} of the a hPG disk electrode at varied glucose concentrations (0.0, 2.8, 5.5, 11, 28, 55 mM) in PBS [131].

The electro-oxidation of glucose on a gold surface in a phosphate buffer has been the subject of numerous studies [167-169]. It has been reported that the main steps involved in the reaction are the formation of an OH layer on the gold surface, followed by glucose adsorption and dehydrogenation to form gluconolactone (Equation 23).

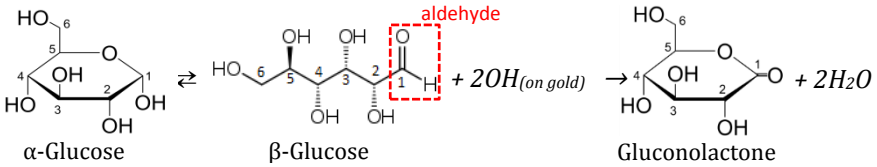

$$\alpha\text{-Glucose} \rightleftarrows \beta\text{-Glucose} + 2OH_{(on\ gold)} \rightarrow \text{Gluconolactone} + 2H_2O$$

Equation 23

The reaction involves the hydrogen atom bounded to the carbon C1 atom of glucose and other aldehyde group containing sugars. This is proven by the inertness of gold surfaces to ketoses and other non-reducing sugars that lack the reactive hydrogen on the carbon C1 atom [169].

To test whether this was in fact the case here, the reactivity of hPG electrodes towards other aldehyde group containing sugars apart from glucose was also tested. The sugars tested were maltose, lactose, and galactose. As a term of comparison, we also tested the hPG electrode response in the presence of fructose (a ketose), and sucrose (a non-reducing sugar).

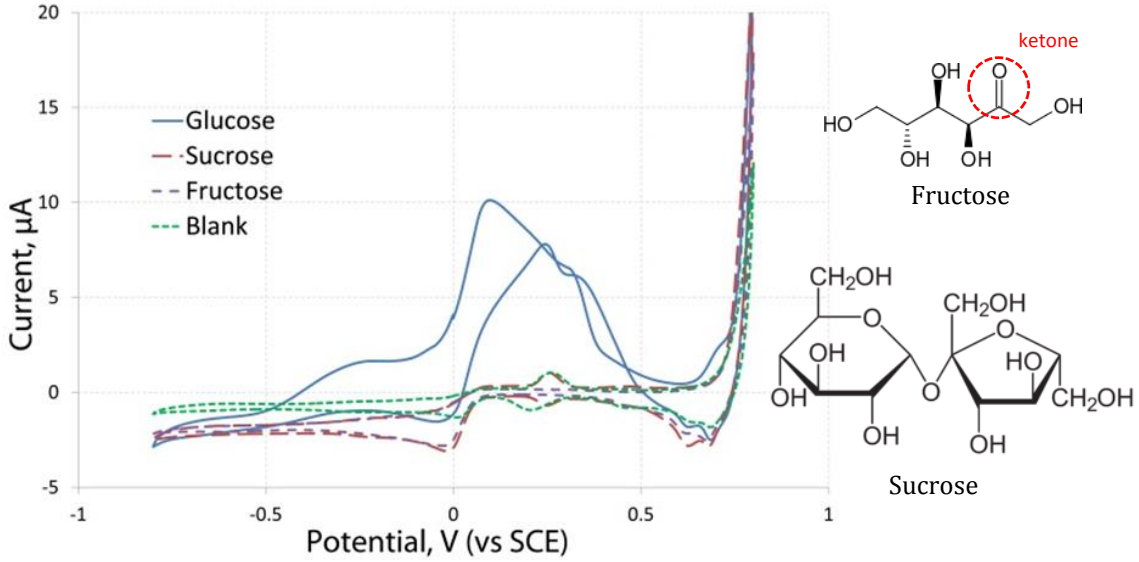

Figure 86: CV scans at 5 mV s^{-1} of hPG disk electrodes in PBS solutions containing 5 g l^{-1} of glucose, fructose, sucrose or no added sugar (blank). 3rd CV scan shown in each case [131].

Figures 86 and 87 show the CV scans obtained with a concentration of 5 g l^{-1} for each sugar in PBS compared with that of 5 g l^{-1} glucose and a blank scan in only PBS. As expected, in the case of fructose and sucrose, no relevant peak currents were observed when compared to blank scans conducted in PBS without any sugars (Figure 86). On the other hand, for each reducing sugar the forward peak at approximately 0.15 V (vs. SCE) was confirmed, although with slightly different shape in each case. This strongly suggests that the reaction detected does indeed involve the C1 in the aldehyde group.

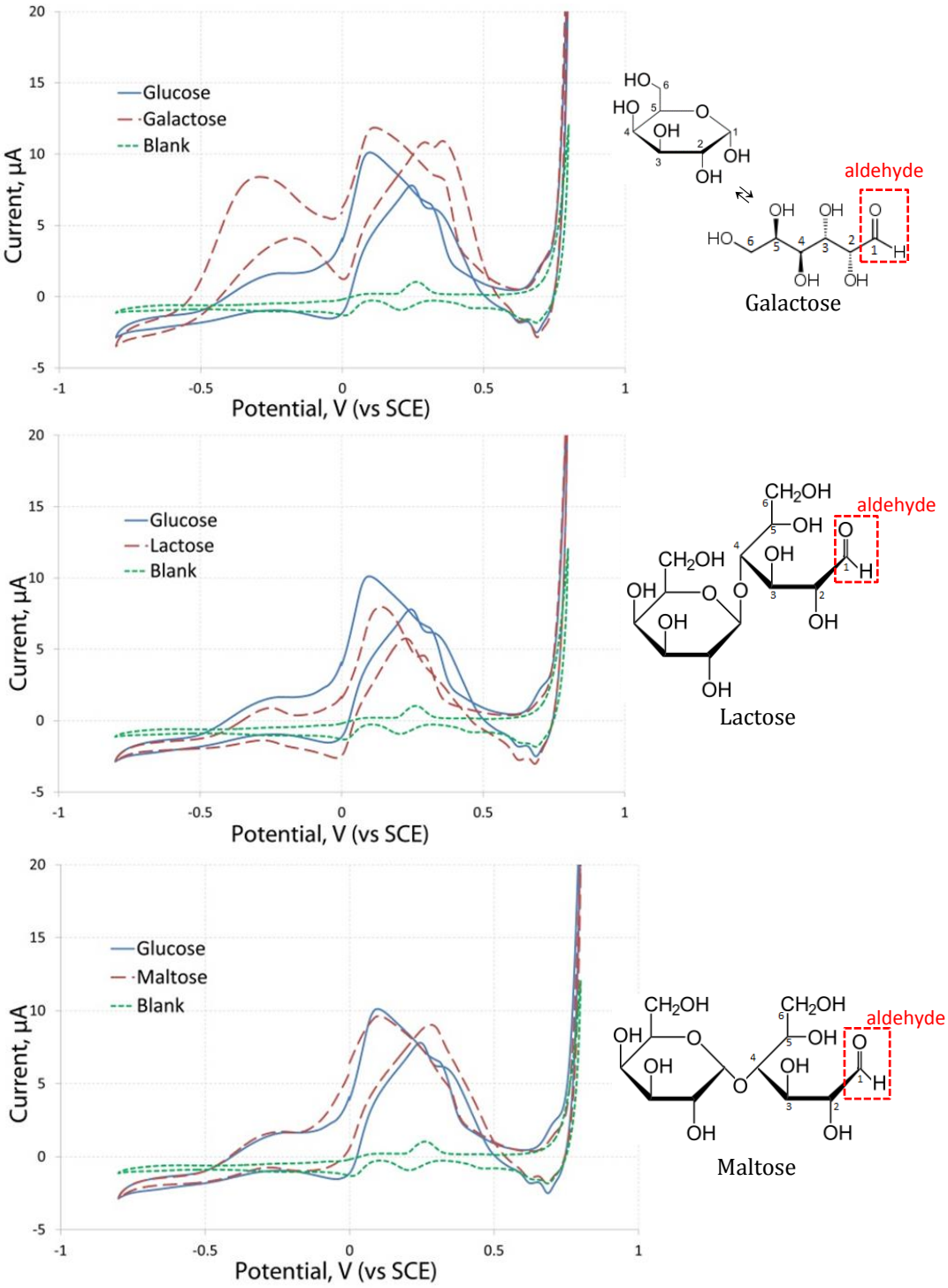

Figure 87: CV scans at 5 mV s^{-1} of hPG disk electrodes in PBS solutions containing 5 g l^{-1} of each different aldehyde group containing sugar considered in comparison to glucose and a no added sugar blank. 3rd CV scan shown in each case [131].

As shown by Figure 87, the general shape of the CV curves obtained was very similar for each sugar, with the exception of galactose. In the case of maltose and lactose the slight differences in the magnitude of the oxidation can be attributed to the fact that their different shapes can the affect the orientation of binding. Interestingly, in the case of galactose, a pronounced peak was also observed in negative scan ranges at around -0.3 V (vs. SCE). Since galactose is the C4

epimer of glucose the only difference in structure is the orientation of an OH group on the opposite side to the aldehyde group (in their ring formations). The peak at -0.3 V is most probably due to an interaction with this OH group, or the OH group of the galactose C6, which could also be affected by this change in orientation. These same OH groups are also present in lactose and thus a slight peak at -0.3 V can also be expected in CV scans of lactose though only a very slight peak was observed here (Figure 87). The CV curves can thus not be used to identify each specific sugar, but can at least be used to determine the presence of aldehyde group containing sugars and could also be used to specifically identify galactose.

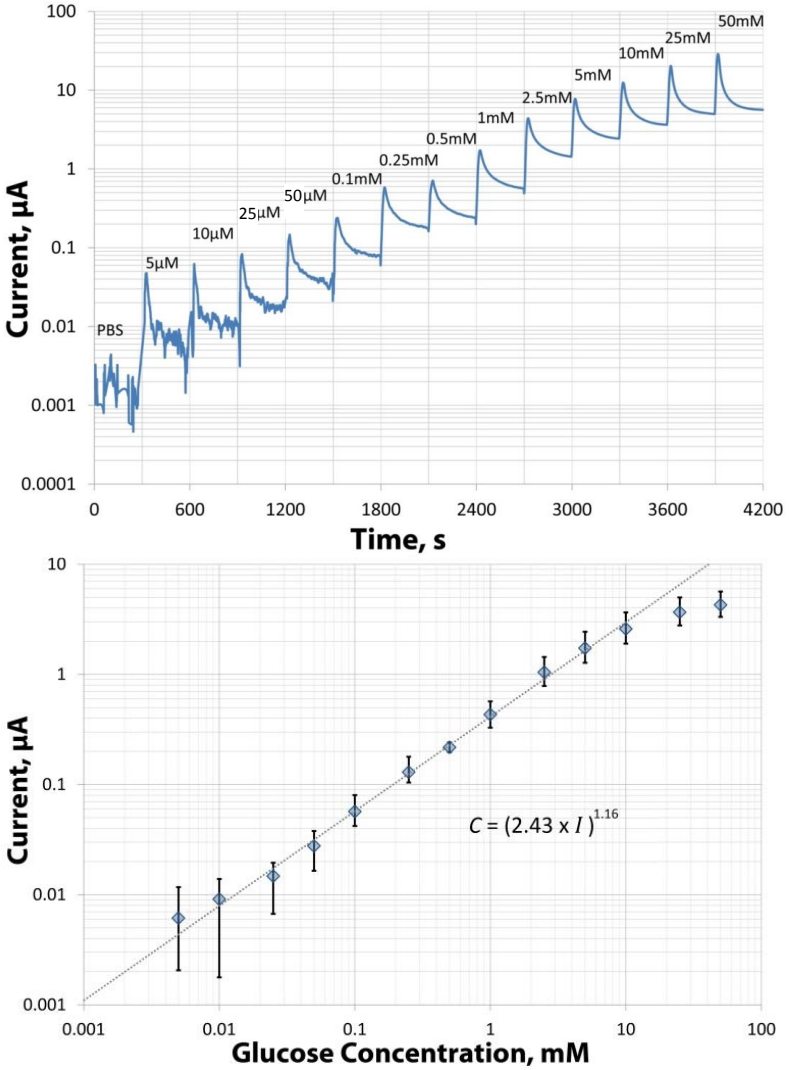

Figure 88: Amperometric response of hPG electrode response to glucose. Raw collected data from a single hPG electrode with repeated injections of glucose and collated data from 3 different hPG electrodes shown respectively. Tests were conducted at 0.15 V (vs. SCE) [131].

Following CV analysis of the different sugars amperometry was used to determine the sensitivity of hPG to glucose. This was achieved by measuring the current response at a constant potential of 0.15 V (vs. SCE), with repeated injections of glucose. Figure 88 shows the raw data collected during the process of injecting increasing amounts of glucose into a test cell, as well as the

overall trend observed with several repeats. A strong correlation between the current and the concentration of glucose in the solution was observed, with a detection limit of approximately 5 µM. This is concurrent with the sensitivity obtained when using nPG electrodes and gold nano-composites produced in much more costly processes [116, 170]. By omitting concentrations below 10 µM and above 10 mM a calibration curve with a coefficient of determination, R^2, of 0.997 can be applied to this set of data [131]. Equation 24 shows the relationship between glucose concentration and current observed (solved for glucose concentration), where *c* is the concentration of glucose (mM), and *I* is the current (µA).

$$c = (2.433 \times I)^{1.16} \qquad \text{Equation 24}$$

As it can be seen by the correlated data in Figure 88 the standard deviation in the current observed between three different electrodes is significant at low concentrations of glucose (up to 80% for a 5 µM glucose solution). This is not due to varied responses from a singular hPG electrode to the same concentration of glucose, but rather due to the variation observed between different hPG electrodes.

$$N = \frac{I - I_0}{I_{50} - I_0} \qquad \text{Equation 25}$$

For the purpose of using these electrodes as sensors it would thus be important to first calibrate these electrodes. In this study a calibration was achieved by the after-the-fact normalisation of collected data sets. The amperometric response in glucose free PBS, I_0, and the amperometric response in a 50 mM glucose and PBS solution, I_{50}, is recorded and then used to calculate the normalised response, *N*, for any given amperometric response, *I*, as per Equation 25.

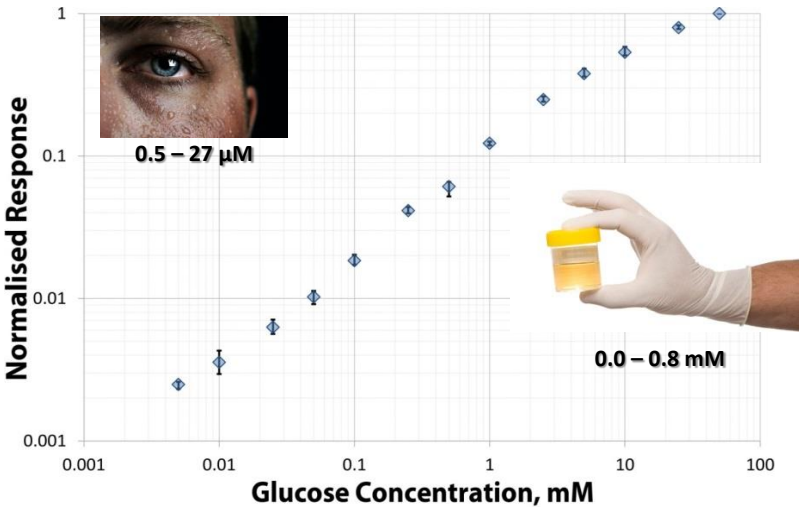

Figure 89: Normalised response of 3 different hPG electrodes to increasing concentrations of glucose (collected by amperometry with sequential injection of glucose). Tests were conducted at 0.15 V (vs. SCE) [131].

The resulting data (Figure 89) shows a much lower percentage standard deviation for all data points, with a maximum standard deviation of 15% observed at a glucose concentration of 5 µM. This high level of sensitivity across such a large range suggests that a sensor of this type could be utilised in a range of different applications, particularly those used in testing biological samples such as urine and sweat tests (see Section 5.2.).

For continuety the other aldyhyde containing reducing sugars were also tested by amperometry with increasing concentrations of each respective sugar.

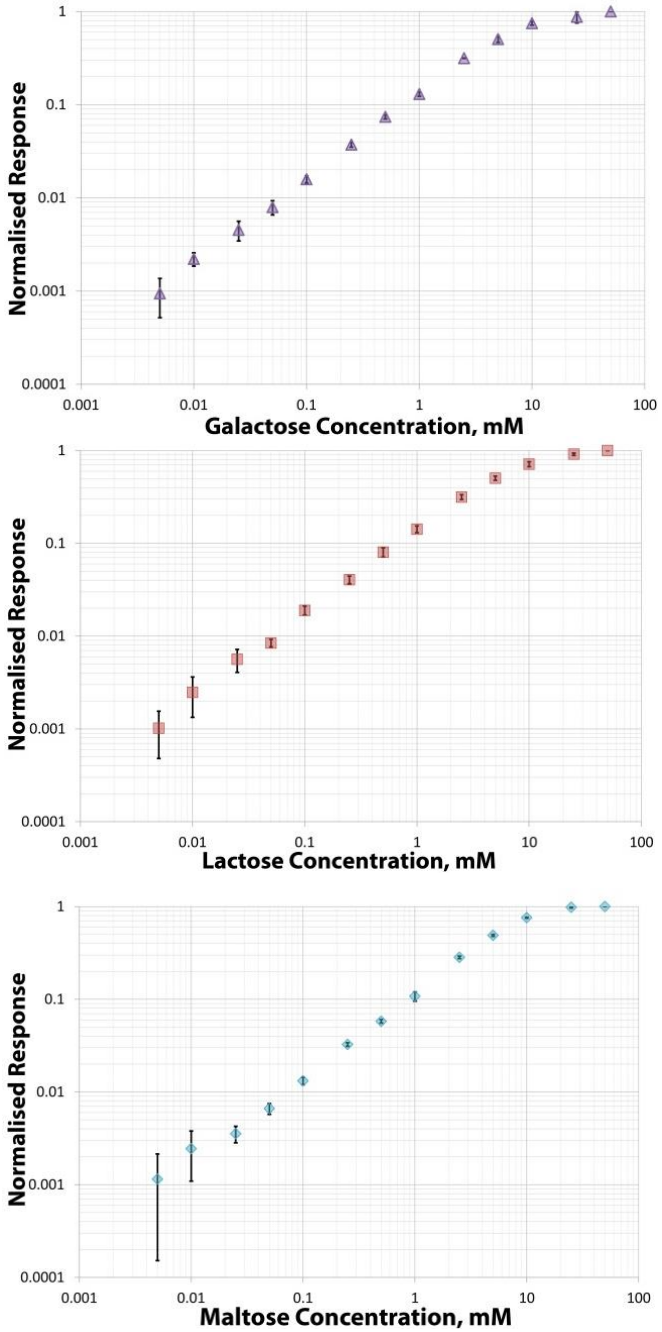

Figure 90: Normalised response from hPG electrodes to increasing concentrations of galactose, lactose and maltose respectively. In each case 3 different hPG electrodes used to collect data. Tests were conducted at 0.15 V (vs. SCE).

As it can be seen in Figure 90, the same sensitivity range is observed for each of the other sugars considered. The sensitivity at low concentrations, however, appears to be much lower for these sugars than with glucose as per the increased standard deviation at low concentrations (illustrated by the error bars).

5.2. GLUCOSE SENSING IN ARTIFICIAL URINE

Typically the range of sensitivity required by a sensor for glucose levels in the human body varies according to the type of test implemented. For example in urine the normal glucose concentration varies between 0.0 and 0.8 mM, and thus an effective sensor needs to be able to accurately determine when glucose levels exceed 0.8 mM [171]. In practice, following an atypical response in a urine glucose test, further more invasive testing of blood or cerebrospinal fluid glucose levels are usually conducted. However, with a view to reducing the amount of invasive tests conducted, sweat glucose tests (with a normal glucose range of between 0.5 and 27 µM) are currently considered as a potential valid alternative to invasive blood tests [172]. Such non-invasive testing methods are of particular interest to patients who suffer from diabetes, who currently have to perform periodic glucose tests every day by taking blood samples [173].

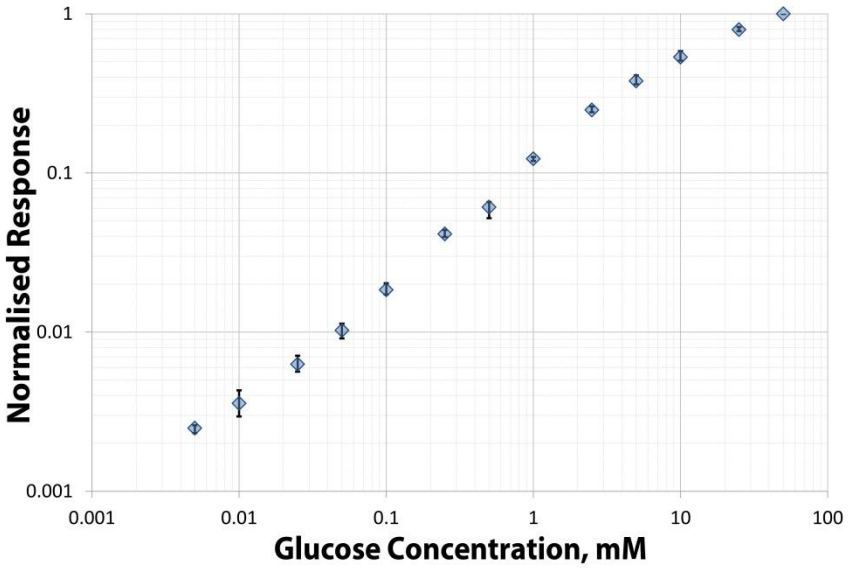

Figure 91: Normalised response of 3 different hPG electrodes to increasing concentrations of glucose in PBS at pH 8.9 and in the presence of 8 g l^{-1} urea. Tests were conducted at 0.15 V (vs. SCE) [131].

To prove the applicability of these hPG electrodes for a urine based glucose test, a glucose detection limit of at least 0.8 mM must be obtained in urine. To test whether or not this is the case here, amperometric tests were conducted with a hPG on gold disk electrode in a simple artificial urine solution. This was simply a PBS solution dosed with 8 g l^{-1} urea and with the pH adjusted to 8.9 (the normal urea concentration and pH of urine [174, 175]).

As it can be seen from Figure 91, the relationship between the current observed and the concentration of glucose is unaffected in this artificial urine. Though significant more testing of the other normal constituents of urine is still required, these electrodes therefore show significant promise for use with urine samples.

5.3 GLUCOSE SENSING IN TRANSDERMAL FLUID

Since existing urine test strips are already capable of the simultaneous testing for abnormal levels of glucose, bilirubin, ketones, specific gravity, blood, pH, proteins, urobilinogen, leukocytes and nitrites, all at very low costs, the development of a gold based urine sensor which is sensitive to only glucose is not cost effective [176].

On the other hand the ability to rapidly analyse the glucose content in sweat and electroosmotic skin extracts would constitute a major development in this field. The current standard for determining glucose levels at such low concentrations is to use high pressure liquid chromatography with a refractive index or UV detector [177]. Such tests take time to setup and have to be performed in a laboratory. The development of a simple and low cost sensor for both laboratory testing, and for use in the home as an alternative to testing glucose levels in the blood, could be a revolutionary.

The following results were obtained from a preliminary investigation into the feasibility of using the hPG on gold disk electrodes constructed in this project for glucose sensing in transdermal fluids.

In order to determine whether or not glucose sensing in transdermal fluids was possible, the sensitivity of these hPG electrodes at extremely low concentrations of glucose first had to be proven. Amperometry tests of 0.5 to 35 µM glucose (a range inclusive of the normal glucose range in sweat) in PBS solutions were therefore conducted.

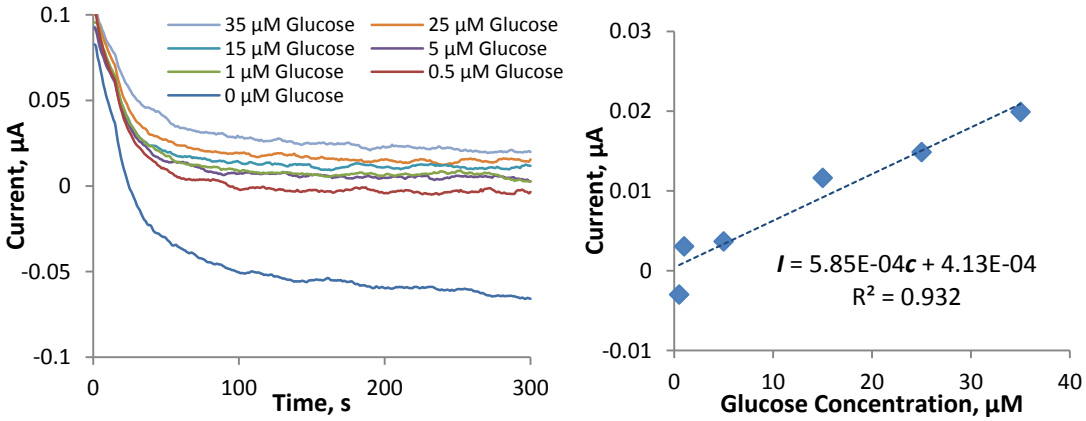

Figure 92: Amperometric response of hPG disk electrode to low glucose concentrations in PBS. Raw data and correlated data from one such test shown respectively. Tests were conducted at 0.15 V (vs. SCE).

As shown in Figure 92, a strong glucose dependant trend is observed even at these very low concentrations. However, since these tests were conducted in ideal solutions they do not give an accurate representation of the types of responses that could be observed in more complex solutions such as sweat. These tests were therefore repeated in biological solutions obtained from the iontophoresis of pig skin. These solutions were dosed with a PBS concentrate and the desired concentration of glucose, so as to closely resemble the PBS solutions used previously.

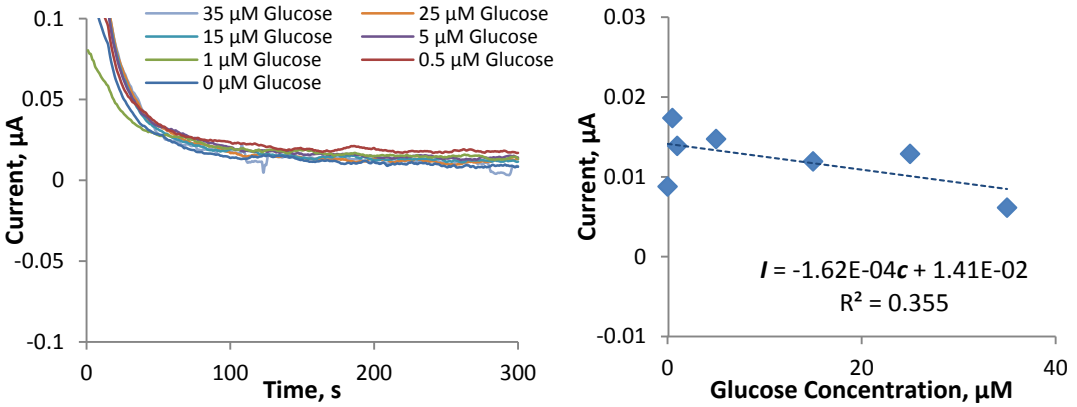

Figure 93: Amperometric response of hPG disk electrode to low glucose concentrations in biological extracts derived from pig skin. Raw data and correlated data from one such test shown respectively. Tests were conducted at 0.15 V (vs. SCE).

As it can be seen in Figure 93 the amperometric response between iontophoresis extracts containing different levels of glucose are practically in indistinguishable. If any correlation is observed, it is actually a weak inverse correlation between the current observed and the concentration of glucose present. This suggests that these biological samples contain certain constituents which interfere with the detection of glucose. To determine the nature of this interference, whether it is a simple interaction between these compounds and glucose, or a fouling of the electrode surface, the hPG electrodes were thoroughly rinsed in PBS and again tested in PBS solutions containing such low concentrations of glucose.

Figure 94 shows the amperometric response obtained when testing electrodes that had previously been used to test the iontophoresis extracts from pig skin in PBS solutions. Only a small degree of sensitivity is restored, since there is a marked difference observed between PBS solutions in the absence and presence of glucose. However, there is very little difference observed between different samples containing glucose, and no clear glucose dependant trend is observed. This suggests that some of the constituent components in the biological samples actually work to foul the hPG surface as the reduction in glucose sensitivity seams permanent.

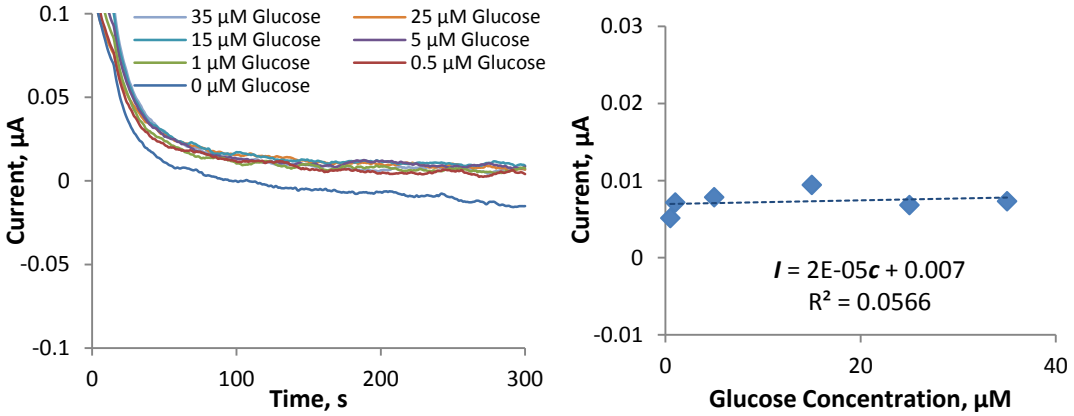

Figure 94: Amperometric response of hPG disk electrode to low glucose concentrations in PBS after exposure to biological samples. Raw data and correlated data from one such test shown respectively. Tests were conducted at 0.15 V (vs. SCE).

It was theorised that this interference and consequent fouling of the hPG electrodes was most likely due to the presence of amino acids which attach to the electrodes during testing due to an electrostatic attraction, much as with the attachment of enzymes to the hPG surface (see Section 6.1.). Further research is required to verify this hypothesis and to take steps to mitigate this interference.

5.4. DISCUSSION AND CONCLUSIONS

The hPG electrodes created here show a very high range of sensitivity to glucose inclusive of all concentrations tested in this project (from 0.5 µM to 50 mM). This means that they could potentially be used in a wide range of applications, from medical applications to process monitoring. This sensitivity range is maintained after repeated use, though the exact current response changes, so a degree of normalisation of data is required.

For the purpose of glucose sensing in medicine, technologies capable of cheaply sensing glucose in blood and in urine are already widely available. Thus new sensing technologies only require sensitivity at extremely low glucose concentrations, since this would open up whole new fields of non-invasive sensing techniques utilising transdermal fluids. The hPG electrodes developed here show high sensitivity in the normal glucose range of sweat (0.5 µM to 27 µM), suggesting that they could potentially serve for this purpose. However, since the hPG electrodes have been found to be susceptible to inference at such low concentrations of glucose, special measures should be taken to isolate and remove any interfering compounds prior to testing.

6. ENZYMATIC ELECTRODES

6.1. hPG-GOx ELECTRODES

6.1.1. ENZYME ATTACHMENT

A fuel cell which can potentially be implanted cannot rely on the use of foreign redox mediators. The enzymatic electrodes developed therefore had to either exhibit DET, or exhibit MET using electron carriers already present in biological systems. In the case of GOx this meant that the electrode had to be capable of the direct oxidation and reduction of the FAD co-factor, or the electrode had to be capable of oxidising H_2O_2 which acts as an electron mediator (as per Equations 4, 5, 7 and 8 in Section 2.2.).

Initially many different techniques for the covalent coupling of GOx onto hPG were trialled. None of the tested techniques resulted in hPG-GOx electrodes which showed any response, either at the redox potential of FAD (at approximately -0.4 V (vs. SCE) [105]), or at the oxidation potential of H_2O_2 (at approximately 0.5 V (vs. SCE) [178]). Consequently it was decided to use a simple electrostatic attraction method to attach GOx onto the hPG since the charge of the enzyme (negative at neutral pH) is complimentary to the charge of the anode during normal fuel cell operation.

Typically DET from GOx is verified by conduction CV scans at a range around -0.4 V (vs. SCE), since this is where the oxidation and reduction of the FAD co-factor would be observed. Unfortunately, by using electrostatic attraction as an immobilisation method, it was not possible to electrochemically determine whether or not DET is achieved with the use of CV scans. This is due to the fact that conducting CV scan at a range around -0.4 V (vs. SCE) would repulse the negatively charged GOx and therefore result in its detachment from the hPG surface. Conversely testing for the oxidation of H_2O_2 was possible since this is achieved at a positive potential range which is complimentary to the charge on GOx.

Figure 95 shows CV scans of a hPG-GOx electrode (on a 2 mm gold disk) in the presence of PBS solutions which contain glucose and are free from glucose. A very clear oxidation peak is observed in the presence of glucose at approximately 0.5 V (vs. SCE). This corresponds to the oxidation potential of H_2O_2 and thus suggests that the enzyme is successfully immobilised onto the hPG surface.

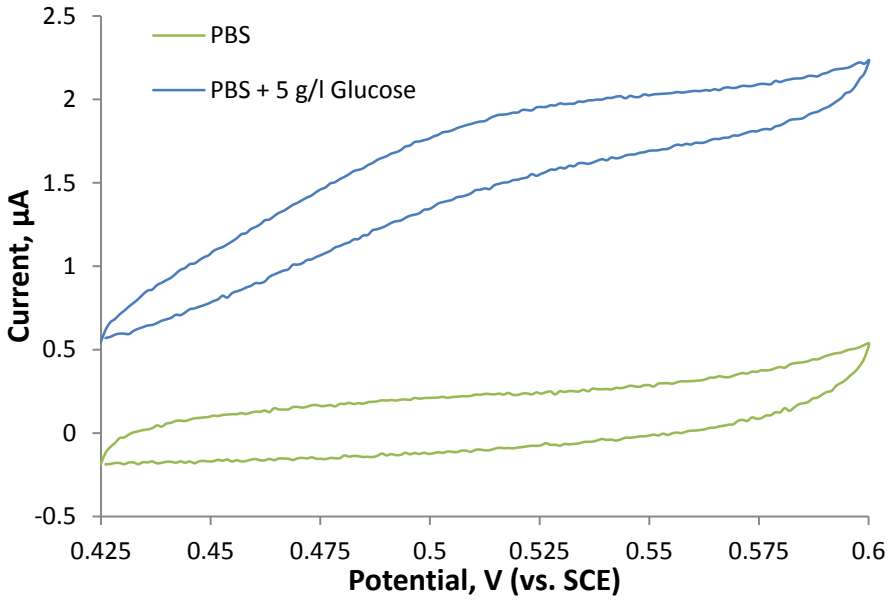

Figure 95: CV scans of a hPG-GOx electrode in the presence and absence of glucose. A 2 mm gold disk electrode was used to deposit the hPG. A scan rate of 1 mV s^{-1} was used and in both cases the third scan is shown here.

For the purpose determining the effectiveness of this immobilisation method the stability of this response over several days was measured. In addition, as a term for comparison, a simple adsorption method was also employed. In this case a hPG electrode was simply submerged in a concentrated GOx solution for a period of 1 hour whilst the electrostatic attraction of GOx took place on another electrode. In between tests the hPG-GOx electrodes were stored in PBS at 4°C.

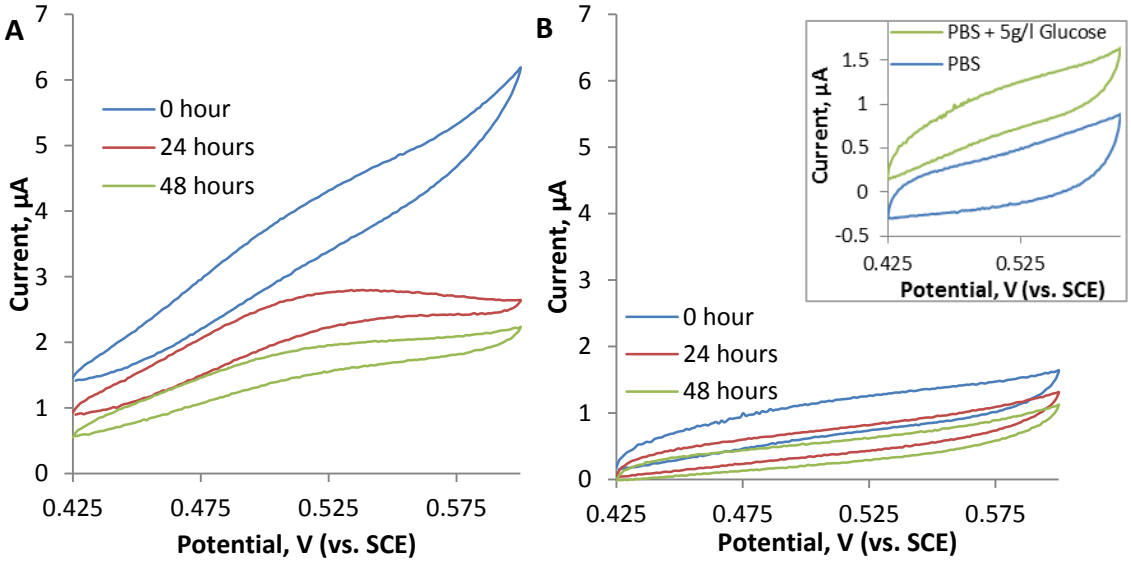

Figure 96: CV scans of hPG-GOx electrodes which utilise different immobilisation techniques and their response to 5 g l^{-1} glucose over 3 days; A- GOx immobilised by electrostatic attraction, B- GOx immobilised by unassisted adsorption (insert shows glucose dependant response at 0 hours). CV scans were conducted at a rate of 1 mV s^{-1} and in each case the third scan is shown here.

Figure 96 shows the CV curves obtained from the hPG-GOx electrodes which employ these two different immobilisation methods. As shown in the insert of Figure 96B, there is still a slight

glucose dependant response observed, which indicates that there is some GOx present. In comparison to the hPG-GOx electrodes which utilised electrostatic attraction, however, the glucose dependent response is very insignificant. In both cases a decay in the response is observed over the 3 days that they were tested. This can be attributed to the deactivation of immobilised enzymes, or to the leeching of enzymes during storage.

The reactivity decay could also be due to the degradation hPG electrode itself resulting in a decreased sensitivity towards H_2O_2. This hypothesis is supported by the fact that the capacitance of bare hPG electrodes also decays over the course of 3 days (as illustrated by Figure 97).

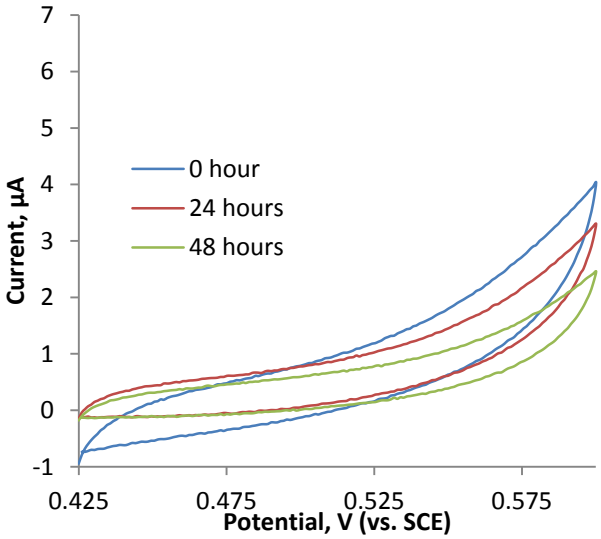

Figure 97: CV scans of hPG electrodes and their response to 5 g l^{-1} glucose over 3 days. CV scans were conducted at a rate of 1 mV s^{-1} and in each case the third scan is shown here.

The GOx loading on the hPG electrodes achieved with electrostatic attraction was evaluated by measing the residual activity of the GOx in PBS solutions after immobilisation and comparing it to activity of the initial solution. in both cases a comercial kinetic assay kit was used as per the manufacturers instructions. As a term for comparison, the loading achieved from the simple physical adsorption method was also determining in this way.

Figure 98 shows the average levels of active enzyme observed before and after immobilisation in each case. As shown an approximate reduction in activity of GOx in solution of 32% is observed with the electrostatic attraction method. This suggests that approximately a third of all of the GOx originally present in solution is immobilised onto the hPG surface. In contrast there is only a very slight difference observed in the amount of active enzyme in solution when solely relying on physical adsorption. In fact the difference observed here lies within the error margins of the measurements, so it can not be concluded the the concentration of active enzyme in solution has at all changed as a consequence of immobilisation. This suggests that the only enzyme

adsorbed in this case is the small amounts of enzyme present in the PBS solution absorbed into the pores.

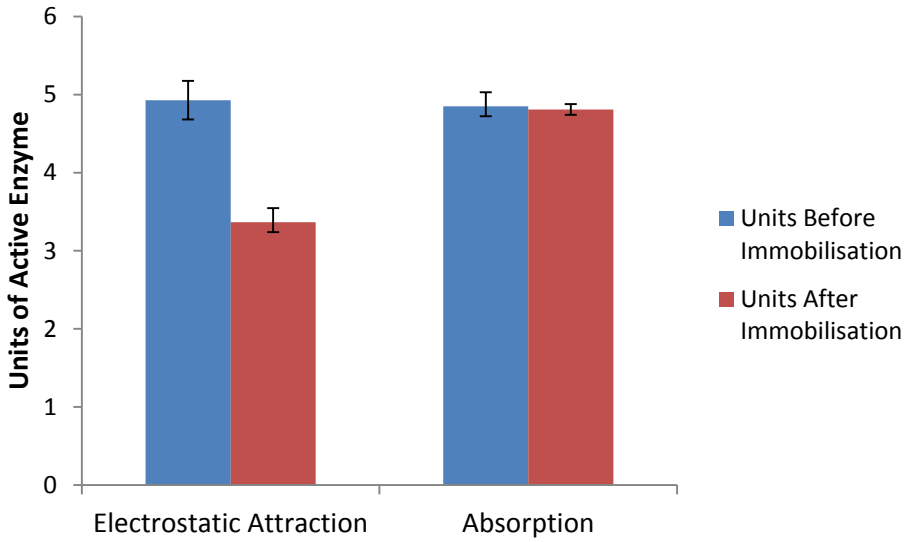

Figure 98: Bar charts indicating activity of GOx solutions before and after each respective immobilisation procedure. Error bars refer to 3 different experiments.

6.1.2. USE AS GLUCOSE BIOSENSORS

Since GOx has specificity and thus only reacts with glucose, a hPG-GOx electrode should be much better suited as a sensor, since it should not be susceptible to the same types of interference as hPG electrodes. The hPG-GOx electrodes' use as glucose sensors was therefore investigated. As was done previously with the hPG electrodes, amperometry was utilised in order to determine their effectiveness as a glucose sensor. This time however, the potential at which the amperometry was conducted was set to 0.52 V (vs. SCE), so as to respond to the presence of H_2O_2.

Initial analysis was conducted in PBS with repeated injections of increasing concentrations of glucose. Figure 99 shows both the raw data collected with each injection of glucose into the cell, as well as the correlated data showing the relationship between the current observed and the glucose concentration present in the cell.

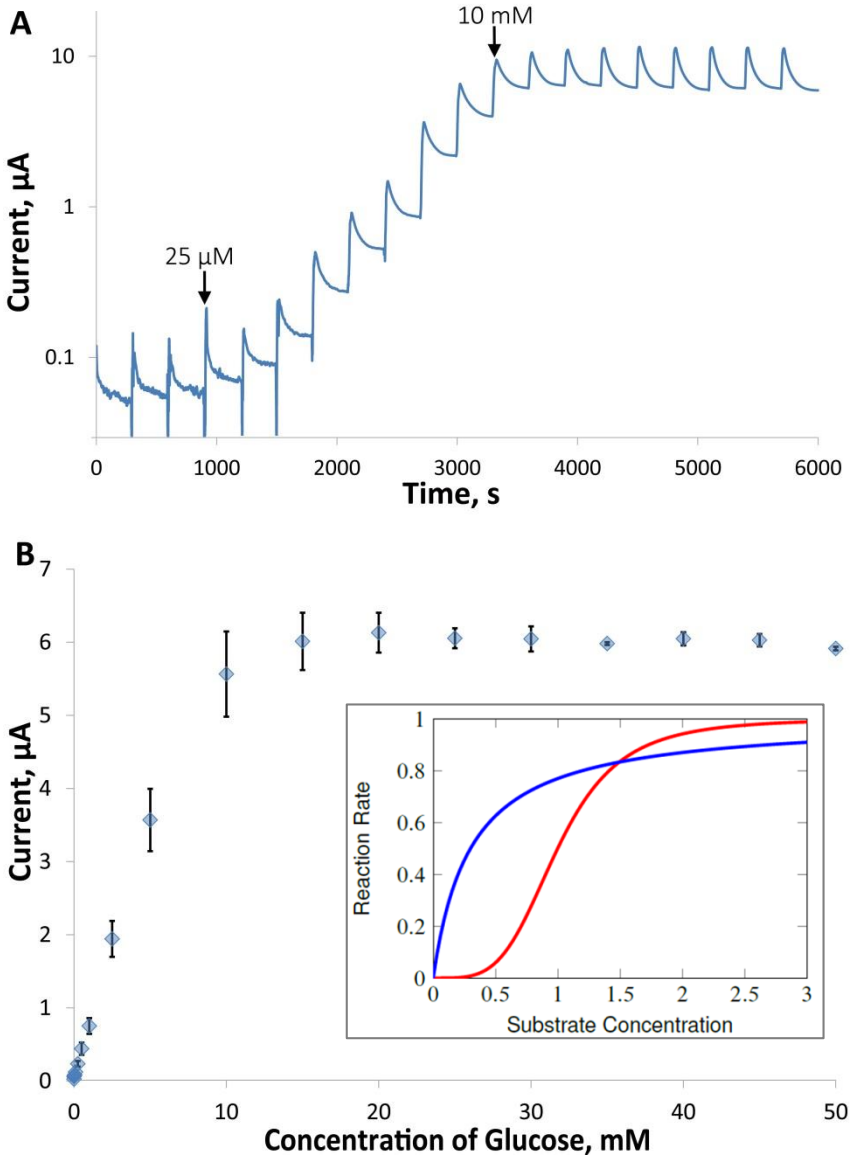

Figure 99: Amperometric response of hPG-GOx electrode to increasing concentrations of glucose in PBS; A- raw data from one experiment, B- correlated data from 3 different electrodes [92], (insert- Enzyme rate kinetics; 1st order Michaelis-Menten kinetics (blue line), and Michaelis-Menthen kinetics for cooperative binding (red line) [179]).

As shown in Figure 99B, the relationship between the current observed and the concentration of glucose present appears to follow classical first order Michaelis-Menten kinetics (see Figure 99 insert). In this case a simple reaction scheme is followed assuming that the product formation and dissociation from the enzyme occurs instantaneously. Equation 26 shows this reaction scheme between the enzyme, *E*, the substrate, *S*, and the resultant evolution of this enzyme-substrate complex, *ES*, to the product, *P*. In this case, the overall rate of product formation, *V*, can be derived from the respective rate equations of each step to give the Michaelis-Menten rate equation, where V_{max} is the maximum rate of reaction, *S* refers to the substrate concentration, and K_M is Michaelis-Menten rate constant (Equation 27).

$$E + S \leftrightarrow ES \rightarrow E + P \qquad \text{Equation 26}$$

$$V = \frac{V_{max}S}{K_M+S}$$ Equation 27

In the case of an electrochemical biosensor, this equation can be adapted for current, since the flow of current is proportional to the rate of reaction [180]. Thus the equation becomes dependant on the maximum current observed, I_{max}, and on the apparent Michaelis-Menten rate constant in this case, K_M^{app} (Equation 28). Taking the reciprocal of this equation gives the electrochemical version of the Lineweaver-Burk equation for enzyme kinetics (Equation 29).

$$I = \frac{I_{max}S}{K_M^{app}+S}$$ Equation 28

$$\frac{1}{I} = \frac{1}{I_{max}} + \frac{K_M^{app}}{I_{max}S}$$ Equation 29

Using this relationship, a plot of the reciprocal of current, 1/I, against the reciprocal of the concentration of glucose, 1/c, should yield a straight line which will allow the values of K_M^{app} and I_{max} to be easily determined. However, as it can be seen in Figure 100, a straight line is not observed in this case, but instead a sigmoidal relationship is observed.

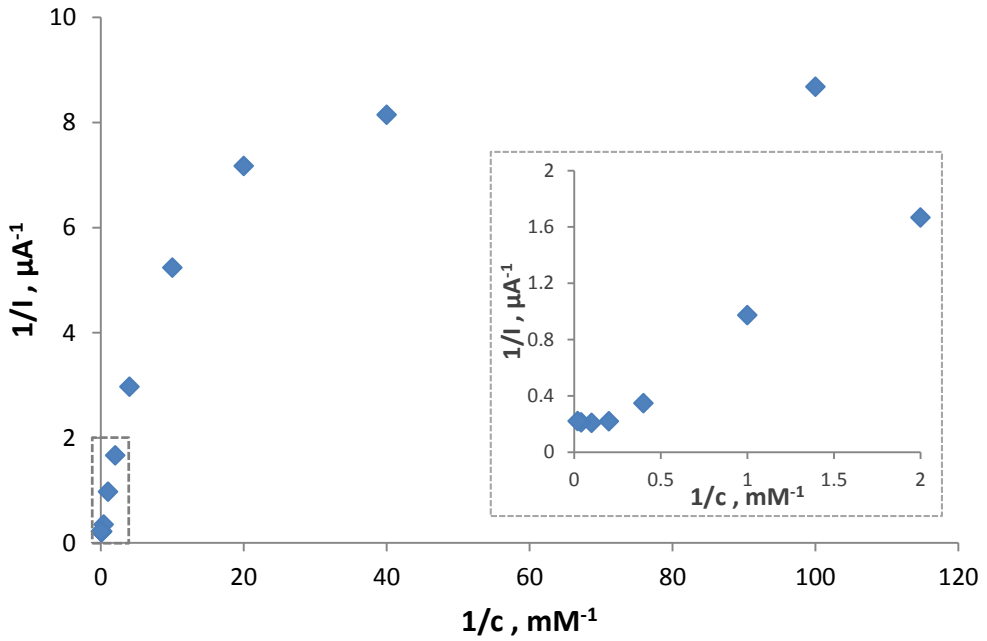

Figure 100: Reciprocal plot of current and glucose concentration in PBS. Insert shows magnification of data collected in dashed box. hPG deposited on 2 mm diameter gold disk electrodes were used here

This is due to the fact that the sensor here does not respond directly to the concentration of glucose. Instead the sensor responds to H_2O_2 which is secondary product produced by the enzyme. The overall reaction scheme for the production of this secondary product is outlined in Equations 30 and 31, where E_{ox} and E_{red} refer to the native and reduced forms of GOx

respectively, S_1 and S_2 refer to the substrates glucose and oxygen respectively, and P_1 and P_2 refer to the products gluconolactone and H_2O_2 respectively [181].

$$E_{ox} + S_1 \leftrightarrow E_{ox}S_1 \leftrightarrow E_{red}P_1 \rightarrow E_{red} + P_1 \qquad \text{Equation 30}$$

$$E_{red} + S_2 \leftrightarrow E_{red}S_2 \leftrightarrow E_{ox}P_2 \rightarrow E_{ox} + P_2 \qquad \text{Equation 31}$$

As it is shown by this reaction scheme, the formation of H_2O_2 is actually first dependant on the production of a reduced form of GOx (which is formed *via* two intermediate complexes), and then by the reaction of this reduced form of GOx with oxygen (again *via* two intermediate complexes). Thus it is not possible to use a simple Michaelis-Menten model in this case, or even to use more complex cooperative binding models. Instead this system would require computer modelling to account for the rates of each reaction, as well as any inefficiencies created by the subsequent reaction of H_2O_2 with the electrode surface.

Fortunately however, a direct linear correlation is evident between the current observed and the glucose concentration over a large range of concentrations as shown by Figure 101.

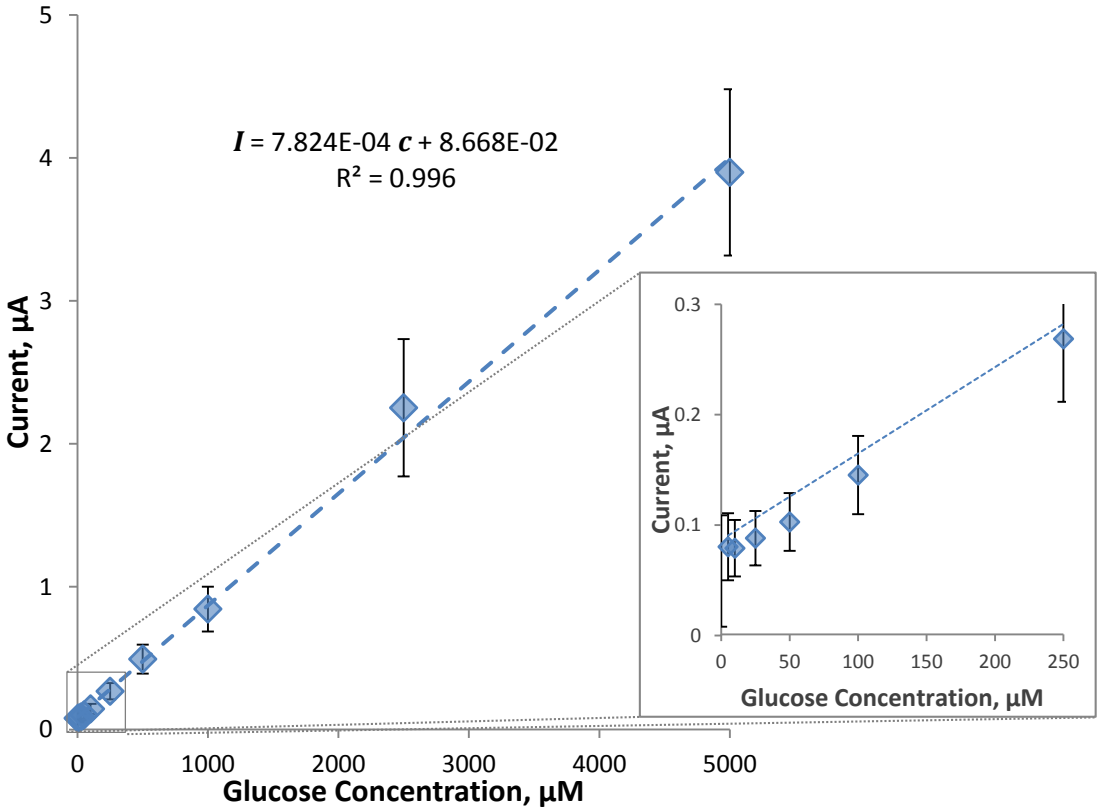

Figure 101: Amperometric response of hPG-GOx electrodes to increasing concentrations of glucose in PBS over linear range (5 µM to 50 mM). Correlated data from 3 different electrodes shown. hPG deposited on 2 mm diameter gold disk electrodes were used here

A direct linear correlation is evident between glucose concentration and current, for glucose concentrations of between 5 µM and 50 mM, with a R^2 value of 0.996. Equation 32 is the

calibration equation for glucose concentration in this case, where *c* is the concentration of glucose (μM), and *I* is the current (μA).

$$c = 1278\, I - 111 \qquad \text{Equation 32}$$

The overall sensitivity of the hPG-GOx electrodes produced here was found to be approximately 22.7 μA mM^{-1} cm^{-2} (based on superficial area of electrodes). This was compared with the sensitivity of other GOx sensors from literature [180, 182-186] (see Table 4). As reported the hPG-GOx electrodes produced in this project have sensitivities which are greater than the majority of the other much more complex methods reviewed, including some that boast direct electron transfer between the FAD centre of GOx and the electrode surface.

Table 4: Comparison of the sensitivity to glucose of several GOx electrodes [92].

Electrode	Sensitivity μA $mM^{-1}cm^{-2}$	Applied Potential V (vs. SCE)	Reference
hPG-GOx	22.7 ± 0.1	0.52	This Study
Naf/GOx-NPG/GCE	0.697	0.40	[182]
Fc/GOx-MWCNT/Chi-BSA- AuE	7.77 ± 0.08	0.17	[180]
GOx-Fc/MWCNT/Chi-GCE	25	0.31	[186]
Gel/GOx-WMCNT/GCE **	2.47	- 0.48	[183]
AuNPs/GOx/Biofilm-MWCNT/GCE **	16.6	- 0.40	[184]
PDDA/AuNPs-MWCNT/GE **	29.72	- 0.49	[185]

**Standard deviation refers to three replicates. **Methods which claim to achieve direct electron transfer.*

Naf: Nafion; GCE: glassy carbon electrode; Fc: Ferrocene; MWCNT: multi-walled carbon nano-tubes; Chi: Chitosan; BSA: bovine serum albumin; AuE: gold electrode; Gel: gelatine; AuNPs: gold nano-particles; PDDA: poly(diallyldimethylammonium chloride); GE: graphene electrode

6.1.3. BIOSENSOR STABILITY

Since enzymatic electrodes are inherently unstable (owing to the gradual decay of the enzymes used), it was important to establish the stability of the amperometric responses observed. A stability study, in which a single hPG-GOx electrode was repeatedly tested over a period of 5 days, was therefore conducted. In between testing the hPG-GOx electrodes were stored in PBS at 4°C.

Figure 102A shows the data obtained on each day. A very clear decay in the current levels was observed in the amperometric tests after each day. However, even though the current observed lowers over time, the range of glucose sensitivity of the hPG-GOx electrodes did not decay. This

is evidenced by the fact that the trend that was initially observed remains throughout the testing period.

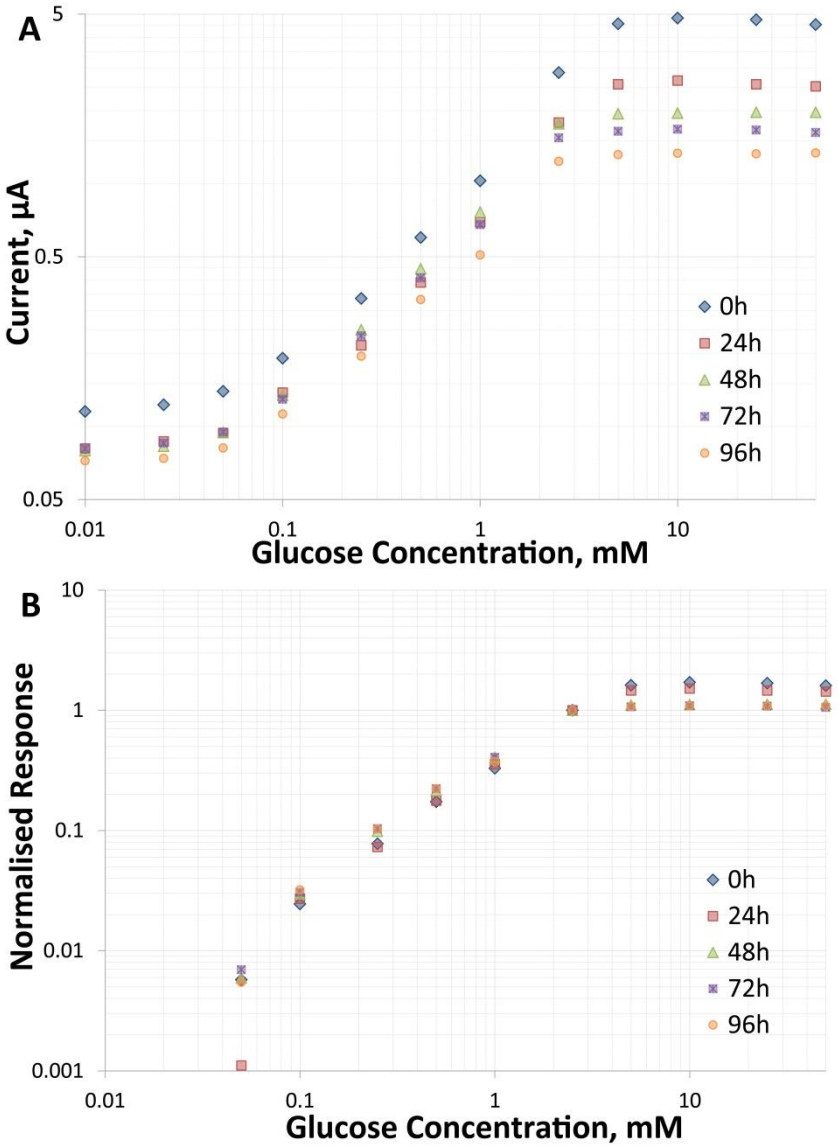

Figure 102: Amperometric response of single hPG-GOx electrode to varied levels of glucose over 5 days; A- data correlated for each day, B- normalised data. hPG deposited on 2 mm diameter gold disk electrodes were used here [92].

To further illustrate this fact, the data obtained on each day was again normalised as for the hPG electrodes and their response to glucose (see Equation 25 in Section 5.1). As shown in Figure 102B, there is very little variance observed between data collected on different days when normalised. This suggests that hPG-GOx electrodes of this sort could be used as effective glucose sensors, providing they were properly calibrated prior to use.

6.2. hPG-LAC ELECTRODES

The immobilisation of LAC was achieved through a well-established covalent coupling technique which employs amino-phenyl groups for the attachment of enzymes [187]. This required a 2-stage surface modification in order to create a conductive monolayer for attachment. For both stages of modification CV was employed to facilitate the surface modification and to monitor the success of each stage of modification.

In the first stage nitrophenyl groups were electrochemically attached to the gold by conducting two reductive CV scans in the presence of p-nitrophenyldiazonium salt. Typically the production of polyaniline is caused by the polymerisation of the phenyl groups through hydrolysis. Thus, in order to limit polyaniline formation, and promote the formation of a monolayer, this stage was conducted in an acetone-based electrolyte.

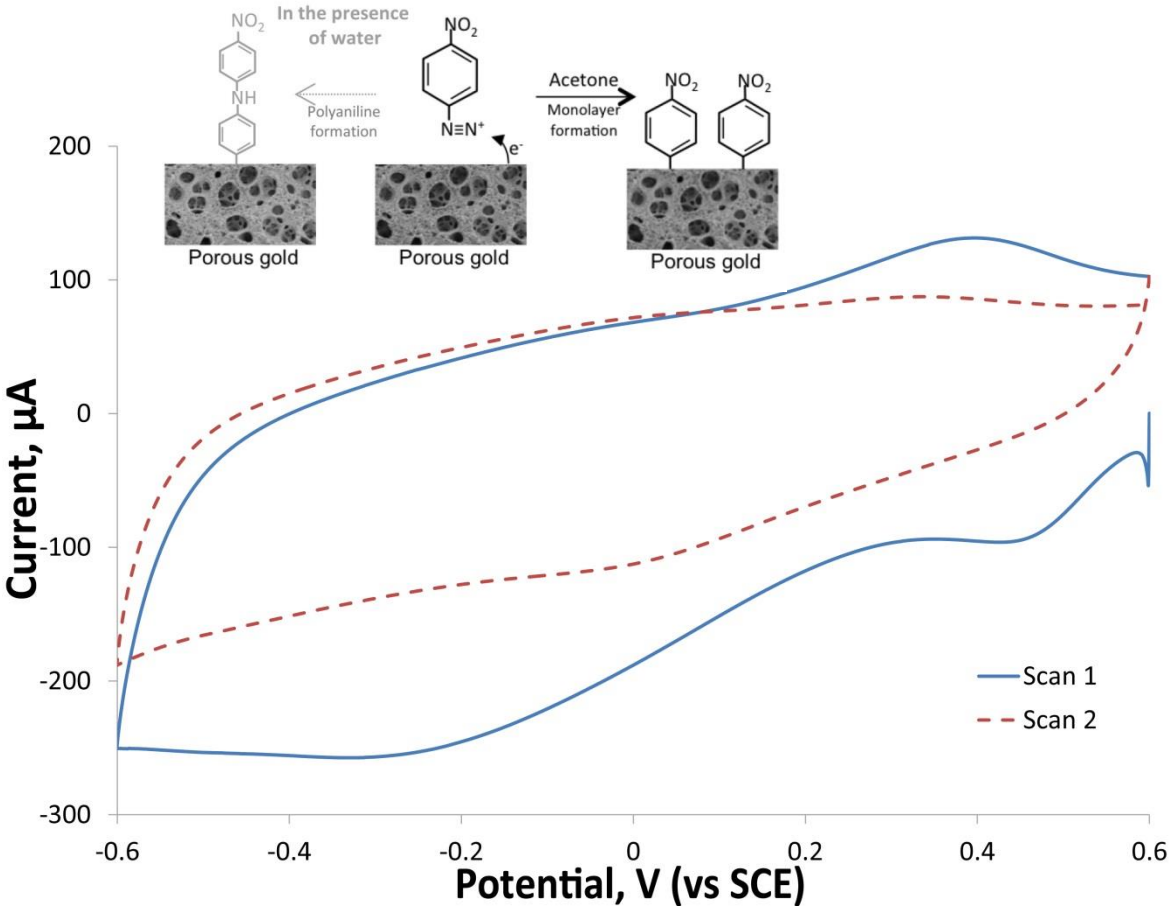

Figure 103: CV scans of the first gold surface modification stage. Scans were conducted at rate of 100 mV s^{-1} in an acetone electrolyte containing 2 mM p-nitrophenyldiazonium tetrafluoroborate and 100 mM tetrabutylammonium tetrafluoroborate.

Figure 103 shows the resulting CV scans from the first surface modification step. Two peaks are visible on the first scan at approximately 400 mV and -200 mV (vs. SCE). These peaks are attributed to the reduction of the diazonium salt on the different planar surfaces of gold and

crystalline gold, as previously suggested for the case of an acetonitrile electrolyte [188]. Since the phenyl-gold bond formed is not oxidised back in this scan range, a large decrease in the magnitude of these peaks are observed on the second scan, which suggests that the surface is quickly becoming saturated with the nitro-phenyl groups [154, 188, 189].

During the second stage, the electrodes were immersed in a 10% ethanol and water based electrolyte and two more reductive CV scans were conducted in a much more negative scan range of between 0.0 V and -1.4 V (vs. SCE). This facilitated the production of amino and hydroxylamino groups through the exchange of oxygen for protons on the nitro groups already formed. As shown in Figure 104, the first scan shows a very clear peak at -820 mV (vs. SCE) which is established as the potential at which nitrophenyl groups are irreversibly reduced to aminophenyl groups [154]. This peak is not evident on the second scan, however, a small redox peak is observed at -700 mV (vs. SCE). This result suggests the presence of some hydroxylamine groups amongst the amine groups [190].

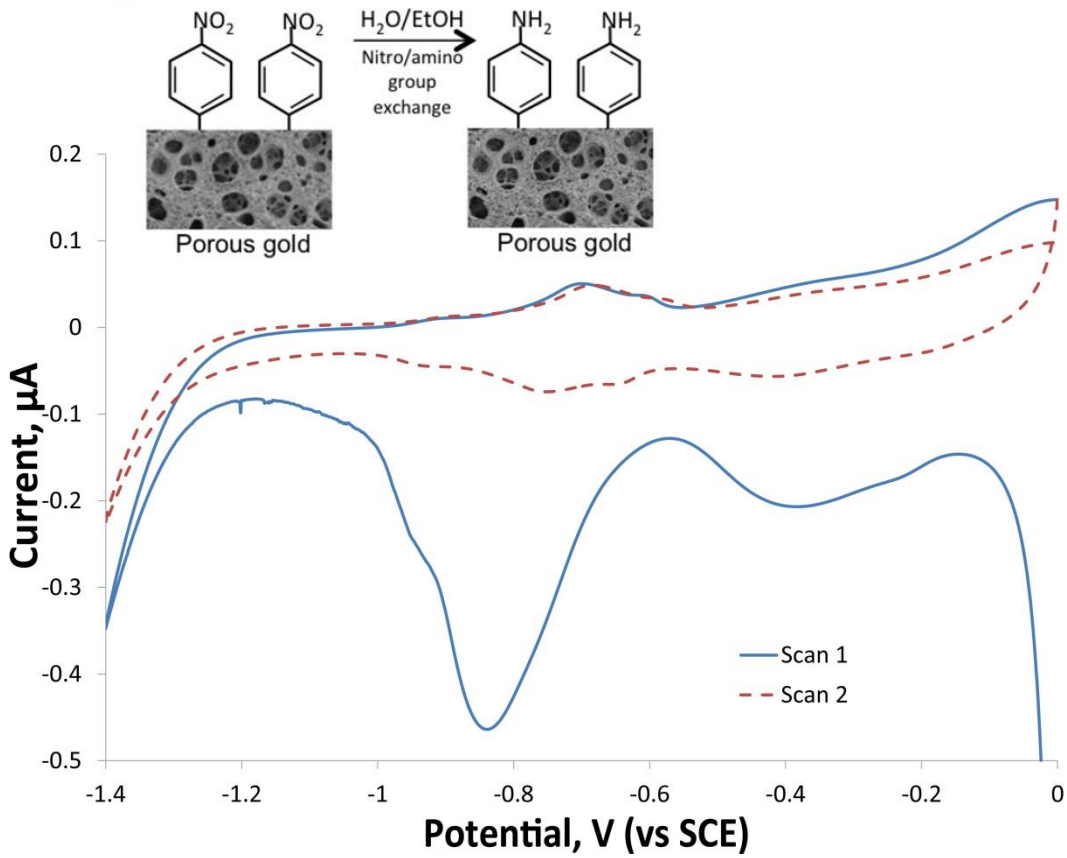

Figure 104: CV scans of the second gold surface modification stage. Scans were conducted at 50 mV s^{-1} from 0.0 V to -1.4 V, in an aqueous electrolyte containing 10 % v/v EtOH and 0.1 M KCl.

Following the modification of the hPG surface, LAC was immobilised by covalently linking its carboxyl-terminal groups with the amines created on the surface. Unfortunately however the performance of the immobilised LAC could not be easily characterised electrochemically. This

was due to the fact that the potential at which LAC is capable of electrochemically reducing oxygen is approximately 0.89 V (vs. SCE) [191]. Applying this high potential to the hPG-LAC electrode would result in oxidation of the gold surface, and it could also reverse the surface modifications which facilitate covalent linkage. The technique for activating the enzymes (by using a weak oxidiser), also prevented any analysis of the enzyme loading achieved here. This was due to the fact that the kinetic assays widely used to measure laccase loading and activity relies on the gradual oxidation of dyes in the presence of laccase. Any residual sodium periodate would instantly react with dyes in the assays. Consequently the performance of the fully constructed EBFCs served as the only metric for determining the hPG-LAC electrodes' performances (see Chapter 7).

6.3. CONCLUSIONS

The hPG electrodes have been proven to be an excellent substrate for the functional immobilisation of enzymes. In particular, when using GOx, the electrostatic attachment of enzymes has been shown to be possible at very high loadings.

The hPG-GOx electrodes have been shown to serve as excellent glucose biosensors with a high specific sensitivity (22.7 μA mM^{-1} cm^{-2}), and a broad sensitivity range. The electrodes also exhibit a direct linear correlation between glucose concentration and current response, thereby making the process of sensor calibration simple and easy. They also show minimal interference in the presence of amino acids commonly found in transdermal fluids so could potentially be used to determine glucose concentrations in sweat and skin extracts derived by iontophoresis or electroosmosis.

The functional immobilisation of LAC onto hPG has also been demonstrated by the performances obtained from EBFCs utilising both hPG-GOx and hPG-LAC electrodes.

7. DEVELOPMENT OF A CONTINUOUS FLOW ENZYMATIC BIOFUEL CELL

7.1. PROOF OF CONCEPT DEVICE

The hPG-GOx and hPG-LAC electrodes were first tested in a simple mock-up EBFC. This EBFC consisted of a hPG-GOx electrode and a hPG-TvLAC electrode, simply submerged in an aerated PBS solution containing 5 g l^{-1} of glucose (see Figure 105A). This concentration of glucose was chosen since, based on the hPG-GOx electrode's performance as a biosensor, it was believed that the performance of the hPG-GOx electrode would be maximised at this concentration (see Section 6.1.2.).

An OCP of 0.58 V was observed, which is greater than the OCPs observed with other EBFCs reported which implement mediators in solution, such as ferrocene, osmium or hydroxyquinoline based mediators [192-194]. This OCP is however much less than the OCPs reported when DET was achieved using CNT aggregate electrodes [44].

Subsequently, the EBFC was polarised by connecting the electrodes to a range of external resistors. Figure 105B shows the cell potential and the power density as a function of the current density. As shown, the peak power density was approximately 6 µW cm^{-2} at a potential difference of 0.2 V. This result is comparable with recently reported miniature enzymatic biofuel cells [62, 195].

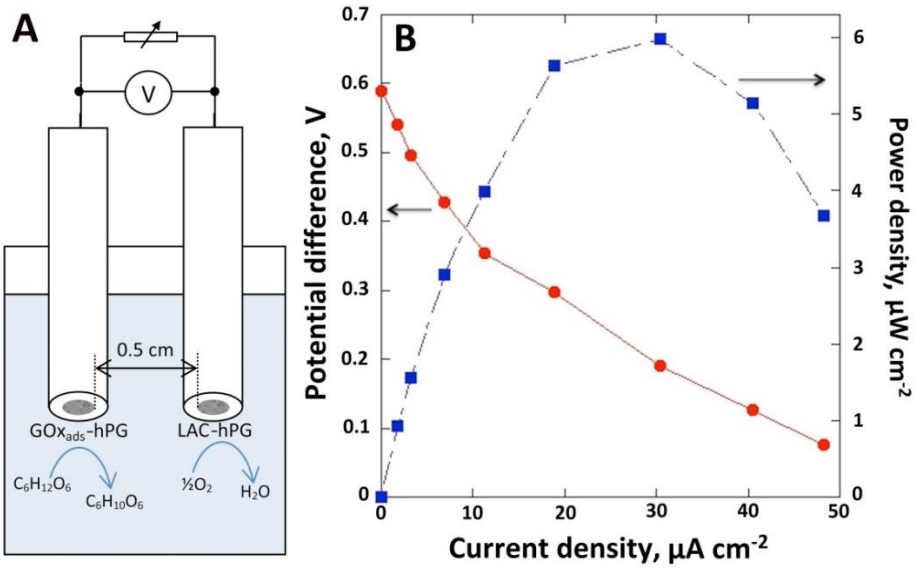

Figure 105: Proof of concept EBFC experiments; A- EBFC setup used, B- correlation between potential difference, current density and power density [92].

Unfortunately, it was not possible to repeat the results obtained with our initial proof of concept device using the TvLAC enzyme. EBFCs constructed to the same initial design yielded little or no

power and, quite curiously, showed the hPG-TvLAC electrode to be acting as an anode and not a cathode. This suggests that the oxidation of glucose and the reduction of oxygen were not the principle reactions occurring at the hPG-GOx and hPG-TvLAC electrodes respectively. Instead a reduction reaction was occurring at the hPG-GOx electrode and an oxidation at the hPG-TvLAC electrode. The oxidation reaction in this case was most likely facilitated by an impurity in the TvLAC preparation purchased here.

It was concluded the TvLAC had denatured since its use for the construction of the proof of concept device. It was decided to instead use a RvLAC preparation (of much higher purity than the TvLAC used) for all subsequent EBFC constructions. This was motivated by the fact that RvLAC has an operating pH range of between 5.5 and 8.3 [196] (compared to TvLAC's normal operating range of between pH 3 and 6 [197]), and would thus actually be better suited for use at near physiological conditions.

7.2. THE EFFECTS OF FLOW ON EBFC DESIGN AND OPERATION

There are several considerations that should be made when using a continuous flow EBFC instead of a simple static or batch EBFC. The most important factor to consider is the rate of flow through the EBFC, since it can have a great impact on the power produced. In both cases, reactants are consumed at the surface of the electrode, thereby leading to a diffusive concentration gradient of reactants from the bulk of the solution to the electrode surface. As illustrated by Figure 106, in the case of a EBFC with flow over the electrodes, the size of this diffusive layer is dependent on the rate of flow (or more specifically, the speed of flow over the electrodes).

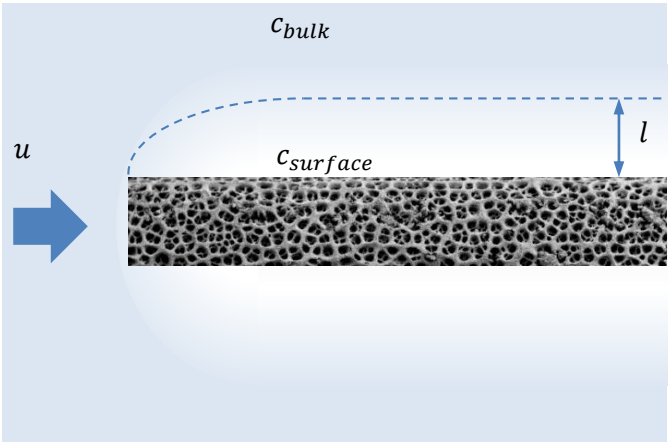

Figure 106: Schematic of diffusive layer formed over electrodes with the flow of reactants.

Changing the size of the diffusive layer (*l*) will also impact the difference between the concentration of reactants at the surface ($c_{surface}$), and the bulk reactant concentration (c_{bulk}). This means that the flow speed (u) will affect the amount of reactants available to the enzymes

on the surface of the electrode and consequently the rate of reaction, and accordingly, the flow of current as well.

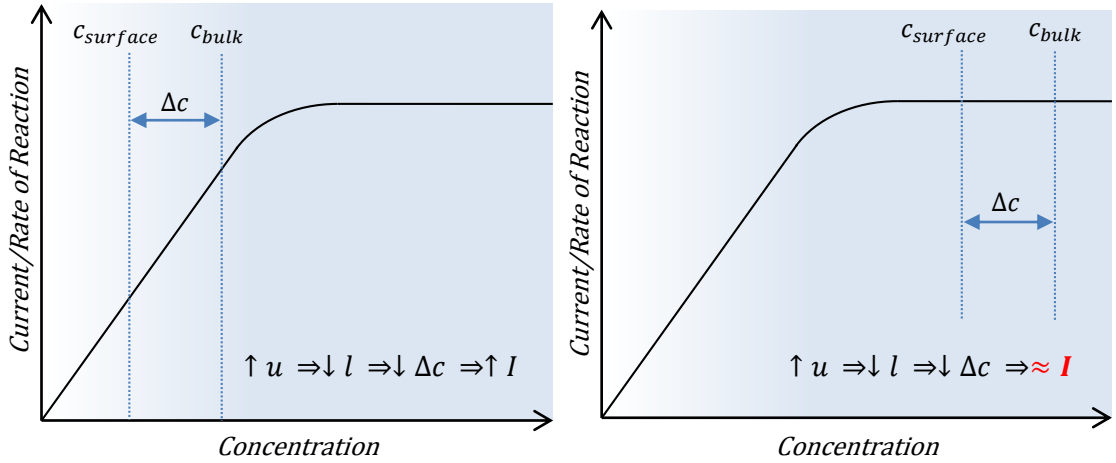

Figure 107: Effect of concentration gradient on an EBFC's performance when bulk concentration is below and above saturation point respectively.

As demonstrated in Figure 107, this effect can be negated by simply using a bulk reactant concentration which is sufficiently high so that the performance of the electrodes are maximised even at the lower surface reactant concentration.

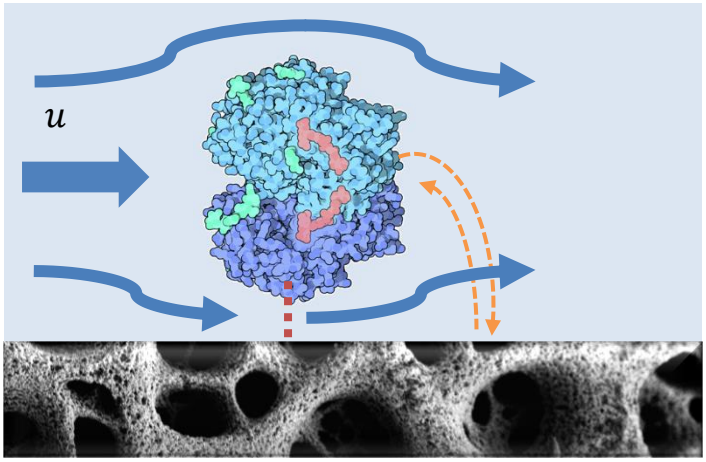

Figure 108: Possible interference to electron transfer caused by high flow speeds.

Alternatively the speed of flow can be increased in order to reduce the size of the diffusive layer and, in so doing, reduce the concentration difference observed. However, in the case of GOx, the apparent K_m (which inversely indicates enzymes' affinity for glucose) typically increases with flow rate [198], and thus a general decay in power output is expected with increasing flow rates. This can be due to interferences caused at high flow speeds in the binding of glucose to the active site of the enzyme, and also in the transfer of electrons between the enzymes and the electrode surface (see Figure 108). Higher flow speeds could also result in the detachment of enzymes due to increased friction at the electrode surface. Thus, in this project, it was decided

to use a glucose concentration at which it was believed the performance of the GOx electrode was maximised.

7.3. EBFC DESIGN AND PERFORMANCE

The EBFCs were constructed as described in Section 3.3.6. First hPG was directly electrodeposited onto platinum wires using a hydrogen bubble template. Since this technique relies on the simultaneous deposition of gold and evolution of hydrogen gas, it is reliant on relatively high deposition potentials and currents. This is easy to achieve and control when using small test electrodes on the laboratory scale with the aid of a potentiostat.

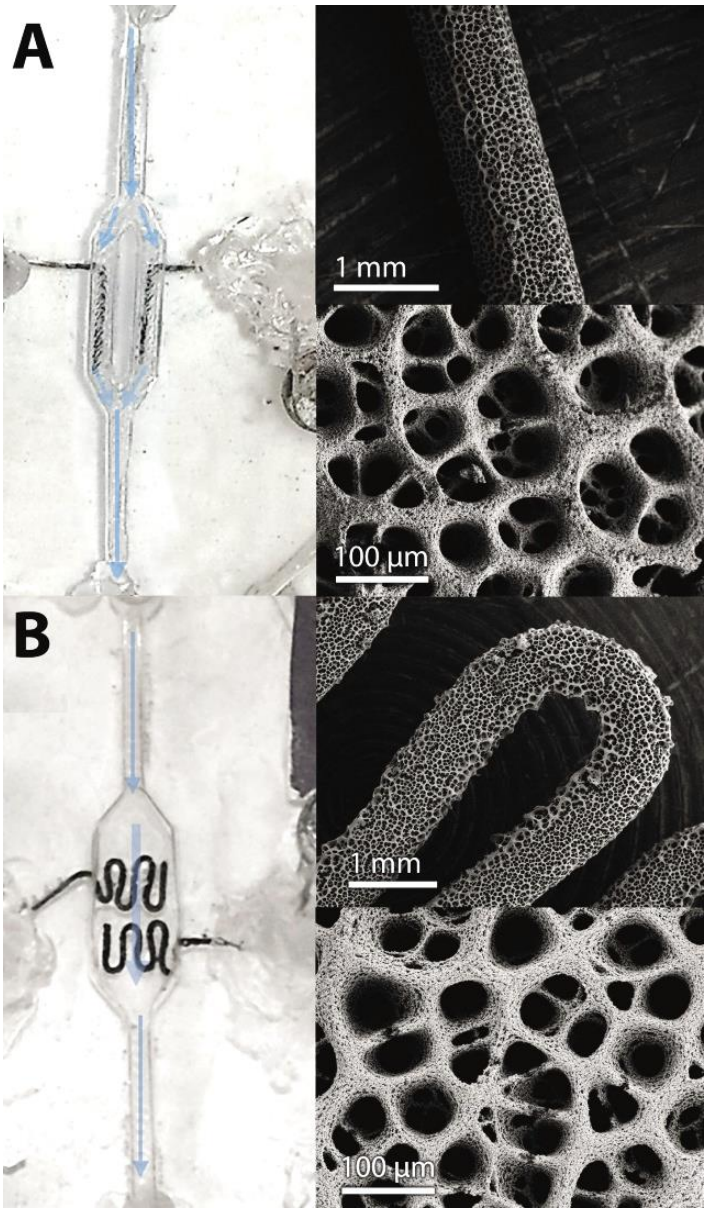

Figure 109: Electrode configurations and their respective morphologies as shown by FESEM; A – dual channel EBFC with hPG electrodes produced under potentiostatic control, B – single channel EBFC with pleated hPG electrodes produced under manual control with bench-top DC power supply [159].

However, when larger surfaces are used or when the manufacture of hPG is required on a more industrial scale, potentiostatic control is harder to maintain. This was found to be the case when using platinum wires of lengths greater than 1 cm. A methodology for simplifying the established hPG deposition method, by eliminating the need for a potentiostat and instead using on a DC power supply, was thus investigated (see section 3.3.1.).

Figure 109 shows the two different EBFC configurations used and FESEM images of the electrodes used in each case. As shown, there is almost no visible difference between the porous structure obtained when using either potentiostatically controlled electrodeposition (Figure 109A), or when using a DC power supply (Figure 109B). This is a significant move towards the low cost production of hPG electrodes on a larger scale.

7.3.1. POLARISATION

Several different metrics were used to determine the performance of the different EBFC designs considered, the first and most common of which was by comparing the EBFCs' polarisation and power output by load. This was achieved by varying the resistance applied across the fuel cell between 1 kΩ and 1 MΩ, as well as by measuring the OCP.

Figure 110 shows the overall polarisation curves observed with the two different EBFC configurations. As it can be seen, there is a marked difference between the two EBFCs, characterised by the specific performance (by electrode surface area) and also by the overall performance. However in both cases the OCP is significantly lower than the value achieved with the proof of concept device. This could be due to the use of a different LAC, or due to the continuous flow employed here. Additionally EBFCs were allowed to stabilise over 24 hours before the polarisation data was collected which could also have impacted the OCP measured.

When comparing the different EBFCs, the power and current density observed with a single channel EBFC (Figure 110B) are much lower than with the EBFC with parallel channels (Figure 110A). More importantly however is the fact that the overall performance of the single channel fuel cell is also shown to be lower than that of the parallel channel fuel cell as demonstrated by the difference in OCP between the two systems.

The difference in OCP observed in the absence of a physical divider suggests that there may be some interference between the two electrodes. This could be due to an exchange of enzymes between the anode and the cathode partially neutralising the EBFC's effectiveness. Then again, it is for this reason that the single channel EBFC was set up so that the feed first passes over the RvLAC electrode first and then the GOx electrode. Since the RvLAC is covalently linked to the

hPG using a widely established method, it was believed to be more stable, and less likely to shed enzymes into solution which could then be absorbed into the porous structure of the GOx electrode.

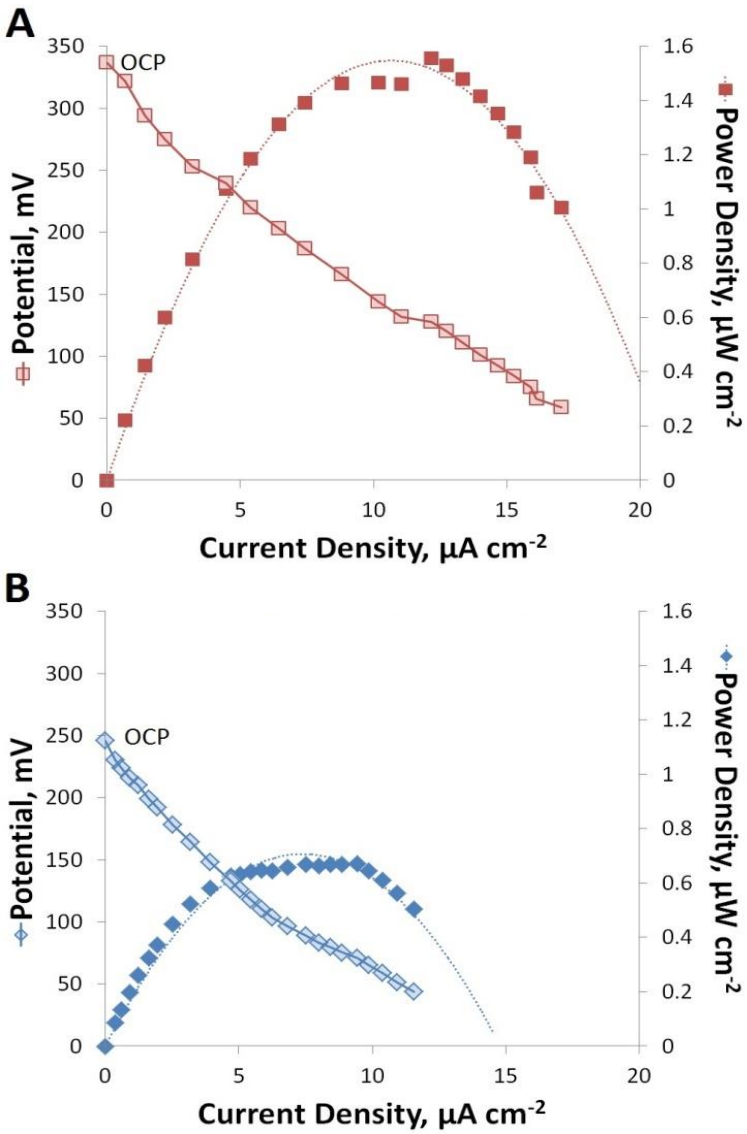

Figure 110: Polarisation by fuel cell load of both fuel cell configurations; A- parallel channel fuel cell, B- single channel fuel cell with pleated electrodes. Tests performed after 24 hours of continuous operation [159].

The more likely scenario is that there is interference caused by the reaction intermediates of the two electrodes. In particular, there is a significant risk of interference from H_2O_2 which is produced when reduced GOx comes in contact with oxygen. This poses no problem at the GOx electrode, as it can improve electron mediation between the enzyme's active site and the hPG surface. Conversely, the back diffusion of H_2O_2 can cause interference at the RvLAC electrode by causing an electrochemical short-circuit. H_2O_2 has also been shown to be toxic to LAC and thus the diffusion of H_2O_2 from the GOx electrode to the RvLAC electrode could result in deactivation of the RvLAC electrode [199].

7.3.2. CONTINUOUS POWER PRODUCTION

Though the specific power output of a fuel cell is the most common metric used for determining fuel cell performance, it does not necessarily have any practical relavance. In this case for example the parallel channel fuel cell has a much higher specific power output but, since it is reliant on the use of a physical divider between electrodes, it will have larger volume. The overall polarisation of a fuel cell can also give a misleading representation of fuel cell performance since it only takes a snapshot of the performance of the fuel cell (often taken at the point of manufacture when performance is maximised).

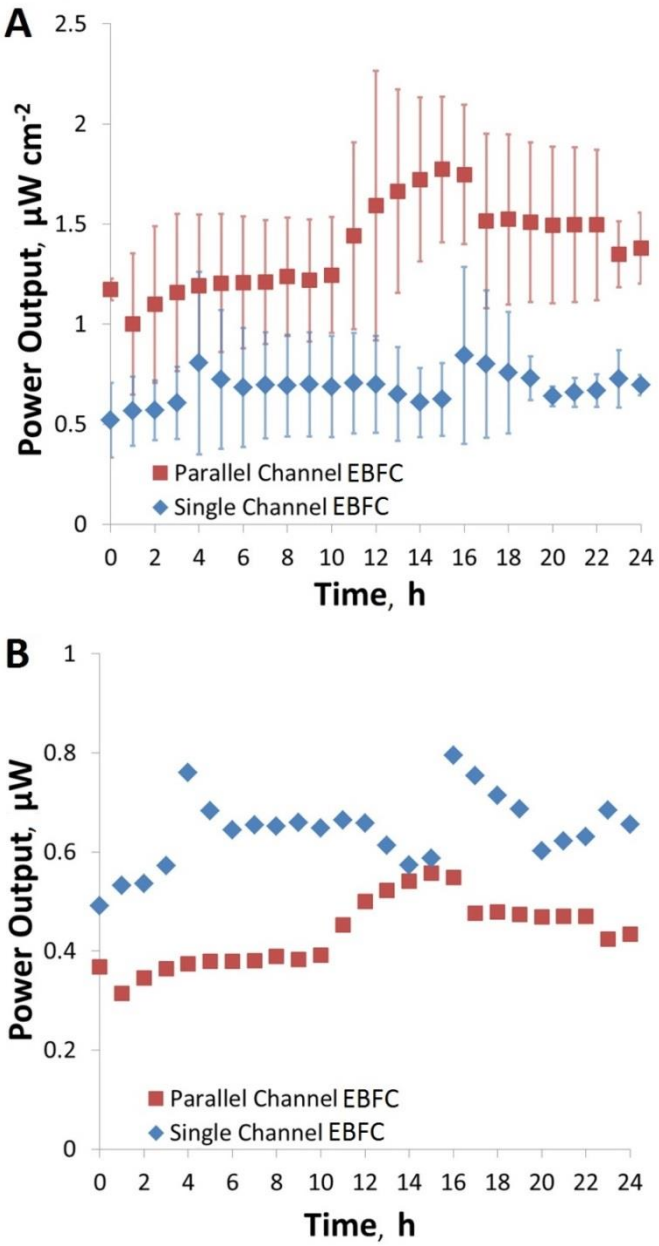

Figure 111: Power output from different fuel cells over first 24 hours of operation; A – specific power output by surface areas of GOx electrodes, B – absolute power output from fuel cells. In both cases data is taken from 3 replicate fuel cells as represented by standard deviation error bars in figure A [159].

For a practical impression of an EBFC's performance it is thus more important to not only consider the surface area of the electrodes but the overall size and shape of the constructed EBFC as well as the power produced during continuous operation. Figure 111 shows the average continuous power produced from EBFCs of both designs during the first 24 hours of operation. In each case the fuel cell load was set so as to maximise power output on the basis of the polarisation curves (30 kΩ and 10 kΩ for the parallel channel and the single channel fuel cells respectively). As can be seen here, when considering the specific power output (by electrode surface area), the parallel channel EBFCs consistently outperform the single channel EBFCs (Figure 111A). However, when considering the total power produced by the EBFCs, the single channel system actually outperforms the parallel channel system (Figure 111B). This shows that there is a potential trade-off between specific power output and the total amount of electrodes that can be used. Essentially if we use a physical divider between electrodes we can increase the power from each electrode, but we can fit fewer electrodes into our fuel cell, so may ultimately produce less power in a device of the same volume.

Alternatively, assuming back diffusion of H_2O_2 is indeed the cause behind the drop in the OCP, a different method can be used to negate this. Instead of using a physical divider the flow rate through the fuel cells can be increased to counteract the diffusion of H_2O_2.

In order to verify that the power produced from the EBFCs was indeed due to the presence of the enzymes, and not merely due to the catalytic activity of the hPG and platinum present in the electrodes, two studies were conducted in which one of the two enzymes were not employed. The parrallel channel fuel cell configuration was used in this case and the electrodes were prepared using all of the other treatments and functionalistion steps as before.

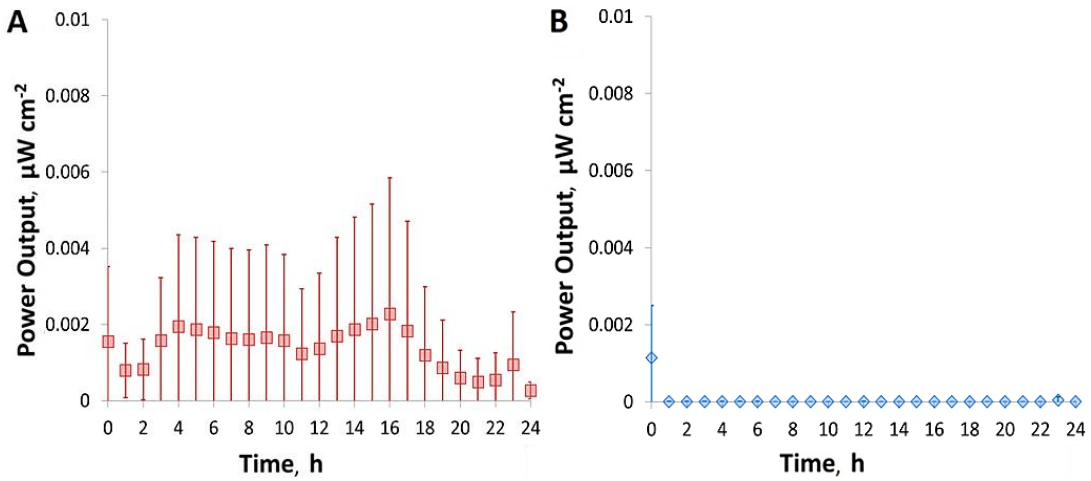

Figure 112: Continuous power production from parallel channel fuel cells in the absence of one of the enzymes; A- GOx-free fuel cells, B- LAC-free fuel cells. Error bars refer to standard deviation from 3 repeats.

Figure 112A shows the continuous power production over 24 hours from a fuel cell which employed a hPG-RvLAC cathode and a hPG anode. Here it is evident that there is some power produced in this case, though it is limited to between 0 and 5 nA, which is approximately 1000 times less than observed with the full EBFC of the same configuration. This suggests that the platinum and hPG electrodes are capable of oxidising glucose when coupled with an oxygen reducing electrode, though much less efficiently that when GOx is employed.

Figure 112B shows the power continuous power production achieved when using a hPG-GOx electrode as an anode and an aminophenyl functionalised hPG electrode as a cathode. The power output is negligible in this case suggesting that the platinum and hPG present in these electrodes cannot effectively reduce oxygen in this context.

7.3.3. SENSITIVITY TO FLOW VELOCITY

Since in both cases the fuel cells were fed with the same volumetric flow rates, but have different geometries and cross-sectional areas, the flow velocities in the fuel cells are different (1.94 cm min^{-1} and 1.17 cm min^{-1} for parallel channel EBFC and the single channel EBFC respectively). This difference in the flow velocity could potentially be the cause behind differing power outputs observed previously. It was thus decided to investigate the effects of flow velocity on the power output of the different fuel cells.

Figure 113 shows preliminary data collected from a study on the impact of different flow velocities on the power output of the different EBFCs. As shown, differences in flow velocity of the same order of magnitude have little effect on power output (note that flow velocity is shown on a logarithmic scale). Thus it is fair to say that the slight differences in flow velocities used previously accounts for little variance in the performance between the two types of EBFCs. However, increasing flow velocity exponentially does seem to have significant effects on fuel cell performance. Since increasing flow adversely affects the affinity of GOx for glucose, an inverse correlation between power output and flow velocity is expected. This is observed in the case of the parallel channel fuel cell.

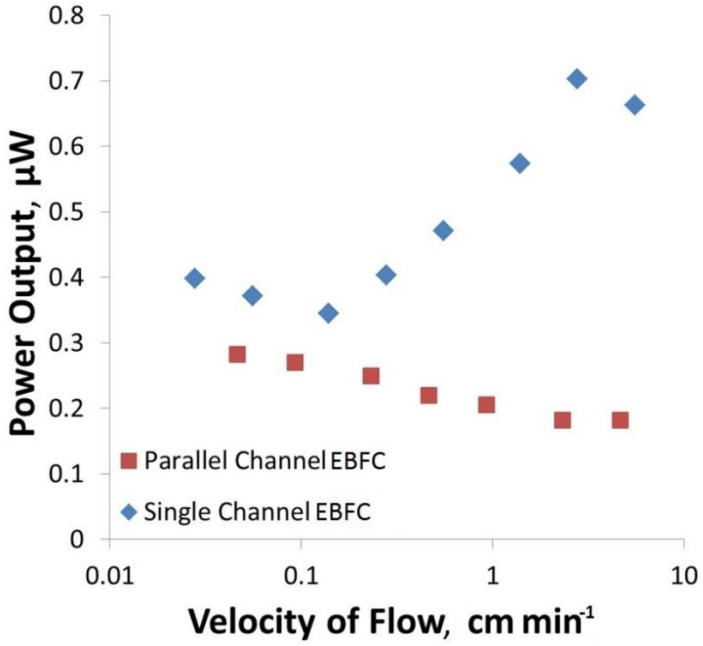

Figure 113: Average power output observed at different flow velocities with each fuel cell configuration. Testing performed on fuel cells which had already operated continuously for 24 hours.

Contrarily, the single channel EBFC shows increasing power output with increasing velocity of flow. The performance increases so much that at high flow rates the specific performance of the single channel fuel exceeds that of the parallel channel fuel cell. This suggests that there is indeed H_2O_2 back diffusion from the hPG-GOx electrodes to the hPG-RvLAC electrodes which is overcome by increasing flow rates. The increased power output could also be due to a better supply of reactants to hard-to-reach regions of the pleated electrodes owing to increased turbulent mixing. The placement of the electrodes in the parallel channel fuel cell does not encourage such turbulent mixing and as such this system would not gain any of the same benefits from higher flow velocities.

Unfortunately higher flow velocities can have adverse effects on the stability of the enzymatic electrodes by causing detachment or leaching of enzymes from the electrode pores. It also means a much higher throughput of fuel, with exponential increases in flow rate yielding only minor increases in performance, so may not be viable for continuous operation.

7.3.4. SENSITIVITY TO GLUCOSE

It was initially assumed that the concentration of glucose used in the feed was above the maximum concentration to which the hPG-GOx electrode was sensitive. This was based on results obtained when testing the performance of the hPG-GOx electrodes as glucose biosensors (Section 6.1.2.). Thus fluctuations in the feed concentration of glucose, or in the flow rate of the feed, should yield minimal changes in the power output of the EBFCs.

To verify whether the validity of this hypothesis, a glucose sensitivity analysis was conducted using one EBFC of each design. The EBFCs were run continuously for 24 hours before being flushed with PBS. The concentration of glucose fed to the EBFCs was then increased in a step-wise fashion, and at each step power output from each EBFC was allowed to stabilise before being recorded.

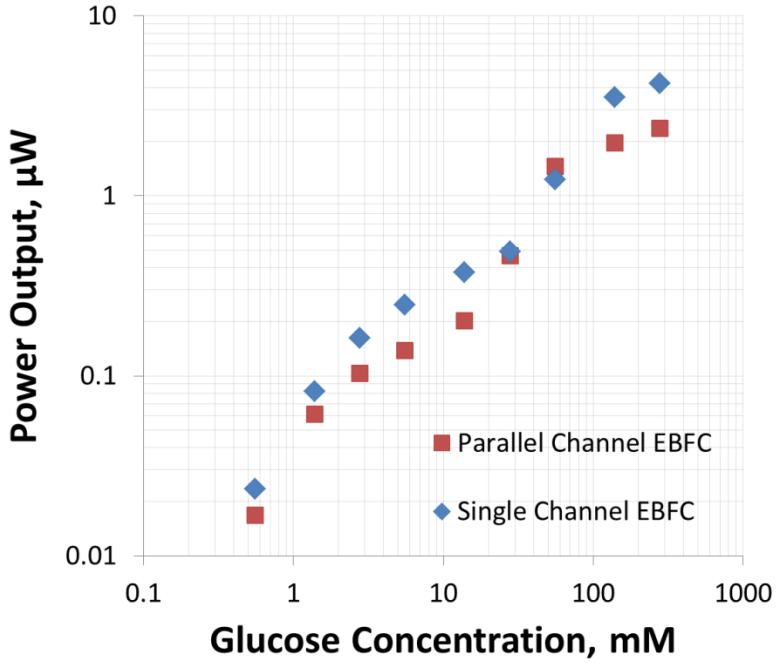

Figure 114: EBFC power output related to glucose concentration in the feed.

Figure 114 shows the power outputs observed from the EBFCs with different feed concentrations of glucose. The power output from both EBFCs is not maximised at the concentration used in the previous tests (approximately 27 mM). Instead the power output continues to increase across the entire concentration range considered. This suggests that the maximum current observed when using the hPG-GOx electrode as a biosensor, was actually due to different limiting factor and not the enzyme's affinity towards glucose. Since the hPG-GOx biosensor actually measured the hPG response to the secondary product H_2O_2, this system could have been limited by the concentration of oxygen, or the affinity of reduced GOx to oxygen.

Since the EBFC does not appear to have the same limitations, it suggests that this system is not reliant on the production of H_2O_2, but instead achieves a degree of DET between the hPG and GOx. Closer examination of the curves created here points towards a possible false plateau of power output that both EBFCs approach at one point (approximately 14 mM and 27 mM for the parallel channel and single channel EBFCs respectively). This suggests that there are elements of both MET by H_2O_2 and DET. As oxygen (or the affinity of reduced GOx to oxygen) becomes a

limiting factor, the power output in relation to glucose concentration levels off slightly. Subsequently the increase in power output in relation to glucose is only dependant on DET.

These are however only preliminary results obtained from one EBFC of each design. A more in depth study is required to confirm the trends observed and to better understand the oxygen dependence or independence of the hPG-GOx electrode in this case. Only then is it possible to prove or disprove the occurrence of DET in this case.

7.3.5. STABILITY

Even though the initial power outputs from EBFCs are frequently reported to be sufficient to power small implantable medical devices such as pacemakers, the long term stability during continuous operation is rarely as respectable. In fact many EBFCs reported so far exhibit a rapid decay in performance with most lasting mere hours [43, 44, 50, 65]. In order to determine the long term stability of the EBFCs it was decided to record the power output during continuous operation for a period of 1 month. The parallel channel fuel cell was selected for this analysis since it produced a more stable power output at low flow rates and it was believed to be the more stable of the two designs due to a minimal risk of deactivation of the hPG-RvLAC electrode by H_2O_2 diffusing from the hPG-GOx electrode.

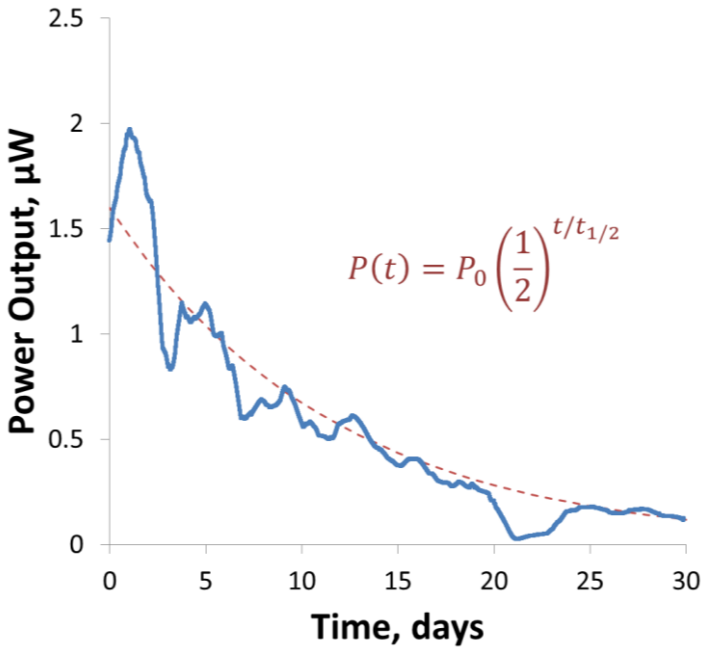

Figure 115: Power output during continuous operation over 1 month period. Dashed line indicates theoretical power output based on half-life of 8 days. EBFC was continuously fed with a PBS solution containing 5 g l^{-1} glucose and maintained at 37°C [159].

Figure 115 shows the continuous power production from a parallel channel fuel cell over a period of 30 days. As shown, the EBFC actually exhibited a growth in power output over the first

48 hours of operation before entering a general decay phase. It is important to note that the noise or large fluctuations in the power output observed is due to the evolution of gas bubbles within the EBFC. Though every effort was taken to prevent this occurring (by for example using drips prior to feeding the EBFC and heating the feed during the aeration stage), some gas bubbles still evolve during long-term continuous operation.

A sharp drop in power output was also observed after 20 days of continuous operation. Power was not restored until the 23rd day of operation when the EBFC was flushed with a fresh PBS solution. This suggests that there may have been some microbial contamination of the feed which inhibited power production.

Regardless of the short-term fluctuations in the power output from the EBFC, a strong trend is maintained with an apparent constant rate of decay. From this decay the half-life of the EBFC was determined to be approximately 8 days. Since there is no other research reported to have used a continuous flow through EBFC design, or to have even tested the long term stability of a glucose and oxygen EBFC for this period of time, it is difficult to make comparisons to existing literature on the subject. However, this EBFC has a half-life which is in line with the half-life of free LAC in solution (3 - 8 days under optimal conditions [200]), and also with that of a carbon based GOx and LAC fuel cell (approximately 6 days based on continuous operation for 72 hours [201]). Since GOx has reported half-lives in excess of 200 days we can assume that the RvLAC electrode is the limiting factor here and the cause of the decay in power output [202]. This is very promising since the majority of such devices exhibit much faster decays in power output owing to deactivation or detachment of enzymes. The fact that the decay in power output is in line with the decay of the enzymes themselves suggests that the methods employed for immobilisation are stable over long periods of time. Thus, in theory, the long term stability of this fuel cell can be improved by simply increasing the stability of the enzymes used, either through genetic modification, or through cross-linking with stabilising polymers.

7.4. DISCUSSION AND CONCLUSIONS

Both EBFC configurations tested show very promising power output levels during continuous operation. There are several factors which have been found to influence power output of these EBFCs including the channel designs, the shape and size of the electrodes used, and flow rate through the few cells.

Since the factors affecting power output have further implications on the cost and size of the EBFC, the design will ultimately come down to priorities. For example if limiting the EBFC volume is the most important factor, then using more or larger electrodes in the same space will

maximise power output, but this will increase cost. Conversely the cost can be minimised, and the specific power output can be maximised, by physically separating the anode and cathode and thus increasing the relative size of the EBFC.

In order to better quantify the cumulative effects of each of these factors, further investigation of both electrode configuration and flow channel design is necessary to determine specific effects of each parameter. Fortunately the methods outlined here allow for the fast prototyping of different fuel cell designs with 3D designed channels taking less than 1 hour to produce (inclusive of 3D printing time and casting in PDMS) and the hPG-GOx electrode and hPG-RvLAC electrodes taking approximately 1 hour and 16 hours to produce respectively. This means that for a given set of parameters, or flow conditions, several prototype EBFC designs can be tested within a very short window of time in order to determine the best design for a given situation.

The most significant finding of this work is the long term stability of the EBFCs during continuous operation. Such devices typically exhibit lifetimes of mere hours owing to the detachment or deactivation of enzymes, or commonly due to the leaching of redox mediators vital for operation. In this case however, there are no mediators utilised and the power output remains seemingly unchanged for the first 24 hours of operation. Only during continual use over days is any decay in performance observed, and even then the half-life of decay is in line with the decay of the enzymes under extremely favourable conditions.

8. CONCLUSIONS AND SUGGESTED FUTURE WORK

The aim of this project was to produce a biocompatible fuel cell that can generate power from metabolites found naturally in blood or interstitial fluids in the human body with a view to potential implantation. The work presented here marks a major step towards achieving this goal, with the successful development of a working EBFC which generates power from glucose. There is however much more work to do in order to develop a prototype device that is safe for implantation. In addition several other potential applications of the technologies developed here should also be investigated, especially the potential use of the enzymatic electrodes as highly specific sensors.

8.1. GLUCOSE SENSORS

8.1.1. ABIOTIC hPG GLUCOSE SENSORS

The hPG electrodes created here show a very high range of sensitivity to glucose (from 0.5 µM to 50 mM) as well as a high degree of stability. Thus these hPG electrodes could potentially be used in a wide range of applications, from medical applications to process monitoring. In this project the potential use of these electrodes for non-invasive blood glucose monitoring were considered. Specifically the potential use of these sensors to monitor glucose levels in urine samples and in transdermal fluids were investigated.

A high sensitivity and stability was observed when using artificial urine samples. For the purpose of monitoring glucose levels in transdermal fluids, a very high level of glucose sensitivity and specificity is required at very low concentrations of glucose (0.5 µM to 27 µM). Currently this has not been shown to be possible since a large degree of inference was observed when using transdermal fluids. One potential source of this interference comes from the relatively high concentrations of amino acids present in these fluids. Further research is required to better understand the exact source of the inference observed in this case, and consequently the removal or mitigation of this interference should also be investigated.

The potential use of hPG as online glucose sensor in process monitoring should also be investigated. For example, the live monitoring of glucose levels in a fermentation vessel could be investigated. The live monitoring of glucose in this case could be used as an indication of fermentation progress, and allow for better batch fed process monitoring.

8.1.2. GLUCOSE BIOSENSORS

hPG electrodes have been proven to be an excellent substrate for the functional immobilisation of GOx using simple electrostatic attachment methods to achieve very high enzyme loading

loadings. These hPG-GOx electrodes have been shown to serve as excellent glucose biosensors with a high specific sensitivity (22.7 µA mM^{-1} cm^{-2}), a broad sensitivity range, and high degree of stability (with concurrent responses to glucose over a period of 5 days).

In theory the use of these enzymes lend a high degree of specificity to the electrodes, and thus they should not be susceptible to the same interference as was observed with abiotic hPG glucose sensors. Thus they could potentially be used to determine glucose concentrations in transdermal fluids, such sweat and skin extracts derived by iontophoresis or electroosmosis, for non-invasive glucose monitoring.

To verify that this is the case a study should be conducted using biological samples such as the pig skin extracts derived by iontophoresis, or electroosmotic extracts from living subjects. The stability in biological solutions (both short and long term) of these hPG-GOx electrodes should be also determined for their use as biosensors.

8.2. EBFCs

8.2.1. IMMOBILISATION TECHNIQUES

The enzyme immobilisation techniques utilised are based on the simplest and most effective methods available. Though non-permanent, the electrostatic attraction and attachment of GOx onto hPG has been shown to be hugely successful even during long term continuous operation (stable power production during continuous operation for up to 30 days has been demonstrated). Conversely the immobilisation of LAC was achieved using established covalent coupling methods. This was due to the fact that the initial use of TvLAC meant that electrostatic immobilisation could not be employed at the cathode since TvLAC had a conflicting charge at neutral pH. When subsequent work with RvLAC was conducted the same established TvLAC immobilisation method was employed. However, since the isoelectric point of RvLAC is at pH 8.2 [203], it would in fact be positively charged at neutral pH and would thus not be repelled by the negatively charged cathode. This means that electrostatic attraction could be used to immobilise RvLAC on hPG.

An investigation should therefore be conducted on the effectiveness of using electrostatic attraction to immobilise RvLAC, either on its own, or in conjunction with covalent coupling at greatly increased loadings.

8.2.2. EBFC DESIGN

Results collected so far from the EBFCs point to some potential advantages of using a physical divider between electrodes to increase stability and specific power output. These findings are

based on the comparison of two different EBFC configurations in which the size and shape of the electrodes used also differed.

To verify and gain a better understanding of the apparent benefits of using a physical divider between electrodes, a control study should be conducted using the same 1 cm long hPG electrodes in the absence of a physical divider (see Figure 116A).

The use of multiple anodes and cathodes in the same channel should also be investigated (Figure 116B). These could simply serve to increase the surface are of the anode and cathode, or could be used in conjunction with different enzymes. For example, a GOx electrode could be placed upstream from an enzymatic electrode capable of further oxidising gluconolactone, or for oxidising unreacted H_2O_2 produced by the GOx electrode.

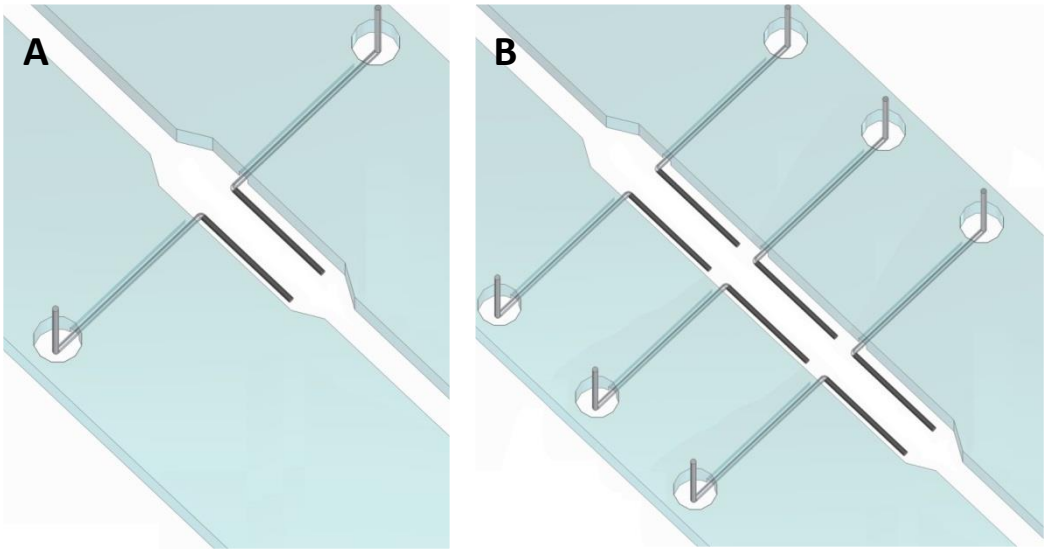

Figure 116: Suggested EBFC designs to consider; A- two electrodes without physical divider, B- six electrode design.

The EBFCs produced here should also be tested in less ideal solutions more closely resembling the composition of blood. Ideally testing would progress to the stage of using plasma derived from whole blood.

Following the development of a better understanding of the design impacts on EBFC performance, and following studies in biological solutions, the EBFCs should be further miniaturised and a prototype could potentially be implanted in a living organism such as a rat.

REFERENCES

1. A. Demirbas, *Political, economic and environmental impacts of biofuels: A review.* Applied Energy, 2009. **86, Supplement 1**(0): p. S108-S117.
2. S. Kerzenmacher, U. Kräling, T. Metz, R. Zengerle and F. von Stetten, *A potentially implantable glucose fuel cell with Raney-platinum film electrodes for improved hydrolytic and oxidative stability.* Journal of Power Sources, 2010. **196**(3): p. 1264-1272.
3. D. Bhatnagar, S. Xu, C. Fischer, R.L. Arechederra and S.D. Minteer, *Mitochondrial biofuel cells: expanding fuel diversity to amino acids.* Physical Chemistry Chemical Physics, 2011. **13**(1): p. 86-92.
4. A.T. Yahiro, S.M. Lee and D.O. Kimble, *Bioelectrochemistry: I. Enzyme utilizing bio-fuel cell studies.* Biochimica et Biophysica Acta (BBA) - Specialized Section on Biophysical Subjects, 1964. **88**(2): p. 375-383.
5. K. Lewis, *Symposium on Bioelectrochemistry of Microorganisms IV. Biochemical Fuel Cells.* Bacteriological Reviews, 1966. **30**(1): p. 101-113.
6. J. Giner, L. Marincic, J.S. Soeldner and C.K. Colton, *Electrochemical Glucose Oxidation on a Platinized Platinum Electrode in Krebs-Ringer Solution.* Journal of The Electrochemical Society, 1981. **128**(10): p. 2106-2114.
7. J. Larminie and A. Dicks, *Fuel Cell Systems Explained*. Second ed. 2003: John Wiley & Sons Ltd.
8. M.C. Potter, *Electrical Effects Accompanying the Decomposition of Organic Compounds.* Proceedings of the Royal Society of London. Series B, Containing Papers of a Biological Character, 1911. **84**(571): p. 260-276.
9. I. Karube, T. Matsunaga, S. Tsuru and S. Suzuki, *Biochemical fuel cell utilizing immobilized cells of clostridium butyricum.* Biotechnology and Bioengineering, 1977. **19**(11): p. 1727-1733.
10. P.S. May, G.C. Blanchard and R.T. Foley, *BIOCHEMICAL FUEL CELL.* US DEPT. OF DEFENSE DOCUMENTATION CENTER, 1963.
11. J.B. Davis and H.F. Yarbrough, *Preliminary Experiments on a Microbial Fuel Cell.* Science, 1962. **137**(3530): p. 615-616.
12. B.C.H. Steele and A. Heinzel, *Materials for fuel-cell technologies.* Nature, 2001. **414**(6861): p. 345-352.
13. H. Liu and B.E. Logan, *Electricity Generation Using an Air-Cathode Single Chamber Microbial Fuel Cell in the Presence and Absence of a Proton Exchange Membrane.* Environmental Science & Technology, 2004. **38**(14): p. 4040-4046.
14. P. Clauwaert, D. van der Ha, N. Boon, K. Verbeken, M. Verhaege, K. Rabaey and W. Verstraete, *Open Air Biocathode Enables Effective Electricity Generation with Microbial Fuel Cells.* Environmental Science & Technology, 2007. **41**(21): p. 7564-7569.
15. N. Kakehi, T. Yamazaki, W. Tsugawa and K. Sode, *A novel wireless glucose sensor employing direct electron transfer principle based enzyme fuel cell.* Biosensors and Bioelectronics, 2007. **22**(9–10): p. 2250-2255.
16. S.N. Thennadil, J.L. Rennert, B.J. Wenzel, K.H. Hazen, T.L. Ruchti and M.B. Block, *Comparison of glucose concentration in interstitial fluid, and capillary and venous blood during rapid changes in blood glucose levels.* Diabetes technology & therapeutics, 2001. **3**(3): p. 357-365.
17. D.A.T. Southgate and J.V.G.A. Durnin, *Calorie conversion factors. An experimental reassessment of the factors used in the calculation of the energy value of human diets.* British Journal of Nutrition, 1970. **24**(02): p. 517-535.
18. S. Cosnier, A. Le Goff and M. Holzinger, *Towards glucose biofuel cells implanted in human body for powering artificial organs: Review.* Electrochemistry Communications, 2014. **38**(0): p. 19-23.

19. D. Simmonds, *A sweet idea*, in *The Economist*. 2012. p. 79-80.
20. D.L. Hayes and S. Furman, *Cardiac pacing: How it started, where we are, where we are going.* PACE - Pacing and Clinical Electrophysiology, 2004. **27**(5): p. 693-704.
21. P.D. Mitcheson, E.M. Yeatman, G.K. Rao, A.S. Holmes and T.C. Green, *Energy harvesting from human and machine motion for wireless electronic devices.* Proceedings of the IEEE, 2008. **96**(9): p. 1457-1486.
22. V. Leonov, T. Torfs, P. Fiorini and C. Van Hoof, *Thermoelectric converters of human warmth for self-powered wireless sensor nodes.* IEEE Sensors Journal, 2007. **7**(5): p. 650-656.
23. M.W. Baker and R. Sarpeshkar, *Feedback analysis and design of RF power links for low-power bionic systems.* IEEE Transactions on Biomedical Circuits and Systems, 2007. **1**(1): p. 28-38.
24. G.A. Covic and J.T. Boys, *Inductive Power Transfer.* Proceedings of the IEEE, 2013. **101**(6): p. 1276-1289.
25. X. Wei and J. Liu, *Power sources and electrical recharging strategies for implantable medical devices.* Frontiers of Energy and Power Engineering in China, 2008. **2**(1): p. 1-13.
26. D. Prutchi. *Nuclear Pacemakers*. 2005 2005 [Accessed: 02/11/2011] Available from: http://home.comcast.net/~dprutchi/nuclear_pacemakers.pdf
27. R.F. Drake, B.K. Kusserow, S. Messinger and S. Matsuda, *A tissue implantable fuel cell power supply.* Transactions - American Society for Artificial Internal Organs, 1970. **16**: p. 199-205.
28. J. Giner, G. Holleck and P.A. Malachesky, *Eine implantierbare Brennstoffzelle zum Betrieb eines mechanischen Herzens.* Berichte der Bunsengesellschaft für physikalische Chemie, 1973. **77**(10-11): p. 782-783.
29. S. Kerzenmacher, J. Ducrée, R. Zengerle and F. von Stetten, *Energy harvesting by implantable abiotically catalyzed glucose fuel cells.* Journal of Power Sources, 2008. **182**(1): p. 1-17.
30. J.R. Rao and G. Richter, *Implantable bio-electrochemical power sources.* Naturwissenschaften, 1974. **61**(5): p. 200-206.
31. E. Weidlich, G. Richter, F. von Sturm, J.R. Rao, A. Thorén and H. Lagergren, *Animal Experiments with Biogalvanic and Biofuel Cells.* Artificial Cells, Blood Substitutes and Biotechnology, 1976. **4**(3-4): p. 277-306.
32. A.P. Chandrakasan, N. Verma and D.C. Daly, *Ultralow-Power Electronics for Biomedical Applications.* Annual Review of Biomedical Engineering, 2008. **10**(1): p. 247-274.
33. F.v. Stetten, S. Kerzenmacher, A. Lorenz, V. Chokkalingam, N. Miyakawa, R. Zengerle and J. Ducree. *A One-Compartment, Direct Glucose Fuel Cell for Powering Long-Term Medical Implants*. in *Micro Electro Mechanical Systems, 2006. MEMS 2006 Istanbul. 19th IEEE International Conference on*. 2006.
34. T. Sharma, Y. Hu, M. Stoller, M. Feldman, R.S. Ruoff, M. Ferrari and X. Zhang, *Mesoporous silica as a membrane for ultra-thin implantable direct glucose fuel cells.* Lab on a Chip, 2011. **11**(14): p. 2460-2465.
35. A. Kloke, B. Biller, U. Kräling, S. Kerzenmacher, R. Zengerle and F. von Stetten, *A Single Layer Glucose Fuel Cell Intended as Power Supplying Coating for Medical Implants.* Fuel Cells, 2011. **11**(2): p. 316-326.
36. A. Kloke, B. Biller, U. Kräling, S. Kerzenmacher, R. Zengerle and F. von Stetten. *A Single Layer Glucose Fuel Cell Intended as Power Supplying Coating for Medical Implants*. 2011 [Accessed: 22/09/2014] Available from: http://www.bioss.uni-freiburg.de/cms/1516.html

37. A. Zebda, S. Cosnier, J.P. Alcaraz, M. Holzinger, A. Le Goff, C. Gondran, F. Boucher, F. Giroud, K. Gorgy, H. Lamraoui, and P. Cinquin, *Single Glucose Biofuel Cells Implanted in Rats Power Electronic Devices.* Sci. Rep., 2013. **3**.
38. L. Halámková, J. Halámek, V. Bocharova, A. Szczupak, L. Alfonta and E. Katz, *Implanted Biofuel Cell Operating in a Living Snail.* Journal of the American Chemical Society, 2012. **134**(11): p. 5040-5043.
39. E. Katz. *Evgeny Katz*. [Accessed: 23/09/2014] Available from: http://people.clarkson.edu/~ekatz/
40. D. Scherson. *New Fuels: Biofuels: Biofuel cell generates electricity when implanted in False Death's Head Cockroach* [Accessed: 23/09/2014] Available from: http://www.acs.org/content/acs/en/pressroom/podcasts/globalchallenges/newfuels1/new-fuels-biofuels-biofuel-cell-generates-electricity-when-implanted-in-false-deaths-head-cockroach.html
41. A. Szczupak, J. Halamek, L. Halamkova, V. Bocharova, L. Alfonta and E. Katz, *Living battery - biofuel cells operating in vivo in clams.* Energy & Environmental Science, 2012. **5**(10): p. 8891-8895.
42. T. Miyake, K. Haneda, N. Nagai, Y. Yatagawa, H. Onami, S. Yoshino, T. Abe and M. Nishizawa, *Enzymatic biofuel cells designed for direct power generation from biofluids in living organisms.* Energy & Environmental Science, 2011. **4**(12): p. 5008-5012.
43. P. Cinquin, C. Gondran, F. Giroud, S. Mazabrard, A. Pellissier, F. Boucher, J.-P. Alcaraz, K. Gorgy, F. Lenouvel, S. Mathé, P. Porcu, and S. Cosnier, *A Glucose BioFuel Cell Implanted in Rats.* PLoS ONE, 2010. **5**(5): p. e10476.
44. K. MacVittie, J. Halamek, L. Halamkova, M. Southcott, W.D. Jemison, R. Lobel and E. Katz, *From "cyborg" lobsters to a pacemaker powered by implantable biofuel cells.* Energy & Environmental Science, 2013. **6**(1): p. 81-86.
45. M. Holzinger, A. Le Goff and S. Cosnier, *Carbon nanotube/enzyme biofuel cells.* Electrochimica Acta, 2012. **82**(0): p. 179-190.
46. S. Cosnier, D. Shan and S.-N. Ding, *An easy compartment-less biofuel cell construction based on the physical co-inclusion of enzyme and mediator redox within pressed graphite discs.* Electrochemistry Communications, 2010. **12**(2): p. 266-269.
47. L. Ren, D. Yan and W. Zhong, *Enhanced enzyme activity through electron transfer between single-walled carbon nanotubes and horseradish peroxidase.* Carbon, 2012. **50**(3): p. 1303-1310.
48. S.C. Barton, J. Gallaway and P. Atanassov, *Enzymatic biofuel cells for implantable and microscale devices.* Chemical reviews, 2004. **104**(10): p. 4867-4886.
49. A. Zebda, C. Gondran, A. Le Goff, M. Holzinger, P. Cinquin and S. Cosnier, *Mediatorless high-power glucose biofuel cells based on compressed carbon nanotube-enzyme electrodes.* Nat Commun, 2011. **2**: p. 370.
50. J.A. Castorena-Gonzalez, C. Foote, K. MacVittie, J. Halámek, L. Halámková, L.A. Martinez-Lemus and E. Katz, *Biofuel Cell Operating in Vivo in Rat.* Electroanalysis, 2013. **25**(7): p. 1579-1584.
51. E. Katz and K. MacVittie, *Implanted biofuel cells operating in vivo - methods, applications and perspectives - feature article.* Energy & Environmental Science, 2013. **6**(10): p. 2791-2803.
52. F.C.P.F. Sales, R.M. Iost, M.V.A. Martins, M.C. Almeida and F.N. Crespilho, *An intravenous implantable glucose/dioxygen biofuel cell with modified flexible carbon fiber electrodes.* Lab on a Chip, 2013. **13**(3): p. 468-474.
53. M. Bottini, S. Bruckner, K. Nika, N. Bottini, S. Bellucci, A. Magrini, A. Bergamaschi and T. Mustelin, *Multi-walled carbon nanotubes induce T lymphocyte apoptosis.* Toxicology Letters, 2006. **160**(2): p. 121-126.

54. A. Bianco, K. Kostarelos and M. Prato, *Making carbon nanotubes biocompatible and biodegradable.* Chemical Communications, 2011. **47**(37): p. 10182-10188.
55. V. Andoralov, M. Falk, D.B. Suyatin, M. Granmo, J. Sotres, R. Ludwig, V.O. Popov, J. Schouenborg, Z. Blum and S. Shleev, *Biofuel Cell Based on Microscale Nanostructured Electrodes with Inductive Coupling to Rat Brain Neurons.* Sci. Rep., 2013. **3**.
56. M. Falk, V. Andoralov, M. Silow, M.D. Toscano and S. Shleev, *Miniature Biofuel Cell as a Potential Power Source for Glucose-Sensing Contact Lenses.* Analytical Chemistry, 2013. **85**(13): p. 6342-6348.
57. B. Otis and B. Parviz. *Introducing our smart contact lens project* 2014 [Accessed: 25/09/2014] Available from: http://googleblog.blogspot.co.uk/2014/01/introducing-our-smart-contact-lens.html
58. A. Ward. *Google and Novartis to develop 'smart' contact lenses for diabetics*. 2014 [Accessed: 25/09/2014] Available from: http://www.ft.com/intl/cms/s/0/a4dd1838-0be1-11e4-a096-00144feabdc0.html
59. A. Habrioux, G. Merle, K. Servat, K.B. Kokoh, C. Innocent, M. Cretin and S. Tingry, *Concentric glucose/O2 biofuel cell.* Journal of Electroanalytical Chemistry, 2008. **622**(1): p. 97-102.
60. B.I. Rapoport, J.T. Kedzierski and R. Sarpeshkar, *A Glucose Fuel Cell for Implantable Brain–Machine Interfaces.* PLoS ONE, 2012. **7**(6): p. e38436.
61. A. Habrioux, E. Sibert, K. Servat, W. Vogel, K.B. Kokoh and N. Alonso-Vante, *Activity of Platinum−Gold Alloys for Glucose Electrooxidation in Biofuel Cells.* The Journal of Physical Chemistry B, 2007. **111**(34): p. 10329-10333.
62. T. Beneyton, I. Putu Mahendra Wijaya, C. Ben Salem, A.D. Griffiths and V. Taly, *Membraneless glucose/O2 microfluidic biofuel cells using covalently bound enzymes.* Chem. Commun., 2012. **49**: p. 1094-1096.
63. A. Zebda, L. Renaud, M. Cretin, C. Innocent, R. Ferrigno and S. Tingry, *Membraneless microchannel glucose biofuel cell with improved electrical performances.* Sensors and Actuators B: Chemical, 2010. **149**(1): p. 44-50.
64. P. Kavanagh, S. Boland, P. Jenkins and D. Leech, *Performance of a Glucose/O2 Enzymatic Biofuel Cell Containing a Mediated Melanocarpus albomyces Laccase Cathode in a Physiological Buffer.* Fuel Cells, 2009. **9**(1): p. 79-84.
65. M. Togo, A. Takamura, T. Asai, H. Kaji and M. Nishizawa, *An enzyme-based microfluidic biofuel cell using vitamin K3-mediated glucose oxidation.* Electrochimica Acta, 2007. **52**(14): p. 4669-4674.
66. R.A. Rincón, C. Lau, H.R. Luckarift, K.E. Garcia, E. Adkins, G.R. Johnson and P. Atanassov, *Enzymatic fuel cells: Integrating flow-through anode and air-breathing cathode into a membrane-less biofuel cell design.* Biosensors and Bioelectronics, 2011. **27**(1): p. 132-136.
67. H. Sakai, T. Nakagawa, Y. Tokita, T. Hatazawa, T. Ikeda, S. Tsujimura and K. Kano, *A high-power glucose/oxygen biofuel cell operating under quiescent conditions.* Energy & Environmental Science, 2009. **2**(1): p. 133-138.
68. M. Hakamada, M. Takahashi and M. Mabuchi, *Enzyme electrodes stabilized by monolayer-modified nanoporous Au for biofuel cells.* Gold Bulletin, 2012. **45**(1): p. 9-15.
69. U. Salaj-Kosla, M. Scanlon, T. Baumeister, K. Zahma, R. Ludwig, P. Conghaile, D. MacAodha, D. Leech and E. Magner, *Mediated electron transfer of cellobiose dehydrogenase and glucose oxidase at osmium polymer-modified nanoporous gold electrodes.* Analytical and Bioanalytical Chemistry, 2013. **405**(11): p. 3823-3830.
70. S.B. Bankar, M.V. Bule, R.S. Singhal and L. Ananthanarayan, *Glucose oxidase — An overview.* Biotechnology Advances, 2009. **27**(4): p. 489-501.
71. G. Wohlfahrt, S. Witt, J. Hendle, D. Schomburg, H.M. Kalisz and H.-J. Hecht, *1.8 and 1.9 A resolution structures of the Penicillium amagasakiense and Aspergillus niger glucose*

oxidases as a basis for modelling substrate complexes. Acta Crystallographica Section D, 1999. **55**(5): p. 969-977.

72. Wellcome Trust Sanger Institute - Genome Research Limited. *Family: Peroxidase (PF00141)*. [Accessed: 25/09/2012] Available from: http://pfam.sanger.ac.uk/family/peroxidase
73. I. Bento, L.O. Martins, G. Gato Lopes, M. Armenia Carrondo and P.F. Lindley, *Dioxygen reduction by multi-copper oxidases; a structural perspective.* Dalton Transactions, 2005(21): p. 3507-3513.
74. A.M. Mayer and R.C. Staples, *Laccase: new functions for an old enzyme.* Phytochemistry, 2002. **60**(6): p. 551-565.
75. A. Chaubey and B.D. Malhotra, *Mediated biosensors.* Biosensors and Bioelectronics, 2002. **17**(6-7): p. 441-456.
76. R.A. Bullen, T.C. Arnot, J.B. Lakeman and F.C. Walsh, *Biofuel cells and their development.* Biosensors and Bioelectronics, 2006. **21**(11): p. 2015-2045.
77. M. Shaolin and X. Huaiguo, *Bioelectrochemical characteristics of glucose oxidase immobilized in a polyaniline film.* Sensors and Actuators B: Chemical, 1996. **31**(3): p. 155-160.
78. Y. Degani and A. Heller, *Direct electrical communication between chemically modified enzymes and metal electrodes. I. Electron transfer from glucose oxidase to metal electrodes via electron relays, bound covalently to the enzyme.* The Journal of Physical Chemistry, 1987. **91**(6): p. 1285-1289.
79. M.J. Moehlenbrock and S.D. Minteer, *Extended lifetime biofuel cells.* Chemical Society Reviews, 2008. **37**(6): p. 1188-1196.
80. N. Yuhashi, M. Tomiyama, J. Okuda, S. Igarashi, K. Ikebukuro and K. Sode, *Development of a novel glucose enzyme fuel cell system employing protein engineered PQQ glucose dehydrogenase.* Biosensors and Bioelectronics, 2005. **20**(10): p. 2145-2150.
81. N. Mano, F. Mao, W. Shin, T. Chen and A. Heller, *A miniature biofuel cell operating at 0.78 V.* Chemical Communications, 2003(4): p. 518-519.
82. J. Lim, N. Cirigliano, J. Wang and B. Dunn, *Direct electron transfer in nanostructured sol-gel electrodes containing bilirubin oxidase.* Physical Chemistry Chemical Physics, 2007. **9**(15): p. 1809-1814.
83. H.R. Bungay, *BASIC Biochemical Engineering: Text & Disk with 75 Programs*. 1989: BiLine Associates.
84. I. Chibata, *Immobilized Enzymes: Research and Development* Kodansha scientific books. 1979: John Wiley & Sons Inc.
85. J.M. Guisan, *Immobilization of enzymes and cells*. Vol. 22. 2006: Springer.
86. J. Porath, *Salting-out adsorption techniques for protein purification.* Biopolymers, 1987. **26**(S0): p. S193-S204.
87. T.-W. Tsai, G. Heckert, L.s.F. Neves, Y. Tan, D.-Y. Kao, R.G. Harrison, D.E. Resasco and D.W. Schmidtke, *Adsorption of glucose oxidase onto single-walled carbon nanotubes and its application in layer-by-layer biosensors.* Analytical chemistry, 2009. **81**(19): p. 7917-7925.
88. A. Guiseppi-Elie, C. Lei and R.H. Baughman, *Direct electron transfer of glucose oxidase on carbon nanotubes.* Nanotechnology, 2002. **13**(5): p. 559.
89. H. Qiu, C. Xu, X. Huang, Y. Ding, Y. Qu and P. Gao, *Immobilization of Laccase on Nanoporous Gold: Comparative Studies on the Immobilization Strategies and the Particle Size Effects.* The Journal of Physical Chemistry C, 2009. **113**(6): p. 2521-2525.
90. M.K. Goel. *IMMOBILIZED ENZYMES*. 1994 [Accessed: 02/10/2014] Available from: http://www.rpi.edu/dept/chem-eng/Biotech-Environ/IMMOB/goel2nd.htm
91. E. Generalic. *"Zwitterion."* Croatian-English Chemistry Dictionary & Glossary. [Accessed: 02/10/2014] Available from: http://glossary.periodni.com/glossary.php?en=zwitterion

92. H. du Toit and M. Di Lorenzo, *Glucose Oxidase Directly Immobilized onto Highly Porous Gold Electrodes for Sensing and Fuel Cell applications.* Electrochimica Acta, 2014. **138**(0): p. 86-92.
93. B. Mattiasson and R. Kaul, *Determination of coupling yields and handling of labile proteins in immobilization technology.* Bioprocess technology, 1990. **14**: p. 161-179.
94. D. Li, Q. He, Y. Cui, L. Duan and J. Li, *Immobilization of glucose oxidase onto gold nanoparticles with enhanced thermostability.* Biochemical and Biophysical Research Communications, 2007. **355**(2): p. 488-493.
95. S. Zhang, N. Wang, H. Yu, Y. Niu and C. Sun, *Covalent attachment of glucose oxidase to an Au electrode modified with gold nanoparticles for use as glucose biosensor.* Bioelectrochemistry, 2005. **67**(1): p. 15-22.
96. ThermoScientific. *Chemistry of Crosslinking*. [Accessed: 01/10/2014] Available from: http://www.piercenet.com/method/chemistry-crosslinking
97. ThermoScientific. *NHS and Sulfo-NHS*. [Accessed: 01/10/2014] Available from: http://www.piercenet.com/product/nhs-sulfo-nhs
98. K.F. O'Driscoll, *[12] Techniques of enzyme entrapment in gels*, in *Methods in Enzymology*, M. Klaus, Editor. 1976, Academic Press. p. 169-183.
99. B.C. Dave, B. Dunn, J.S. Valentine and J.I. Zink, *Sol-gel encapsulation methods for biosensors.* Analytical Chemistry, 1994. **66**(22): p. 1120A-1127A.
100. A.C. Pierre, *The sol-gel encapsulation of enzymes.* Biocatalysis and Biotransformation, 2004. **22**(3): p. 145-170.
101. R.B. Bhatia, C.J. Brinker, A.K. Gupta and A.K. Singh, *Aqueous Sol–Gel Process for Protein Encapsulation.* Chemistry of Materials, 2000. **12**(8): p. 2434-2441.
102. J. Wang, *Glucose Biosensors: 40 Years of Advances and Challenges.* Electroanalysis, 2001. **13**(12): p. 983-988.
103. R. Sahney, S. Anand, B.K. Puri and A.K. Srivastava, *A comparative study of immobilization techniques for urease on glass-pH-electrode and its application in urea detection in blood serum.* Analytica Chimica Acta, 2006. **578**(2): p. 156-161.
104. K. Zeng, H. Tachikawa, Z. Zhu and V.L. Davidson, *Amperometric Detection of Histamine with a Methylamine Dehydrogenase Polypyrrole-Based Sensor.* Analytical Chemistry, 2000. **72**(10): p. 2211-2215.
105. Y. Liu, M. Wang, F. Zhao, Z. Xu and S. Dong, *The direct electron transfer of glucose oxidase and glucose biosensor based on carbon nanotubes/chitosan matrix.* Biosensors and Bioelectronics, 2005. **21**(6): p. 984-988.
106. D. Ivnitski, B. Branch, P. Atanassov and C. Apblett, *Glucose oxidase anode for biofuel cell based on direct electron transfer.* Electrochemistry Communications, 2006. **8**(8): p. 1204-1210.
107. S. Zhang, N. Wang, Y. Niu and C. Sun, *Immobilization of glucose oxidase on gold nanoparticles modified Au electrode for the construction of biosensor.* Sensors and Actuators B: Chemical, 2005. **109**(2): p. 367-374.
108. T.J. Thomas, K.E. Ponnusamy, N.M. Chang, K. Galmore and S.D. Minteer, *Effects of annealing on mixture-cast membranes of Nafion® and quaternary ammonium bromide salts.* Journal of Membrane Science, 2003. **213**(1–2): p. 55-66.
109. C.M. Moore, N.L. Akers, A.D. Hill, Z.C. Johnson and S.D. Minteer, *Improving the Environment for Immobilized Dehydrogenase Enzymes by Modifying Nafion with Tetraalkylammonium Bromides.* Biomacromolecules, 2004. **5**(4): p. 1241-1247.
110. M.C. Dixon, T.A. Daniel, M. Hieda, D.M. Smilgies, M.H.W. Chan and D.L. Allara, *Preparation, Structure, and Optical Properties of Nanoporous Gold Thin Films.* Langmuir, 2007. **23**(5): p. 2414-2422.

111. P.N. Ciesielski, A.M. Scott, C.J. Faulkner, B.J. Berron, D.E. Cliffel and G.K. Jennings, *Functionalized Nanoporous Gold Leaf Electrode Films for the Immobilization of Photosystem I.* ACS Nano, 2008. **2**(12): p. 2465-2472.
112. C. Xu, J. Su, X. Xu, P. Liu, H. Zhao, F. Tian and Y. Ding, *Low Temperature CO Oxidation over Unsupported Nanoporous Gold.* Journal of the American Chemical Society, 2006. **129**(1): p. 42-43.
113. X. Yan, X. Ge and S. Cui, *Pt-decorated nanoporous gold for glucose electrooxidation in neutral and alkaline solutions.* Nanoscale Research Letters, 2011. **6**(1): p. 313.
114. B. Seo and J. Kim, *Electrooxidation of Glucose at Nanoporous Gold Surfaces: Structure Dependent Electrocatalysis and Its Application to Amperometric Detection.* Electroanalysis, 2010. **22**(9): p. 939-945.
115. J.F. Huang and I.W. Sun, *Fabrication and Surface Functionalization of Nanoporous Gold by Electrochemical Alloying/Dealloying of Au–Zn in an Ionic Liquid, and the Self-Assembly of L-Cysteine Monolayers.* Advanced Functional Materials, 2005. **15**(6): p. 989-994.
116. F. Jia, C. Yu, Z. Ai and L. Zhang, *Fabrication of Nanoporous Gold Film Electrodes with Ultrahigh Surface Area and Electrochemical Activity.* Chemistry of Materials, 2007. **19**(15): p. 3648-3653.
117. H. Zhang, J.-J. Xu and H.-Y. Chen, *Shape-Controlled Gold Nanoarchitectures: Synthesis, Superhydrophobicity, and Electrocatalytic Properties.* The Journal of Physical Chemistry C, 2008. **112**(36): p. 13886-13892.
118. L. Kashefi-Kheyrabadi and M.A. Mehrgardi, *Aptamer-based electrochemical biosensor for detection of adenosine triphosphate using a nanoporous gold platform.* Bioelectrochemistry, 2013. **94**(0): p. 47-52.
119. D. van Noort and C.-F. Mandenius, *Porous gold surfaces for biosensor applications.* Biosensors and Bioelectronics, 2000. **15**(3–4): p. 203-209.
120. Y. Xia, W. Huang, J. Zheng, Z. Niu and Z. Li, *Nonenzymatic amperometric response of glucose on a nanoporous gold film electrode fabricated by a rapid and simple electrochemical method.* Biosensors and Bioelectronics, 2011. **26**(8): p. 3555-3561.
121. Y. Deng, W. Huang, X. Chen and Z. Li, *Facile fabrication of nanoporous gold film electrodes.* Electrochemistry Communications, 2008. **10**(5): p. 810-813.
122. R. Zhang and H. Olin, *Porous Gold Films—A Short Review on Recent Progress.* Materials, 2014. **7**(5): p. 3834-3854.
123. Y.-G. Zhou, S. Yang, Q.-Y. Qian and X.-H. Xia, *Gold nanoparticles integrated in a nanotube array for electrochemical detection of glucose.* Electrochemistry Communications, 2009. **11**(1): p. 216-219.
124. P. Evans, W.R. Hendren, R. Atkinson, G.A. Wurtz, W. Dickson, A.V. Zayats and R.J. Pollard, *Growth and properties of gold and nickel nanorods in thin film alumina.* Nanotechnology, 2006. **17**(23): p. 5746.
125. Y. Lu, Q. Wang, J. Sun and J. Shen, *Selective Dissolution of the Silver Component in Colloidal Au and Ag Multilayers: A Facile Way to Prepare Nanoporous Gold Film Materials.* Langmuir, 2005. **21**(11): p. 5179-5184.
126. Y. Bai, W. Yang, Y. Sun and C. Sun, *Enzyme-free glucose sensor based on a three-dimensional gold film electrode.* Sensors and Actuators B: Chemical, 2008. **134**(2): p. 471-476.
127. C.H. Wang, C. Yang, Y.Y. Song, W. Gao and X.H. Xia, *Adsorption and Direct Electron Transfer from Hemoglobin into a Three-Dimensionally Ordered Macroporous Gold Film.* Advanced Functional Materials, 2005. **15**(8): p. 1267-1275.
128. X. Chen, Y. Wang, J. Zhou, W. Yan, X. Li and J.-J. Zhu, *Electrochemical Impedance Immunosensor Based on Three-Dimensionally Ordered Macroporous Gold Film.* Analytical Chemistry, 2008. **80**(6): p. 2133-2140.

129. B. Zhao and M.M. Collinson, *Hierarchical porous gold electrodes: Preparation, characterization, and electrochemical behavior.* Journal of Electroanalytical Chemistry, 2012. **684**(0): p. 53-59.
130. S. Cherevko and C.-H. Chung, *Direct electrodeposition of nanoporous gold with controlled multimodal pore size distribution.* Electrochemistry Communications, 2011. **13**(1): p. 16-19.
131. H. du Toit and M. Di Lorenzo, *Electrodeposited highly porous gold microelectrodes for the direct electrocatalytic oxidation of aqueous glucose.* Sensors and Actuators B: Chemical, 2014. **192**(0): p. 725-729.
132. Y. Li, Y.-Y. Song, C. Yang and X.-H. Xia, *Hydrogen bubble dynamic template synthesis of porous gold for nonenzymatic electrochemical detection of glucose.* Electrochemistry Communications, 2007. **9**(5): p. 981-988.
133. J.C. Slater, *Atomic Radii in Crystals.* The Journal of Chemical Physics, 1964. **41**(10): p. 3199-3204.
134. M. Mohl, A. Kumar, A.L.M. Reddy, A. Kukovecz, Z. Konya, I. Kiricsi, R. Vajtai and P.M. Ajayan, *Synthesis of Catalytic Porous Metallic Nanorods by Galvanic Exchange Reaction.* The Journal of Physical Chemistry C, 2009. **114**(1): p. 389-393.
135. A.J. Bard and L.R. Faulkner, *ELECTROCHEMICAL METHODS: Fundamentals and Applications*. Second ed. 2001: JOHN WILEY & SONS, INC.
136. *Tech Note, Rev. 3.0*. 26/04/2011 [cited 2012 [Accessed: 30/06/2011] Available from: http://www.gamry.com/assets/Application-Notes/2-3-4-Electrodes.pdf
137. C.M. Brett, A.M.O. Brett and J. Heinze, *Electrochemistry: principles, methods, and applications*. Vol. 4. 1993: Oxford university press Oxford.
138. A.J. Bard and L.R. Faulkner, *Electrochemical methods: fundamentals and applications*. Vol. 2. 1980: Wiley New York.
139. C. Andrade, M. Danielly Oliveira, T. Faulin, V. Hering and D.S.P. Abdalla, *Biosensors for detection of Low-Density Lipoprotein and its modified forms* in *Biosensors for Health, Environment and Biosecurity*, P.P.A. Serra, Editor. 2011: InTech.
140. R.S. Kelly. *Analytical Electrochemistry: The Basic Concepts*. [Accessed: 30/09/2012] Available from: http://www.asdlib.org/onlineArticles/ecourseware/Kelly_Potentiometry/PDF-12-CV-Additional.pdf
141. O. Barbieri, M. Hahn, A. Herzog and R. Kötz, *Capacitance limits of high surface area activated carbons for double layer capacitors.* Carbon, 2005. **43**(6): p. 1303-1310.
142. R.A. Marusak, K. Doan and S.D. Cummings, *Appendix 6: A Brief Guide to Writing in Chemistry*, in *Integrated Approach to Coordination Chemistry*. 2006, John Wiley & Sons, Inc. p. 252-259.
143. J. Wang, *Carbon-Nanotube Based Electrochemical Biosensors: A Review.* Electroanalysis, 2005. **17**(1): p. 7-14.
144. J. Wang, *Amperometric biosensors for clinical and therapeutic drug monitoring: a review.* Journal of Pharmaceutical and Biomedical Analysis, 1999. **19**(1–2): p. 47-53.
145. R. Baker and J. Zhang. *PROTON EXCHANGE MEMBRANE or POLYMER ELECTROLYTE MEMBRANE (PEM) FUEL CELLS*. 2011 [Accessed: 02/11/2014] Available from: http://knowledge.electrochem.org/encycl/art-f04-fuel-cells-pem.htm
146. J. Zhang, *PEM fuel cell electrocatalysts and catalyst layers: fundamentals and applications*. 2008: Springer Science & Business Media.
147. Clariant Corporation. *AZ® nLOF™ 2000 Series i-Line Photoresists*. 2002 [Accessed: 08/12/2011] Available from: http://www.first.ethz.ch/infrastructure/Chemicals/Photolithography/Data_AZnLof2070.pdf

148. *Materials Group: Thin Films*. [Accessed: 30/06/2012] Available from: http://materials.web.psi.ch/Research/Introduction.htm
149. M. Winter. *Web Elements*. 2012 [Accessed: 30/09/2012] Available from: http://www.webelements.com/
150. Sigma-Aldrich. *Glucose Oxidase from Aspergillus niger* [Accessed: 07/10/2014] Available from: http://www.sigmaaldrich.com/catalog/product/sigma/g2133?lang=en&region=GB
151. P. Cassland and L.J. Jönsson, *Characterization of a gene encoding Trametes versicolor laccase A and improved heterologous expression in Saccharomyces cerevisiae by decreased cultivation temperature.* Applied Microbiology and Biotechnology, 1999. **52**(3): p. 393-400.
152. H.-J. QIU, C.-X. XU, G.-L. JI, X.-R. HUANG, S.-H. HAN, Y. DING and Y.-B. QU, *Immobilization of Laccase on Nanoporous Gold and Its Enzymatic Properties.* Acta Chimica Sinica, 2008. **66**(18): p. 2075-2080.
153. D. Yinghui, W. Qiuling and F. Shiyu, *Laccase stabilization by covalent binding immobilization on activated polyvinyl alcohol carrier.* Letters in Applied Microbiology, 2002. **35**(6): p. 451-456.
154. M. Pita, C. Gutierrez-Sanchez, D. Olea, M. Velez, C. Garcia-Diego, S. Shleev, V.M. Fernandez and A.L. De Lacey, *High Redox Potential Cathode Based on Laccase Covalently Attached to Gold Electrode.* The Journal of Physical Chemistry C, 2011. **115**(27): p. 13420-13428.
155. C. Vaz-Dominguez, S. Campuzano, O. Rüdiger, M. Pita, M. Gorbacheva, S. Shleev, V.M. Fernandez and A.L. De Lacey, *Laccase electrode for direct electrocatalytic reduction of O2 to H2O with high-operational stability and resistance to chloride inhibition.* Biosensors and Bioelectronics, 2008. **24**(4): p. 531-537.
156. D. Wan, S. Yuan, G.L. Li, K.G. Neoh and E.T. Kang, *Glucose Biosensor from Covalent Immobilization of Chitosan-Coupled Carbon Nanotubes on Polyaniline-Modified Gold Electrode.* ACS Applied Materials & Interfaces, 2010. **2**(11): p. 3083-3091.
157. S.K. Arya, A. Dey and S. Bhansali, *Polyaniline protected gold nanoparticles based mediator and label free electrochemical cortisol biosensor.* Biosensors and Bioelectronics, 2011. **28**(1): p. 166-173.
158. V. Madhavi and S. Lele, *Laccase: properties and applications.* BioResources, 2009. **4**(4): p. 1694-1717.
159. H. du Toit and M. Di Lorenzo, *Continuous Power Generation from Glucose with Miniature Flow-Through Enzymatic Biofuel Cells.* 2014.
160. W. Zhao, J.-J. Xu, C.-G. Shi and H.-Y. Chen, *Fabrication, characterization and application of gold nano-structured film.* Electrochemistry Communications, 2006. **8**(5): p. 773-778.
161. A. Sarapuu, K. Tammeveski, T.T. Tenno, V. Sammelselg, K. Kontturi and D.J. Schiffrin, *Electrochemical reduction of oxygen on thin-film Au electrodes in acid solution.* Electrochemistry Communications, 2001. **3**(8): p. 446-450.
162. L.D. Burke and P.F. Nugent, *The electrochemistry of gold: I the redox behaviour of the metal in aqueous media.* Gold Bulletin, 1997. **30**(2): p. 43-53.
163. Y. Rong, R. Malpass-Evans, M. Carta, N.B. McKeown, G.A. Attard and F. Marken, *Intrinsically Porous Polymer Protects Catalytic Gold Particles for Enzymeless Glucose Oxidation.* Electroanalysis, 2014. **26**(5): p. 904-909.
164. H. Yin, C. Zhou, C. Xu, P. Liu, X. Xu and Y. Ding, *Aerobic Oxidation of d-Glucose on Support-Free Nanoporous Gold.* The Journal of Physical Chemistry C, 2008. **112**(26): p. 9673-9678.
165. J.H. Shim, A. Cha, Y. Lee and C. Lee, *Nonenzymatic Amperometric Glucose Sensor Based on Nanoporous Gold/Ruthenium Electrode.* Electroanalysis, 2011. **23**(9): p. 2057-2062.

166. J. Wang, *Electrochemical Glucose Biosensors.* Chemical Reviews, 2007. **108**(2): p. 814-825.
167. M. Pasta, F. La Mantia and Y. Cui, *Mechanism of glucose electrochemical oxidation on gold surface.* Electrochimica Acta, 2010. **55**(20): p. 5561-5568.
168. I. Rattalino, P. Motto, I. Taurino, F. Cortes-Salazar, G. Piccinini, D. Demarchi, G. De Micheli and S. Carrara. *Nanogap-based enzymatic-free electrochemical detection of glucose*. in *Biomedical Circuits and Systems Conference (BioCAS), 2013 IEEE*. 2013.
169. M.W. Hsiao, R.R. Adžić and E.B. Yeager, *Electrochemical Oxidation of Glucose on Single Crystal and Polycrystalline Gold Surfaces in Phosphate Buffer.* Journal of The Electrochemical Society, 1996. **143**(3): p. 759-767.
170. J.H. Shim, A. Cha, Y. Lee and C. Lee, *Nonenzymatic Amperometric Glucose Sensor Based on Nanoporous Gold/Ruthenium Electrode.* Electroanalysis, 2011. **23**(9): p. 2057 – 2062.
171. D.C. Dugdale. *Glucose test - urine*. 2013 [Accessed: 10/07/2013] Available from: http://www.nlm.nih.gov/medlineplus/ency/article/003581.htm
172. J. Moyer, D. Wilson, I. Finkelshtein, B. Wong and R. Potts, *Correlation between sweat glucose and blood glucose in subjects with diabetes.* Diabetes Technology & Therapeutics, 2012. **14**(5): p. 398-402.
173. *Testing*. 2014 [Accessed: 29/10/2014] Available from: http://www.diabetes.org.uk/Guide-to-diabetes/Monitoring/Testing/
174. J.E. Hall, *Guyton and Hall Textbook of Medical Physiology: Enhanced E-book*. 2010: Elsevier Health Sciences.
175. H. Kirchmann and S. Pettersson, *Human urine - Chemical composition and fertilizer use efficiency.* Fertilizer research, 1994. **40**(2): p. 149-154.
176. *Mission Urinalysis Reagent Strips*. [Accessed: 03/11/2014] Available from: http://www.aconlabs.com/pdf/uspdf/1150457901%20Mission%20urinalysis%20sell%20sheet-for%20US%20110708.pdf
177. N.A. Rahman, M. Hasan, M.A. Hussain and J. Jahim, *Determination of Glucose and Fructose from Glucose Isomerization Process by High performance Liquid Chromatography with UV Detection.* Modern Applied Science, 2008. **2**(4): p. 151-154.
178. M. Gerlache, Z. Senturk, G. Quarin and J.-M. Kauffmann, *Electrochemical behavior of H2O2 on gold.* Electroanalysis, 1997. **9**(14): p. 1088-1092.
179. H.M. Sauro, *Enzyme Kinetics for Systems Biology*. Second ed. 2012: Ambrosius Publishing. 382.
180. A. Fatoni, A. Numnuam, P. Kanatharana, W. Limbuta, C. Thammakhet and P. Thavarungkul, *A highly stable oxygen-independent glucose biosensor based on a chitosan-albumin cryogel incorporated with carbon nanotubes and ferrocene.* Sensors and Actuators B, 2013. **185**: p. 725– 734.
181. Q.H. Gibson, B.E.P. Swoboda and V. Massey, *Kinetics and Mechanism of Action of Glucose Oxidase.* Journal of Biological Chemistry, 1964. **239**(11): p. 3927-3934.
182. H. Qiu, L. Xue, G. Ji, G. Zhou, X. Huang, Y. Qu and P. Gao, *Enzyme-modified nanoporous gold-based electrochemical biosensors.* Biosensors and Bioelectronics, 2009. **24**(10): p. 3014-3018.
183. A.P. Periasamy, Y.-J. Chang and S.-M. Chen, *Amperometric glucose sensor based on glucose oxidase immobilized on gelatin-multiwalled carbon nanotube modified glassy carbon electrode.* Bioelectrochemistry, 2011. **80**(2): p. 114-120.
184. H. Zhang, Z. Meng, Q. Wang and J. Zheng, *A novel glucose biosensor based on direct electrochemistry of glucose oxidase incorporated in biomediated gold nanoparticles–carbon nanotubes composite film.* Sensors and Actuators B: Chemical, 2011. **158**(1): p. 23-27.
185. Y. Yu, Z. Chen, S. He, B. Zhang, X. Li and M. Yao, *Direct electron transfer of glucose oxidase and biosensing for glucose based on PDDA-capped gold nanoparticle modified*

graphene/multi-walled carbon nanotubes electrode. Biosensors and Bioelectronics, 2014. **52**: p. 147–152.

186. J.D. Qiu, W.M. Zhou, J. Guo, R. Wang and R.P. Liang, *Amperometric sensor based on ferrocene modified multiwalled carbon nanotube nanocomposites as electron mediator for the determination of glucose.* Analytical Biochemistry, 2009. **385**: p. 264-269.
187. P. Olejnik, B. Palys, A. Kowalczyk and A.M. Nowicka, *Orientation of Laccase on Charged Surfaces. Mediatorless Oxygen Reduction on Amino- and Carboxyl-Ended Ethylphenyl Groups.* Journal of Physical Chemistry, 2012. **116**: p. 25911-25918.
188. A. Benedetto, M. Balog, P. Viel, F. Le Derf, M. Sallé and S. Palacin, *Electro-reduction of diazonium salts on gold: Why do we observe multi-peaks?* Electrochimica Acta, 2008. **53**(24): p. 7117-7122.
189. P.A. Brooksby and A.J. Downard, *Electrochemical and Atomic Force Microscopy Study of Carbon Surface Modification via Diazonium Reduction in Aqueous and Acetonitrile Solutions.* Langmuir, 2004. **20**(12): p. 5038-5045.
190. N. Mano and A. Kuhn, *Cation induced amplification of the electrocatalytic oxidation of NADH by immobilized nitro-fluorenone derivatives.* Journal of Electroanalytical Chemistry, 2001. **498**(1–2): p. 58-66.
191. M.S. Thorum, C.A. Anderson, J.J. Hatch, A.S. Campbell, N.M. Marshall, S.C. Zimmerman, Y. Lu and A.A. Gewirth, *Direct, Electrocatalytic Oxygen Reduction by Laccase on Anthracene-2-methanethiol-Modified Gold.* The Journal of Physical Chemistry Letters, 2010. **1**(15): p. 2251-2254.
192. F. Barrière, P. Kavanagh and D. Leech, *A laccase–glucose oxidase biofuel cell prototype operating in a physiological buffer.* Electrochimica Acta, 2006. **51**(24): p. 5187-5192.
193. E. Katz, I. Willner and A.B. Kotlyar, *A non-compartmentalized glucose/O2 biofuel cell by bioengineered electrode surfaces.* Journal of Electroanalytical Chemistry, 1999. **479**(1): p. 64-68.
194. L. Brunel, J. Denele, K. Servat, K.B. Kokoh, C. Jolivalt, C. Innocent, M. Cretin, M. Rolland and S. Tingry, *Oxygen transport through laccase biocathodes for a membrane-less glucose/O2 biofuel cell.* Electrochemistry Communications, 2007. **9**(2): p. 331-336.
195. M. Falk, V. Andoralov, M. Silow, M.D. Toscano and S. Shleev, *Miniature biofuel cell as potential power source for glucose sensing contact lenses.* Analytical chemistry, 2013. **85**: p. 6342-6348.
196. D.L. Johnson, J.L. Thompson, S.M. Brinkmann, K.A. Schuller and L.L. Martin, *Electrochemical characterization of purified Rhus vernicifera laccase: voltammetric evidence for a sequential four-electron transfer.* Biochemistry, 2003. **42**(34): p. 10229-37.
197. S. Ivanka, K. Albert and S. Veselin, *Properties of crude laccase from Trametes versicolor produced by solid-substrate fermentation.* Advances in Bioscience and Biotechnology, 2010. **2010**.
198. G.H. Seong, J. Heo and R.M. Crooks, *Measurement of Enzyme Kinetics Using a Continuous-Flow Microfluidic System.* Analytical Chemistry, 2003. **75**(13): p. 3161-3167.
199. R.D. Milton, F. Giroud, A.E. Thumser, S.D. Minteer and R.C.T. Slade, *Hydrogen peroxide produced by glucose oxidase affects the performance of laccase cathodes in glucose/oxygen fuel cells: FAD-dependent glucose dehydrogenase as a replacement.* Physical Chemistry Chemical Physics, 2013. **15**(44): p. 19371-19379.
200. A. Zille, T. Tzanov, G. Gübitz and A. Cavaco-Paulo, *Immobilized laccase for decolourization of Reactive Black 5 dyeing effluent.* Biotechnology Letters, 2003. **25**(17): p. 1473-1477.
201. T. Chen, S.C. Barton, G. Binyamin, Z. Gao, Y. Zhang, H.-H. Kim and A. Heller, *A Miniature Biofuel Cell.* Journal of the American Chemical Society, 2001. **123**(35): p. 8630-8631.

202. D. Rando, G.W. Kohring and F. Giffhorn, *Production, purification and characterization of glucose oxidase from a newly isolated strain of Penicillium pinophilum.* Applied Microbiology and Biotechnology, 1997. **48**(1): p. 34-40.
203. W. Yun-Yang, Y.-M. Du, Y. Fang-Xing, X. Ying, C. Rong-Zhi and J.F. Kennedy, *Purification and characterization of hydrosoluble components from the sap of Chinese lacquer tree Rhus vernicifera.* International Journal of Biological Macromolecules, 2006. **38**(3–5): p. 232-240.

PUBLICATIONS IN PEER REVIEWED JOURNALS

- ***Electrodeposited highly porous gold microelectrodes for the direct electrocatalytic oxidation of aqueous glucose***

  Hendrik du Toit, Mirella Di Lorenzo

  Sensors and Actuators B: Chemical, Volume 192, 1 March 2014, Pages 725-729, ISSN 0925-4005, http://dx.doi.org/10.1016/j.snb.2013.11.017

- ***Glucose Oxidase Directly Immobilized onto Highly Porous Gold Electrodes for Sensing and Fuel Cell applications***

  Hendrik du Toit, Mirella Di Lorenzo

  Electrochimica Acta, Volume 138, 20 August 2014, Pages 86-92, ISSN 0013-4686, http://dx.doi.org/10.1016/j.electacta.2014.06.074

- ***Continuous power generation from glucose with two different miniature flow-through enzymatic biofuel cells***

  Hendrik du Toit, Mirella Di Lorenzo

  Biosensors and Bioelectronics, Volume 69, 15 July 2015, Pages 199-205, ISSN 0956-5663, http://dx.doi.org/10.1016/j.bios.2015.02.036

Sensors and Actuators B 192 (2014) 725–729

Contents lists available at ScienceDirect

Sensors and Actuators B: Chemical

journal homepage: www.elsevier.com/locate/snb

Short communication

Electrodeposited highly porous gold microelectrodes for the direct electrocatalytic oxidation of aqueous glucose

Hendrik du Toit, Mirella Di Lorenzo *

University of Bath, Department of Chemical Engineering, Bath BA2 7AY, UK

ARTICLE INFO

Article history:
Received 16 September 2013
Received in revised form 25 October 2013
Accepted 6 November 2013
Available online 15 November 2013

Keywords:
Nanoporous gold
Glucose sensor
Lab-on-a-chip
Nanostructure
Electrocatalysis

ABSTRACT

High-surface area electrode materials are particularly relevant for a vast range of applications, especially in the field of catalysis and electrochemical energy conversion (e.g. fuel cells).

In this work high surface area gold electrodes were produced by direct electrodeposition of highly porous gold (hPG) films onto gold electrodes via a very fast (15 s), simple, and cost-effective methodology that involves a hydrogen bubble template. This methodology was also successfully applied to gold microelectrodes produced by lift-off lithography, thus paving the way for interesting lab-on-a-chip applications.

The hPG electrodes showed very high sensitivity towards glucose, with a detection limit of 5 μM. This reactivity was maintained when the electrodes were tested in artificial urine, thus encouraging their use in healthcare.

The hPG electrodes showed high sensitivity also towards other aldoses and other reducing sugars (maltose, lactose, galactose).

1. Introduction

Glucose monitoring is essential for the effective treatment of diabetes. For the past three decades enzymatic glucose tests have been the prevailing technology [1]. Non-enzymatic glucose-sensitive electrodes, however, can potentially lead to sensors that are less affected by temperature and pH, and generally more stable than those dependent on immobilised enzymes [2].

In this context, considerable attention has recently been given to the development of glucose sensors based on highly porous gold (hPG) electrodes, such as nanoporous gold electrodes, due to the observed reactivity of these electrodes towards glucose [3]. The non-enzymatic aerobic oxidation of glucose to gluconic acid at neutral pH by nanoporous gold was reported as far back as 2008 [4]. Only much more recently the use of hPG electrodes as a glucose sensor has been investigated [3,5,6].

Key features of hPG electrodes are: very large specific surface area, high electrocatalytic activity, conductivity, and biocompatibility [3,7,8].

The establishment of efficient, simple and low-cost processes for the manufacture of such electrodes is therefore key. The development of methodologies that could easily be transferred to the microscale is particularly attractive for the use of hPG electrodes in lab-on-a-chip sensors and microfluidic electrochemical devices.

The main techniques so far reported to produce hPG films required the selective etching of silver from thick layers of gold and silver alloys [9,10]. Other more complicated templated methods have also been used [11,12]. Only recently two simple and rapid methods that target the deposition of gold, and avoid the use of any harsh or expensive reagents were reported [3,13]. Cherevko et al., in particular, developed a hydrogen template assisted electrodeposition of hPG onto a Pt/Ti/Si electrode in conjunction with a gold (III) electrolyte [13]. Yet, this technique has not been proven to be transferable to lab-on-a-chip scale thin film gold electrodes.

This study reports a rapid, easy, cost-effective, and targeted direct electrodeposition method to produce hPG electrodes, which has been also applied for the first time to thin film electrodes produced by lift-off lithography. The resulting electrode was then tested for the amperometric detection of aqueous glucose. The nature of the electrochemical reaction occurring at the electrode surface was then investigated by comparing the electrode response towards a selection of sugars. Finally, the hPG electrodes were tested in artificial urine to explore their potential implementation in healthcare.

2. Experimental

2.1. Materials

AZ nLOF 2070 photoresist and AZ 326 MIF Developer were purchased from Microchemicals. All other reagents were of analytical grade and purchased from Sigma–Aldrich.

* Corresponding author. Tel.: +44 01225 385574.
E-mail address: M.Di.Lorenzo@bath.ac.uk (M. Di Lorenzo).

0925-4005/$ – see front matter © 2013 Elsevier B.V. All rights reserved.
http://dx.doi.org/10.1016/j.snb.2013.11.017

Gold disk electrodes (2 mm diameter), saturated calomel electrodes (SCE) and platinum counter electrodes were purchased from IJCambria Ltd.

The hPG film electrodeposition and all the electrochemical processes were conducted using the Autolab PGSTAT128N potentiostat. All potentials are referred to against SCE.

2.2. Patterning electrodes onto glass slides

Gold electrodes (1 mm × 10 mm) were patterned onto glass slides by lift-off lithography as described in the supplementary data (Fig. SS1).

2.3. Electro-deposition of porous gold film and

Gold electrodeposition was performed in an aqueous electrolyte consisting of 0.1 M $HAuCl_4$ and 1 M NH_4Cl.

The morphology of the resulting electrodes was characterised using a Hitachi S-4300 field emission scanning electron microscope (FESEM).

2.4. Electrochemical characterisation

The electrochemical characterisation regarded only the hPG electrodes fabricated on gold disks. All the experiments were carried in phosphate buffered saline (PBS), prepared in distilled water with: 137 mM NaCl, 2.7 mM KCl, 10 mM Na_2HPO_4, 2 mM KH_2PO_4. The pH was adjusted to 7. Artificial urine was prepared by adding urea (8 g l^{-1}) to PBS and by adjusting the pH of the resulting solution to 8.9 [14,15].

Cyclic voltammetry (CV) and amperometric tests were performed in a three-electrode electrochemical cell with a SCE reference electrode and a platinum rod counter electrode.

CV scans were performed at the potential range of −0.8 V to 0.8 V (vs. SCE). The amperometric tests were performed at 0.15 V (vs. SCE). A concentration range of 0.005–50 mM was considered for all the sugars tested. During the addition of the target sugar the solution was agitated for 20 s. In order to minimise the amperometric noise observed, the agitation was stopped and the solution was left for 270 s to allow for stabilisation of the amperometric response under natural convection. The average response over a period of 10 s was then recorded. Three replicates were performed per experiment.

The electrochemically effective surface area (ESA) of the porous gold electrodes was determined using Eq. (1):

$$\mathrm{ESA} = \Delta I_{\mathrm{porous}} \times \frac{\mathrm{SA}_{\mathrm{flat}}}{\Delta I_{\mathrm{flat}}} \quad (1)$$

where SA_{flat} is the surface area of the bare electrode, and ΔI is the charging current, or capacitance, of the system measured at 0.5 V during a CV scan between 0.42 V and 0.6 V (vs. SCE) at 1 mV s^{-1}.

3. Results and discussion

The electrodeposition of porous gold films via a hydrogen bubble template is a new technique to produce hPG electrodes which requires small amount of gold; is fast; does not involve harsh reagents; and is easy to perform [13].

In our group we observed, however, that the resulting gold structures were unstable, as pieces of black hPG film would easily flake off the surface of the gold disk. A better control of the evolution and removal of hydrogen gas during the electrodeposition process could improve the adhesion of the porous gold film onto the electrode surface. A gradual potential step down process was therefore developed. Firstly, the working potential was set to −0.7 V vs. SCE (potential at which the evolution of hydrogen gas first occurs) for a period of 5 s. This first step (S1) would create an uneven gold surface for the adhesion of the hPG film. The set potential was then stepped down to −4.0 V (vs. SCE) for a period of 10 s (S2). This highly negative potential ensures intense hydrogen bubbling that is key for the final foam-shape of the electrode

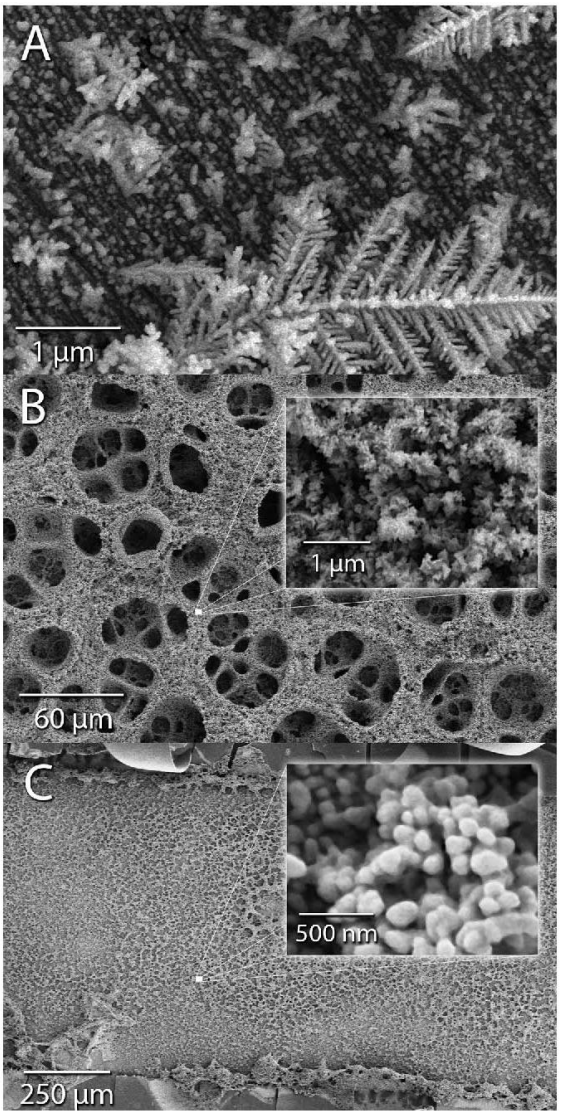

Fig. 1. FESEM images of the hPG electrodes: (A) obtained from gold disk taken after 5 s of electroplating at a potential of −0.7 V (S1); (B) obtained from gold disk taken after subsequent electroplating at −4.0 V (S2) and (C) obtained from lithographically produced gold microelectrodes after S2 (note that the flaking on the electrode edges is due to the photoresist chemical treatment).

After S1, a crystalline feather-like framework of gold developed on the surface of the gold disk electrode (Fig. 1A), which would serve as an anchoring point for the subsequent electrodeposition of the porous gold film. At the end of the electro-deposition process, the electrode presented a 3D foam-like structure with a wide pore size distribution ranging from 10 nm to 30 µm (Fig. 1B). The nanostructure inside the large pores was comparable with the structure of nanoporous gold films previously reported [13].

This large distribution in pore size is crucial for the high amperometric reactivity observed. The larger pores (lined with nano-pores) allow for the free movement of the electrolyte deep into the porous gold structure of the electrode resulting in an ESA of $29 \pm 5.3\ cm^2$, approximately 10^3 times higher than the ESA of the bare gold disk ($0.031\ cm^2$).

The direct electrodeposition of hPG films was subsequently applied on thin-film gold electrodes patterned on glass slides by lift-off lithography.

Initial tests showed that these electrodes were more fragile than the commercial ones, as the rapid evolution of hydrogen gas at −4.0 V (vs. SCE), during S2, damaged the patterned electrodes (data not shown). It was, therefore, decided to reduce the hydrogen evolution by using a potential of only −2.5 V (vs. SCE) during this stage, for the same period of time (10 s).

A much greater variance in the deposited gold morphology was observed in this case (Fig. 1C). Inside the large pores, some feather-like structures, similar to those obtained on gold disks after S1, were observed, which might be a result of the weaker deposition potential adopted.

The electrodeposition methodology for these microelectrodes must be further optimised, and a further characterisation of the resulting structure is required. Nonetheless, this result demonstrates for the first time the direct electrodeposition of highly porous gold on thin film (100 nm thick) gold microelectrodes, paving the way for the easy and fast fabrication of high surface area gold microelectrodes for lab-on-a-chip sensors and microfluidic devices.

In future work electrodeposition times longer than 10 s, during S2, will be investigated to search for the time that optimises the hPG structure without damaging the microelectrode.

Long range CV scans conducted on freshly prepared porous gold disk electrodes in the presence of glucose and at a scan rate of $5\ mV\ s^{-1}$, revealed a clear glucose-dependent response. In particular, a strong current peak on the forward scan was observed at approximately 0.15 V (vs. SCE), as previously found [5]. The magnitude of the current peak changed with the concentration of glucose in the electrolyte (Fig. 2).

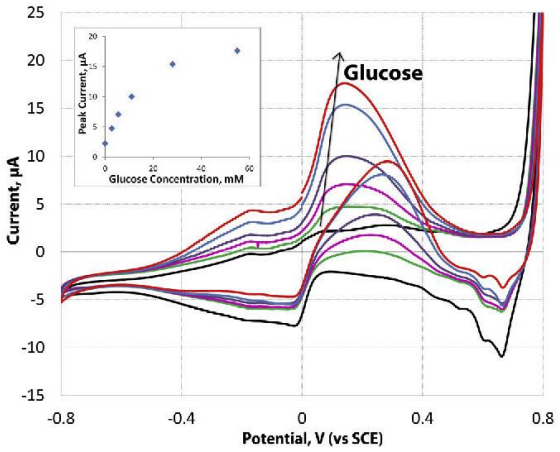

Fig. 2. Cyclic voltammetry tests at $5\ mV\ s^{-1}$ of the hPG disk electrode at varied glucose concentrations (0.0, 2.8, 5.5, 11, 28, 55 mM) in PBS. Evolution of the peak current in function of the glucose concentration.

The reactivity of the porous gold electrodes was also tested on other reducing sugars, such as maltose, lactose and galactose. A ketose (fructose), and a non-reducing sugar (sucrose) were also considered for comparison.

Fig. 3 reports the cyclic voltammetry tests obtained with a concentration of $5\ g\ l^{-1}$ for each sugar. In the case of fructose and sucrose, no relevant peak currents were observed when compared to blank scans conducted in PBS (Fig. 3D). On the other hand, for each aldose the forward peak at approximately 0.15 V (vs. SCE) was confirmed. The electro-oxidation of each sugar tested might involve the dehydrogenation of the aldehyde group, as for glucose [16]. The oxidation peak observed for all the aldoses tested might, in particular, refer to the hydrogen atom bounded to the carbon C1 atom of the aldehyde group of the sugars [16]. This justifies the inertness

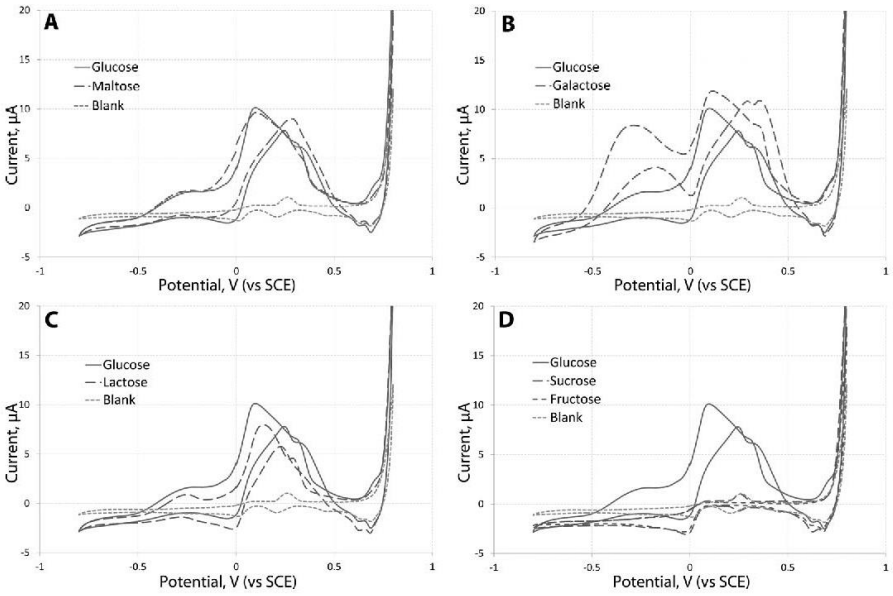

Fig. 3. Comparison of the cyclic voltammetry tests of the hPG disk electrodes performed with several sugars at a concentration of $5\ g\ l^{-1}$ and at a scan rate of $2\ mV\ s^{-1}$.

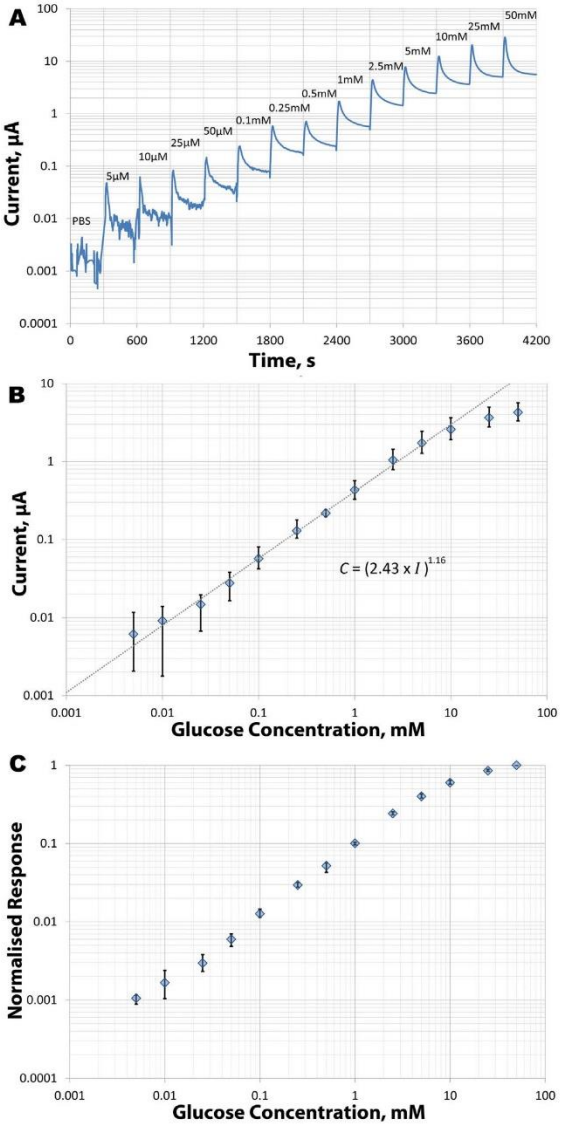

Fig. 4. Amperometric response of the hPG disk electrodes to increasing concentrations of glucose in PBS at pH 7. (A) Current change with time after drop-wise glucose concentration increases; (B) amperometric response versus glucose concentration. The equation shows the relationship between glucose concentration (C, range 10 µM–10 mM) and current observed (I), $R^2 = 0.997$ and (C) Electrode response normalisation between 0 and 1. Error bars refer to three replicates.

of sucrose and fructose that both lack the reactive hydrogen on the carbon C1 atom.

The shape of the cyclic voltammetry curves was generally different for each sugar. An exception was observed for maltose with a CV curve very similar to the one obtained with glucose (Fig. 3A).

By considering the results from the CV scans, the potential of 0.15 V (vs. SCE) was chosen for the amperometric tests. Fig. 4A and B shows the increase in current observed by step-increasing the concentration of glucose. A very strong correlation between the current observed and the concentration of glucose in the solution was observed, with a detection limit of 5 µM. This is concurrent with the sensitivity obtained when using similar porous gold electrodes and gold nano-composites produced in much more costly processes [5,17]. The standard deviation in the current observed between three different electrodes was substantial at low concentrations of glucose (up to 80% for a 5 µM glucose solution, Fig. 4B). For the purpose of using these electrodes as sensors the data sets were therefore normalised. This was achieved by calibrating the electrodes between 0 and 50 mM glucose in PBS. The amperometric response in glucose free PBS, I_0, and the amperometric response in a 50 mM glucose and PBS solution, I_{50}, was recorded and then used to calculate the normalised response, N, for any given amperometric response, I (Eq. (2)).

$$N = \frac{I - I_0}{I_{50} - I_0} \quad (2)$$

The resulting data (Fig. 4C) shows a much lower percentage standard deviation for all data points, with a maximum standard deviation of 15% observed for a 5 µM glucose solution.

The hPG electrodes showed the same sensitivity with the other reducing sugars tested (supplementary data, Fig. SS2).

The range of sensitivity required by a sensor for glucose levels in the human body varies according to the type of test implemented. In urine the normal glucose concentration varies between 0.0 and 0.8 mM [18].

Following a positive urine test, further more invasive testing of blood or cerebrospinal fluid glucose levels are usually conducted. Currently, sweat glucose tests (glucose range: 0.5–27 µM) are considered as a potential valid alternative to invasive tests [19].

The reactivity of the hPG electrode towards glucose was consequently investigated in artificial urine (supplementary data, Fig. SS3). The relationship between current observed and concentration of glucose was unaffected by the presence of urea and by the higher pH (from 7 to 8.9).

Future work will regard the analysis of the influence that other compounds present in biological fluids, such as uric and ascorbic acid, and catecholamine, might have on the hPG amperometric response. Due to the high sensitivity of hPG, its potential use to detect glucose in sweat will also be investigated.

4. Conclusions

A rapid method (15 s) for the direct electrodeposition of highly porous gold electrodes was developed, which is easily transferable to thin-film microelectrodes lithographically produced. The resulting electrodes have a wide pore size distribution and an electrochemically effective surface area 10^3 times greater than bare gold.

The porous gold electrodes showed high sensitivity towards glucose with a detection limit of 5 µM, which was maintained when the electrodes were tested in artificial urine.

Acknowledgements

The authors acknowledge Prof Frank Marken, University of Bath and the Royal Society Research Grant (RG110344).

Appendix A. Supplementary data

Supplementary data associated with this article can be found, in the online version, at http://dx.doi.org/10.1016/j.snb.2013.11.017.

References

[1] N.S. Oliver, C. Toumazou, A.E.G. Cass, D.G. Johnston, Glucose sensors: a review of current and emerging technology, Diabet. Med. 26 (2009) 197–210.
[2] J. Wang, Electrochemical glucose biosensors, Chem. Rev. 108 (2007) 814–825.

[3] Y. Xia, W. Huanga, J. Zheng, Z. Niub, Z. Li, Nonenzymatic amperometric response of glucose on a nanoporous gold film electrode fabricated by a rapid and simple electrochemical method, Biosens. Bioelectron. 26 (2011) 3555–3561.
[4] H. Yin, C. Zhou, C. Xu, P. Liu, X. Xu, Y. Ding, Aerobic oxidation of D-glucose on support-free nanoporous gold, J. Phys. Chem. C 112 (2008) 9673–9678.
[5] J.H. Shim, A. Cha, Y. Lee, C. Lee, Nonenzymatic amperometric glucose sensor based on nanoporous gold/ruthenium electrode, Electroanalysis 23 (2011) 2057–2062.
[6] X. Yan, X. Ge, S. Cui, Pt-decorated nanoporous gold for glucose electrooxidation in neutral and alkaline solutions, Nanoscale Res. Lett. 6 (2011) 313.
[7] M.a.D. Scanlon, U. Salaj-Kosla, S. Belochapkine, D. MacAodha, D.o. Leech, Y. Ding, et al., Characterization of nanoporous gold electrodes for bioelectrochemical applications, Langmuir 28 (2012) 2251–2261.
[8] A. Wittstock, A. Wichmann, M. Bäumer, Nanoporous gold as a platform for a building block catalyst, ACS Catal. 2 (2012) 2199–2215.
[9] P.N. Ciesielski, A.M. Scott, C. Faulkner, J.B.J. Berron, D.E. Cliffel, G.K. Jennings, Functionalized nanoporous gold leaf electrode films for the immobilization of photosystem I, ACS Nano 2 (2008) 2465–2472.
[10] M.C. Dixon, T.A. Daniel, M. Hieda, D.M. Smilgies, M.H.W. Chan, D.L. Allara, Preparation, structure, and optical properties of nanoporous gold thin films, Langmuir 23 (2007) 2414–2422.
[11] Y.-G. Zhou, S. Yang, Q.-Y. Qian, X.-H. Xia, Gold nanoparticles integrated in a nanotube array for electrochemical detection of glucose, Electrochem. Commun. 11 (2009) 216–219.
[12] Y. Bai, Y. Weiwei, S. Ying, S. Changqing, Enzyme-free glucose sensor based on a three-dimensional gold film electrode, Sens. Actuators B 13 (2008) 471–476.
[13] S. Cherevko, C.-H. Chung, Direct electrodeposition of nanoporous gold with controlled multimodal pore size distribution, Electrochem. Commun. 13 (2011) 16–19.
[14] J.E. Hall, Guyton and Hall Textbook of Medical Physiology: Enhanced E-book, 2010.
[15] H. Kirchmann, S. Pettersson, Human urine – chemical composition and fertilizer use efficiency, Fert. Res. 40 (1994) 149–154.
[16] M. Pasta, F. La Mantia, Y. Cui, Mechanism of glucose electrochemical oxidation on gold surface, Electrochim. Acta 55 (2010) 5561–5568.
[17] Y. Li, Y.-Y. Song, C. Yang, X.-H. Xia, Hydrogen bubble dynamic template synthesis of porous gold for nonenzymatic electrochemical detection of glucose, Electrochem. Commun. 9 (2007) 981–988.
[18] D.C. Dugdale, Glucose Test – Urine, 2013, Available from: http://www.nlm.nih.gov/medlineplus/ency/article/003581.htm (accessed 10.07.13).
[19] J. Moyer, D. Wilson, I. Finkelshtein, B. Wong, R. Potts, Correlation between sweat glucose and blood glucose in subjects with diabetes, Diabetes Technol. Ther. 14 (2012) 398–402.

Biographies

Hendrik du Toit is a Ph.D. student in the Department of Chemical Engineering, University of Bath, UK. He received his M.Eng. in Chemical Engineering from Imperial College London in 2011. He is currently conducting research into the production of biocompatible biosensors and biofuel cells.

Mirella Di Lorenzo received her M.Eng. degree in Chemical Engineering from Federico II University, Italy, in 2003. She received her Ph.D. degree in Industrial Biotechnology from the same University in the year 2006. Presently, she is an Assistant Professor in the Department of Chemical Engineering, University of Bath, UK. Her current research interests include biofuel cells, high surface microelectrodes, and microfluidics. She is the member of the Editorial Advisory Board of the Sustainable Energy Technologies and Assessments Journal.

SUPPLEMENTARY DATA

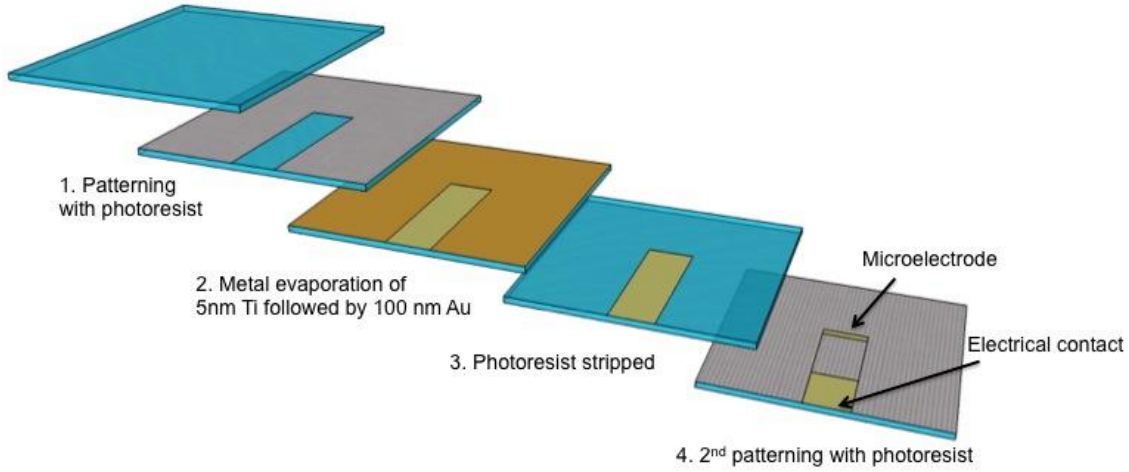

Figure SS1 *Schematic of gold microelectrodes manufacture process.*

AZ nLOF 2070 photoresist was spin coated (3000 rpm, 30 s) onto clean glass slides. The slides were pre-baked (110°C, 120 s); exposed to 180 mJ cm^{-2} ultraviolet light through a photomask carrying the positive image of the electrode pattern; and post-baked (110°C, 120 s), before being treated with the AZ 326 MIF developer. Subsequently, the slides were coated by metal evaporation with a 5 nm thick titanium adhesion layer followed by a 100 nm layer of gold. Metal lift-off in DMSO followed. A second layer of photoresist was spin coated onto the electrode surface to confine the porous gold film electrodeposition to the area of 1 mm x 10 mm. This served as electrical insulation for the conductive tracks leading to the electrodes.

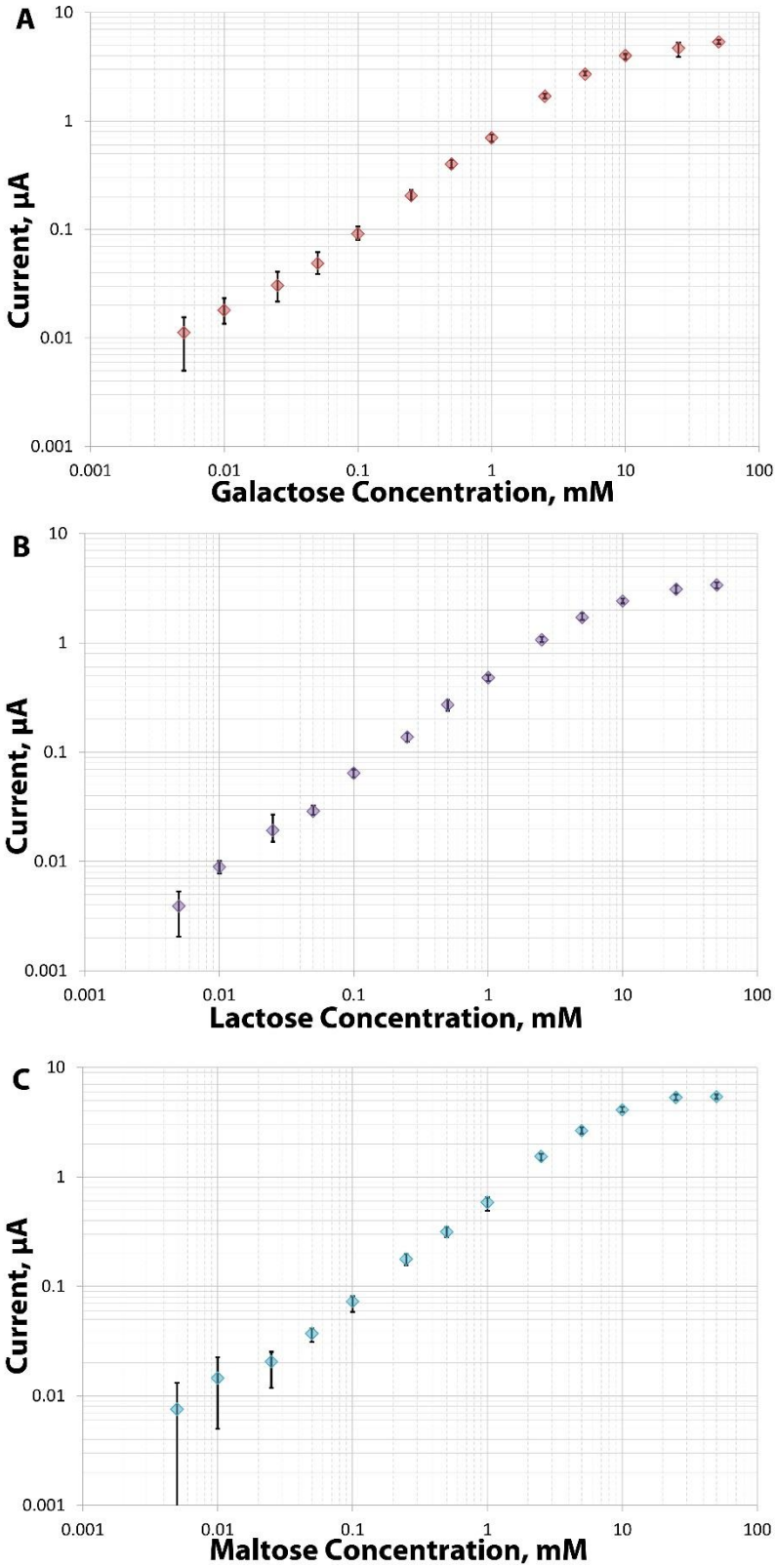

Figure SS2 *Amperometric response of the hPG electrode to increasing concentrations of aldoses in PBS at pH 7. A) galactose; B) lactose; C) maltose. Error bars refer to three replicates.*

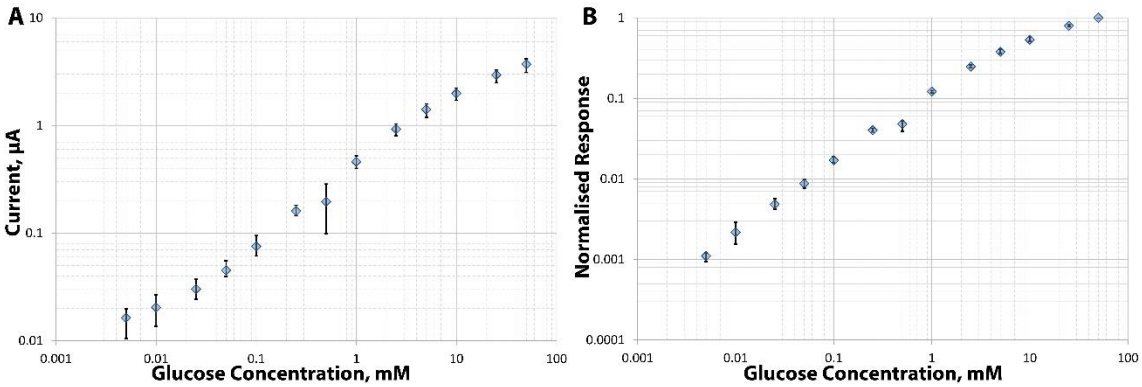

Figure SS3 *Amperometric response of the hPG electrode to increasing concentrations of glucose in artificial urine. A) Current change with time after drop-wise glucose concentration increases; B) Electrode response normalisation between 0 and 1. Error bars refer to three replicates.*

Electrochimica Acta 138 (2014) 86–92

Contents lists available at ScienceDirect

Electrochimica Acta

journal homepage: www.elsevier.com/locate/electacta

Glucose Oxidase Directly Immobilized onto Highly Porous Gold Electrodes for Sensing and Fuel Cell applications

Hendrik du Toit, Mirella Di Lorenzo *

University of Bath, Department of Chemical Engineering, Bath, BA2 7AY, UK

ARTICLE INFO

Article history:
Received 12 April 2014
Received in revised form 11 June 2014
Accepted 12 June 2014
Available online 19 June 2014

Keywords:
Biofuel cell
glucose oxidase
laccase
porous gold
glucose sensor

ABSTRACT

The successful implementation of redox-enzyme electrodes in biosensors and enzymatic biofuel cells has been the subject of extensive research.

For high sensitivity and high energy-conversion efficiency, the effective electron transfer at the protein-electrode interface has a key role. This is difficult to achieve in the case of glucose oxidase, due to the fact that for this enzyme the redox centre is buried inside the structure, far from any feasible electrode binding sites.

This study reports, a simple and rapid methodology for the direct immobilisation of glucose oxidase into highly porous gold electrodes. When the resulting electrode was tested as glucose sensor, a Michaelis-Menten kinetic trend was observed, with a detection limit of 25 μM. The bioelectrode sensitivity, calculated against the superficial surface area of the bioelectrode, was of 22.7 ± 0.1 $\mu A\,mM^{-1}\,cm^{-2}$.

This glucose oxidase electrode was also tested as an anode in a glucose/O_2 enzymatic biofuel cell, leading to a peak power density of 6 $\mu W\,cm^{-2}$ at a potential of 0.2 V.

1. Introduction

The functional immobilisation of redox enzymes, such as laccase and glucose oxidase, onto electrode material surfaces is of keen interest for sensors and biofuel cells development.

Enzymes are the most common bioreceptor molecules used in biosensors due to their extremely high specificity that leads to minimal risk of false positive responses. The implementation of enzymes in biofuel cells allows for the development of membraneless and compartment-less devices, which not only can be easily miniaturised, but can also be used in situations where it is not feasible to separate the fuel and oxidant [1].

For these applications, the achievement of efficient electron transfer between the enzyme active centre and the electrode is critical. Usually a mediated electron transfer (MET) mechanism is required. This might involve the use of small redox active particles and polymers as electron carriers (mediators), such as organic dyes, ferrocene and its derivatives, modified vitamin complexes, and conducting salts [2]. If the mediator is in solution their diffusion to the electrode surface allows for a more rapid electron transfer compared to the direct transfer from the enzyme itself [3]. Alternatively, the mediators can be polymerised directly onto the electrode surface or co-immobilised with the reacting enzymes to further enhance the rate of electron transfer [4,5].

However, the use of redox active electron carriers can have several drawbacks, such as short lifespans, poor biocompatibility, risk of leaching away from the electrode surface, potential toxicity. Consequently, the achievement of a direct electron transfer (DET) process is preferred.

Major advancements have come as far back as the 1980s from examining transition metal rich enzymes, such as laccase (LAC), capable of catalysing the reduction of oxygen to water through DET [6]. This is because LAC contains several copper centres that allow the electrons transport through the enzyme redox centre to the electrode surface. Consequently, the achievement of DET with LAC-immobilised electrodes is now well established [7–9].

In the case of glucose oxidase (GOx), DET is more difficult to achieve, due to the fact that the GOx redox centre is buried inside the enzyme structure, and is far from any feasible electrode binding sites. To achieve efficient electron transfer, the use of GOx has been often combined with mediator compounds, of which ferrocene is the most common [10]. Most of the GOx immobilisation protocols reported, while effective, are usually very expensive, due to the reagents required. These protocols are often very laborious, involving multi-steps in the immobilization procedure that can be sources of experimental errors [11–14]. Moreover the resulting bioelectrodes can be unstable and inefficient with limited opportunity for practical implementations, due to the leaching of

* Corresponding author. Tel.: +44 0 1225 385574.
E-mail address: M.Di.Lorenzo@bath.ac.uk (M. Di Lorenzo).

http://dx.doi.org/10.1016/j.electacta.2014.06.074

the mediator implemented and the dependence of the electron transfer process on the capability of the mediator to be rapidly oxidised and reduced [15].

In recent years, some progress has been reported when using nanostructured electrodes, such as carbon nanotubes (CNTs), as electron acceptors. Due to their size and shape, these electrodes are able to intertwine with the enzyme and come in very close proximity to the enzyme FAD centre. Successful DET of GOx immobilised onto CNTs-based electrodes has been reported [16–18]. High surface area microelectrodes are also preferred in the context of an increasing trend towards the miniaturization of bioelectrochemical devices for applications such as implantable healthcare devices. However, the not yet fully addressed potential long-term toxicity of CNTs leads to controversial opinions on the feasibility of using CNTs for *in vivo* or cutaneous applications [19–23].

Nano-porous gold (nPG) electrodes (porous gold electrodes with a pore size distribution limited to the nanometre range) are considered a very promising alternative for the development of new generation bioelectrochemical devices with implantable capability. These non-toxic electrodes have remarkable properties, such as high conductivity, large surface area, three-dimensional open porosity, and biocompatibility [24]. In this context, an even more promising material for the production of high sensitivity biosensors is highly porous gold (hPG). While retaining the morphology observed with nPG, hPG electrodes present large micro-pores that are lined with nano-pores themselves [25]. As a consequence, hPG electrodes have a very wide pore size distribution, leading to extremely large surface areas and hence larger current densities in comparison to conventional nPG.

A new and rapid method of producing hPG electrodes by direct electrodeposition of porous gold films onto gold electrodes was recently reported [26]. These electrodes were characterised by a 3D foam-like structure, with a wide pore size distribution (ranging from 10 nm to 30 μm), and a roughness factor (calculated in terms of electrochemically effective surface area) approximately 10^3 times higher than polished gold. The hPG electrodes showed excellent glucose electrooxidation activity with a detection limit as low as 5 μM [26]. However, the high specificity required for some applications, such as implantable biofuel cell devices where the fuel (e.g. glucose) and the oxidant (e.g. oxygen) are fed to the system as a mixture, demands the implementation of enzymatic electrodes [27].

The large surface area of hPG electrodes and their complex morphology make them an ideal support for enzyme immobilisation at high loadings. This hypothesis is encouraged by the successful production of GOx-immobilised nPG electrodes recently reported. In these cases the GOx immobilisation protocols involved the nPG functionalization with thiol-linker molecules or with conductive polymers, such as poly(3,4-ethylenedioxythiophene), to enhance the electron transfer process [24,28,29].

This study reports for the first time, an efficient, simple, cost-effective, and rapid method for the functional immobilisation of GOx onto hPG surfaces. The immobilisation protocol does not require any electrode pre-treatments with linker molecules or polymers and it is simple to reproduce. In particular, GOx is immobilised onto the hPG surface *via* a one-step electrochemical adsorption process in a phosphate buffer with no additional chemicals. The use of the resulting GOx-immobilised hPG electrode is tested for glucose sensing and for energy harvesting in a glucose/O_2 enzymatic biofuel cell.

2. Experimental

2.1. Materials

Glucose Oxidase (GOx) from *Aspergillus niger*, Laccase (LAC) from *Trametes versicolor*, and all other reagents used were of analytical grade and purchased from Sigma-Aldrich. All aqueous solutions were prepared with reverse osmosis purified water. Gold disk electrodes (2 mm diameter), saturated calomel electrodes (SCE) and platinum counter electrodes were purchased from IJCambria Ltd. Gold disk electrodes were polished between uses with a 0.3 micron aluminium oxide polish (Buehler).

All analytical experiments were performed in phosphate buffered saline (PBS). This was prepared with the following constituents: 137 mM NaCl, 2.7 mM KCl, 10 mM Na_2HPO_4, 2 mM KH_2PO_4. The pH of this solution was then adjusted to 7 with the drop wise addition of 1 M solutions of HCl and NaOH.

2.2. Deposition of highly Porous Gold (hPG) onto gold electrodes

The hPG was fabricated with a two-step potential process as previously described [26]. Briefly, the gold disk electrodes were immersed in an aqueous electrolyte consisting of 0.1 M $HAuCl_4$ and 1 M NH_4Cl. Gold was then potentiostatically deposited in two steps. Firstly, the system was set at a working potential of -0.7 V (vs. SCE) for 5 s. Afterwards, the potential was stepped down to a value of -4.0 V (vs. SCE) for 15 s.

2.3. Immobilisation of GOx onto hPG electrodes

GOx was electrochemically adsorbed onto the prepared hPG disk electrodes by conducting a total of 6 CV scans between 0.42 V and 0.60 V (vs. SCE) at a scan rate of 1 mV s^{-1}, in a PBS solution containing 0.45 mg ml^{-1} GOx (approximately 8 U ml^{-1} as per activity rating of manufacturer).

As a term of comparison of performance, GOx was also immobilised by absorption. In this case, the hPG electrodes were incubated with the GOx solution in PBS (0.45 mg ml^{-1}) for 1 hour at room temperature, without conducting any CV scans. In both cases, the GOx-hPG electrodes were then thoroughly rinsed three times with PBS to remove any weakly bonded enzyme, and stored in PBS at 4 °C until used.

The amount of GOx immobilised onto the hPG electrodes, was estimated by performing a kinetic assay (provided by Megazyme Ltd.) of the enzyme solution before and after the immobilisation procedure and assuming no enzyme losses during the process.

2.4. Immobilisation of LAC onto hPG electrodes

The surface of the hPG electrodes was modified with a layer of amino-phenyl groups through a simple two-stage process. Firstly, a layer of nitro-phenyl groups was attached by performing two reductive CV scans at 100 mV s^{-1} from 0.6 V to -0.6 V (vs. SCE), in the presence of an acetone electrolyte containing 2 mM p-nitrophenyldiazonium tetrafluoroborate and 100 mM tetrabutylammonium tetrafluoroborate. In the second stage, the nitro groups were exchanged for amino groups by conducting two reductive CV scans at 50 mV s^{-1} from 0.0 V to -1.4 V (vs. SCE), in an aqueous electrolyte containing 10% v/v EtOH and 0.1 M KCl. Afterwards, the electrodes were transferred to a PBS solution containing 80 U ml^{-1} of LAC. The electrodes were kept in this solution overnight at 4 °C in order to facilitate the covalent linkage between the amine functional groups on the gold, and the carboxylate groups on LAC. Finally, the electrodes were rinsed three times with PBS and stored in PBS at 4 °C until required.

2.5. Electrochemical Characterisation

All electrochemical processes were conducted using the Autolab PGSTAT128 N (Metrohm, UK) potentiostat. Cyclic voltammetry (CV) and amperometry tests were performed in a three-electrode electrochemical set-up with a SCE reference electrode and a platinum

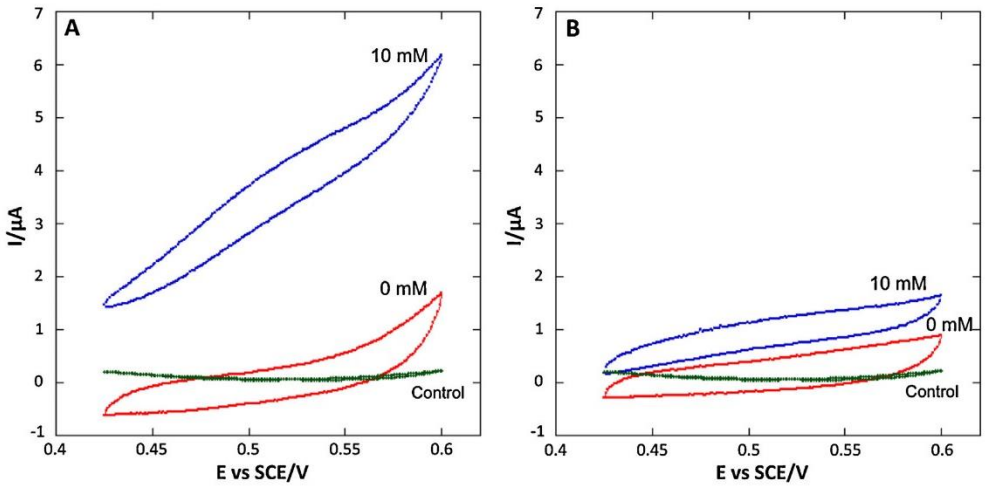

Fig. 1. Electrochemical response to glucose in PBS of the hPG electrodes. A: CV scans of the GOx_{ads}-hPG electrode in the absence and presence of 10 mM of glucose. B: CV scans of the GOx_{abs}-hPG electrode in the absence and presence of 10 mM of glucose. The control was performed with the hPG electrode (no GOx) in the presence of 10 mM of glucose. The scan rate for each test was 1 mV s^{-1}.

rod counter electrode. CV scans were performed at a scan rate of 1 mV s^{-1} in the potential range of 0.42 - 0.60 V (vs. SCE) in order to determine the optimum potential for the amperometric analysis (this range incorporates the normal oxidation potential of H_2O_2 on polished gold). CV analyses were repeated over a period of three days to determine the stability of the GOx-hPG electrodes.

The amperometry tests were performed at a fixed potential (0.52 V) during the step-wise increase of glucose concentration. After each concentration increase, the solution was agitated for 20 s and then left for 270 s to allow the amperometric response under convectional mixing to stabilise. The average amperometric response over a period of 10 s was then reported. Three replicates were performed per each experiment. In each case, a glucose concentration range of 5 µM - 50 mM was considered.

2.6. Biofuel Cell Setup

The biofuel cell consisted of a glass vial (28 ml in volume) containing a GOx_{abs}-hPG electrode and a LAC-hPG electrode as anode and cathode respectively. The electrode spacing was approximately of 0.5 cm. The system was fed with 12 ml of an aerated PBS solution containing 27.8 mM glucose at pH 7. The potential difference (ΔV) between the two electrodes was measured in open circuit mode until steady state conditions were achieved. Afterwards, the cell potential was measured under a range of different external resistances applied to the system.

3. Results and Discussion

3.1. GOx-hPG electrodes

The purpose of this study was to investigate the possibility to develop a more rapid and reproducible immobilization protocol of GOx onto hPG electrodes with respect to those so far reported that involve the use of thiol groups or conductive polymers [24,28]. This was achieved by running a series of CV scans of a hPG electrode in a GOx buffer solution, with the aim of increasing enzyme loading and affinity through the use of electrostatic forces.

The performance of the resulting bioelectrode was compared with a hPG electrode with GOx immobilised by absorption, as described in Section 2.3. Fig. 1 compares the CV curves produced with the two GOx-hPG electrodes in the presence of glucose. In both cases, no mediators were added to the electrolyte solution. As shown, when the GOx-hPG electrode was prepared electrochemically (GOx_{ads}-hPG electrode) a more prominent response to glucose was observed compared to the electrode produced by absorption (GOx_{abs}-hPG electrode). The CV scan of the GOx_{ads}-hPG electrode shows in particular a shoulder peak between 0.5 V and 0.525 V vs. SCE.

The difference in the CV curves for the two electrodes suggests that a different type of linkage between the enzyme and hPG electrode surface occurs in the two cases. The immobilisation mechanism achieved during the CV scans in the presence of GOx is not merely *absorption*, but an electrochemically driven physical *adsorption*. Since GOx is anionic at pH 7.0, and since a relatively high positive scan range is used, the CV scans are likely to promote an electrostatic attraction between the gold surface and the free enzyme. In contrast, when the electrodes are simply placed in contact with the enzymatic solution, absorption occurs into the pores of the electrode. Consequently, the resulting electrode is less stable as GOx can easily leach out.

The CV scans might actively draw the enzyme to the surface of the electrode, thus significantly increasing the loading. For the case of electrochemical adsorption in fact an average of 31.7% reduction of activity in solution after the immobilisation process was observed. On the other hand, the amount of enzyme immobilised by absorption was so low that no significant changes were observed with the activity tests in solution prior and after the incubation with the hPG electrode.

The amperometric response of the two GOx-hPG electrodes to glucose (10 mM) was tested and compared at a potential of 0.52 V vs SCE (the potential at which the electrodes showed the highest sensitivity to glucose).

This potential is within the 0.4 - 0.6 V range of values previously reported for the oxidation peak of H_2O_2 on polished gold [11,24]. H_2O_2 is formed through the oxidation of glucose by GOx and, since its formation is related to the amount of glucose in solution (see Equation (1)), many glucose sensors rely on the resultant oxidation of H_2O_2 on gold to determine the concentration of glucose in a sample [30].

$$Glucose + O_2 + H_2O \xrightarrow[GOx]{} Gluconic\ \ acid + H_2O_2 \quad (1)$$

Table 1
Comparison of the amperometric response at 0.52 V vs SCE of the GOx-hPG electrode to 10 mM of glucose, according to the immobilisation methodology. Standard deviation refers to three replicates.

Electrode	I/μA	Sensitivity/μA mM^{-1} cm^{-2}
hPG	0.07 ± 0.03	
GOx_{abs}-hPG	1.6 ± 0.2	2.42 ± 0.05
GOx_{ads}-hPG	6.10 ± 0.12	22.7 ± 0.1

The amperometric tests confirmed that the GOx_{ads}-hPG electrode performed better than the GOx_{abs}-hPG electrode. As reported in Table 1, the response of the GOx_{ads}-hPG electrode is in fact approximately four times higher than the GOx_{abs}-hPG electrode, with a sensitivity of 22.7 ± 0.1 μA mM^{-1} cm^{-2}, calculated against the superficial surface area of the bioelectrode (0.03 cm^2). In comparison, the amperometric response of a blank hPG electrode to glucose at 0.52 V is negligible. This is because the current peak related to glucose electrooxidation by the non-enzymatic hPG electrode occurs at a potential of 0.15 V [26].

3.2. The use of the GOx_{ads}-hPG electrode as glucose sensor

The amperometric response of the GOx_{ads}-hPG electrode to increasing concentrations of glucose at a constant potential of 0.52 V (vs SCE) was investigated. A typical Michaelis-Menten kinetic trend was observed. This was characterised by a linear increase in the current output up to a concentration of 10 mM as shown in Fig. 2. The detection limit the system was found to be 25 μM, which is lower compared to other GOx electrodes reported previously [28,31]. At least three replicates were performed using different electrodes, showing a good reproducibility of the electrode performance with a maximum standard deviation factor of 0.38 (at 5 μM of glucose).

The enzymatic affinity towards glucose was estimated in terms of the apparent Michaelis-Menten constant (K_m^{app}), and was calculated by using the electrochemical version of the Lineweaver-Burk equation of enzyme kinetics (Equation (2)) [13].

$$\frac{1}{i} = \frac{1}{i_{max}} + \frac{K_M^{app}}{i_{max} C} \quad (2)$$

Where i is the steady-state current observed after the addition of glucose; i_{max} is the maximum current under the saturated concentration of glucose; c is the glucose concentration. The reciprocal of the current was plotted versus the reciprocal of the glucose

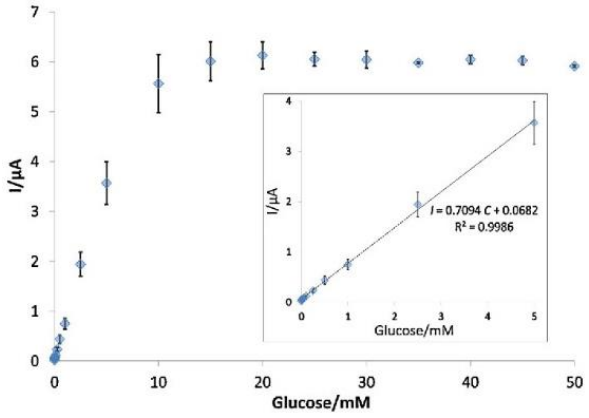

Fig. 2. Amperometric tests (at 0.52 V vs SCE) of the GOx_{ads}-hPG electrode in the presence of various glucose concentrations in the electrolyte (range of 5 μM - 50 mM). Error bars refer to three replicates.

concentration in the range of 0.005- 10 mM. This gave a value of K_m^{app} equal to 6.3 ± 0.7 mM, which was calculated from the slope (K_m^{app}/i_{max}) and the intercept ($1/i_{max}$) of the plot. This value is much lower than the one reported for the native GOx from *Aspergillus niger* in solution (27 mM) [32]. This indicates that the immobilised GOx onto hPG electrodes has high enzymatic activity and higher affinity for glucose than the soluble enzyme with a low diffusion barrier. Although this value is slightly higher than the value of 1.5 mM recently reported for a GOx/chitosan/ferrocene carbon nanotubes electrode [13], it is, however, comparable with the value (6.3 mM) reported for a ferrocene-modified multiwalled carbon nanotube [12], and much lower than other reported GOx electrodes [33,34].

Table 2 compares the sensitivity to glucose of the GOx_{ads}-hPG electrode with other GOx electrodes created by using much more complex immobilisation procedures [12–14,21,35,36]. As reported, the GOx_{ads}-hPG electrode sensitivity is greater than the majority of the other methods reviewed, including some that boast direct electron transfer between the FAD centre of GOx and the electrode surface.

3.3. Stability

The GOx_{ads}-hPG electrodes were stored in PBS at 4 °C and tested again at regular intervals of time to investigate their stability. In particular, Fig. 3A compares the CV scans obtained immediately after the electrode fabrication, and after 24 and 48 hours, respectively.

A reduction in the current signal was observed within the three days, with the largest variation occurring after 24 hours of storage. After the first 24 hours of storage, a 35% reduction in the current peak at 0.52 V was observed. Interestingly, after the first 24 hours of storage, a marked change in the blank (e.g. CV test in the absence of glucose) was also observed, while no further changes occurred in the following days. The reduction in the response observed was lower after 48 hours, with a 25% decrease in the current peak at 0.52 V with respect to data collected at 24 hours.

This suggests that the initial variation in the activity of the bioelectrodes might be caused by a reduction in the hPG sensitivity towards H_2O_2, rather than simply to enzyme deactivation and/or leaching. The reduction in the electrochemical activity of nPG structures with the time has been previously reported and attributed to a coarsening process [37]. This hypothesis was supported by stability tests carried out on the hPG electrode with no enzyme immobilised. When the hPG electrode was tested in PBS after one day, a change in the CV curve was observed, which was minimal after another day of storage (see supplementary data, Figure S1).

The stability of the GOx_{ads}-hPG electrodes in terms of amperometric response was also investigated during a period of time of five days. As shown in Fig. 3B, the linearity range and the detection limit did not change. However, the magnitude of the amperometric response diminished by a maximum factor of 3.60 over the 5 days tested. In considering practical applications, the GOx_{ads}-hPG electrode response should be normalised and calibrated prior to use to achieve concurrent data sets. After data normalisation, the variance observed between data sets obtained on different days for concentrations of glucose between 50 μM and 5 mM was minimal (see supplementary data, Figure S2).

3.4. GOx electrode in enzymatic biofuel cell

The functional immobilisation of LAC was achieved by activating the hPG surface with amino-phenyl groups as previously reported [38]. The steps in the immobilisation protocols are reported in Fig. 4. Firstly, nitrophenyl groups were electrochemically attached to the gold by conducting two reductive CV scans in the presence of p-nitrophenyldiazonium salt. In order to limit the production

Table 2
Comparison of the sensitivity to glucose of several GOx electrodes. *Standard deviation refers to three replicates. **Methods which claim to achieve direct electron transfer.

Electrode	Sensitivity/μA mM^{-1} cm^{-2}	E vs SCE/V	Reference
GOx_{ads}-hPG *	22.7 ± 0.1	0.52	This Study
Naf/GOx-NPG/GCE	0.697	0.40	[14]
Fc/GOx-MWCNT/Chi-BSA- AuE	7.77 ± 0.08	0.17	[13]
GOx-Fc/MWCNT/Chi-GCE	25	0.31	[12]
Gel/GOx-WMCNT/GCE **	2.47	- 0.48	[35]
AuNPs/GOx/Biofilm-MWCNT/GCE **	16.6	- 0.40	[36]
PDDA/AuNPs-MWCNT/GE **	29.72	- 0.49	[21]

Naf: Nafion; GCE: glassy carbon electrode; Fc: Ferrocene; MWCNT: multi-walled carbon nano-tubes; Chi: Chitosan; BSA: bovine serum albumin; AuE: gold electrode; Gel: gelatine; AuNPs: gold nano-particles; PDDA: poly(diallyldimethylammonium chloride); GE: graphene electrode

of polyaniline (by the polymerisation of the phenyl groups through hydrolysis), and to promote the formation of a monolayer, this stage was conducted in an acetone-based electrolyte. The CV scans conducted show two peaks (at 400 mV and -200 mV vs. SCE) on the first scan that greatly decrease on the second scan (Figure S3). These peaks are attributed to the reduction of the diazonium salt on the different planar surfaces of gold and crystalline gold as previously suggested for the case of an acetonitrile electrolyte [39]. Since the phenyl-gold bond formed is not oxidised back in this scan range, the large decrease in the magnitude of the peaks on the second scan suggests that the surface is quickly becoming saturated with the nitro-phenyl groups [8,39,40].

During the second stage, the treated electrodes were immersed in a 10% ethanol and water based electrolyte and two more reductive CV scans were conducted in a much more negative scan range (0.0 V and -1.4 V vs. SCE). This facilitated the exchange of oxygen for protons on the nitro groups resulting in the production of amino and hydroxylamino groups. The voltammogram of the first scan shows a very clear peak at -820 mV which is established as the potential at which nitrophenyl groups are irreversibly reduced to aminophenyl groups [8]. This peak is not evident on the second scan though a small redox peak is observed at -700 mV (Figure S4). This results suggests the presence of hydroxylamine groups amongst the amine groups [41].

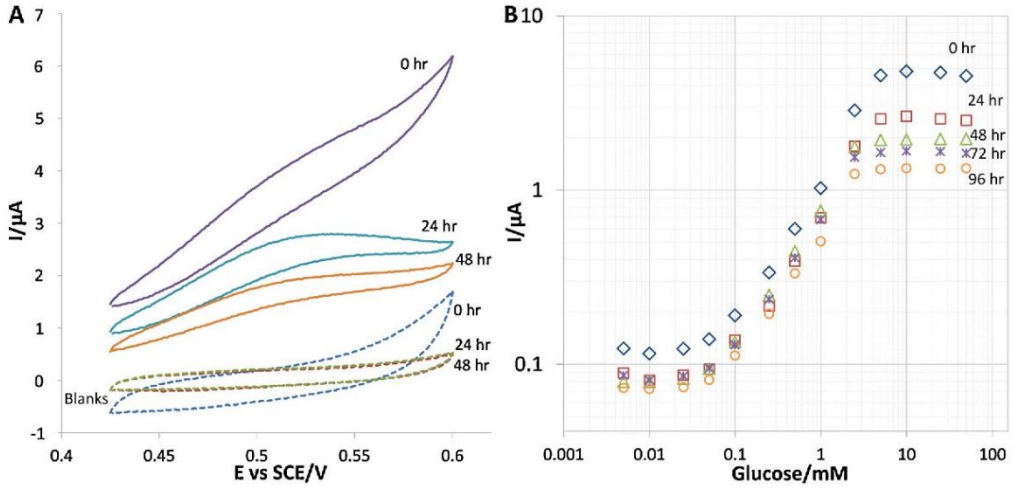

Fig. 3. Stability tests. A: CV scans of the GOx_{ads}-hPG electrode after 0, 24, and 48 hours for a glucose concentration of 10 mM. The blanks were performed in the absence of glucose in the electrolyte. B: Amperometric response of the GOx_{ads}-hPG electrode to increasing concentration of glucose over a period of five days of storage.

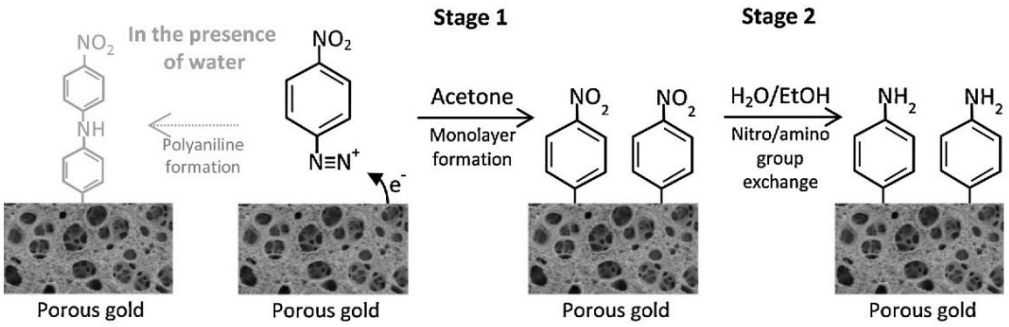

Fig. 4. Schematic of gold surface modification prior to LAC immobilisation.

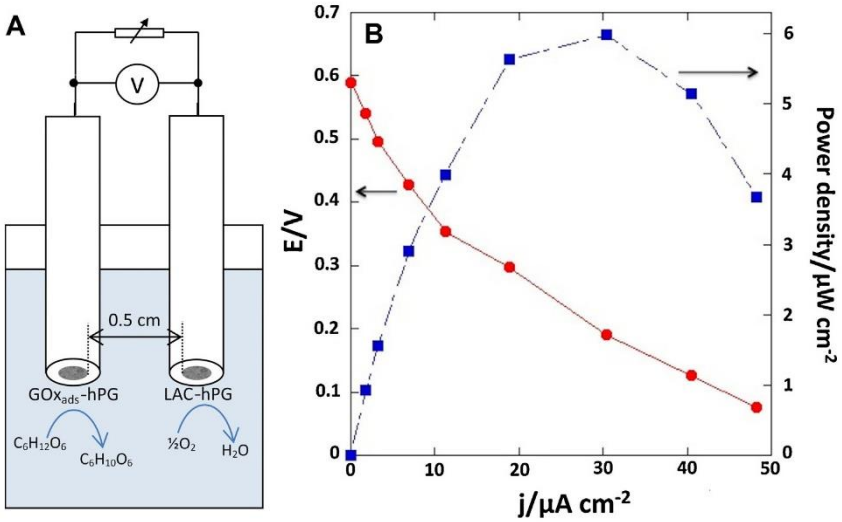

Fig. 5. A: Scheme of the enzymatic biofuel cell set up. B: Polarisation and power density curve of the GOx$_{ads}$-hPG and LAC-hPG biofuel cell. The power and the current density refer to the total superficial surface area of the electrodes used (0.03 cm^2).

The GOx$_{ads}$-hPG and the LAC-hPG electrodes were subsequently tested as anode and cathode respectively of a glucose/oxygen enzymatic biofuel cell. The electrodes were immerged in an aerated PBS solution containing 27.8 mM of glucose, and the potential difference of the cell was monitored by means of a potentiostat (Fig. 5). An open circuit voltage of 0.58 V was observed, comparable with the value previously reported [27]. Subsequently, the cell was polarised by connecting the electrodes to a range of external resistors. Fig. 5B shows the cell voltage and the power density as a function of the current density. As shown, the peak power density was of 6 μW cm^{-2} at 0.2 V vs SCE. This result, although obtained with a very simple design, is comparable with recently reported miniature enzymatic biofuel cells [27,42].

4. Conclusions

Glucose oxidase was immobilised onto highly porous gold electrodes by electrochemical adsorption, with a rapid one-step protocol that did not involve the use of expensive and/or harsh reagents. The GOx$_{ads}$-hPG electrode exhibits Michaelis-Menten kinetics with a wide linearity range between 50 μM and 10 mM of glucose, and a detection limit of 25 μM.

The sensitivity, calculated against the total superficial surface area of the bioelectrode was of 22.7 ± 0.1 μA mM^{-1} cm^{-2}. After five days of storage the bioelectrode amperometric response to glucose was 3.6 times lower compared to the initial value. However, the linearity range and the detection limit were maintained.

Preliminary experiments encourage the implementation of the GOx$_{ads}$-hPG electrode as the anode of an enzymatic biofuel cell. When the electrode was coupled with a LAC-hPG electrode as a cathode, a peak power density of 6 μW cm^{-2} at 0.2 V vs SCE was achieved. Future work will be regarding the implementation of the enzyme hPG electrodes in a micro biofuel cell for healthcare applications.

Acknowledgments

The authors acknowledge: Prof Frank Marken, University of Bath, for valuable discussions; the Royal Society Research Grant (RG110344) and EPSRC (EP/K031597/1) for funding.

Appendix A. Supplementary data

Supplementary data associated with this article can be found, in the online version, at http://dx.doi.org/10.1016/j.electacta.2014.06.074.

References

[1] M. Falk, V. Andoralov, M. Silow, M.D. Toscano, S. Shleev, Miniature Biofuel Cell as a Potential Power Source for Glucose-Sensing Contact Lenses, Anal Chem 85 (2013) 6342–6348.
[2] A. Chaubey, B.D. Malhotra, Mediated biosensors, Biosens Bioelectron 17 (2002) 441–456.
[3] R.A. Bullen, T.C. Arnot, J.B. Lakeman, F.C. Walsh, Biofuel cells and their development, Biosens Bioelectron 21 (2006) 2015–2045.
[4] M. Shaolin, X. Huaiguo, Bioelectrochemical characteristics of glucose oxidase immobilized in a polyaniline film, Sensor Actuat B-Chem 31 (1996) 155–160.
[5] Y. Degani, A. Heller, Direct electrical communication between chemically modified enzymes and metal electrodes. I. Electron transfer from glucose oxidase to metal electrodes via electron relays, bound covalently to the enzyme, J Phys Chem 91 (1987) 1285–1289.
[6] M.J. Moehlenbrock, S.D. Minteer, Extended lifetime biofuel cells, Chem Soc Rev 37 (2008) 1188–1196.
[7] C. Vaz-Dominguez, S. Campuzano, O. Rüdiger, M. Pita, M. Gorbacheva, S. Shleev, V.M. Fernandez, A.L. De Lacey, Laccase electrode for direct electrocatalytic reduction of O2 to H2O with high-operational stability and resistance to chloride inhibition, Biosens Bioelectron 24 (2008) 531–537.
[8] M. Pita, C. Gutierrez-Sanchez, D. Olea, M. Velez, C. Garcia-Diego, S. Shleev, V.M. Fernandez, A.L. De Lacey, High Redox Potential Cathode Based on Laccase Covalently Attached to Gold Electrode, J Phys Chem C 115 (2011) 13420–13428.
[9] S. Timur, N. Pazarlıolu, R. Pilloton, A. Telefoncu, Thick film sensors based on laccases from different sources immobilized in polyaniline matrix, Sensor Actuat B-Chem 97 (2004) 132–136.
[10] J. Wang, Glucose Biosensors: 40 Years of Advances and Challenges, Electroanalysis 13 (2001) 983–988.
[11] Y. Xiao, F. Patolsky, E. Katz, J.F. Hainfeld, I. Willner, Plugging into Enzymes: Nanowiring of Redox Enzymes by a Gold Nanoparticle, Science 299 (2003) 1877–1881.
[12] J.D. Qiu, W.M. Zhou, J. Guo, R. Wang, R.P. Liang, Amperometric sensor based on ferrocene modified multiwalled carbon nanotube nanocomposites as electron mediator for the determination of glucose, Anal Biochem 385 (2009) 264–269.
[13] A. Fatoni, A. Numnuam, P. Kanatharana, W. Limbuta, C. Thammakhet, P. Thavarungkul, A highly stable oxygen-independent glucose biosensor based on a chitosan-albumin cryogel incorporated with carbon nanotubes and ferrocene, Sensor Actuat B-Chem 185 (2013) 725–734.
[14] H. Qiu, L. Xue, G. Ji, G. Zhou, X. Huang, Y. Qu, P. Gao, Enzyme-modified nanoporous gold-based electrochemical biosensors, Biosens Bioelectron 24 (2009) 3014–3018.
[15] J. Kim, H. Jia, P. Wang, Challenges in biocatalysis for enzyme-based biofuel cells, Biotechnol Adv 24 (2006) 296–308.

[16] A. Guiseppi-Elie, C. Lei, R.H. Baughman, Direct electron transfer of glucose oxidase on carbon nanotubes, Nanotechnology 13 (2002) 559.
[17] D. Ivnitski, B. Branch, P. Atanassov, C. Apblett, Glucose oxidase anode for biofuel cell based on direct electron transfer, Electrochem Commun 8 (2006) 1204–1210.
[18] Y. Liu, M. Wang, F. Zhao, Z. Xu, S. Dong, The direct electron transfer of glucose oxidase and glucose biosensor based on carbon nanotubes/chitosan matrix, Biosens Bioelectron 21 (2005) 984–988.
[19] N. German, A. Ramanaviciene, J. Voronovi, A. Ramanavicius, Glucose biosensor based on graphite electrodes modified with glucose oxidase and colloidal gold nanoparticles, Microchim Acta 168 (2010) 221–229.
[20] H.-F. Cui, K. Zhang, Y.-F. Zhang, Y.-L. Sun, J. Wang, W.-D. Zhang, J.H.T. Luong, Immobilization of glucose oxidase into a nanoporous TiO2 film layered on metallophthalocyanine modified vertically-aligned carbon nanotubes for efficient direct electron transfer, Biosens Bioelectron 46 (2013) 113–118.
[21] Y. Yu, Z. Chen, S. He, B. Zhang, X. Li, M. Yao, Direct electron transfer of glucose oxidase and biosensing for glucose based on PDDA-capped gold nanoparticle modified graphene/multi-walled carbon nanotubes electrode, Biosens Bioelectron 52 (2014) 147–152.
[22] A.J. Thorley, T.D. Tetley, New perspectives in nanomedicine, Pharmacol Therapeut 140 (2013) 176–185.
[23] M. Bottini, S. Bruckner, K. Nika, N. Bottini, S. Bellucci, A. Magrini, A. Bergamaschi, T. Mustelin, Multi-walled carbon nanotubes induce T lymphocyte apoptosis, Toxicol Lett 160 (2006) 121–126.
[24] L.Y. Chen, T. Fujita, M.W. Chen, Biofunctionalized nanoporous gold for electrochemical biosensors, Electrochim Acta 67 (2012) 1–5.
[25] S. Cherevko, C.-H. Chung, Direct electrodeposition of nanoporous gold with controlled multimodal pore size distribution, Electrochem Commun 13 (2011) 16–19.
[26] H. du Toit, M. Di Lorenzo, Electrodeposited highly porous gold microelectrodes for the direct electrocatalytic oxidation of aqueous glucose, Sensor Actuat B-Chem 192 (2014) 725–729.
[27] M. Falk, V. Andoralov, M. Silow, M.D. Toscano, S. Shleev, Miniature biofuel cell as potential power source for glucose sensing contact lenses, Anal Chem 85 (2013) 6342–6348.
[28] X. Xiao, M.e. Wang, H. Li, P. Si, One-step fabrication of bio-functionalised nanoporous gold/poly(3,4-ethylenedioxythiophene) hybrid electrodes for amperometric glucose sensing, Talanta 116 (2013) 1054–1059.
[29] M. Hakamada, M. Takahashi, M. Mabuki, Enzyme electrodes stabilized by monolayer-modified nanoporous Au for biofuel cells, Gold Bull 45 (2012) 9–15.
[30] F. He, Y. Tang, M. Yu, S. Wang, Y. Li, D. Zhu, Fluorescence-Amplifying Detection of Hydrogen Peroxide with Cationic Conjugated Polymers, and Its Application to Glucose Sensing, Adv Funct Mater 16 (2006) 91–94.
[31] G. Wang, N.M. Thai, S.-T. Yau, Preserved enzymatic activity of glucose oxidase immobilized on an unmodified electrode, Electrochem Commun 8 (2006) 987–992.
[32] M.J. Rogers, K.G. Brandt, Interaction of d-glucal with Aspergillus niger glucose oxidase, Biochemistry 10 (1971) 4624–4630.
[33] J.C. Vidal, E. Garcia, J.R. Castillo, Electropolymerization of pyrrole and immobilization of glucose oxidase in a flow system: influence of the operating conditions on analytical performance, Biosens Bioelectron 13 (1998) 371–382.
[34] X. Chen, J.B. Jia, S.J. Dong, Organically modified sol–gel/chitosan composite based glucose biosensor, Electroanalysis 15 (2003) 608–612.
[35] A.P. Periasamy, Y.-J. Chang, S.-M. Chen, Amperometric glucose sensor based on glucose oxidase immobilized on gelatin-multiwalled carbon nanotube modified glassy carbon electrode, Bioelectrochemistry 80 (2011) 114–120.
[36] H. Zhang, Z. Meng, Q. Wang, J. Zheng, A novel glucose biosensor based on direct electrochemistry of glucose oxidase incorporated in biomediated gold nanoparticles–carbon nanotubes composite film, Sensor Actuat B-Chem 158 (2011) 23–27.
[37] S. Cattarin, D. Kramer, A. Lui, M.M. Musiani, Preparation and Characterization of Gold Nanostructures of Controlled Dimension by Electrochemical Techniques, J Phys Chem C 111 (2007) 12643–12649.
[38] P. Olejnik, B. Palys, A. Kowalczyk, A.M. Nowicka, Orientation of Laccase on Charged Surfaces. Mediatorless Oxygen Reduction on Amino- and Carboxyl-Ended Ethylphenyl Groups, J Phys Chem 116 (2012) 25911–25918.
[39] A. Benedetto, M. Balog, P. Viel, F. Le Derf, M. Sallé, S. Palacin, Electro-reduction of diazonium salts on gold: Why do we observe multi-peaks? Electrochim Acta 53 (2008) 7117–7122.
[40] P.A. Brooksby, A.J. Downard, Electrochemical and Atomic Force Microscopy Study of Carbon Surface Modification via Diazonium Reduction in Aqueous and Acetonitrile Solutions, Langmuir 20 (2004) 5038–5045.
[41] N. Mano, A. Kuhn, Cation induced amplification of the electrocatalytic oxidation of NADH by immobilized nitro-fluorenone derivatives, J Electroanal Chem 498 (2001) 58–66.
[42] T. Beneyton, I. Putu Mahendra Wijaya, C. Ben Salem, A.D. Griffiths, V. Taly, Membraneless glucose/O2 microfluidic biofuel cells using covalently bound enzymes, Chem Commun 49 (2012) 1094–1096.

SUPPLEMENTARY DATA

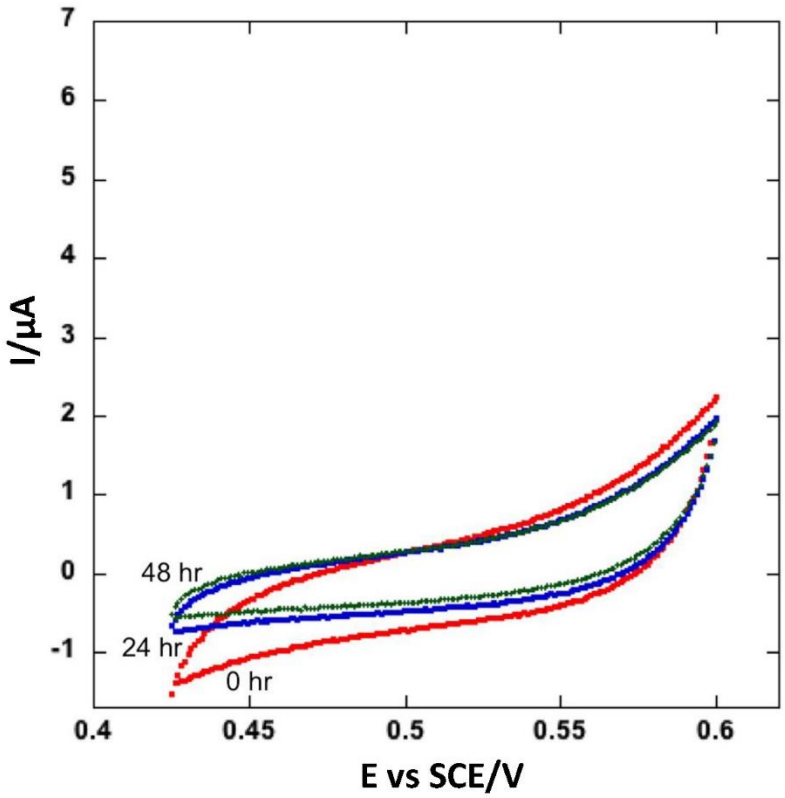

Figure S1. CV scans of the hPG electrode in PBS, pH7 in the absence of glucose after 0, 24, and 48 hours. Scan rate of 1 mV s^{-1} (the final of 3 cyclic scans is shown here).

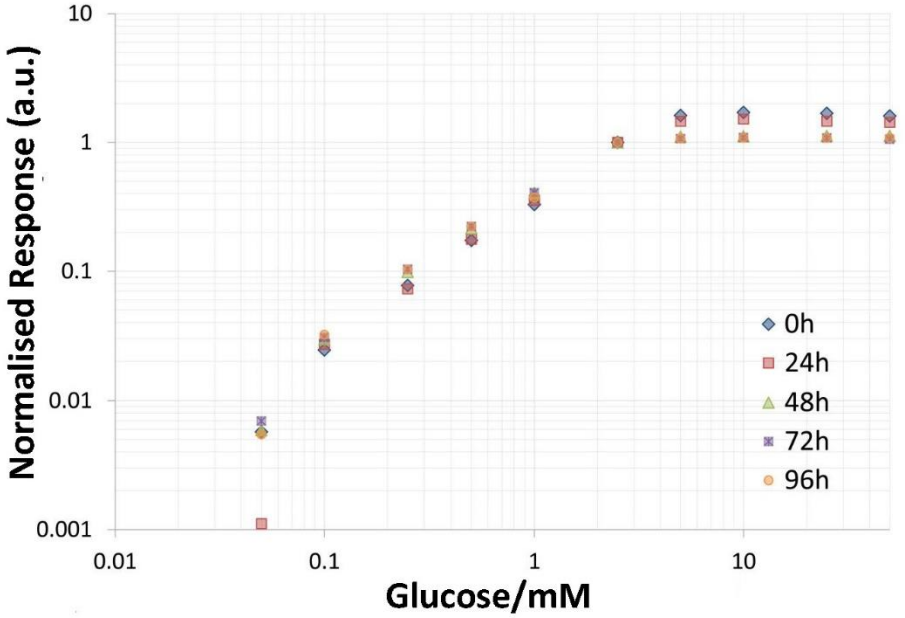

Figure S2: Normalised response of GOx_{ads}-hPG electrode over period of five days. Results were normalised between 0 and 2.5 mM glucose in PBS (this range was chosen since a linear relationship is evident here). The amperometric response in glucose free PBS, I_0, and the amperometric response in a 2.5 mM glucose and PBS solution, $I_{2.5}$, is used to calculate the normalised response, N, for any given amperometric response, I ;

$$N = \frac{I - I_0}{I_{2.5} - I_0}$$

The resulting data shows a very strong trend in data obtained over the five- day period considered.

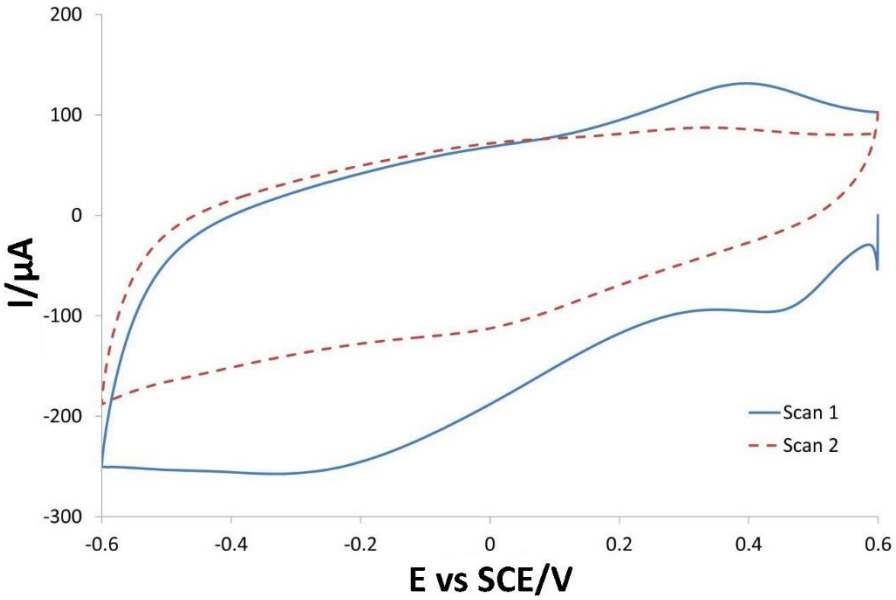

Figure S3: Cyclic voltammograms of the first gold surface modification stage prior to laccase immobilisation. Scans were conducted in an acetone electrolyte containing 2 mM p-nitrophenyldiazonium tetrafluoroborate and 100 mM tetrabutylammonium tetrafluoroborate, and at a scan rate of 100 mV s^{-1}.

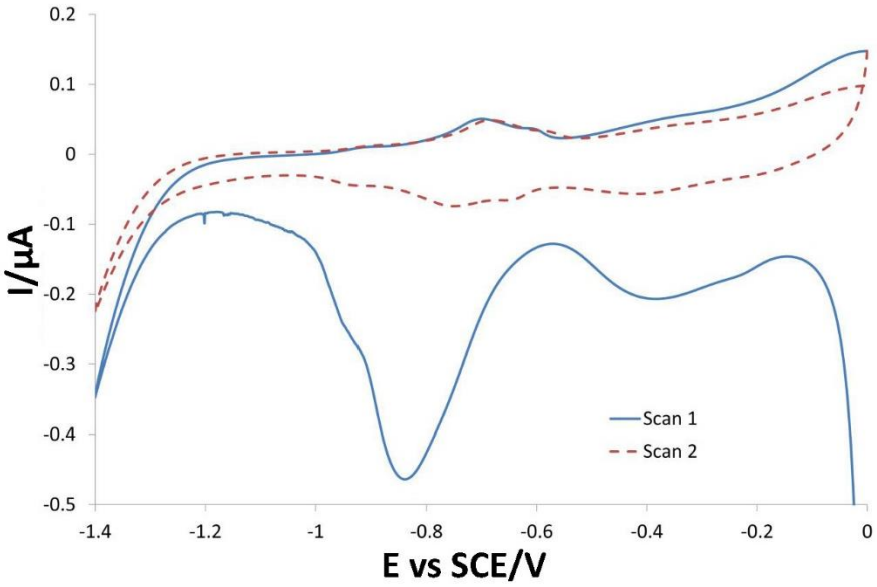

Figure S4: Cyclic voltammograms of the second gold surface modification stage prior to laccase immobilisation. Scans were conducted at 50 mV s^{-1} from 0.0 V to -1.4 V, in an aqueous electrolyte containing 10 % v/v EtOH and 0.1 M KCl.

Biosensors and Bioelectronics 69 (2015) 199–205

Contents lists available at ScienceDirect

Biosensors and Bioelectronics

journal homepage: www.elsevier.com/locate/bios

Continuous power generation from glucose with two different miniature flow-through enzymatic biofuel cells

Hendrik du Toit, Mirella Di Lorenzo *

University of Bath, Department of Chemical Engineering, Bath BA2 7AY, UK

ARTICLE INFO

Article history:
Received 5 January 2015
Received in revised form
17 February 2015
Accepted 24 February 2015
Available online 26 February 2015

Keywords:
Enzymatic biofuel cells
Bioenergy
Highly porous gold
Flow-through
Glucose oxidase
Laccase

ABSTRACT

Enzymatic biofuel cells (EBFCs) can generate energy from metabolites present in physiological fluids. They represent an attractive alternative to lithium batteries to power implantable devices, as they work at body temperature, are light and easy-to-miniaturise. To be implantable in blood vessels, EBFCs should not only be made of non-toxic and biocompatible compounds but should also be able to operate in continuous flow-through mode. The EBFC devices reported so far, however, implement carbon-based materials of questionable toxicity and stability, such as carbon nanotubes, and rely on the use of external redox mediators for the electrical connection between the enzyme and the electrode. With this study, we demonstrate for the first time continuous power generation by flow through miniature enzymatic biofuel cells fed with an aerated solution of glucose and no redox mediators. Non-toxic highly porous gold was used as the electrode material and the immobilisation of the enzymes onto the electrodes surface was performed via cost-effective and easy-to-reproduce methodologies. The results presented here are a significant step towards the development of revolutionary implantable medical devices that extract the power they require from metabolites in the body.

1. Introduction

Millions of patients worldwide suffer from serious diseases such as bradycardia, fibrillation or diabetes, and consequently require active medical implants (WHO 2014). Size, weight, and reliability are fundamental characteristics of these devices, and are typically determined by the power source utilised. Active medical implants are traditionally powered by lithium batteries, which are heavy and difficult to miniaturise, leading to disproportionately large energy sources compared to the systems that they power (Bazaka and Jacob 2012). The search for alternative power sources, which are light, non-toxic, and easy-to-miniaturise, is therefore crucial.

Enzymatic biofuel cells (EBFCs) are power sources that can be employed in the human body (Barton et al. 2004). EBFCs are a specific type of fuel cell that implements redox enzymes as catalysts at the anode and cathode. They can mimic many of the metabolic pathways found within living cells (in particular the oxidation of glucose), and thus produce power from energy sources naturally found in biological fluids at body temperature (Cosnier et al. 2014). EBFCs have also the added benefit of producing the same waste products as the living organism that hosts them, and could thus use established waste metabolism routes to dispose of the by-products produced during the production of power. These features make EBFCs an attractive alternative to lithium batteries.

For the purpose of *in vivo* use, EBFCs could either be implanted in soft tissue or in blood vessels (Barton et al., 2004; Cinquin et al., 2010; Kerzenmacher et al., 2008). In the case of devices to be implanted in the soft tissue, the system is limited by lower fuel and oxidant concentrations (glucose and oxygen), and is thus reliant solely on diffusion for the supply and removal of reactants and waste products respectively. Devices designed for use in blood vessels, would instead exhibit continuous flow through operation. In this case, the EBFC would benefit by having higher concentrations of glucose and oxygen, continuously supplied by the flow of blood. The continuous flow could however lead to enzyme leaching from the electrodes, and could interfere with the electron transfer between enzymes and the electrode surface (Kerzenmacher et al., 2008).

Currently the practical application of EBFCs is prevented by several major hindrances, the most significant of which are poor stability and extremely low power yields (Wei and Liu, 2008). However, the poor stability is not necessarily caused by the deactivation of the enzymes used, but rather by a decay in the efficiency of electron transfer between the enzymes and the electrode surface. This is due to the fact that most EBFCs reported so far rely on mediated electron transfer (MET) techniques, which typically require foreign redox active particles to transfer electrons between

* Corresponding author.
E-mail address: M.Di.Lorenzo@bath.ac.uk (M. Di Lorenzo).

http://dx.doi.org/10.1016/j.bios.2015.02.036

the active site of the enzyme and the electrode surface (Cooney et al., 2008; Degani and Heller, 1987; Minteer et al., 2007). Over time, these free moving redox mediators can leach out from the fuel cell's electrodes causing a decay in power output.

The development of new enzyme immobilisation techniques in recent years, which achieve direct electron transfer (DET) between the enzyme and the electrode, together with major advances in material sciences allowing for much higher enzyme loading, and advances in electronics leading to ultra-low power medical devices (with a typical pacemaker now only requiring 10 μW) have opened new perspectives and reinforced the interest for EBFCs (Cosnier et al., 2014).

Power generation by EBFCs from biological fluids has been recently proven (Kim et al., 2006; Rincón et al., 2011; Sokic-Lazic and Minteer, 2009; Togo et al., 2007). Nonetheless, there is currently very little reported on fully-fledged devices capable of continuous operation under physiological conditions. The majority of devices reported so far show the use of separate enzymatic electrodes simply placed in the living organism and externally wired. In the case of continuous flow-through operation, these devices still rely on the use of mediators in the feed solution. There are no reported EBFCs that exhibit continuous flow-through operation without mediators for the potential use in line with blood vessels. Instead the few studies that have progressed to the development of devices capable of sustained operation have thus far focused on implantation in the soft tissue of animals (Castorena-Gonzalez et al., 2013; Cinquin et al., 2010; Halámková et al., 2012; MacVittie et al., 2013; Rasmussen et al., 2012; Sales et al., 2013; Szczupak et al., 2012).

All of these reported studies rely on the use of carbon-based electrodes. In particular, carbon nanotube (CNT) aggregates have been widely implemented, since they allow DET with glucose oxidase (GOx), which is the most prevalent enzyme used for glucose oxidation at the anode of EBFCs (Anthony et al., 2002; Ivnitski et al., 2006; Liu et al., 2005). However, the long term toxicity and stability of CNTs is still unknown. CNTs have been reported to cause the destruction of T lymphocyte cells in mammals (Bottini et al., 2006). Direct contact between the CNTs electrode and physiological fluids should therefore be carefully prevented in implantable applications. Some researchers have tackled this obstacle by enclosing their devices in semi-permeable membranes which would prevent direct contact between the electrodes and white blood cells (Cinquin et al., 2010). This may, however, not be possible when designing a device for implantation in or around blood vessels, since the device would have to be small enough to cause minimal disruption to normal blood flow. The search for electrode materials, as an alternative to carbon-based systems is therefore critical for implantable EBFCs. In this context, highly porous gold (hPG) electrodes are a promising alternative. These non-toxic electrodes have remarkable properties, such as high conductivity, large surface area, three-dimensional open porosity, and biocompatibility. Moreover, their large surface area and foam-like morphology make hPG electrodes the ideal support for enzyme immobilisation at high loadings as previously demonstrated by this group and others (Chen et al., 2012; du Toit and Di Lorenzo, 2014b; Hakamada et al., 2012; Xiao et al., 2013).

In this study, we demonstrate for the first time sustained power production from continuous flow-through enzymatic biofuel cells (CFEBFCs) for periods of up to one month without the use of external redox mediators. We also demonstrate a simple and low cost methodology for fast prototyping of CFEBFCs using 3D printed moulds, as well as the electrochemical production of hPG electrodes without the need for potentiostatic control. Moreover, GOx, implemented at the anode, is electrostatically immobilisation onto the hPG surface *via* the simple and easy-to-reproduce method that we have previously reported (du Toit and Di Lorenzo, 2014b).

2. Experimental

2.1. Materials

GOx from *Aspergillus niger*, laccase (LAC) from *Rhus vernicifera*, and all other reagents used were of analytical grade and purchased from Sigma-Aldrich. Unless stated otherwise, all the aqueous solutions used were prepared with reverse osmosis purified water. Saturated calomel electrodes (SCE) were purchased from IJCambria Ltd. Platinum wire was purchased from Cookson Precious Metals Ltd. Polydimethylsiloxane (PDMS, Dow Corning Sylgard 184) was purchased from Ellsworth Adhesives.

All analytical experiments were performed in phosphate buffered saline (PBS). This was prepared with the following constituents: 137 mM NaCl, 2.7 mM KCl, 10 mM Na_2HPO_4, 2 mM KH_2PO_4. The pH of this solution was then adjusted to 7 with the drop wise addition of 1 M solutions of HCl and NaOH.

All potentiostatically-controlled electrochemical processes were conducted using the Autolab PGSTAT128 N (Metrohm, UK) potentiostat. The load on the fuel cells was controlled using a Cropico variable resistance box (RS Components) and the potential difference was monitored and recorded using a PicoLog ADC-24 multichannel data logger. The moulds for the PDMS replicas were 3D printed in polylactic acid using a Makerbot Replicator.

2.2. Deposition of hPG onto platinum wires

The hPG was fabricated with a two-stage process similar to the process previously described (du Toit and Di Lorenzo, 2014a). Briefly, controlled lengths of platinum wire electrodes were immersed in an electrolyte consisting of 0.1 M $HAuCl_4$ and 1 M NH_4Cl. Gold was deposited in two steps. For platinum wire lengths of 1 cm or less, the working potential was first gradually stepped down to −4.0 V (vs. SCE) over a period 10 s using the Autolab PGSTAT128N (Metrohm, UK) potentiostat. This potential was then maintained for a further 10 s. For platinum wire lengths greater than 1 cm (where the required deposition current exceeded the capabilities of the potentiostat), a simple two-electrode system was used with a second platinum wire as the counter electrode. This time the potential applied across the two electrodes was gradually stepped down to −10 V and then maintained at this potential for 10 s using the Basetech BT-305 variable bench-top power supply unit. This was done in accordance with the actual potential applied across the working electrode and counter electrode when using a potentiostat with a three-electrode setup.

The morphology of the resulting electrodes was characterised using a Hitachi S-4300 field emission scanning electron microscope (FESEM).

2.3. Enzyme immobilisation onto hPG electrodes

GOx and LAC were immobilised onto the hPG anode and cathode respectively to facilitate the oxidation of glucose at the anode and the reduction of oxygen at the cathode according to the following reactions:

$$\underbrace{C_6H_{12}O_6}_{glucose} \xrightarrow{GOx} \underbrace{C_6H_{10}O_6}_{D-glucono-1,5-lactone} + 2e^- + 2H^+$$

$$\frac{1}{2}O_2 + 2e^- + 2H^+ \xrightarrow{LAC} H_2O$$

GOx was electrochemically adsorbed onto the prepared hPG wire electrodes using a process based on the method described previously (du Toit and Di Lorenzo, 2014b). Simply, 6 CV scans were conducted between 0.42 V and 0.60 V (vs. SCE) at a scan rate

of 1 mV s^{-1}, in a PBS solution containing 15 mg ml^{-1} GOx (approximately 270 U ml^{-1} as per activity rating of manufacturer).

LAC was immobilised using a multistage method based on a method previously reported by this research group and a thiol blotting method reported by other researchers for the immobilisation of laccase from *Trametes versicolor* (du Toit and Di Lorenzo, 2014b; Pita et al., 2011). The surface of the hPG wire electrodes was modified with a layer of amino-phenyl groups through a simple two-stage process. Firstly, a layer of nitro-phenyl groups was attached by performing two reductive CV scans at 100 mV s^{-1} from 0.6 V to −0.6 V (vs. SCE), in the presence of an acetone electrolyte containing 2 mM p-nitrophenyldiazonium tetrafluoroborate and 100 mM tetrabutylammonium tetrafluoroborate. In the second stage, the nitro groups were exchanged for amino groups by conducting two reductive CV scans at 50 mV s^{-1} from 0.0 V to −1.4 V (vs. SCE), in an electrolyte containing 10%v/v EtOH and 0.1 M KCl. Afterwards, the electrodes were transferred to a solution containing 10 mM 6-mercapto-1-hexanol and left overnight at room temperature. The following morning 1 mg of LAC (270 U as per activity rating of manufacturer) was added to 0.38 ml of a 50 mM sodium periodate solution. After 30 minutes of incubation at room temperature this LAC solution was made up to 1.0 ml by the addition of 0.62 ml of a 100 mM Na_2HPO_4 solution. The amino-phenyl and thiol functionalised hPG electrodes were then submerged in this LAC solution for 90 min. Finally the electrodes were taken from the LAC solution and, after repeated rinsing in a 10 mM 2-morpholinoethanesulfonate (MES) buffer, were submerged in a solution containing 10 mM MES, 20 mM N-hydroxysuccinimide and 40 mM 1-(3-dimethylaminopropyl)-3-ethylcarbodiimide for 2 h before being rinsed with and stored in PBS until required.

3. Results and discussion

3.1. Enzymatic biofuel cell fabrication

Two different CFEBFC designs were considered in this study. In the first design, the anode and the cathode (1 cm long each) were fit in two parallel channels, each with a 3 mm × 3 mm cross-sectional area, separated by a PDMS wall (Fig. 1A). The second design was characterised by a single channel (10 mm × 3 mm cross-sectional area) containing the two electrodes, which were positioned so that the electrolyte would flow over the cathode and the anode sequentially (Fig. 1B). In this design, the electrode's projected surface area was increased by repeatedly folding 3 cm long electrodes to occupy a total cross-sectional area of 1 cm by 0.5 cm. The negative of the CFEBFC was 3D printed and then used as a mould over which PDMS was cast to create the final fuel cell design (Fig. 1C). Once the enzymatic electrodes were inserted, the PDMS structure was clamped between two pieces of acrylic plastic (Fig. 1D).

The electrodes were manufactured by directly electrodepositing hPG films onto platinum wires *via* a hydrogen bubble template (du Toit and Di Lorenzo, 2014a). This technique relies on the simultaneous deposition of gold and evolution of hydrogen gas, and thus is reliant on relatively high deposition potentials and currents. The deposition is therefore easy to achieve and control with a potentiostat in the case of small test electrodes (such as for the electrodes used in the parallel channels design). When larger surfaces are used, such as the platinum wires used in the single channel design, potentiostatic control is, however, harder to maintain. The use of a DC power supply as an alternative to the potentiostat was therefore investigated to simplify the established hPG deposition method. Fig. 2 compares the FESEM images of the

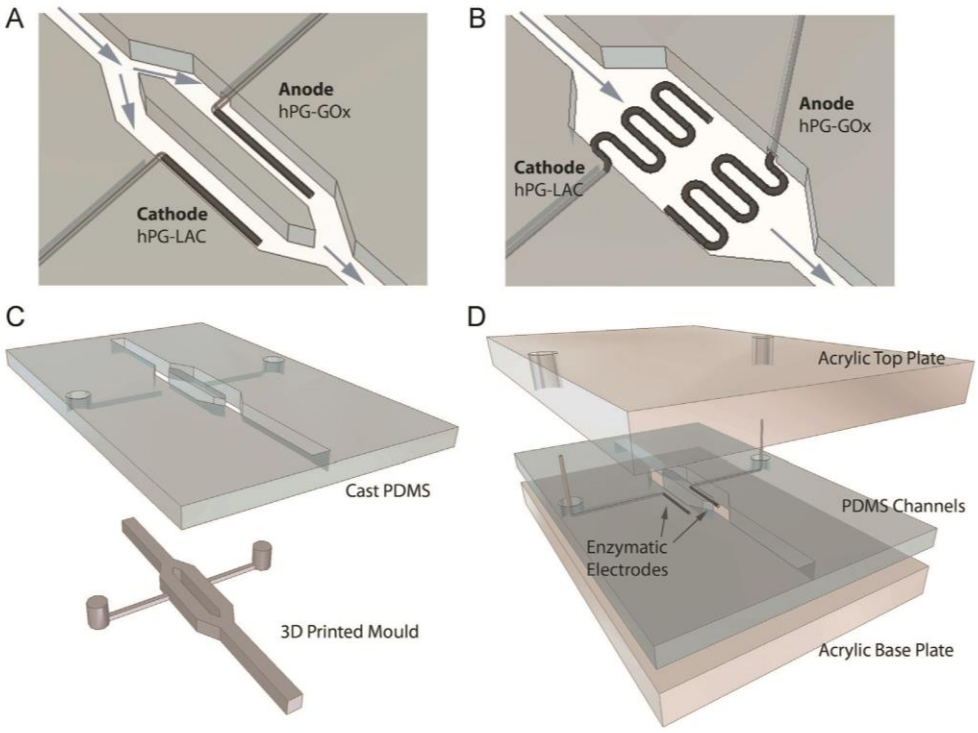

Fig. 1. Schematic and construction of the two different CFEBFC configurations; (A) parallel channel fuel cell design (top view), (B) single channel fuel cell with pleated electrodes (top view), (C) casting of PDMS channels from 3D printed negative, (D) exploded view of a CFEBFC.

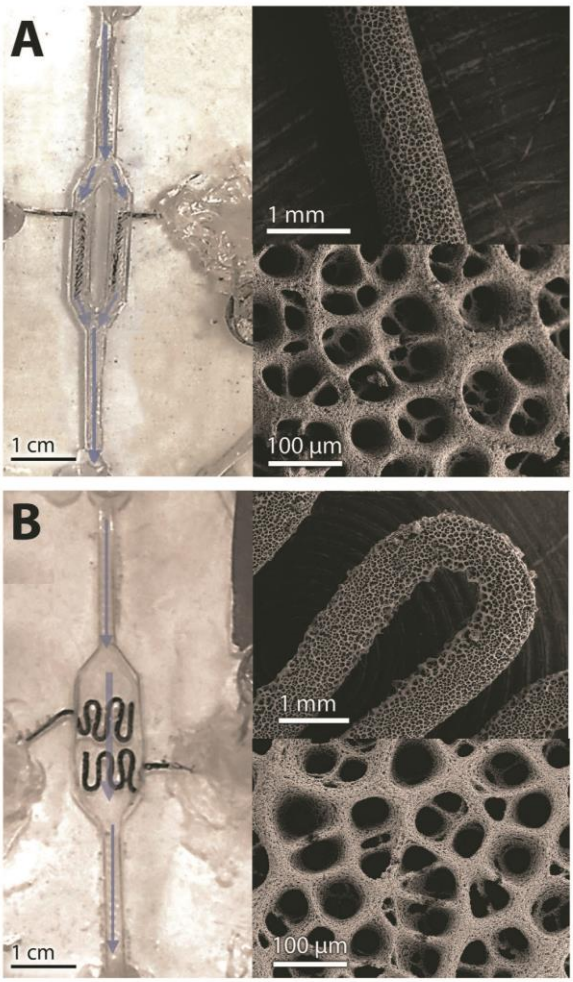

Fig. 2. Electrode configurations and their respective morphologies as shown by FESEM (A) dual channel fuel cell with hPG electrodes produced under potentiostatic control and (B) single channel fuel cell with pleated hPG electrodes produced under manual control with bench-top DC power supply.

electrodes used in the two different CFEBFC configurations obtained either *via* a potentiostatically controlled electrodeposition (Fig. 2A), or by using a DC power supply (Fig. 2B). As shown, the two methodologies led to the same porous structure. This is a significant move towards the low cost production of hPG electrodes on a larger scale.

3.2. Performance of the CFEBFCs

The CFEBFCs were tested by continuously feeding them with an aerated PBS solution containing 27 mM glucose, at a rate of 0.35 ml min^{-1} and under the constant temperature of 37 °C as shown in Supplementary data.

The performances of the two CFEBFCs were firstly compared on the basis of their polarisation and power curves. These were obtained by step-increasing the resistance applied across the fuel cell between 1 kΩ and 1 MΩ, as well as by measuring the open circuit potential (OCP). Fig. 3 shows the results obtained. A marked difference in performance (either specific by electrode surface area, or overall) was observed between the two CFEBFCs. The power and current density obtained with the single channel CFEBFC (Fig. 3B) are in fact much lower than the case of two channels CFEBFC (Fig. 3A).

Moreover, in the case of the single chamber CFEBFC, a drop in OCP of approximately 90 mV was observed. The potential interference of reaction intermediates, such as H_2O_2, could be the cause of the poorer performance of the single chamber CFEBFC. H_2O_2 is produced when reduced GOx comes in contact with oxygen as described by the following reactions:

$$\underbrace{C_6H_{12}O_6}_{\text{glucose}} + GOx \rightarrow \underbrace{C_6H_{10}O_6}_{\text{D-glucono-1,5-lactone}} + GOx.H_2$$

$$GOx.H_2 + O_2 \rightarrow GOx + H_2O_2$$

This poses no problem at the GOx electrode as H_2O_2 is can be involved in improving electron mediation between the enzyme's active site and the hPG surface, according to the following reaction:

$$H_2O_2 \xrightarrow{\text{hPG electrode}} O_2 + 2H^+ + 2e^-$$

The back diffusion of H_2O_2 can however cause interference at the LAC electrode by causing an electrochemical short-circuit. Laccase could also be deactivated by H_2O_2 as previously reported (Milton et al. 2013). Enzyme migration from one electrode to another could also be a risk. If, as a consequence of the continuous

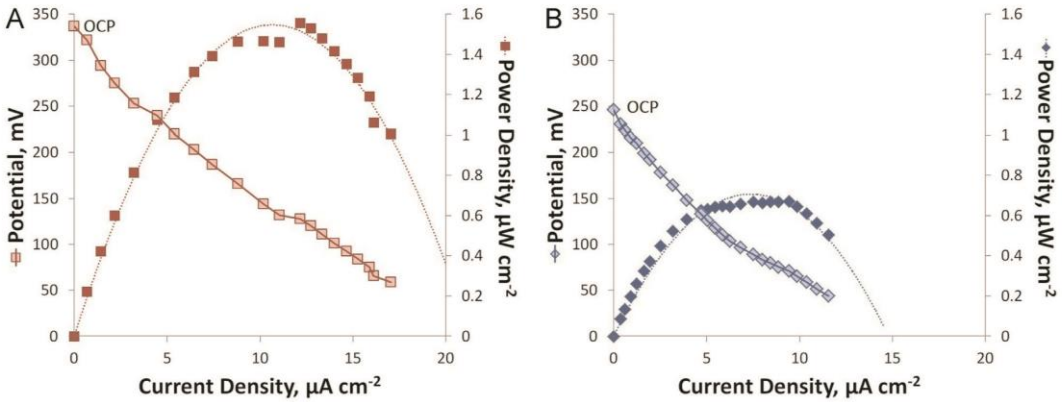

Fig. 3. Polarisation by fuel cell load of both CFEBFC configurations (A) parallel channel CFEBFC and (B) single channel CFEBFC. Tests performed during continuous operation 24 h after setup. Current and power densities refer to geometric surface area of anode (0.31 cm^2).

flow, the enzyme from the first electrode is released in the solution it could be absorbed into the porous structure of the following electrode with the result of short-circuiting the electricity production. In our case, however, this risk is believed to be minimal since the electrodes were rinsed thoroughly prior to use to remove any poorly attached enzyme. Moreover, the single channel CFEBFC was set-up so that the feed would first pass over the cathode and then to the anode. This was done on the assumption that, the LAC, covalently attached to the electrode contrarily to GOx, presented minimum risk of leaching.

The specific power output by the geometric surface area of an electrode is the most common metric used for determining fuel cell performance, however it does not always have practical relevance. In this study, the highest specific power output by anode surface was obtained with the parallel channels CFEBFC; with a value (1.6 μW cm^{-2}) more than two times greater than the single channel CFEBFC (0.7 μW cm^{-2}). Nonetheless, since the parallel channels CFEBFC is reliant on the use of a physical divider between electrodes, it has a larger overall volume relative to the electode size. A more practical evaluation of the CFEBFCs' performance should therefore consider not only the surface area of the electrodes but also the overall size and shape of the constructed fuel cells.

The overall polarisation of a fuel cell can also give a misleading characterisation of the fuel cells since it only takes a snapshot of their performance. The power produced by the two types of fuel cells was therefore investigated during continuous operation.

Fig. 4 shows the average continuous power production from the two CFEBFC designs during the first 24 h of operation. In each case, the fuel cell load was chosen so as to maximise power output (30 kΩ and 10 kΩ for the parallel channel and the single channel CFEBFC respectively). According to the parameter used for comparison, the two designs give apparently controversial results. When the specific power output is considered, the parallel channel CFEBFC consistently outperforms the single channel CFEBFC (Fig. 4A). On the contrary, when the total power produced is taken into account, the single channel system presents better performance than the parallel channel system (Fig. 4B). This suggests that there is a potential trade-off between the CFEBFC's specific power output by area and its specific power output by volume.

Alternatively, assuming that H_2O_2 is the cause for the lower power density by electrode area for the single chamber system, the use of a physical divider could be overcame by operating the cell at flow velocities high enough to counteract H_2O_2 diffusion. The CFEBFCs were in fact fed with the same volumetric flow rate (0.35 ml min^{-1}). Due to their different cross-sectional areas, the flow velocities in the CFEBFCs were however different: 1.94 cm min^{-1} and 1.17 cm min^{-1} for parallel channels CFEBFC and single channel CFEBFC respectively. This difference could affect the mass transfer both from the bulk of the solution to the enzymes on the electrodes, and subsequently between the enzymes and the hPG. The impact that different flow velocities have on the power output generated by the two CFEBFCS was consequently investigated.

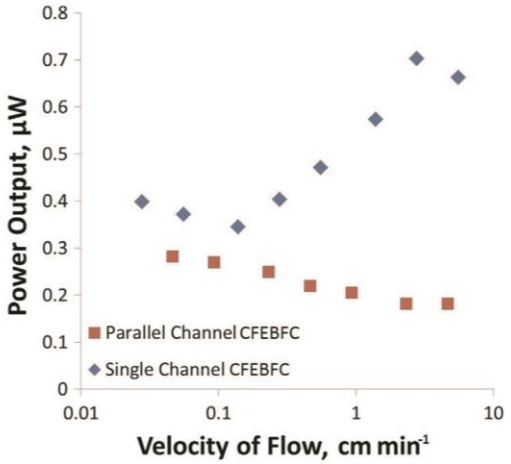

Fig. 5. Power output observed at different flow velocities with each CFEBFC configuration. Testing performed on fuel cells which had already operated continuously for 24 h. Note that flow velocity is on logarithmic scale.

Fig. 5 shows the power output produced by the two CFEBFCs at increasing velocities of flow. As shown, differences in flow velocity had little effect on the parallel channels CFEBFC. On the other hand, exponential increases of the flow velocities had a significant impact on the performance of the single chamber CFEBFC. It has been reported that the GOx's apparent K_m (which inversely indicates enzymes' affinity for glucose) increases with flow rate

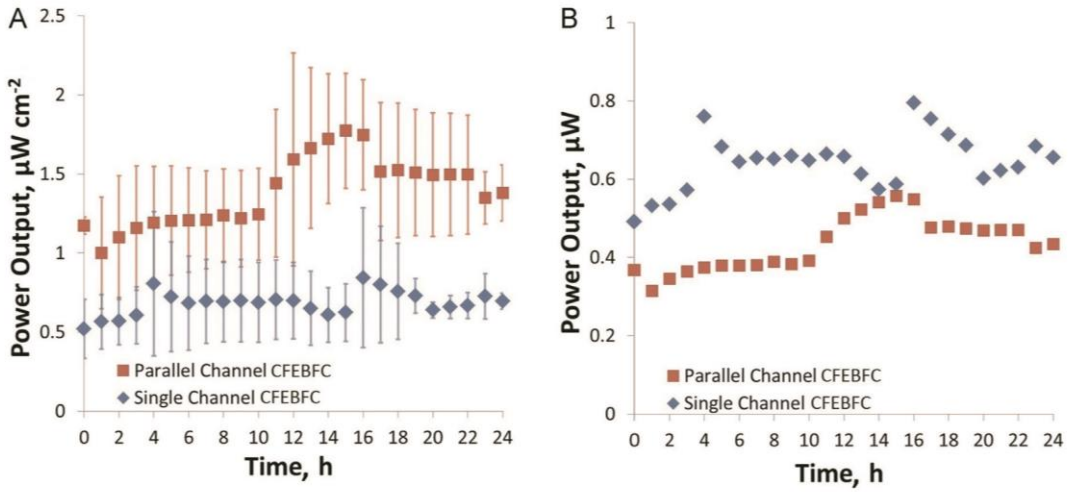

Fig. 4. Power output from the two CFEBFC designs over the first 24 h of operation; (A) specific power output by geometric surface areas of anodes, (B) absolute power output from the CFEBFCs. In both cases data is taken from 3 replicate fuel cells as represented by standard deviation error bars in Fig. 4A.

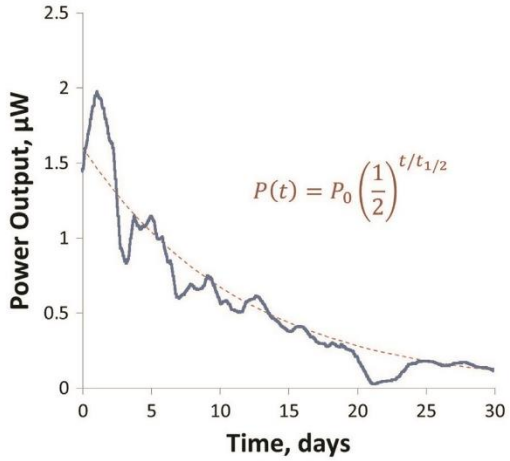

Fig. 6. Power output during continuous operation over 1 month period. Dashed line indicates theoretical power output based on half-life of 8 days. Flow rate: 0.35 ml min^{-1}.

(Seong et al., 2003). A general decay in power output is therefore expected at high flow rates. This decay was observed in the case of the parallel channel CFEBFC. Contrarily, in the case of the single channel CFEBFC the power output increased at flow velocities higher than 0.04 cm min^{-1}. This result supports the hypothesis that H_2O_2 back diffusion is one of the causes of poor performance at low flow rates. The high flow rates could also provide a better supply of reactants to hard-to-reach regions of the pleated electrode surfaces owing to increased turbulent mixing. Higher flow velocities are however associated with a much higher throughput of fuel, with exponential increases in flow rate yielding only minor increases in performance. An increase in the flow velocity of one order of magnitude (from 0.03 cm min^{-1} to 0.7 cm min^{-1}) led in fact to a power output only 0.75 times higher. Future work is, however required to take a more in-depth look at the flow phenomena in the two cells and further investigate and quantify the effects of flow rate on their operation.

Although the initial power output generated by enzymatic biofuel cells is frequently reported to be sufficient for ultra-low power implantable medical devices, their long-term stability during continuous operation is very poor. Many enzymatic fuel cells reported so far exhibit in fact a rapid decay in performance, with most lasting only a few hours (Castorena-Gonzalez et al., 2013; Cinquin et al., 2010; MacVittie et al., 2013; Togo et al., 2007). In order to determine the long-term stability of the CFEBFC it was decided to record the power output during continuous operation for one month. To the best of our knowledge, this is the first study performed over such a period of time with an enzyme immobilised EBFC operating in continuous flow with no addition of external mediators.

The parallel channel fuel cell was selected for this analysis since it produced a more stable power output at low flow rates with low risk for H_2O_2 diffusion from the anode to the cathode.

Fig. 6 shows the continuous power production from the parallel channel EBFC over a period of 30 days. As shown, during the first 48 h of operation, the CFEBFC exhibited a growth in the power produced, before entering a general decay phase. The fluctuations in the power output observed are attributed to the evolution of gas bubbles within the fuel cell. Although every effort was taken to prevent this happening by using drips prior to feeding the CFEBFC (see Supplementary data), some gas bubbles would still evolve during long-term continuous operation. A sharp drop in power was observed after 20 days of continuous operation, which continued until the 23rd day when the CFEBFC was washed with a fresh PBS solution. This suggests that there might have been some contamination in the feed that inhibited the power production.

Regardless of the short-term fluctuations in the power output from the CFEBFC, a strong trend was maintained with an apparent constant rate of decay. From this decay, the half-life of the fuel cell was determined to be approximately eight days. Since there is no other research reported to have used a continuous flow through enzymatic biofuel cell or to have even tested the long-term stability for over 30 days, it is difficult to make comparisons to the existing state-of-the-art on the subject. However, it can be reported that this CFEBFC has a half-life which is in line with the half-life of free laccase in solution (3–8 days under optimal conditions (Zille et al., 2003)), and also with that of a carbon-based GOx-LAC fuel cell (approximately six days based on continuous operation for 72 h (Chen et al., 2001)). Since GOx has reported half-lives in excess of 200 days, the LAC electrode is likely to be the limiting electrode and the cause of the decay in power output (Rando et al., 1997). This result is very promising since the majority of enzyme-immobilised devices exhibit much faster decays in power output owing to deactivation or detachment of enzymes. The fact that the decay in power output is in line with the decay of the enzymes themselves suggests that the methods employed for immobilisation are stable over long periods of time. The long-term stability of this CFEBFC could therefore be improved by simply increasing the stability of the enzymes used, either though protein engineering, or through cross-linking with stabilising polymers.

4. Conclusions

In this study we report continuous power generation from two innovative continuous flow enzymatic biofuel cell configurations that implement highly porous gold electrodes and glucose oxidase and laccase as the catalysts. The fabrication methodology here presented is cost-effective, easy-to-reproduce and fast, allowing for large scale-production and for further in-depth investigation on optimal electrode configuration and flow channel design.

By comparing the performance of the two CFEBFCS, we demonstrated that the power output generated is influenced by the channel designs; shape and size of the electrodes; and flow rate through the fuel cells. The design and operation of the CFEBFC can therefore be customised depending on the intended use. If miniaturisation is a major requirement, then using larger electrodes in a single channel device will maximise power output, but this will require high flow rates. Conversely, if space is not limited, then the specific power output can be maximised by physically separating the anode and cathode and thus increasing the relative size of the fuel cell.

This study also reports for the first time the long-term stability of a CFEBFC under continuous operation. Typically enzymatic biofuel cells exhibit lifetimes of only a few hours owing to the detachment or deactivation of enzymes, or commonly due to the leaching of redox mediators. In this study, however, the power output produced by the CFEBFC is stable during the first 24 h of operation. Furthermore, though decay in performance is observed during continual use over many days, the half-life of decay is in line with the state-of-the-art decay of the enzymes implemented under extremely favourable conditions (e.g. aqueous conditions).

Acknowledgments

The authors acknowledge: Prof Frank Marken, University of Bath, for valuable discussions and EPSRC (EP/K031597/1) for funding.

Appendix A. Supplementary information

Supplementary data associated with this article can be found in the online version at http://dx.doi.org/10.1016/j.bios.2015.02.036.

References

Anthony, G.-E., Chenghong, L., Ray, H.B., 2002. Nanotechnology 13 (5), 559.
Barton, S.C., Gallaway, J., Atanassov, P., 2004. Chem. Rev. 104 (10), 4867–4886.
Bazaka, K., Jacob, M., 2012. Electronics 2 (1), 1–34.
Bottini, M., Bruckner, S., Nika, K., Bottini, N., Bellucci, S., Magrini, A., Bergamaschi, A., Mustelin, T., 2006. Toxicol. Lett. 160 (2), 121–126.
Castorena-Gonzalez, J.A., Foote, C., MacVittie, K., Halámek, J., Halámková, L., Martinez-Lemus, L.A., Katz, E., 2013. Electroanalysis 25 (7), 1579–1584.
Chen, L.Y., Fujita, T., Chen, M.W., 2012. Electrochim. Acta 67 (0), 1–5.
Chen, T., Barton, S.C., Binyamin, G., Gao, Z., Zhang, Y., Kim, H.-H., Heller, A., 2001. J. Am. Chem. Soc. 123 (35), 8630–8631.
Cinquin, P., Gondran, C., Giroud, F., Mazabrard, S., Pellissier, A., Boucher, F., Alcaraz, J.-P., Gorgy, K., Lenouvel, F., Mathé, S., Porcu, P., Cosnier, S., 2010. PLoS One 5 (5), e10476.
Cooney, M.J., Svoboda, V., Lau, C., Martin, G., Minteer, S.D., 2008. Energy Environ. Sci. 1 (3), 320–337.
Cosnier, S., Le Goff, A., Holzinger, M., 2014. Electrochem. Commun. 38 (0), 19–23.
Degani, Y., Heller, A., 1987. J. Phys. Chem. 91 (6), 1285–1289.
du Toit, H., Di Lorenzo, M., 2014a. Sens. Actuators B: Chem. 192 (0), 725–729.
du Toit, H., Di Lorenzo, M., 2014b. Electrochim. Acta 138 (0), 86–92.
Hakamada, M., Takahashi, M., Mabuchi, M., 2012. Gold Bull. 45 (1), 9–15.
Halámková, L., Halámek, J., Bocharova, V., Szczupak, A., Alfonta, L., Katz, E., 2012. J. Am. Chem. Soc. 134 (11), 5040–5043.
Ivnitski, D., Branch, B., Atanassov, P., Apblett, C., 2006. Electrochem. Commun. 8 (8), 1204–1210.
Kerzenmacher, S., Ducrée, J., Zengerle, R., von Stetten, F., 2008. J. Power Sources 182 (1), 1–17.
Kim, J., Jia, H., Wang, P., 2006. Biotechnol. Adv. 24 (3), 296–308.
Liu, Y., Wang, M., Zhao, F., Xu, Z., Dong, S., 2005. Biosens. Bioelectron. 21 (6), 984–988.
MacVittie, K., Halamek, J., Halamkova, L., Southcott, M., Jemison, W.D., Lobel, R., Katz, E., 2013. Energy Environ. Sci. 6 (1), 81–86.
Milton, R.D., Giroud, F., Thumser, A.E., Minteer, S.D., Slade, R.C.T., 2013. Phys. Chem. Chem. Phys. 15 (44), 19371–19379.
Minteer, S.D., Liaw, B.Y., Cooney, M.J., 2007. Curr. Opin. Biotechnol. 18 (3), 228–234.
Pita, M., Gutierrez-Sanchez, C., Olea, D., Velez, M., Garcia-Diego, C., Shleev, S., Fernandez, V.M., De Lacey, A.L., 2011. J. Phys. Chem. C 115 (27), 13420–13428.
Rando, D., Kohring, G.W., Giffhorn, F., 1997. Appl. Microbiol. Biotechnol. 48 (1), 34–40.
Rasmussen, M., Ritzmann, R.E., Lee, I., Pollack, A.J., Scherson, D., 2012. J. Am. Chem. Soc. 134 (3), 1458–1460.
Rincón, R.A., Lau, C., Luckarift, H.R., Garcia, K.E., Adkins, E., Johnson, G.R., Atanassov, P., 2011. Biosens. Bioelectron. 27 (1), 132–136.
Sales, F.C.P.F., Iost, R.M., Martins, M.V.A., Almeida, M.C., Crespilho, F.N., 2013. Lab on a Chip 13 (3), 468–474.
Seong, G.H., Heo, J., Crooks, R.M., 2003. Anal. Chem. 75 (13), 3161–3167.
Sokic-Lazic, D., Minteer, S.D., 2009. Electrochem. Solid-State Lett. 12 (9), F26–F28.
Szczupak, A., Halamek, J., Halamkova, L., Bocharova, V., Alfonta, L., Katz, E., 2012. Energy Environ. Sci. 5 (10), 8891–8895.
Togo, M., Takamura, A., Asai, T., Kaji, H., Nishizawa, M., 2007. Electrochim. Acta 52 (14), 4669–4674.
Wei, X., Liu, J., 2008. Front. Energy Power Eng. China 2 (1), 1–13.
WHO, 2014. Fact Sheets. World Health Organisation, (Accessed: 01/10/2014) Available from: ⟨http://www.who.int/mediacentre/factsheets/en/⟩.
Xiao, X., Wang, Me, Li, H., Si, P., 2013. Talanta 116 (0), 1054–1059.
Zille, A., Tzanov, T., Gübitz, G., Cavaco-Paulo, A., 2003. Biotechnol. Lett. 25 (17), 1473–1477.

SUPPLEMENTARY DATA

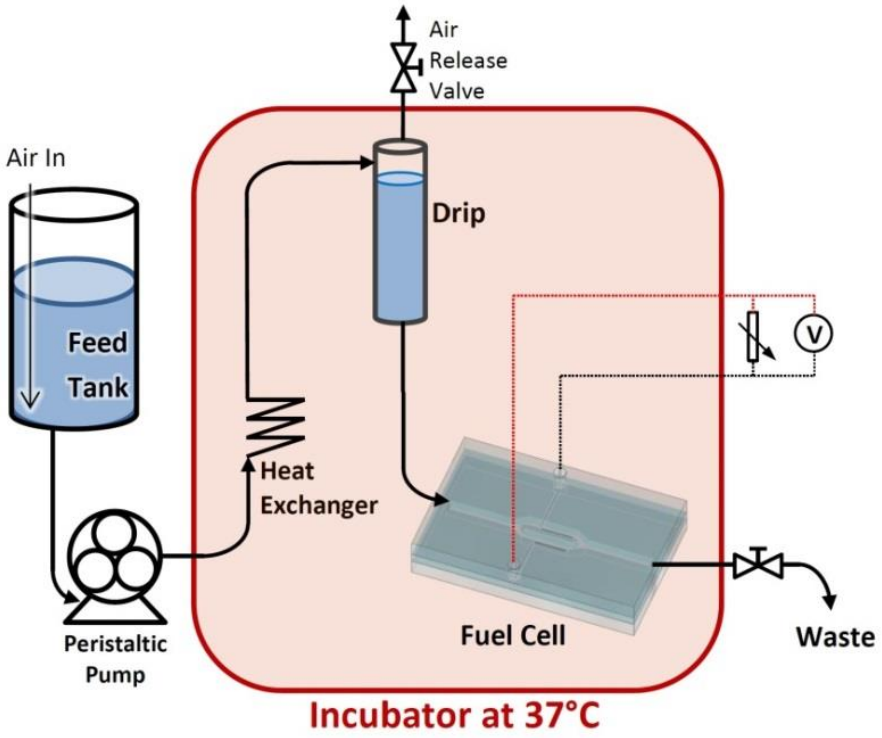

Figure S1: Experimental setup (not to scale) used during fuel cell operation

Figure S1 shows the experimental set-up used for testing the CFEBFCs. The feed solution was aerated prior to entering the incubator and passed through a tubing coil inside the incubator. This ensured that both the feed and the CFEBFC were maintained at 37°C. Finally, the feed passed through a drip prior to remove any gas bubbles that evolved in the heating process. This served to minimise to air bubbles entering the fuel cell and thus reduce fluctuations in power output due to the presence of air in the channels.